

Ring Opening of Mono- and Bicyclic Naphthenes via Hydrogenolysis on Noble Metal Catalysts

Von der Fakultät Chemie der Universität Stuttgart
zur Erlangung der Würde eines
Doktors der Naturwissenschaften (Dr. rer. nat.)
genehmigte Abhandlung

Vorgelegt von
Andreas Haas
aus Schramberg

Hauptberichter: Prof. Dr.-Ing. Jens Weitkamp

Mitberichter: Prof. Dr. Thomas Schleid

Tag der mündlichen Prüfung: 27.04.2012

Institut für Technische Chemie
der Universität Stuttgart

2012

Die vorliegende Arbeit entstand in der Zeit von Oktober 2008 bis November 2011 am Institut für Technische Chemie der Universität Stuttgart.

Mein Dank gilt besonders Herrn Prof. Dr.-Ing. Jens Weitkamp für die Überlassung dieses aktuellen und spannenden Themas, sowie für die engagierte Betreuung meiner Arbeit.

Herrn Prof. Dr.-Ing. Elias Klemm danke ich für die guten Rahmenbedingungen am Institut für Technische Chemie.

Herrn Prof. Dr. Thomas Schleid danke ich für die Übernahme des Koreferats.

Ferner danke ich Herrn Dr. Vincenzo Calemma und Herrn Dr. Marco Ferrari von Eni S.p.A. für die gute Zusammenarbeit im Rahmen des Industrieprojekts und für die Bereitstellung des Modellkohlenwasserstoffs Perhydroindan.

Ein besonderer Dank gilt Simon Schulze und Nelli Pfaff, die im Rahmen ihrer Diplomarbeiten einen wichtigen Beitrag zu dieser Arbeit geleistet haben.

Dank gebührt ebenfalls Julia Kreis, Yvonne Krämer und Melanie Mechler, die im Rahmen von Praktika zu dieser Arbeit beigetragen haben.

Besonders danke ich meinen Kollegen Tobias Holl, Sandra Rabl und Dominic Santi für die sehr angenehme Zusammenarbeit im Projekt. Zusammen mit Frank Salzbauer waren sie anspruchsvolle Diskussionspartner und eine große Unterstützung bei verschiedensten Fragestellungen und Problemen.

Für die Durchführung verschiedener Analysen und Charakterisierungsmethoden bedanke ich mich bei Heike Fingerle, Barbara Gehring, Ines Kley, Dominic Santi und Matthias Scheibe.

Ein großer Dank gilt meinen Eltern, die mir viele Freiheiten ließen, mich unterstützen und mir das Studium ermöglichten. Meinen Freunden und besonders meiner Partnerin möchte ich für die Geduld und Unterstützung während des Studiums und der Anfertigung der Arbeit danken.

I Table of Contents

1	Zusammenfassung	1
2	Summary.....	6
3	Introduction and Objectives	10
4	Literature Review	12
4.1	Preparation of Noble-Metal-Containing Catalysts.....	12
4.1.1	Monofunctional Metal Catalysts	12
4.1.2	Bifunctional Zeolite Catalysts	14
4.2	Catalytic Reactions of Saturated Hydrocarbons in the Presence of Hydrogen	15
4.2.1	Reactions on Monofunctional Noble Metal Catalysts.....	15
4.2.1.1	Dehydrocyclization and Dehydrogenation.....	15
4.2.1.2	Skeletal Isomerization of Hydrocarbons.....	16
4.2.1.3	Hydrogenolysis of Alkanes	18
4.2.1.4	Hydrogenolysis of Naphthenes	21
4.2.2	Reactions on Bifunctional Catalysts.....	28
4.2.2.1	Skeletal Isomerization of Hydrocarbons.....	28
4.2.2.2	Hydrocracking of Alkanes	30
4.2.2.3	Hydrocracking of Naphthenes	32
4.2.3	Ring Opening of Naphthenes <i>via</i> Skeletal Isomerization and Subsequent Hydrogenolysis	35
5	Experimental Section.....	40
5.1	Preparation of the Catalysts.....	41
5.1.1	Preparation of [Si]SBA-15	41
5.1.2	Ion Exchange with Ammonium Ions.....	42
5.1.3	Incorporation of the Noble Metals	42
5.1.3.1	Ion Exchange.....	42
5.1.3.2	Strong Electrostatic Adsorption	42

5.1.3.3	Impregnation	43
5.1.4	Calcination of Catalyst Precursors	44
5.1.5	Forming of the Catalyst Powder.....	45
5.1.6	Oxidative Treatment.....	45
5.1.7	Reduction of the Noble Metals.....	45
5.2	Characterization of the Starting Materials and Catalysts.....	47
5.2.1	X-Ray Diffraction.....	47
5.2.2	Chemical and Thermogravimetric Analysis.....	47
5.2.3	Scanning Electron Microscopy.....	48
5.2.4	FT-Infrared Spectroscopy.....	48
5.2.5	Nitrogen Physisorption and Hydrogen Chemisorption	48
5.3	Procedures of the Catalytic Experiments	49
5.3.1	Hydroconversion of n-Octane as Test Reaction.....	49
5.3.1.1	Experimental Set-Up of the Flow Apparatus.....	50
5.3.1.2	Conditions in the Catalytic Experiments	50
5.3.2	Isomerization of n-Nonane and n-Undecane	50
5.3.3	Hydroconversion of n-Decane, Ethylcyclohexane, Butylcyclohexane, Perhydroindan, cis-Decalin, Spiro[4.5]decane and Methyldecalin	52
5.3.3.1	Experimental Set-Up of the High-Pressure Flow-Type Apparatuses.....	52
5.3.3.2	Conditions in the Catalytic Experiments with n-Decane	54
5.3.3.3	Conditions in the Catalytic Experiments with Ethylcyclohexane.....	55
5.3.3.4	Conditions in the Catalytic Experiments with Butylcyclohexane	55
5.3.3.5	Conditions in the Catalytic Experiments with Perhydroindan.....	56
5.3.3.6	Conditions in the Catalytic Experiments with cis-Decalin	56
5.3.3.7	Conditions in the Catalytic Experiments with Spiro[4.5]decane.....	57
5.3.3.8	Conditions in the Catalytic Experiments with Methyldecalin	58
5.4	Product Analysis by Capillary Gas Chromatography	58
5.4.1	On-line Gas Chromatography.....	58
5.4.2	Off-line Gas Chromatography / Mass Spectrometry.....	61

5.5	Evaluation of the Catalytic Experiments.....	62
5.5.1	Terminology of the Reactions and Products	62
5.5.1.1	Hydroconversion of n-Octane	63
5.5.1.2	Hydroconversion of n-Decane	63
5.5.1.3	Hydroconversion of Ethylcyclohexane.....	64
5.5.1.4	Hydroconversion of Butylcyclohexane.....	64
5.5.1.5	Hydroconversion of Perhydroindan	65
5.5.1.6	Hydroconversion of cis-Decalin	66
5.5.1.7	Hydroconversion of Spiro[4.5]decane	66
5.5.1.8	Hydroconversion of Methyldecalin	67
5.5.2	Assignment of the GC Signals	69
5.5.3	Conversions, Yields and Selectivities	69
5.5.4	Liquid Hourly Space Velocity.....	70
6	Characterization of the Catalyst Precursors and Catalysts	72
6.1	Zeolite Y	72
6.2	Silica	72
6.3	[Si]SBA-15	73
6.4	Metal Dispersions of the Catalysts.....	74
7	Preliminary Experiments	76
7.1	Co-Injection of n-Alkane Isomers.....	76
7.2	Blank Tests	79
8	Hydroconversion of n-Octane as Test Reaction.....	81
8.1	Palladium-Containing Y Zeolite as Bifunctional Reference Catalyst.....	81
8.2	Iridium- or Platinum-Containing Catalysts Supported on Silica or [Si]SBA-15	83
8.3	Iridium- or Platinum-Containing Catalysts Supported on γ -Alumina, Titania or Carbon Black	88
8.4	Conclusions	90
9	Hydrogenolysis on Monofunctional Noble Metal Catalysts	91
9.1	n-Decane.....	91

9.2	Ethylcyclohexane	94
9.3	Butylcyclohexane	100
9.4	Perhydroindan	106
9.5	cis-Decalin.....	114
9.5.1	Stereoisomerization of cis- and trans-Decalin.....	114
9.5.2	Hydroconversion on Ir/Silica and Ir/[Si]SBA-15 Catalysts.....	115
9.5.3	Hydroconversion on Pt/Silica and Pt/[Si]SBA-15 Catalysts.....	125
9.5.4	Hydroconversion on Rh/Silica Catalysts.....	132
9.6	Spiro[4.5]decane.....	134
9.7	Methyldecalin.....	142
9.8	Influence of the Hydrogen Pressure	145
9.8.1	Hydrogenolysis of Perhydroindan on Platinum	145
9.8.2	Hydrogenolysis of cis-Decalin on Iridium	149
9.9	Conclusions	153
9.9.1	Influence of the Nature of the Noble Metal.....	153
9.9.2	Influence of the Type of Hydrocarbon	156
10	Hydrocracking on Metal Catalysts Containing Brønsted Acid Sites.....	160
10.1	n-Decane.....	160
10.2	Butylcyclohexane	166
10.2.1	Hydroconversion on High-Performance Ring-Opening Catalysts	166
10.2.2	Hydroconversion on a Bifunctional Isomerization Catalyst and a Two-Bed Arrangement with 2.69Pt/Silica	177
10.3	Perhydroindan	181
10.4	Spiro[4.5]decane.....	187
10.5	Conclusions	191
11	References.....	192
12	Appendices.....	197
12.1	Retention Times	197
12.2	Calculation of Conversion, Yields and Selectivities in the Catalytic Conversion of Hydrocarbons with Hydrogen	197

12.2.1	Nomenclature.....	197
12.2.1.1	Symbols.....	197
12.2.1.2	Indices	198
12.2.1.3	Abbreviations	198
12.2.2	Conversion X_{feed}	199
12.2.2.1	Fundamentals	199
12.2.2.2	Calculation of $(m_{\text{feed}})_{\text{GSL}}$ from the Area in the Gas Chromatogram.....	201
12.2.2.3	Calculation of $(m_{\text{feed}})_{\text{GSL}}$ at $X = 0$	202
12.2.3	Yield Y_j	204
12.2.4	Selectivity S_j	205
12.2.5	Modified Selectivity S_j^*	205
12.2.6	References	206
12.3	Simulation of the Distribution of Hydrocracked Products in the Hydroconversion of Decalin on Ir/silica	207
12.3.1	Underlying Reaction Network.....	207
12.3.1.1	Hydrogenolytic Ring Opening of One Six-Membered Ring in Decalin	207
12.3.1.2	Consecutive Hydrogenolysis of the Direct ROPs and Direct OCDs.....	209
12.3.2	Calculation Method for the Distribution of the Hydrocracked Products	209
12.3.3	Results	210

II Symbols, Indices and Abbreviations

Symbols

Symbol	Unit	Designation
α	-	Fraction of hydrogenolyzed C-C bonds of a certain type that undergo hydrogenolysis
A	-	Dimensionless peak area in the chromatogram
A_{BET}	$\text{m}^2 \cdot \text{g}^{-1}$	Specific surface area according to Brunauer, Emmett and Teller
d	m	Diameter
D	-	Dispersion
f	-	Compound-specific correction factor of the flame-ionization detector
$LHSV$	h^{-1}	Liquid hourly space velocity
m	kg	Mass
M	$\text{g} \cdot \text{mol}^{-1}$	Molar mass
\dot{m}	$\text{g} \cdot \text{h}^{-1}$	Mass flux
n	mol	Molar amount
n_{C}	-	Number of carbon atoms in the carbenium ion
p	Pa	Pressure
pH	-	Negative decimal logarithm of the oxonium ion concentration
PZC	-	Point of zero charge
S	-	Selectivity
S_j^*	-	Modified selectivity
T	K or °C	Temperature
\dot{V}	$\text{m}^3 \cdot \text{s}$	Volumetric flow rate
X	-	Conversion
Y	-	Yield
θ	°	Angle

ν - Stoichiometric factor

Indices

cat	Catalyst
j	A product or group of products in the stoichiometric equation
max.	Maximum
r	Reaction
red	Reduction
RT	Room temperature
subst.	Substituted
unsubst.	Unsubstituted

Abbreviations

a.u.	Arbitrary units
C ₅ -	Hydrocarbons with less than 6 carbon atoms (hydrocracked products)
C ₆ -	Hydrocarbons with less than 7 carbon atoms (hydrocracked products)
C ₇ -	Hydrocarbons with less than 8 carbon atoms (hydrocracked products)
C ₈ -	Hydrocarbons with less than 9 carbon atoms (hydrocracked products)
C ₉ -	Hydrocarbons with less than 10 carbon atoms (hydrocracked products)
C ₁₀ -	Hydrocarbons with less than 11 carbon atoms (hydrocracked products)
CCD	Charge-coupled device
CH _x -ROPs	Alkylcyclohexanes with 9 carbon atoms
CP _n -ROPs	Alkylcyclopentanes with 9 carbon atoms
DEPT	Distortionless enhancement by polarization transfer
DFT	Density functional theory
DHP(s)	Dehydrogenated product(s)
DRIFT	Diffuse reflectance infrared Fourier transform

EDS	Energy-dispersive X-ray spectroscopy
FI	Flow indicator
FID	Flame-ionization detector
FT-IR	Fourier transform infrared
GC	Gas chromatograph(y)
GC/MS	Gas chromatograph(y) / mass spectrometer, spectrometry
HIPEROC(s)	High-performance ring-opening catalyst(s)
HRTEM	High-resolution transmission electron microscopy
ICP-OES	Optical emission spectrometer with an inductively coupled plasma
M	Metal
MBDe	Multiply branched decanes
MBNo	Multiply branched nonanes
MCM	Mobil Composition of Matter
NMR	Nuclear magnetic resonance
NV	Needle valve
OCD(s)	Open-chain decane(s)
OCO(s)	Open-chain octane(s)
OCN(s)	Open-chain nonane(s)
OCU(s)	Open-chain undecane(s)
PCP	Protonated cyclopropane
PHI	Perhydroindan
RCP(s)	Ring closure product(s)
Ref.	Reference
ROP(s)	Ring-opening product(s)
SBA	University of California, Santa Barbara
SEA	Strong electrostatic adsorption
SEM	Scanning electron microscopy
sk-Iso(s)	Skeletal isomer(s)
spiro	Spiro[4.5]decane

TCD	Thermal conductivity detector
TEM	Transmission electron microscopy
TGA	Thermogravimetric analyzer, analysis
TPR	Temperature-programmed reduction
USY	Ultrastable Y zeolite
V	Valve
wt.-%	Mass fraction
XPS	X-ray photoelectron spectroscopy
XRD	X-ray diffractometry, diffractogram
ZO ⁻	Anionic framework oxygen of the zeolite

Abbreviations of Hydrocarbons

B-	Butyl-
Bz	Benzene
c-	cis-
CH _x	Cyclohexane
CP _n	Cyclopentane
De	Decane
Dec	Decalin
DE-	Diethyl-
DM-	Dimethyl-
E-	Ethyl-
Hp	Heptane
Hx	Hexane
M-	Methyl-
No	Nonane
Oc	Octane
P-	Propyl-
P _n	Pentane

Pr	Propane
tr-	trans-

Nomenclature of the Catalysts

The designation of the catalyst composition was always related to the dry mass, as determined by thermogravimetric analysis (TGA). In the catalyst designation the mass fractions of the noble metals are given in weight-% in front of a slash as determined by optical emission spectrometer with an inductively coupled plasma (ICP-OES). They were separated by comma and sorted by mass fraction in descending order.

After the slash, the catalyst support is identified. In case of aluminum-containing zeolites, also the charge-compensating cations are given in front of a hyphen that separates the cation composition and the type of zeolite. After each cation, a subscript indicates the mole fraction as determined by ICP-OES. The molar amount of protons is calculated as the molar amount of aluminum minus the sum of equivalents of all metal cations. The symbols are separated by comma and sorted by mole fraction in descending order.

1 Zusammenfassung

Polycyclische aromatische Kohlenwasserstoffe besitzen im Dieselkraftstoff mehrere unerwünschte Eigenschaften, dies sind eine geringe Cetanzahl, eine starke Neigung zur Rußbildung, eine ungünstige Kältefließfähigkeit und eine hohe spezifische Kohlendioxidemission. Die EU hat den maximal erlaubten Gehalt an polycyclischen aromatischen Kohlenwasserstoffen im Dieselkraftstoff auf 8 Ma.-% reduziert. Deshalb können in einer Raffinerie Stoffströme, die einen hohen Anteil dieser Verbindungen enthalten, nur in geringem Umfang dem Dieselkraftstoff beigemischt werden. Zur Umwandlung dieser Komponenten in Kohlenwasserstoffe mit besseren Eigenschaften scheint deren Hydrierung zu polycyclischen Naphthenen (polycyclische Kohlenwasserstoffe), gefolgt von einer selektiven Ringöffnung ohne Verlust von Kohlenstoffatomen der attraktivste Weg zu sein.

Da die Ringöffnung mittels bifunktionellen Hydrocrackens nur sehr langsam erfolgt, wurden vor Kurzem Katalysatoren entwickelt, die eine geringe Konzentration an sauren Zentren besitzen und mit Iridium oder Platin beladen sind („high-performance ring-opening catalysts“, HIPEROs). An den Brønsted-Säurezentren findet zunächst eine Gerüstisomerisierung des Naphthens statt, wohingegen die Ringöffnung vermutlich durch Hydrogenolyse an den Edelmetallen Iridium oder Platin erfolgt. Trotz der herausragenden Rolle der metallkatalysierten Hydrogenolyse an HIPEROs ist nur wenig über die Reaktionen von polycyclischen Naphthenen an nicht sauren Edelmetallkatalysatoren bekannt.

In der vorliegenden Arbeit wurden zwei Themengebiete behandelt: Welche Reaktionen und Reaktionspfade werden in der Umsetzung von polycyclischen Naphthenen an Edelmetallen, vor allem Iridium und Platin, unter Wasserstoffeinfluss katalysiert? Wie werden an HIPEROs offenkettige Alkane in hohen Ausbeuten gebildet?

Um ausschließlich metallkatalysierte Reaktionen untersuchen zu können, war es notwendig, einen Katalysatorträger zu finden, der keine katalytisch aktiven Brønsted-Säurezentren enthält. Hierzu wurden verschiedene Materialien mit Iridium oder Platin beladen und in der katalytischen Umsetzung von n-Octan unter Wasserstoffatmosphäre untersucht. In dieser Testreaktion konnte bei den Trägermaterialien Silica (amorphes Siliciumdioxid) und dem mesoporösen Material [Si]SBA-15 keine Beteiligung saurer Zentren beobachtet werden. Durch FT-IR-spektroskopische Untersuchungen mit Pyridin als Sondenmolekül konnte ebenfalls bestätigt werden, dass auf Silica keine Brønsted-Säurezentren existieren, deren Stärke ausreicht, um

Pyridin zu protonieren. Folglich wurde Silica für alle Experimente zur Untersuchung der reinen Metallkatalyse als Katalysatorträger verwendet. Die Beladung mit 0,7 bis 2,7 Ma.-% des jeweiligen Edelmetalls erfolgte durch starke elektrostatische Adsorption („strong electrostatic adsorption“, SEA) eines entsprechenden Metallkomplexkations. Auch [Si]SBA-15 wurde für eine Reihe von Vergleichsexperimenten als Trägermaterial eingesetzt. Die Ergebnisse waren denen mit Silica sehr ähnlich.

Im Allgemeinen konnte eine Abnahme der katalytischen Aktivität der Edelmetalle in der Reihe Ir > Rh > Pt > Pd beobachtet werden. Da mit den weniger aktiven Metallen höhere Reaktionstemperaturen notwendig waren, kam es zu einer verstärkten Bildung von Aromaten durch Dehydrierung. Alle vier Metalle katalysierten als schnelle Reaktion die cis/trans-Isomerisierung von Perhydroindan und Decalin, anschließend wurden die Mischungen der Stereoisomere durch Gerüstisomerisierung, Hydrogenolyse und Dehydrierung zu verschiedenen Produkten umgesetzt. Die weiteren Einsatzkohlenwasserstoffe waren n-Decan, Ethylcyclohexan, Butylcyclohexan und Methyldecalin.

Vor allem für Naphthene, die aus Sechsringen aufgebaut sind, war Iridium das am besten geeignete Metall für die rein hydrogenolytische Ringöffnung. Bei der Umsetzung von cis-Decalin an 2.73Ir/Silica wurde bei einem Wasserstoffdruck von 8,0 MPa und einer Reaktionstemperatur von 310 °C eine maximale Ausbeute an offenkettigen Decanen von 22 % erreicht. An Iridium fand keine Gerüstisomerisierung statt und es wurden bevorzugt unsubstituierte C-C-Bindungen, d. h. primär-sekundäre und sekundär-sekundäre Bindungen, gebrochen. Dies führte zu einem hohen Verzweigungsgrad in den gebildeten offenkettigen Alkanen mit gleicher Zahl an Kohlenstoffatomen wie im Reaktanden. Bei der Umsetzung von Decalin enthielten die Crackprodukte sehr große Anteile an C₁- und C₉-Produkten, große Anteile an C₂- und C₈-Produkten sowie sehr kleine Anteile an C₃- bis C₇-Produkten. Eine solche Form der Verteilungskurve, auch als Hängematten-Kurve bezeichnet, scheint typisch für die Umsetzung verschiedener bicyclischer Naphthene an nicht sauren Iridiumkatalysatoren zu sein.

Aus der Abhängigkeit der Produktselektivitäten vom Umsatz bei der Umsetzung von Decalin wurde die folgende Reaktionsfolge abgeleitet, die auch für die Simulation der Crackproduktverteilung angenommen wurde: Durch Hydrogenolyse einer C-C-Bindung in Decalin entstehen die drei direkten Ringöffnungsprodukte („direct ring-opening products“, direct ROPs) Butylcyclohexan, 1-Methyl-2-propylcyclohexan und 1,2-Diethylcyclohexan. In einem weiteren Hydrogenolyseschritt wird entweder eine

C-C-Bindung in einer Alkylseitenkette gespalten (exocyclische Hydrogenolyse) unter Bildung von Crackprodukten, oder es erfolgt Hydrogenolyse im Sechsring (endocyclische Hydrogenolyse), wobei sieben Konstitutionsisomere von Decan gebildet werden können („direct open-chain decanes“, direct OCDs). Für die Simulation wurde außerdem angenommen, dass auch alle direct OCDs durch Hydrogenolyse in Crackprodukte umgesetzt werden. Eine gute Übereinstimmung der simulierten Ergebnisse mit den im Experiment erhaltenen konnte erreicht werden, indem die plausible Annahme getroffen wurde, dass an Iridium unsubstituierte C-C-Bindungen bevorzugt gespalten wurden.

Platin ist wesentlich weniger hydrogenolyseaktiv als Iridium. Dieser Trend ist besonders ausgeprägt, wenn die C-C-Bindungen Teil eines Sechsrings sind. Zur Ringöffnung von Fünfringen, wie beispielweise in Perhydroindan, kann aber auch Platin ein geeignetes Edelmetall sein. Eine Untersuchung der Reaktionspfade auf nicht sauren Pt/Silica-Katalysatoren wurde durch die Isomerisierungsaktivität von Platin stark beeinträchtigt. So wurden bei der Umsetzung von cis-Decalin an Pt/Silica bei kleinen Umsätzen vor allem die Produkte Butylcyclohexan und Spiro[4.5]decan gebildet. Auch mit anderen Reaktanden, wie z. B. Ethylcyclohexan oder Butylcyclohexan, fand bevorzugt eine Spaltung der substituierten C-C-Bindungen in Sechsringen statt, was zu einer bevorzugten Bildung von Butylcyclohexan aus Decalin führte. Die hohe Selektivität der Spiroverbindung kann durch eine rein metallkatalysierte Isomerisierung über den „bond-shift“-Mechanismus oder über eine 1,5-Dehydrocyclisierung von Butylcyclohexan erklärt werden. An 2.68Pt/Silica wurde in der Umsetzung von cis-Decalin eine maximale OCD-Ausbeute von 2 % erreicht.

Es war nicht möglich, eine Verteilung der Hydrocrackprodukte zu simulieren, die der im Experiment erhaltenen Zusammensetzung dieser Produkte in der Umsetzung von Decalin an Pt/Silica ähnelt. Jedoch konnte eine Erklärung für die Bildung der sehr großen Mengen an C₁ und C₃ und der großen Mengen an C₂ und C₄ durch Umsetzung des wichtigsten Ringöffnungsprodukts Butylcyclohexan an einem identischen Katalysator gefunden werden: Die hohen Reaktionstemperaturen, die zur Öffnung eines Ringes in Decalin notwendig sind, begünstigen die exocyclische Hydrogenolyse von Butylcyclohexan unter der Bildung von großen Mengen an Methan und Propan.

Bei der Umsetzung an Pt/Silica war Spiro[4.5]decan reaktiver als Decalin. Die Hauptreaktion bei geringen Umsätzen war die Gerüstisomerisierung zu Decalin. Vermutlich verlief diese über den „bond-shift“-Mechanismus. Ähnliche Ausbeuten an Ringöffnungsprodukten wurden bei der Umsetzung beider Reaktanden bei vergleichbaren Reaktionstemperaturen erhalten. Es konnte gezeigt werden, dass die

wahrscheinlichste Ursache die Bildung einer ähnlichen Mischung von Gerüstisomeren ist, welche durch anschließende Hydrogenolyse Ringöffnungsprodukte bilden. Bei der Umsetzung von Spiro[4.5]decan an Ir/Silica erfolgte eine direkte Ringöffnung: Nach einer Öffnung des Fünfringes erfolgte die Öffnung des Sechsrings in den entsprechenden Ringöffnungsprodukten. Iridium öffnet bevorzugt die unsubstituierten C-C-Bindungen, was auch mit anderen Reaktanden beobachtet wurde, und erhält die Bindungen zwischen den quaternären und den benachbarten C-Atomen.

Pd/Silica erwies sich in erster Linie als Dehydrierungskatalysator und war beinahe inaktiv in der Hydrogenolyse. Bei der Umsetzung von cis-Decalin an Rhodiumkatalysatoren wurde ein Einfluss der Metallpartikelgröße auf die katalytischen Eigenschaften beobachtet. Kleine Rhodiumpartikel mit einer Metalldispersion von 0,57 katalysierten beinahe ausschließlich die Hydrogenolyse von C-C-Bindungen, wohingegen auf größeren Metallpartikeln mit einer Dispersion von 0,17 auch Gerüstisomere von Decalin gebildet wurden. Rhodium war weniger aktiv als Iridium. Es mussten ca. 50 °C höhere Reaktionstemperaturen angewandt werden, um denselben Umsatz zu erreichen. Dies führte zu mehrfacher Hydrogenolyse und damit zu einer starken Methanbildung.

Der Einfluss des Wasserstoffdrucks auf die Metallkatalyse wurde in einem Druckbereich von 1,0 bis 8,0 MPa untersucht. An Ir/Silica wurde cis-Decalin und an Pt/Silica Perhydroindan umgesetzt. An Pt/Silica ging der Umsatz mit steigendem Wasserstoffdruck zurück. Um hohe Ausbeuten an offenkettigen Nonanen zu erhalten, waren jedoch Drücke von 4,0 und 8,0 MPa optimal. An Ir/Silica war die Katalysatoraktivität bei der Umsetzung von cis-Decalin bei $p_{\text{H}_2} = 4,0$ MPa maximal. Die höchste Ausbeute an offenkettigen Decanen wurde jedoch bei $p_{\text{H}_2} = 8,0$ MPa erzielt. In beiden Kombinationen aus Reaktand und Katalysator begrenzte die Dehydrierung zu Aromaten die Ringöffnungsaktivität. An Ir/Silica führt scheinbar der hohe Wasserstoffdruck von $p_{\text{H}_2} = 8,0$ MPa zu einer langsameren Hydrogenolyse in den Alkylseitenketten. Da gleichzeitig die Hydrogenolyse der endocyclischen C-C-Bindungen scheinbar nicht beeinflusst wird, resultiert eine hohe Ringöffnungsaktivität.

Es wurden außerdem katalytische Experimente mit Zweibett-Arrangements durchgeführt, in denen zwei unterschiedliche Katalysatoren räumlich voneinander getrennt in den Reaktor eingebracht waren. Im ersten Katalysatorbett befand sich der bifunktionelle Isomerisierungskatalysator Pd/Na,H-Y und im zweiten Bett Pt/Silica als Hydrogenolysekatalysator. Die katalytischen Ergebnisse mit den Reaktanden n-Decan und Butylcyclohexan waren eine Mischung der Ergebnisse, die mit den einzelnen Katalysatoren beobachtet wurden. Es konnte keine Produktverteilung beobachtet

werden, die anzeigt, dass die an dem Zeolithkatalysator gebildeten Decanisomere an Pt/Silica anschließend durch Hydrogenolyse gespalten wurden. Dies zeigt, dass für solche Untersuchungen eine bessere Anpassung der Katalysatoraktivitäten notwendig ist.

HIPEROcs sind zeolithische, mit Iridium oder Platin beladene Katalysatoren, die eine geringe Konzentration an Brønsted-Säurezentren aufweisen. Diese wurden in der katalytischen Umsetzung von n-Decan, Butylcyclohexan und Spiro[4.5]decan getestet. Es konnte gezeigt werden, dass die Spaltung von C-C-Bindungen an diesen Katalysatoren zum allergrößten Teil durch Hydrogenolyse am Edelmetall erfolgt. Außerdem wurden die Ergebnisse der Umsetzung von Butylcyclohexan an den nicht sauren Katalysatoren mit denen an HIPEROcs verglichen. Es konnte die folgende Reaktionsfolge abgeleitet werden: Durch bifunktionelle Katalyse wird zunächst der Sechs- zu einem Fünfring isomerisiert. Anschließend erfolgt eine schnelle Öffnung des Fünfrings durch Hydrogenolyse am Edelmetall. An iridiumhaltigen HIPEROcs wird der Sechsring auch direkt durch Hydrogenolyse geöffnet. Da auch Platin selbst isomerisierungsaktiv ist, konnte an Pt/Silica eine ähnliche Reaktionsfolge beobachtet werden, jedoch mit einer geringeren Isomerisierungsaktivität als an zeolithischen Platinkatalysatoren.

An bifunktionellen Zeolithkatalysatoren mit Palladium als Edelmetall wurden in der Umsetzung von Butylcyclohexan und Perhydroindan vor allem Gerüstisomerisierungen katalysiert. Ringöffnungsprodukte wurden nur in geringen Mengen und bei hohen Temperaturen gebildet. Die Ringöffnung durch Hydrogenolyse an Palladium kann ausgeschlossen werden, da bei der Umsetzung von Perhydroindan an Pd/Silica nur sehr geringe Mengen an Ringöffnungsprodukten gebildet wurden. Dies zeigt, dass eine langsame Ringöffnung auch mittels bifunktionellen Hydrocrackens durch β -Spaltung von Carbokationen möglich ist.

Spiro[4.5]decan ist eines der Hauptprodukte in der Umsetzung von Decalin an HIPEROcs bei geringen Umsätzen. In der vorliegenden Arbeit wurde dieses Zwischenprodukt an HIPEROcs umgesetzt, und es wurde eine ähnliche Produktzusammensetzung wie bei der Umsetzung von Decalin erhalten. Dies zeigt, dass Spiro[4.5]decan höchstwahrscheinlich ein wichtiges Zwischenprodukt in der Umsetzung von Decalin ist.

2 Summary

In this work, the following two topics were covered: (i) What are the reactions and reaction paths that are catalyzed by noble metals, mainly iridium and platinum, in the hydroconversion of bicyclic naphthenes and their respective ring-opening products when Brønsted acid sites are absent? (ii) How are high yields of open-chain alkanes formed on high-performance ring-opening catalysts (HIPEROCS)?

For studies about pure metal catalysis it was required to identify a catalyst support that does not contain catalytically active Brønsted acid sites. In a test reaction, *viz.* the hydroconversion of n-octane on iridium- and platinum-loaded materials, it turned out that amorphous silica and the mesoporous silica modification [Si]SBA-15 show no contribution of catalysis on Brønsted acid sites. By FT-IR spectroscopy with pyridine as probe molecule it was also demonstrated that no Brønsted acid sites of sufficient strength for the protonation of pyridine are present on silica. Hence, for all experiments about pure metal catalysis silica was used as catalyst support, loaded with *ca.* 0.7 to 2.7 wt.-% of the respective noble metal by strong electrostatic adsorption of metal complex cations. Also [Si]SBA-15 was used as catalyst support for one series of comparative experiments. The catalytic results were similar to those obtained on the silica-supported catalysts.

In general the catalytic activity of the noble metals decreased in the order Ir > Rh > Pt > Pd, resulting in an increasing tendency of dehydrogenation to aromatics at the high reaction temperatures that are required. All metals were active in the *cis/trans*-isomerization of perhydroindan or decalin which preceded the other reactions, *viz.* hydrogenolysis, skeletal isomerization and dehydrogenation. Other feed hydrocarbons were n-decane, ethylcyclohexane, butylcyclohexane and methyldecalin.

Iridium was the best noble metal for purely metal-catalyzed ring opening, especially if naphthenes were converted that consist of two six-membered rings. For example, in the hydroconversion of *cis*-decalin a maximal yield of open-chain decanes of 22 % was obtained on 2.73Ir/silica at a reaction temperature of 310 °C and a hydrogen pressure of 8.0 MPa. Iridium was not active in skeletal isomerization and cleaved preferentially unsubstituted C-C bonds, *i.e.* primary-secondary and secondary-secondary bonds. One result of this regioselectivity was a high degree of branching in the open-chain alkanes with the same number of carbon atoms as the reactant that are formed by cleaving one C-C bond in each naphthenic ring. In the group of hydrocracked products mainly methane and C₉ products, smaller amounts of ethane and C₈ products and very small amounts of C₃ to C₇ hydrocarbons were formed in the

hydroconversion of decalin. Such a distribution, denoted as hammock-type curve, seems to be typical also for the hydroconversion of other bicyclic naphthenes like perhydroindan and methyldecalin on non-acidic iridium catalysts.

This type of distribution curve was simulated by assuming the following reaction sequence that was also deduced from the dependence of product selectivities on conversion: One ring in decalin is opened by hydrogenolysis under the formation of the three direct ring-opening products (direct ROPs) butylcyclohexane, 1-methyl-2-propylcyclohexane and 1,2-diethylcyclohexane. Subsequently, hydrogenolysis occurs either in the alkyl side-chains of direct ROPs (exocyclic hydrogenolysis), resulting in the formation of hydrocracked products (C_9 -), or in the six-membered ring (endocyclic hydrogenolysis) under the formation of seven constitutional decane isomers (direct open-chain decanes, direct OCDs). For the simulation it is assumed that also direct OCDs undergo complete hydrogenolysis under the formation of C_9 - products. To obtain a good agreement between the simulated and the experimentally obtained curve it turned out that the catalytic property of iridium to cleave preferentially unsubstituted C-C bonds is important.

Platinum was much less active in the hydrogenolysis of C-C bonds, especially of those that are part of a six-membered ring, in comparison to iridium. However, for the ring opening of five-membered rings, *e.g.* in perhydroindan, also platinum can be an appropriate type of noble metal. An examination of reaction paths on non-acidic Pt/silica catalysts was strongly hampered by its isomerization activity. For example, in the conversion of *cis*-decalin the main products at low conversion were the ring-opening product butylcyclohexane and the skeletal isomer spiro[4.5]decane. A preference of platinum to cleave preferentially the substituted C-C bonds in six-membered rings was observed with several reactants and can explain the butylcyclohexane formation from decalin. The high selectivity of the spiro compound can be rationalized by a purely metal-catalyzed isomerization *via* the bond-shift mechanism or via 1,5-dehydrocyclization of butylcyclohexane. OCD formation was negligible with a maximal yield of 2 % on 2.68Pt/silica.

It was not possible to calculate a simulated distribution curve of the hydrocracked products for the hydroconversion of *cis*-decalin on Pt/silica that correlates well with the one obtained in the catalytic experiment. However, an explanation for the formation of large amounts of C_1 and C_3 and high amounts of C_2 and C_4 was found by comparative experiments with butylcyclohexane which is the main ring-opening product of the decalin conversion on this catalyst. The high reaction temperatures that

are required to open the six-membered ring in decalin favor exocyclic hydrogenolysis in butylcyclohexane under the formation of mainly methane and propane.

Spiro[4.5]decane was more reactive on Pt/silica in comparison with decalin but at low conversions mainly decalin was formed by skeletal isomerization, presumably *via* the bond-shift mechanism. Similar yields of ring-opening products were obtained at comparable reaction temperatures in the conversion of decalin and spiro[4.5]decane. It was concluded that, with both reactants, at first a similar mixture of skeletal isomers is generated which undergoes a consecutive hydrogenolysis under the formation of ROPs. On Ir/silica a direct ring-opening mechanism occurred: The first reaction is a hydrogenolytic ring opening of the five-membered ring, followed by hydrogenolysis of the six-membered ring in the respective ring-opening products. Iridium cleaves with a strong preference the bisecondary C-C bonds and conserves the bonds between the quaternary and the neighbored carbon atoms.

Palladium was mainly active in dehydrogenation and of very low activity in hydrogenolysis. A particle size effect was observed with rhodium. On small rhodium particles with a metal dispersion of 0.57 only hydrogenolysis occurred in the hydroconversion of decalin whereas on larger particles with a dispersion of 0.17 also skeletal isomers were formed. Rhodium was less active than iridium, *ca.* 50 °C higher reaction temperatures had to be applied to obtain similar conversions, resulting in multiple hydrogenolysis under the formation of relatively large amounts of methane.

The influence of hydrogen pressure on metal catalysis was studied in the range of $p_{\text{H}_2} = 1.0$ to 8.0 MPa. In the reaction of perhydroindan on Pt/silica the conversion decreased monotonously with increasing hydrogen pressure. For obtaining high yields of open-chain nonanes, however, hydrogen pressures of 4.0 and 8.0 MPa were optimal. On Ir/silica in the conversion of cis-decalin the catalyst activity was maximal at $p_{\text{H}_2} = 4.0$ MPa but the highest yield of open-chain decanes was reached at $p_{\text{H}_2} = 8.0$ MPa. In both combinations of catalyst and reactant, at low hydrogen pressures up to 2.0 MPa dehydrogenation to aromatic hydrocarbons limited the ring-opening performance. On Ir/silica it seemed that the highest pressure of $p_{\text{H}_2} = 8.0$ MPa led to a reduced extent of hydrogenolysis in alkyl chains whereas the hydrogenolysis of endocyclic C-C bonds seemed to be not affected, resulting in a good ring-opening performance.

Catalytic experiments with a two-bed arrangement being comprised of a bifunctional isomerization catalyst Pd/Na,H-Y in the first bed and Pt/silica as hydrogenolysis catalyst in the second bed were conducted. In the hydroconversion of n-decane and

butylcyclohexane an intermediate catalytic behavior compared to the experiments with the single catalysts was observed. The expected hydrogenolysis of skeletal isomers on platinum, which were formed on the zeolite catalyst, was not observed. Hence, for such studies a better adjustment of the catalyst activities is required.

High-performance ring-opening catalysts (HIPEROs) are zeolitic, iridium- or platinum-containing catalysts with a small concentration of Brønsted acid sites. They were tested in the hydroconversion of n-decane, butylcyclohexane and spiro[4.5]decane. By a detailed examination of the product distribution it turned out that on these zeolitic iridium- or platinum-containing catalysts with a small concentration of Brønsted acid sites C-C bond cleavage occurs virtually only on the noble metal *via* hydrogenolysis. By comparing the results of butylcyclohexane conversion on the non-acidic catalysts with those on HIPEROs evidence for the following reaction sequence on HIPEROs was obtained: *Via* bifunctional catalysis the six-membered ring is isomerized into a five-membered ring. Subsequently, a fast opening of the five-membered ring occurs by hydrogenolysis on the noble metal. On iridium-containing HIPEROs the six-membered ring is in addition also opened directly by hydrogenolysis. On Pt/silica a similar reaction sequence was observed since skeletal isomerization occurs also on platinum by metal catalysis. However, on this non-acidic support the isomerization activity is much lower compared to catalysts that contain Brønsted acid sites.

Bifunctional zeolite catalysts with palladium as noble metal component were mainly isomerization active in the hydroconversion of butylcyclohexane and perhydroindan. Small amounts of ring-opening products were formed on these catalysts at relatively high reaction temperatures. This demonstrates that ring opening is, to a small extent, also possible by bifunctional hydrocracking *via* β -scission of carbocations. Ring opening by hydrogenolysis can be ruled out since in the hydroconversion of perhydroindan on Pd/silica almost no ring opening occurred.

Spiro[4.5]decane is an important product in the hydroconversion of decalin on HIPEROs at low conversions. Therefore, spiro[4.5]decane was also converted on these catalysts and a similar product mixture was obtained as in the decalin conversion. This indicates that spiro[4.5]decane could indeed be an important intermediate on these catalysts.

3 Introduction and Objectives

An increasing production rate of liquid fuels from unconventional resources of fossil fuel, *e.g.* from oil sands or extra-heavy crude oils, is expected for the next decades [1]. Due to the low n_H/n_C ratio of the contained compounds an increased fraction of polycyclic aromatics is found in different refinery streams. In diesel fuel, polycyclic aromatics have several undesired properties. These are low cetane numbers, high propensity for soot formation, unfavorable cold-flow properties and a high specific carbon dioxide emission. This led the EU legislative to reduce the maximum allowed content of polycyclic aromatics to 8 wt.-% [2] and even a further reduction is under discussion. It seems, the most attractive route for the upgrading of refinery streams which contain such compounds is their hydrogenation to polycyclic naphthenes, which is a state-of-the-art technology, and further their selective ring opening under retention of the number of carbon atoms [3].

For a long time the hydrogenolysis of carbon-carbon bonds in hydrocarbons was an undesired side reaction in the hydroconversion of refinery streams. In hydrocrackers the cleavage of C-C bonds is realized by bifunctional hydrocracking, *inter alia*, since this type of reaction does not require very high temperatures and only very small amounts of the low-value products methane and ethane are formed. However, for the ring opening of naphthenes typical bifunctional catalysis turned out to be inappropriate. The reason is an unfavorable orbital overlap in the cyclic carbocation, resulting in a slow β -scission of such C-C bonds which are part of a naphthenic ring [3].

If the ring is opened on a noble metal by hydrogenolysis and not by bifunctional catalysis *via* carbocations, the limitation that was mentioned above does not apply. However, hydrogenated polycyclic aromatics, *i.e.* polycyclic naphthenes, are composed mainly of six-membered rings. For the opening of those by hydrogenolysis relatively high reaction temperatures are required, whereas the five-membered ones are readily opened by hydrogenolysis on noble metals like iridium or platinum [4]. Hence, an isomerization function is required for the transformation of six-membered rings into five-membered rings. Recently it was demonstrated with decalin as model hydrocarbon that the combination of a mild isomerization function and a noble metal that is active in hydrogenolysis on the same catalyst can result in high-performance ring-opening catalysts (HIPEROCS) [5].

Due to the supposed important role of hydrogenolysis in the ring opening reaction a better knowledge of purely metal-catalyzed reactions of naphthenes on non-acidic

noble metal catalysts is required. A literature study revealed that very little is known about the hydrogenolytic mechanisms and product distributions in the hydroconversion of polycyclic naphthenes. Most studies about hydrogenolysis deal with monocyclic naphthenes with no more than eight carbon atoms. However, for an understanding of the hydrogenolytic reaction paths of hydrocarbons in the boiling point range of diesel fuel, naphthenes with at least nine carbon atoms have to be used.

In this work mainly naphthenic hydrocarbons with up to eleven carbon atoms were studied in the hydroconversion on non-acidic supported noble metal catalysts. Moreover, a very important question to be answered is: Does the ring opening on HIPEROs occur on the noble metal by hydrogenolysis or by bifunctional hydrocracking? Hence, also HIPEROs were tested in the hydroconversion of important intermediate products that are observed in the ring opening of decalin, *viz.* n-decane, butylcyclohexane and spiro[4.5]decane. These studies allowed an insight in the reaction networks on such catalysts.

4 Literature Review

4.1 Preparation of Noble-Metal-Containing Catalysts

4.1.1 Monofunctional Metal Catalysts

In order to prepare a well-dispersed metal phase, a catalyst support with a high specific surface area is required. Moreover, for studies about pure metal catalysis it is essential to prepare catalysts which contain no catalytically active Brønsted acid sites. Hence, aluminum-containing zeolites are inappropriate for this purpose due to the formation of Brønsted acid sites during reduction of the noble-metal-loaded zeolite with hydrogen (see Eqs. (4.2) and (4.3), page 14).

Widely used non-zeolitic support materials are the inorganic oxides γ -alumina and amorphous silica which are utilized for the catalytic hydroconversion of hydrocarbons after loading with noble metals. For the present study a chlorine-free type of γ -alumina has to be chosen, whereas in the refinery process of catalytic reforming, γ -alumina is typically made acidic by incorporation of chlorine [6]. Also metal-loaded titania and carbon black are frequently used as catalysts. However, on titania so-called strong metal-support interactions can alter the catalytic properties of the metal strongly [7], *e.g.* titania can migrate onto the metal clusters and block catalytically active sites. On carbon black the surface chemistry is rather complex and depends strongly on the preparation methods and pretreatment conditions [8].

Commercially available amorphous silica is a highly porous material with specific surface areas of up to $380 \text{ m}^2 \cdot \text{g}^{-1}$ [9]. Other modifications of highly porous silicon dioxide are ordered mesoporous materials like [Si]SBA-15 [10] or [Si]MCM-41 [11] with specific surface areas around $1000 \text{ m}^2 \cdot \text{g}^{-1}$.

Besides the incorporation of a metal during the synthesis of the support, several methods for the loading of a support material with a metal component are known. Most convenient is the impregnation with a solution of a metal salt. There are principally two different types of impregnation [12]: During capillary or incipient wetness impregnation the dry support is contacted with that volume of a solution of a metal salt that equals the volume of the pores in the support. Afterwards the material looks dry. A high pressure that can build up inside the pore space when the solution is adsorbed can result in a destruction of the pore system. Diffusional or wet impregnation is conducted, for example, when the metal salt is of low solubility. In

this method, the support, in which the pores are filled with the solvent, usually water, is contacted with a solution of a metal salt. Obviously, the latter method requires more time depending on the diffusion properties. After drying of the loaded catalyst precursors, they are usually oxidized with air prior to the reduction with hydrogen. However, disadvantages of impregnation can be a rather low metal dispersion [13].

For reaching high metal dispersions, ion exchange with metal salts on materials which possess surface charges is the preferred method. Such materials can be natural ion exchangers like aluminum-containing zeolites (see Section 4.1.2). Alternatively, surface charges can be generated by acid-base reactions with the hydroxyl groups on amphoteric oxides [12]. In the following the later method is described which is often referred to as strong electrostatic adsorption (SEA).

When a material is covered with water, that pH value at which most of the surface hydroxyl groups are uncharged is defined as point of zero charge (PZC). In Figure 4.1 the protonation and deprotonation of surface hydroxyl groups at $\text{pH} < \text{PZC}$ and $\text{pH} > \text{PZC}$, respectively, is illustrated. A positive surface charge leads to a favored adsorption of an anionic metal complex like $[\text{PtCl}_6]^{2-}$ and a negative charge favors the adsorption of a cationic metal complex like $[\text{Pt}(\text{NH}_3)_4]^{2+}$.

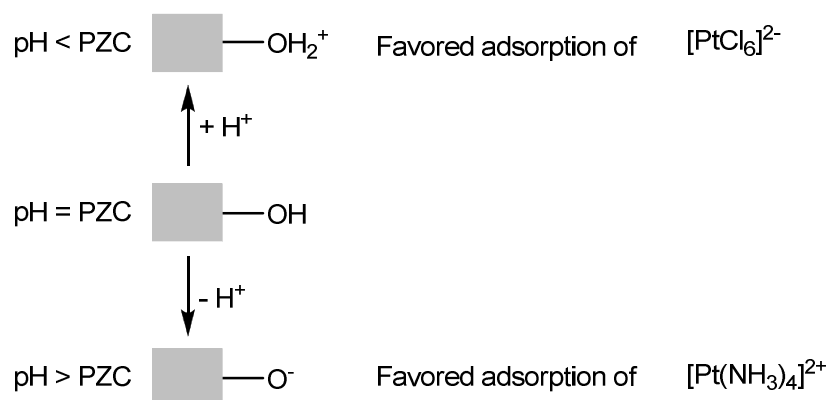


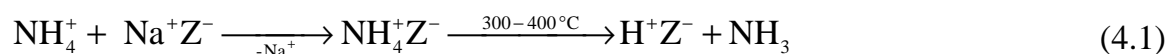
Figure 4.1: Strong electrostatic adsorption of platinum complexes on hydroxyl groups in dependence on the pH and point of zero charge (PZC). After Ref. [14].

In several publications [13-15] it was demonstrated that the SEA of complexes like $[\text{Pd}(\text{NH}_3)_4]\text{Cl}_2$ or $[\text{Pt}(\text{NH}_3)_4]\text{Cl}_2$ on amorphous silica and mesoporous $[\text{Si}]\text{SBA-15}$ results in the formation of highly dispersed metal particles. At first, the material is suspended in water, and the addition of an ammonium hydroxide solution until $\text{pH} \approx 10$ deprotonates most of the surface silanol groups, due to a $\text{PZC} \approx 4$. When the pH of the suspension remains constant, an aqueous solution of $[\text{Pt}(\text{NH}_3)_4]\text{Cl}_2$ is added. Due

to a strong Coulomb interaction, the complex is well adsorbed on the deprotonated silanol groups and remains adsorbed even after filtration and washing with water. Moreover, with $[\text{Pt}(\text{NH}_3)_4]\text{Cl}_2$ on amorphous silica it was demonstrated that an oxidative treatment of the dried catalyst precursor at 100 to 150 °C prior to reduction is crucial for a good dispersion value of 1.00 [13]. At these temperatures platinum remains in an oxidation state of +2, while higher oxidation temperatures generate Pt^{4+} species which are believed to be responsible for the formation of larger metal particles after reduction.

4.1.2 Bifunctional Zeolite Catalysts

There are essentially two possibilities for the preparation of bifunctional zeolitic catalysts, *i.e.* catalysts that contain a noble metal and Brønsted acid sites as catalytically active components [16]. One method is the loading of a metal on a zeolite that contains Brønsted acid sites already. The most common method for the generation of Brønsted acid sites in a zeolite is the ion exchange with an ammonium salt and subsequent calcination. At temperatures of 300 to 400 °C all ammonium ions are decomposed into ammonia and protons in the zeolite, see Eq. (4.1). Z^- is the negatively charged zeolite framework in the vicinity of framework aluminum atoms.



The second method is the formation of Brønsted acid sites during the reduction of a zeolite that was ion-exchanged with a metal complex cation and calcined:



Also a sequential ion exchange with ammonium and metal complex ions followed by one calcination step and one reduction step allows the formation of bifunctional zeolite catalysts.

4.2 Catalytic Reactions of Saturated Hydrocarbons in the Presence of Hydrogen

4.2.1 Reactions on Monofunctional Noble Metal Catalysts

As introduced in Section 4.1.1, monofunctional noble metal catalysts possess a metal function only. Most important is the absence of Brønsted acid sites, otherwise an examination of metal-catalyzed reaction mechanisms is not possible due to simultaneously occurring bifunctional reaction mechanisms, see Section 4.2.2. In hydrocarbon chemistry, the knowledge about catalysis on metal clusters is much less developed than the relatively well-understood carbocation chemistry on catalysts with Brønsted acid sites [17].

A simplified reaction network of the most important reactions that can occur in the hydroconversion of n-hexane on noble metal catalysts is shown in Figure 4.2 [18]. In the following Sections these different types of metal-catalyzed reactions will be described.

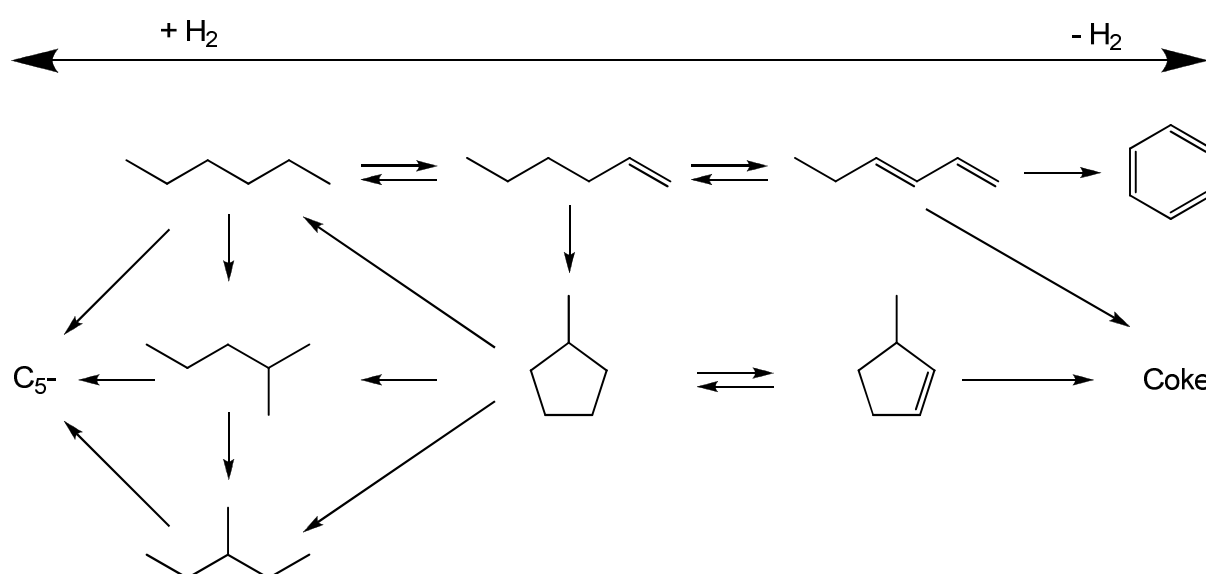


Figure 4.2: Simplified reaction network of the possible reactions of n-hexane on noble metal catalysts. C₅-: hydrocarbons with five or less carbon atoms. From Ref. [18].

4.2.1.1 Dehydrocyclization and Dehydrogenation

When a hydrocarbon undergoes dehydrocyclization, a cyclic structure or substructure of the carbon chain is formed under co-production of hydrogen. Generally,

dehydrocyclization and dehydrogenation of a hydrocarbon are endothermic reactions [19] and, consequently, their formation is facilitated by high temperatures. In the dehydrocyclization of hydrocarbons, olefinic structures are thought to be intermediates. As shown in Figure 4.2, the formation of methylcyclopentane from n-hexane, *e.g.*, is possibly preceded by an intermediate formation of 1-hexene [18].

Both, dehydrocyclization and aromatization occur in an important refinery process, *i.e.*, catalytic reforming. Due to Le Chatelier's principle the process is conducted at relatively low hydrogen pressures of 0.3 to 3.5 MPa [6, 20]. Since platinum is the best metal for these types of reactions, a platinum-containing catalyst supported on chlorinated alumina is typically used for this process [6].

Despite the extensive research in this field, the reaction path for the formation of an aromatic molecule like benzene from n-hexane on non-acidic platinum catalysts is still not sufficiently understood. As shown in Figure 4.2, intermediates in the benzene formation could be mono- and diolefins [18]. Other authors assume that at first cyclohexane is formed by dehydrocyclization, followed by dehydrogenation to benzene [21]. Cyclohexane, in turn, can be formed from hexane by direct 1,6-dehydrocyclization and also by 1,5-dehydrocyclization to methylcyclopentane and subsequent isomerization to cyclohexane [22]. Depending on the reactant and reaction conditions, the relative contributions of the different reaction paths can vary. When the extent of aromatization is lowered by applying a hydrogen pressure of at least 0.5 MPa, also direct 1,6-dehydrocyclization of n-octane, mainly to 1,2-dimethylcyclohexane can occur [23].

4.2.1.2 Skeletal Isomerization of Hydrocarbons

For the metal-catalyzed skeletal isomerization of alkanes two mechanisms are well-established: (i) the bond-shift mechanism *via* cyclopropanoid species [24, 25] and (ii) the cyclic mechanism *via* substituted cyclopentanes [22, 26].

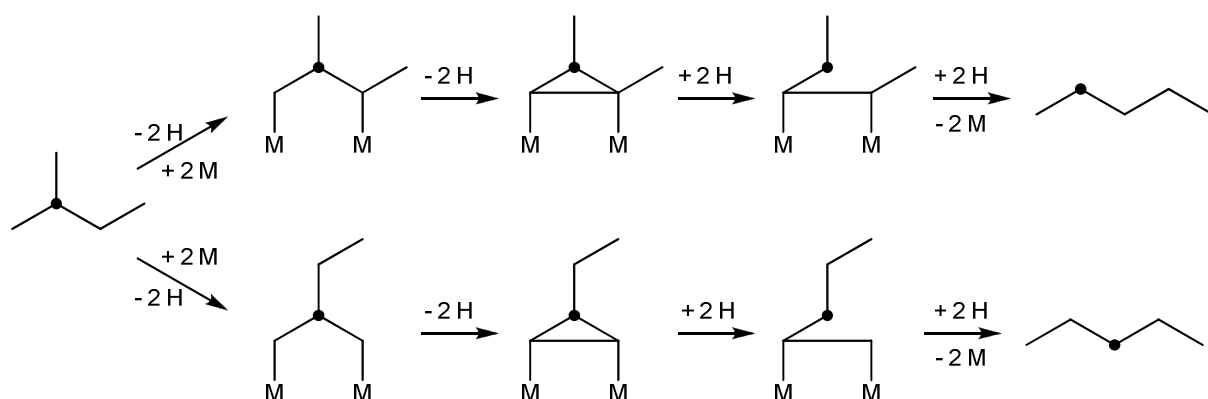


Figure 4.3: Skeletal isomerization of 2-methylbutane-2-¹³C according to the bond-shift mechanism *via* cyclopropanoid species. After Ref. [27, 28].

In the hydroconversion of 2-methylbutane-2-¹³C on a Pt/ γ -alumina catalyst hints for the bond-shift mechanism were found [27]. Most likely it proceeds *via* adsorbed cyclopropanoid species as shown in in Figure 4.3, which are re-opened at a C-C bond in the three-membered ring other than the new one formed. An alternative description of the bond-shift mechanism proceeds *via* metallacyclobutane species [22] (see Figure 4.4). There, the cleavage of a metal-carbon and a carbon-carbon bond in the metallacyclobutane substructure leads to a metal-carbene complex with a π -adsorbed allylic species. A rotation of the π -adsorbed allylic intermediate, followed by reformation of a metallacyclobutane species and subsequent desorption under hydrogenation of the metal-carbon bonds furnishes 2-methylbutane-3-¹³C as skeletal isomer.

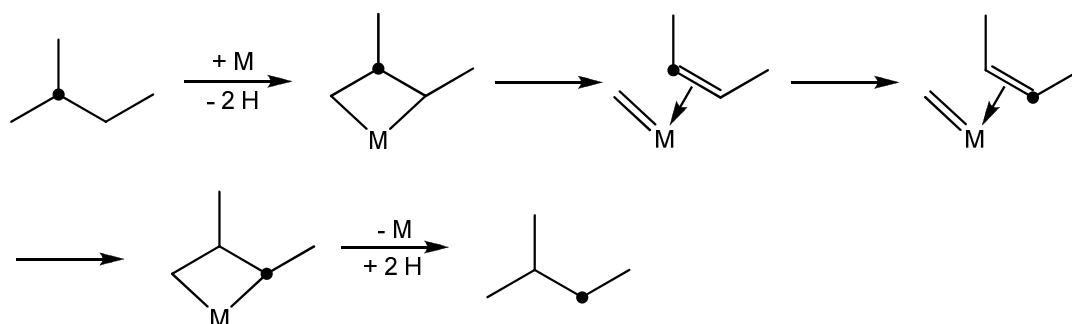


Figure 4.4: Skeletal isomerization of 2-methylbutane-2-¹³C *via* the bond-shift mechanism and metallacyclobutane species. From Ref. [22].

In the cyclic mechanism [26, 29] the first step is a 1,5-dehydrocyclization of the alkane to substituted cyclopentanes. Subsequently, the five-membered ring is opened at a position other than the new one formed, furnishing a skeletal isomer of the original alkane.

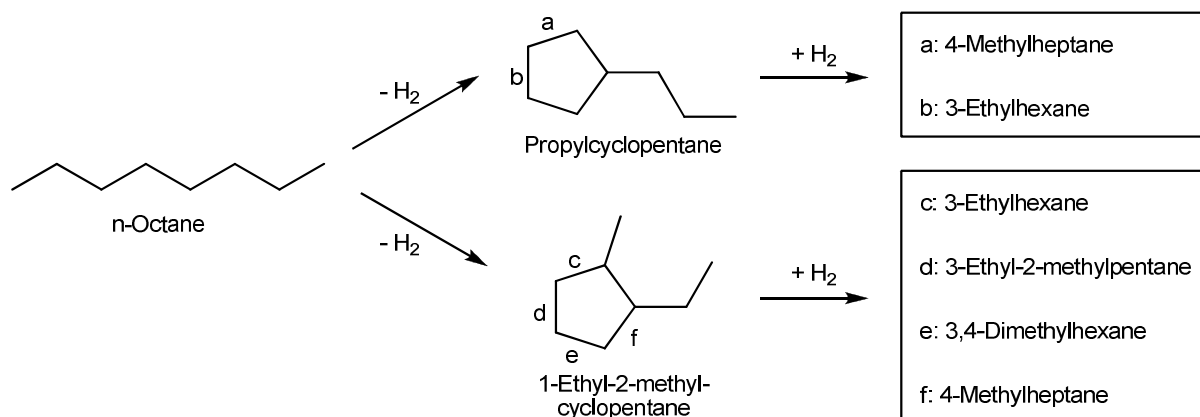


Figure 4.5: Isomerization of n-octane *via* the cyclic mechanism on 2.0Pt/alumina. After Ref. [23].

For example, in the hydroconversion of n-octane on 2.0Pt/alumina [23], propylcyclopentane and 1-ethyl-2-methylcyclopentane were the major C₈ naphthenes formed, see Figure 4.5. All open-chain octanes that can be formed by the cleavage of C-C bonds in the five-membered rings occurred (see Figure 4.5). An increase of the hydrogen pressure from 0.5 to 2.0 MPa leads to a favored formation of skeletal isomers that can be formed by the bond-shift mechanism only (2-methylheptane and 3-methylheptane). Although 1,6-dehydrocyclization, mainly to 1,2-dimethylcyclohexane occurred, the products indicative of a ring-opening of the six-membered ring were absent. This finding can easily be explained by the slow ring opening of six-membered rings on platinum (see Section 4.2.1.4). In the isomerization of 2-methylpentane on Pt/γ-alumina, it was found that a low metal dispersion leads to a higher contribution of the cyclic mechanism whereas at a high metal dispersion the bond-shift mechanism is favored [29].

4.2.1.3 Hydrogenolysis of Alkanes

From the product distribution of alkane hydrogenolysis on noble metals different mechanisms have been suggested. On platinum catalysts the cleavage of C-C bonds in an α,β-position related to a tertiary carbon atom is favored [22]. To account for this catalytic behavior, the Anderson-Avery mechanism [30], shown in Figure 4.6 exemplarily for 2-methylpentane, was proposed. Its first reaction step is the adsorption of the hydrocarbon on two metal atoms under formation of a 1,1,3-triadsorbed species. Subsequently, in this species the C-C bond between C₁ and C₂ is cleaved and a π-adsorbed olefinic species and a carbyne species are formed. Hydrogenation and desorption of the hydrocarbons results in the formation of two hydrocarbons.

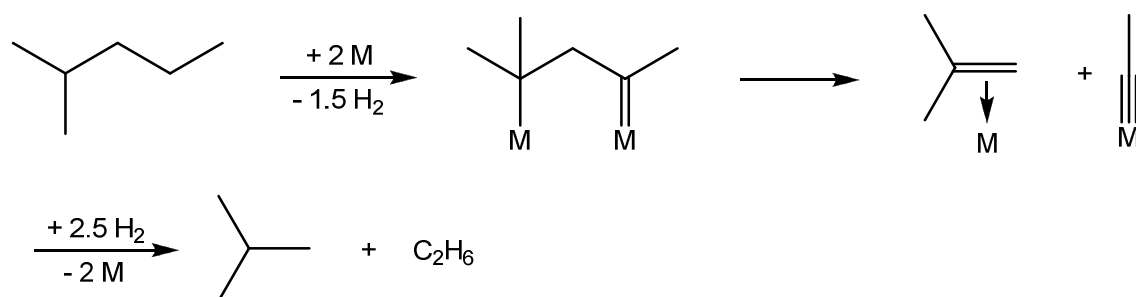


Figure 4.6: Hydrogenolysis of 2-methylpentane according to the Anderson-Avery mechanism. After Ref. [22].

On iridium, hydrogenolysis of alkanes occurs mainly between primary-secondary and secondary-secondary C-C bonds. Gault [22] interprets this regioselectivity with a mechanism involving a 1,2-dicarbene species, see Figure 4.7. A cleavage of the C-C bond between both adsorbed carbon atoms yields two carbyne species which form two alkanes after hydrogenation and desorption.

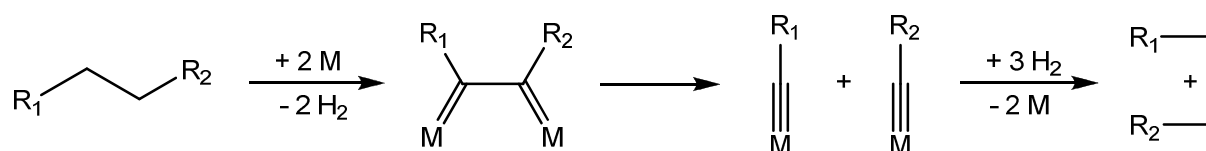


Figure 4.7: Hydrogenolysis of an alkane *via* a 1,2-dicarbene species. R₁, R₂: hydrogen or hydrocarbon substituents. After Ref. [22].

A quantitative distribution of the hydrocracked products obtained in the hydroconversion of n-heptane on unsupported metal catalysts is presented in Figure 4.8. Two types of curve shapes can be found: (i) On palladium and rhodium hydrogenolysis occurs with a high regioselectivity at the primary-secondary C-C bonds, generating mainly methane and C₆ hydrocarbons. (ii) On iridium, platinum and ruthenium cleavage of C-C bonds occurs with a rather equal probability for all bonds, as indicated by the almost horizontal curve shape. However, as the metal particle size can have a strong influence on the reaction mechanisms, these results with very big metal particles can only be compared to a limited extent with results obtained on supported metal catalysts with a high metal dispersion.

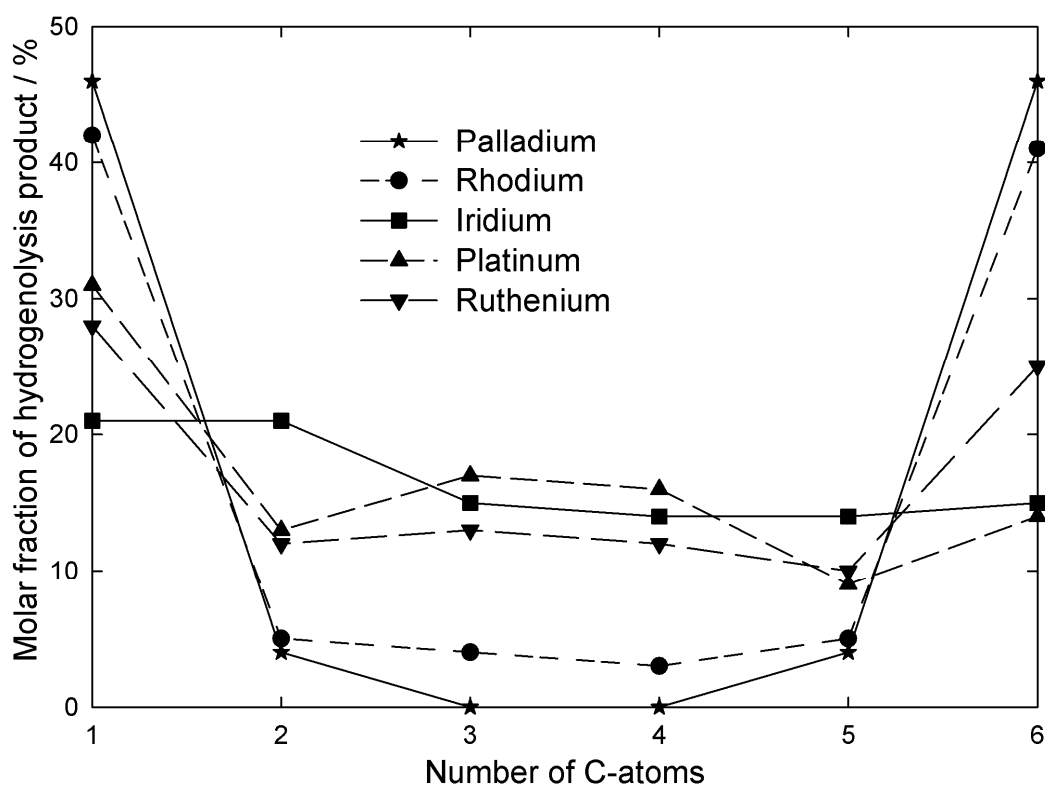


Figure 4.8: Distribution of the hydrocracked products in the catalytic hydroconversion of n-heptane on unsupported metal particles. Data from Ref. [31].

On hydrogenolysis catalysts like 0.3Pt/ γ -alumina, the hydrogen pressure at which a maximal hydrogenolysis reaction rate of n-alkanes is observed depends strongly on the chain length of the hydrocarbon. An increase of the chain length from ethane to propane to n-butane shifts the maximal rate to higher hydrogen pressures from *ca.* 0.02 to *ca.* 0.05 to *ca.* 0.1 MPa [32] as shown in Figure 4.9. Garin and Gault [27] found a negative reaction order with respect to hydrogen in the hydrogenolysis of n- and iso-pentane on Pt/alumina at hydrogen pressures up to $p_{\text{H}_2} = 0.16$ MPa. A decreasing conversion with increasing hydrogen pressure from 0.5 to 2.0 MPa was observed in the hydroconversion of n-octane on 2.0Pt/alumina [23]. These results suggest that the maximum of the reaction rate with n-octane as reactant could be located at $p_{\text{H}_2} \leq 2.0$ MPa. However, the higher number of carbon atoms in n-octane allows more different types of reaction, *e.g.* dehydrocyclization and aromatization, to occur simultaneously. Since the selectivity or yield of hydrogenolysis products at the different pressures were not given, the influence of the hydrogen pressure on the hydrogenolysis cannot be estimated. No reports are available concerning the hydrogenolysis of hydrocarbons with more than eight carbon atoms at varying hydrogen pressures on non-acidic noble metal catalysts.

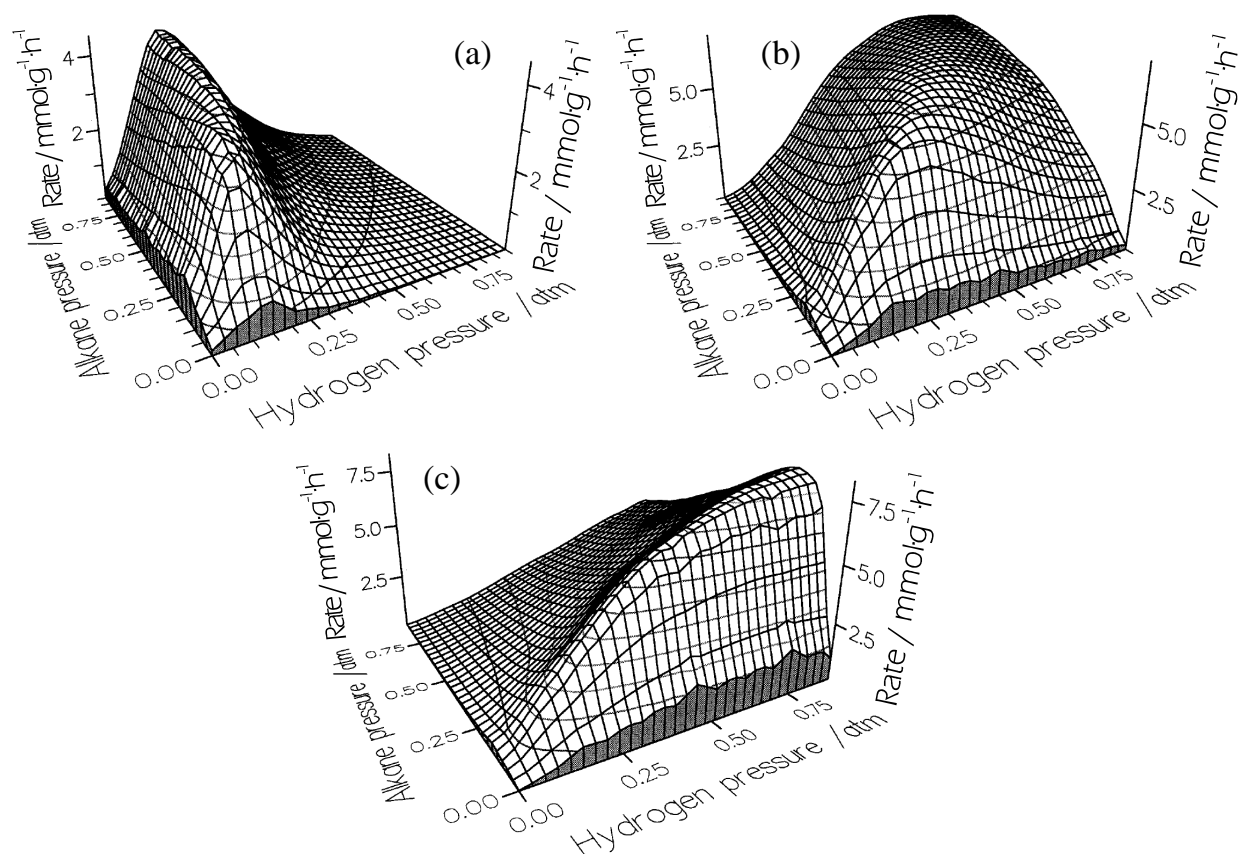


Figure 4.9: Influence of the partial pressures of the respective alkane and of hydrogen on the reaction rates in the hydrogenolysis of (a) ethane, (b) propane and (c) n-butane on 0.3Pt/ γ -alumina. After Ref. [32].

4.2.1.4 Hydrogenolysis of Naphthenes

In today's literature the nomenclature proposed by Maire *et al.* [33] concerning the various hydrogenolysis mechanisms for the hydrodecyclization of naphthenes is mostly adopted. There are three basic mechanisms for metal-catalyzed ring opening which have been discussed in detail by Gault [22]: In the so-called non-selective mechanism, the likelihood of all endocyclic carbon-carbon bonds for cleavage is considered to be equal. By contrast, the salient feature of the selective mechanism is that bonds between two secondary carbon atoms are broken exclusively. Finally, the partially selective mechanism envisages a rupture of endocyclic carbon-carbon bonds substituted by at least one methyl group.

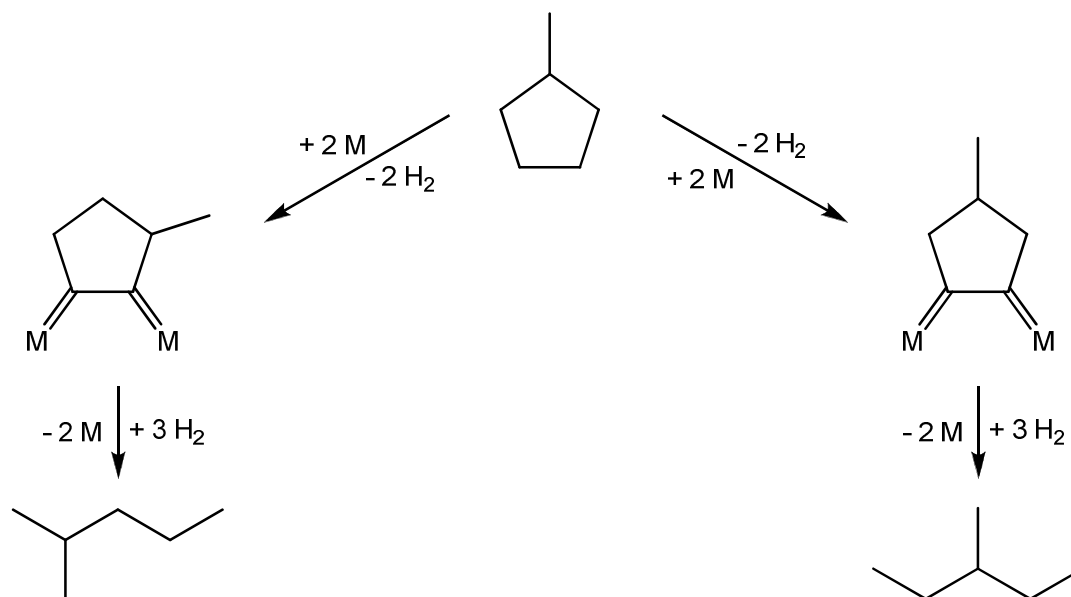


Figure 4.10: Selective hydrogenolysis of methylcyclopentane on iridium or platinum of low dispersion *via* the dicarbene mechanism. After Ref. [22].

When converting methylcyclopentane on non-acidic catalysts with iridium, nickel, rhodium or ruthenium as metal, the ring is opened with a high selectivity at bissecondary positions [4]. The high regioselectivity for the cleavage of bissecondary C-C bonds is explained by the intermediate formation of dicarbenes. As shown in Figure 4.10 for methylcyclopentane as reactant, the main products are 2-methylpentane and 3-methylpentane. Also platinum of low dispersion catalyzes a selective ring opening of methylcyclopentane [33].

In contrast, when platinum is highly dispersed, a non-selective ring opening occurs [33]. Intermediates in the non-selective or multiplet mechanism are probably unsaturated species that are π -adsorbed on the metal. In the conversion of methylcyclopentane, dehydrogenation can occur in every endocyclic C-C bond (see Figure 4.11). For the ring opening of such an adsorbed olefin to the corresponding open-chain alkane no generally accepted mechanistic step is available in the present literature.

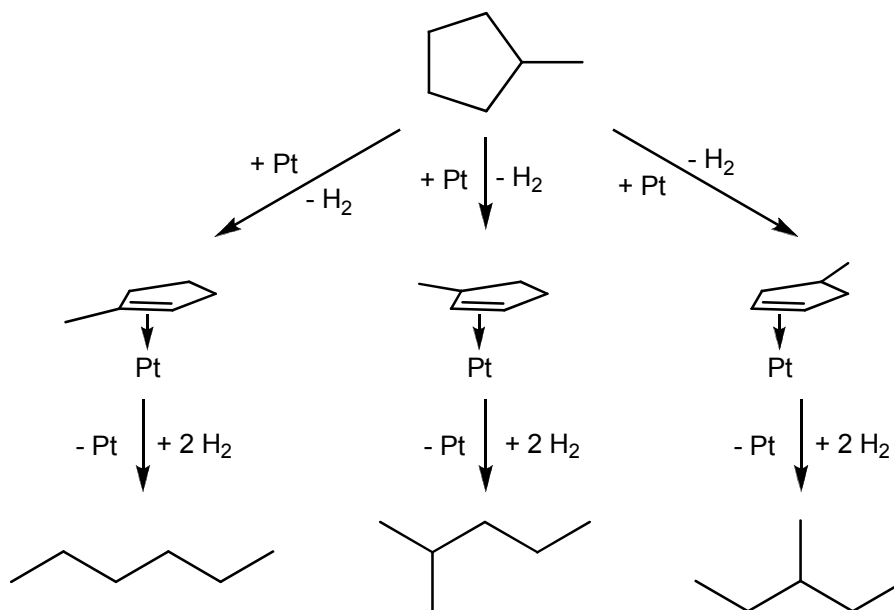


Figure 4.11: Non-selective hydrogenolysis of methylcyclopentane on highly dispersed platinum *via* the multiplet mechanism. After Ref. [22].

At increased reaction temperatures, Maire *et al.* [33] found a relatively high selectivity of n-hexane in the hydroconversion of methylcyclopentane on non-acidic 10Pt/ γ -alumina with a low metal dispersion. The authors explained this specific behavior with the occurrence of a third mechanism, called partially selective mechanism. Ring opening *via* the partially selective mechanism occurs most probably *via* metallacyclobutane intermediates, as shown in Figure 4.12 for the ring opening of methylcyclopentane. Accordingly, this intermediate is re-opened to a species containing a carbenoid and a π -adsorbed olefinic entity, and further to a diolefinic intermediate that forms n-hexane after hydrogenation and desorption.

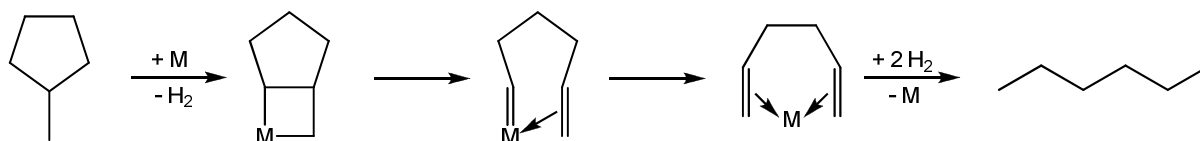


Figure 4.12: Partially selective hydrogenolysis of methylcyclopentane on iridium or low dispersed platinum *via* metallacyclobutane. After Ref. [22].

On non-acidic rhodium catalysts at high metal dispersions [34-36] or high reaction temperatures [37] also n-hexane was detected as ring-opening product in the hydroconversion of methylcyclopentane. Hence, under these conditions also the non-selective or partially selective mechanism can contribute on rhodium.

Five-membered rings are easy to open on non-acidic noble metal catalysts without forming hydrocarbons with a smaller number of carbon atoms. Also six-membered

rings can be opened on this type of catalyst but lower yields and high amounts of by-products were observed. The faster cleavage of C-C bonds that are part of a five-membered ring is usually interpreted in terms of a higher ring strain in five-membered compared to six-membered rings [4, 38] In several publications it was demonstrated that iridium is the most active and selective metal for the ring opening of naphthenes on non-acidic supports [4, 39].

In the hydroconversion of methylcyclohexane (see Figure 4.13) on non-acidic noble metal catalysts, three products of a direct ring opening can be obtained. In Table 4.1 the product distributions on iridium-, nickel-, palladium- or platinum-containing catalysts are shown [4]. There, the experimental results are opposed to the product distributions that are expected theoretically by applying the three different hydrogenolysis mechanisms for the ring opening of naphthenes. On platinum neither one mechanism nor a linear combination of the three mechanisms can explain the product distribution with a preference for the substituted bond a and the bisecundary bond b without cleaving bond c. Both, the iridium and the nickel catalyst open the ring essentially according to the selective mechanism while on ruthenium several mechanisms occur simultaneously.

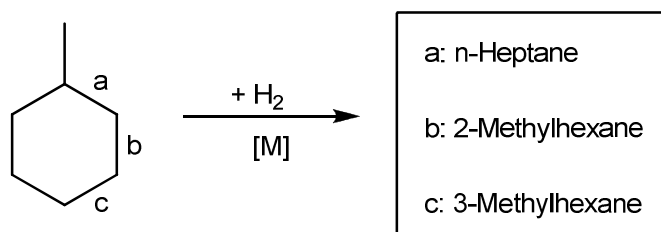


Figure 4.13: Methylcyclohexane and products of a hydrogenolytic ring opening.

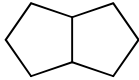
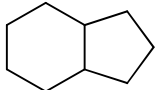
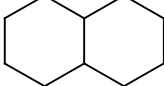
Table 4.1: Ring-opening products in the hydrogenolysis of methylcyclohexane [4].

Catalyst	Distribution of ring-opening products in the experiments		
	a: n-Heptane	b: 2-Methylhexane	c: 3-Methylhexane
0.6Pt/silica	65	35	traces
15Ni/ γ -alumina	4	48	48
0.9Ir/ γ -alumina	5	37	58
1.5Ru/silica	13	38	49

Mechanism	Theoretical product distribution		
Non-selective	33	33	33
Selective	0	50	50
Partially selective	100	0	0

Publications about the ring opening of multi-ring naphthenes on monofunctional metal catalysts are scarce. McVicker *et al.* [4] tested three bicyclic naphthenes in the hydroconversion on a 0.9Ir/ γ -alumina catalyst, see Table 4.2. In bicyclo[3.3.0]octane, the ring opening of both five-membered rings to open-chain alkanes was relatively fast. When a bicyclic naphthene composed of a five-membered and a six-membered ring, *i.e.* perhydroindan (or bicyclo[4.3.0]nonane), was converted, higher reaction temperatures were applied but a lower conversion was reached. Moreover, the five-membered ring was opened relatively fast but only traces of open-chain alkanes were detected, indicating that the six-membered ring can hardly be opened. In decalin which is composed of two six-membered rings the conversion was very low, the endocyclic hydrogenolysis of one naphthenic ring was very slow and open-chain alkanes were found only in traces at the reaction conditions given.

Table 4.2: Hydrogenolysis of bicyclic naphthenes on 0.9Ir/ γ -alumina [4].

Reactant	Temperature / °C	Conversion / %	Yield / %	
			One-ring naphthenes	Open-chain alkanes
Bicyclo[3.3.0]octane 	225	81	60	21
Perhydroindan 	275	68	56	traces
Decalin 	275	4	4	traces

In another work [40] indan was converted on 1.56Ir,0.08Pt/ceria at a total pressure of 4.0 MPa. Prior to endocyclic C-C bond cleavage complete hydrogenation to perhydroindan occurred. In spite of the high iridium content only mono-alkylated cyclohexanes like propylcyclohexane were formed whereas dialkylated cyclohexanes were absent in the product mixture. No interpretation of this regioselectivity that cannot be explained by the selective ring-opening mechanism on iridium was given by the authors. A maximal yield of ring-opening products of 47 % was reported at $T_r = 325$ °C which included, however, significant amounts of cracking products of n-tetradecane since a mixture of indan and n-tetradecane was used as feed.

For iridium catalysts it is also characteristic that with an increasing number of substituents and when converting a six-membered instead of a five-membered ring, higher reaction temperatures have to be applied. Moreover, at least two ring-opening mechanisms occur simultaneously [4, 41-43]. Do *et al.* [43] explained the variance of the different modes of ring opening by comparing their activation energies. Since a reaction uses the path of minimal activation energy this should be the selective mechanism. However, in the case that this low-energy path is blocked, another mechanism with higher activation energy is followed, *i.e.* the partially selective mechanism *via* a metallacyclobutane intermediate.

Exemplarily, the distribution of the ring-opening products obtained on 0.9Ir/ γ -alumina in the hydroconversion of 1,2,4-trimethylcyclohexane is shown in Figure 4.14 [4]. Due to the limited separation of the products in the capillary gas chromatograph, it was not possible to differentiate between the formation of 2,5- and 3,5-dimethylheptane.

Surprisingly, no selective hydrogenolysis of the bissecondary bond e occurred as expected by the selective mechanism. Moreover, the two secondary-tertiary bonds c and d are not cleaved, whereas a cleavage of the two secondary-tertiary bonds b or f occurred. Even a cleavage of the highly substituted tertiary-tertiary bond a was observed. Two reasons could account for this regioselectivity: (i) A preference for cleaving bonds that can be adsorbed easily due to sterical reasons, since several diastereomers of 1,2,4-trimethylcyclohexane are possible. Such an influence of the stereochemical configuration on the reactivity was found with the cis- and trans-isomers of 1,2- and 1,3-dimethylcyclohexane on non-acidic iridium catalysts [43]. (ii) The formation of a metallacyclopentane intermediate could explain the cleavage of the highly substituted bond a. Such an intermediate was assumed to be responsible for the cleavage of the quaternary-quaternary C-C bond in 2,2,3,3-tetramethylbutane under the formation of iso-butane on a ruthenium catalyst [44].

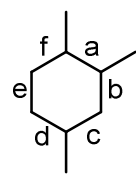
		Distribution of ring-opening products / %	
		Observed	Selective mechanism
	a	19	0
	b/f	44	0
	c	0	0
	d	0	0
	e	37	100

Figure 4.14: Endocyclic hydrogenolysis of 1,2,4-trimethylcyclohexane on 0.9Ir/ γ -alumina. After Ref. [4].

With an increasing length of the alkyl side-chain in a naphthene, the selectivity of products that are formed by exocyclic hydrogenolysis increases [4]. For example, in the hydroconversion of methylcyclohexane compared to butylcyclohexane on 0.9Ir/ γ -alumina at $T_r = 275$ °C the selectivity of ring-opening products drops from 87

to 35 % while the selectivity of products with less carbon atoms than the reactant increases.

Only one study about the influence of the hydrogen pressure on the ring opening of cyclic hydrocarbons with a ring size larger than four-membered rings on non-acidic metal catalysts was found. There, cyclohexane and methylcyclohexane are hydroconverted on 0.54Ir/ γ -alumina at $p_{\text{H}_2} = 0.1$ to 1.7 MPa [45]. In the cyclohexane hydroconversion at $T_r = 280$ °C and conversions below 10 % a maximal rate of the n-hexane formation is observed at $p_{\text{H}_2} = 0.3$ MPa for catalysts with metal dispersions of 0.30 and 0.46. In the methylcyclohexane conversion on 0.54Ir/ γ -alumina with a metal dispersion of 0.30 the rate of ring opening to heptane isomers is not influenced by the hydrogen pressure. However, the rate of demethylation, *i.e.* of cyclohexane formation, decreases strongly with increasing hydrogen pressure. On a similar catalyst with an iridium dispersion of 0.58 both reaction rates decrease with increasing hydrogen pressure.

One approach to reach higher selectivities of ring-opening products in the hydroconversion of naphthenes with a six-membered ring is the combination of (i) an isomerization catalyst for the ring contraction to five-membered rings and (ii) a hydrogenolysis catalyst for the hydrogenolytic ring opening. More details will be given in Section 4.2.3.

As conclusion, studies that examine purely metal-catalyzed hydrogenolytic ring-opening mechanisms of bicyclic naphthenes are lacking. Also the influence of the hydrogen pressure on the hydrogenolysis of such reactants is unknown.

4.2.2 Reactions on Bifunctional Catalysts

On bifunctional catalysts the two following catalytic functions co-exist: (i) A noble metal as dehydrogenation/hydrogenation component for the formation of olefinic intermediates and the hydrogenation of unsaturated products, and (ii) Brønsted acid sites for the formation of carbocations by protonation of olefinic intermediates [46].

4.2.2.1 Skeletal Isomerization of Hydrocarbons

Skeletal isomerizations of hydrocarbons can be classified into two types. In skeletal isomerizations of type A, the number of branchings remains constant, just their

position changes. In the catalytic cycle, the most important steps are intramolecular alkyl and hydride shifts in the corresponding carbenium ions [46].

An increase or decrease of the number of branchings occurs in skeletal isomerizations of type B. In Figure 4.15 the catalytic cycle for such an isomerization of an n-alkane to a mono-branched iso-alkane is depicted. As widely accepted, in the first step the noble metal catalyzes the dehydrogenation of the n-alkane to an n-alkene, followed by protonation on the Brønsted acid site of the zeolite. Subsequently, the resulting secondary n-alkyl carbenium ion undergoes a rearrangement *via* protonated cyclopropane (PCP) intermediates [47]. In a bimolecular step, the formed tertiary iso-alkyl carbenium ion undergoes an intermolecular hydride transfer with a new n-alkane molecule. This results in the formation of a mono-branched iso-alkane and a secondary n-alkyl carbenium ion, which closes the catalytic cycle.

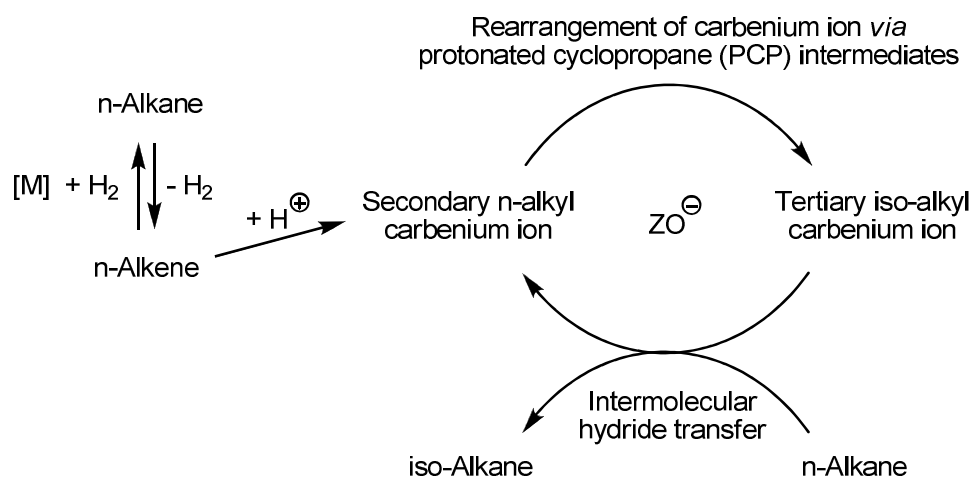


Figure 4.15: Skeletal type B isomerization of n-alkanes on bifunctional catalysts *via* PCP intermediates. ZO[⊖]: Anionic framework oxygen of the zeolite. Adapted from Ref. [46, 48].

Also naphthenic rings can be transferred into skeletal isomers. For example, in the hydroconversion of methylcyclohexane on the bifunctional 1.0Pt/H-Y zeolite at a total pressure of 2.0 MPa and $T_r = 240$ to 280 °C all four possible skeletal isomers with a five-membered ring were formed [49]. These were ethylcyclopentane by an isomerization of type A and 1,1-, trans-1,2- and cis- and trans-1,3-dimethylcyclopentane by a type B isomerization.

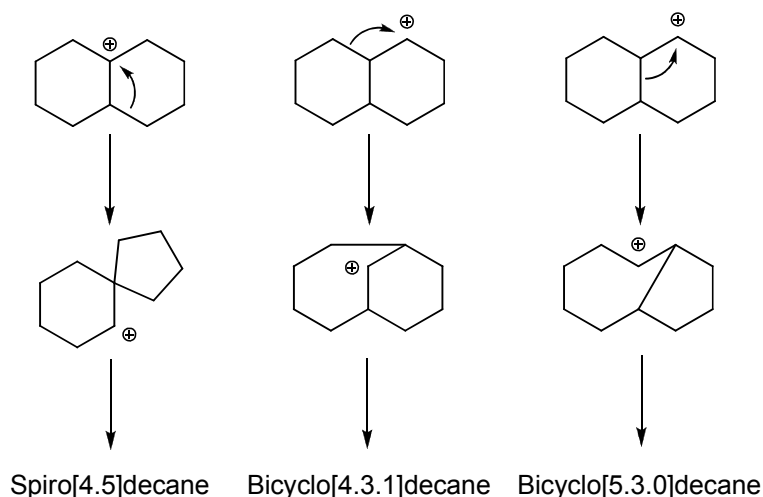


Figure 4.16: Type A rearrangements of the tertiary and secondary carbenium ions derived from decalin. From Ref. [52].

When a bicyclic naphthene like decalin is hydroconverted on a bifunctional catalyst, skeletal isomerization occurs and a complex mixture of skeletal isomers is formed [50, 51]. Recently, Rabl *et al.* [52] detected spiro[4.5]decane as one of the major skeletal isomers that were formed on $0.85\text{Ir}/\text{La}_{0.30}, \text{H}_{0.06}, \text{Na}_{0.04}\text{-X}$ and $1.0\text{Pt}/\text{La}_{0.30}, \text{H}_{0.06}, \text{Na}_{0.04}\text{-X}$ catalysts at low decalin conversions. A rationale was given by applying the carbocation chemistry that is known from alkanes. Hence, the fast type A rearrangement can start from the three possible carbenium ions that are depicted in Figure 4.16. Since tertiary carbenium ions are generally more stable than secondary ones, the route starting from the tertiary carbenium ion that forms spiro[4.5]decane after a 1,2-alkyl shift is more likely.

4.2.2.2 Hydrocracking of Alkanes

On a bifunctional hydrocracking catalyst, the cleavage of a C-C bond by β -scission is often preceded by skeletal isomerization of the carbenium ion, see Section 4.2.2.1. In Figure 4.17 a catalytic cycle for the ideal bifunctional hydrocracking of n-hexane into propane is shown exemplarily [46].

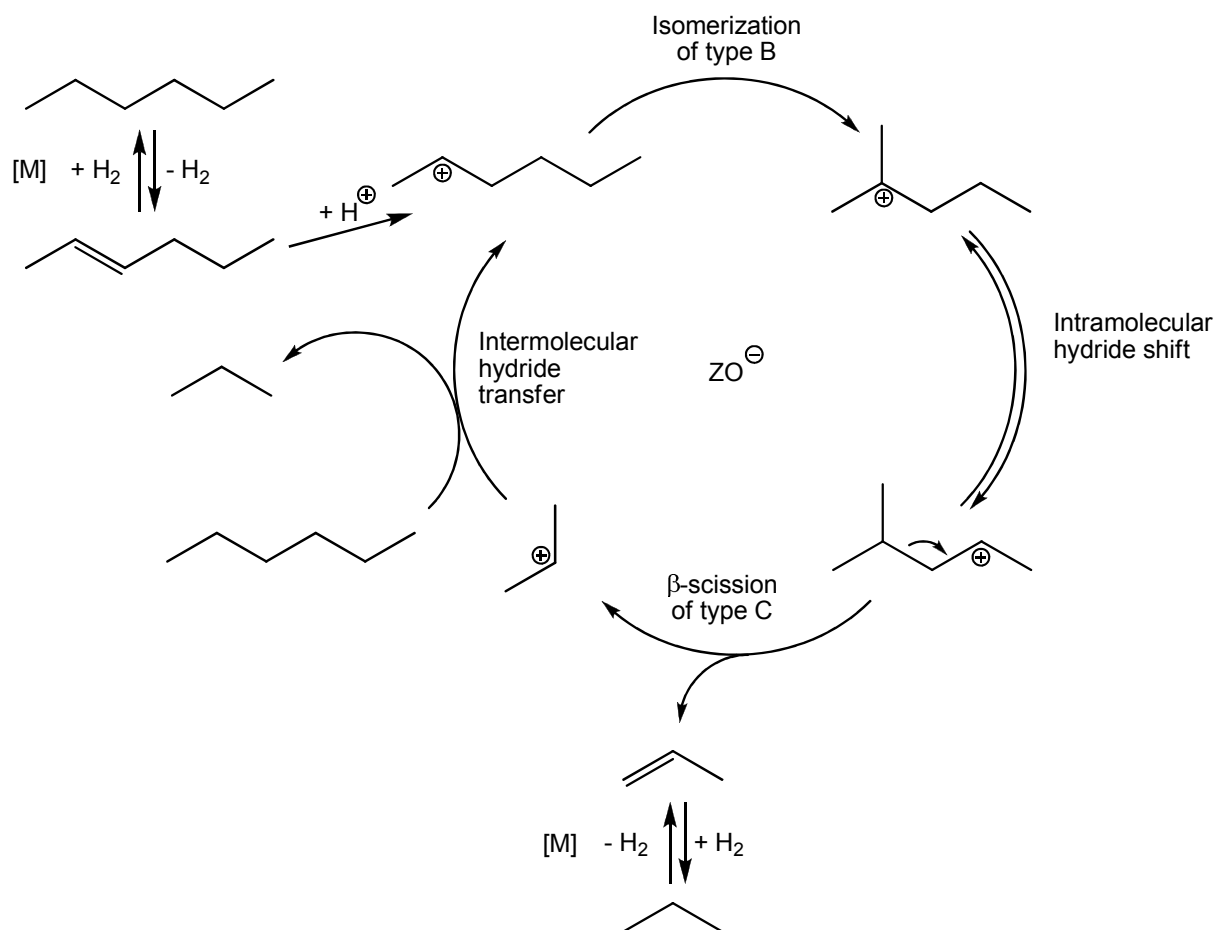


Figure 4.17: Catalytic cycle for the ideal bifunctional hydrocracking of n-hexane into propane. After Ref. [46].

The first steps are similar to those described for the bifunctional isomerization of type B, see Figure 4.15. In addition, now an intramolecular hydride shift in the tertiary carbenium ion generates a precursor for the β -scission, resulting in propene and propyl-(2) cation. On the noble metal, the olefinic product is hydrogenated to propane. *Via* an intermolecular hydride transfer with n-hexane, the carbenium ion forms a new secondary hexyl cation and propane.

With an increasing degree of branching in an alkylcarbenium ion the rate of β -scission increases due to an increasing stability in the series primary < secondary < tertiary carbenium ion. In Figure 4.18 the different types are listed together with the number of carbon atoms n in the carbenium ion that are required for each type of β -scission [53]. When a tertiary carbenium ion undergoes β -scission to form a smaller tertiary carbenium ion and an olefin, this type A β -scission is very fast due to the high stability of tertiary alkylcarbenium ions.

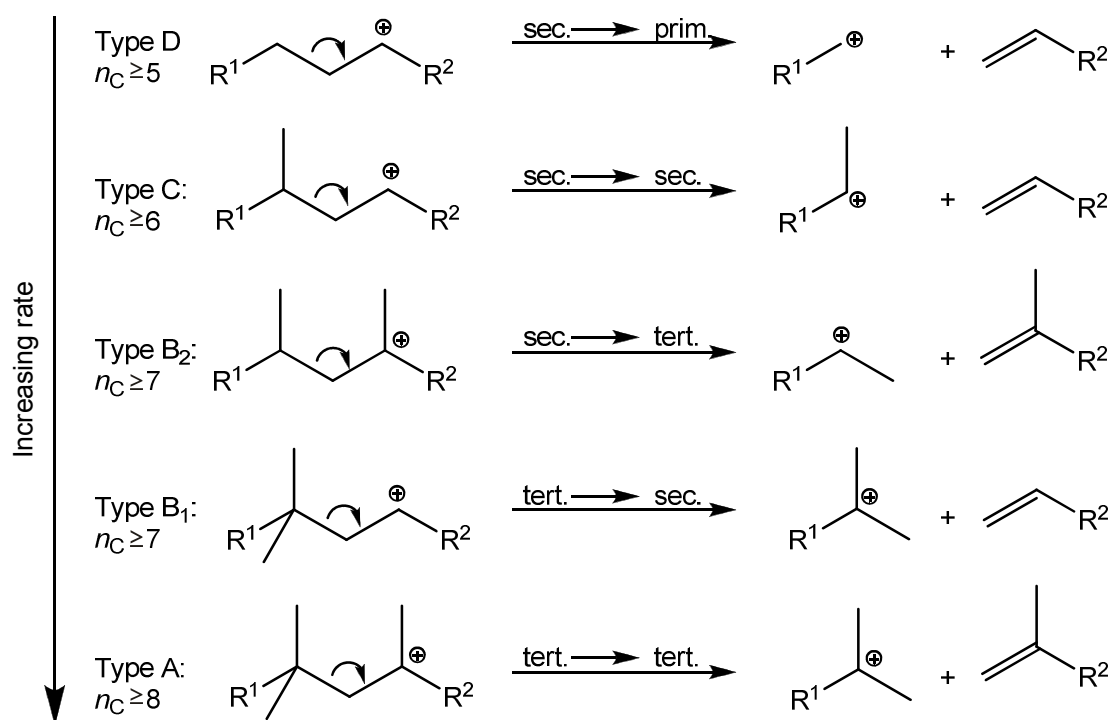


Figure 4.18: Classification of β -scissions of alkylcarbenium ions. n_C : number of carbon atoms in the carbenium ion that can undergo the respective type of β -scission. After Ref. [53].

The influence of the hydrogen pressure on the hydroconversion of n-decane was studied on a bifunctional Pt/Ca-Y zeolite [54] in a range of $p_{\text{H}_2} = 0.3$ to 9.7 MPa. A maximal conversion was measured at a hydrogen pressure of *ca.* 1.5 MPa. At a pressure of 2.0 MPa the selectivity of hydrocracked products was maximal and a further increased pressure led to a higher selectivity of isomerization products.

Also when a noble metal as dehydrogenation/hydrogenation component is absent, cracking of hydrocarbons can occur on the Brønsted acid sites. This mechanism of hydrocracking is known as catalytic cracking and can generate saturated and unsaturated products simultaneously [46]. Moreover, cleavage of C-C bonds can also occur by thermal cracking and hydrocracking without a catalyst [55]. This mechanism requires high temperatures above 500 °C, proceeds *via* radicals and forms large amounts of methane and other light alkanes.

4.2.2.3 Hydrocracking of Naphthenes

The features of hydrocracking of alkanes can be applied largely to the hydrocracking of naphthenes. However, especially for the ring opening of naphthenes to alkanes with the same number of carbon atoms there is a limitation. This is the strongly hindered β -

scission of endocyclic C-C bonds in a cycloalkylcarbenium ion [3]. An explanation that is now widely accepted was given by Brouwer and Hogeveen [56]: In contrast to an aliphatic carbenium ion, the rotation around the α -bond is not possible in a cycloalkylcarbenium ion. However, for a fast β -scission a coplanar orientation of the vacant p-orbital in the carbenium ion and the β -bond to be broken is required. The inability of cycloalkylcarbenium ions to allow this orientation can explain the hindered ring opening of naphthenes.

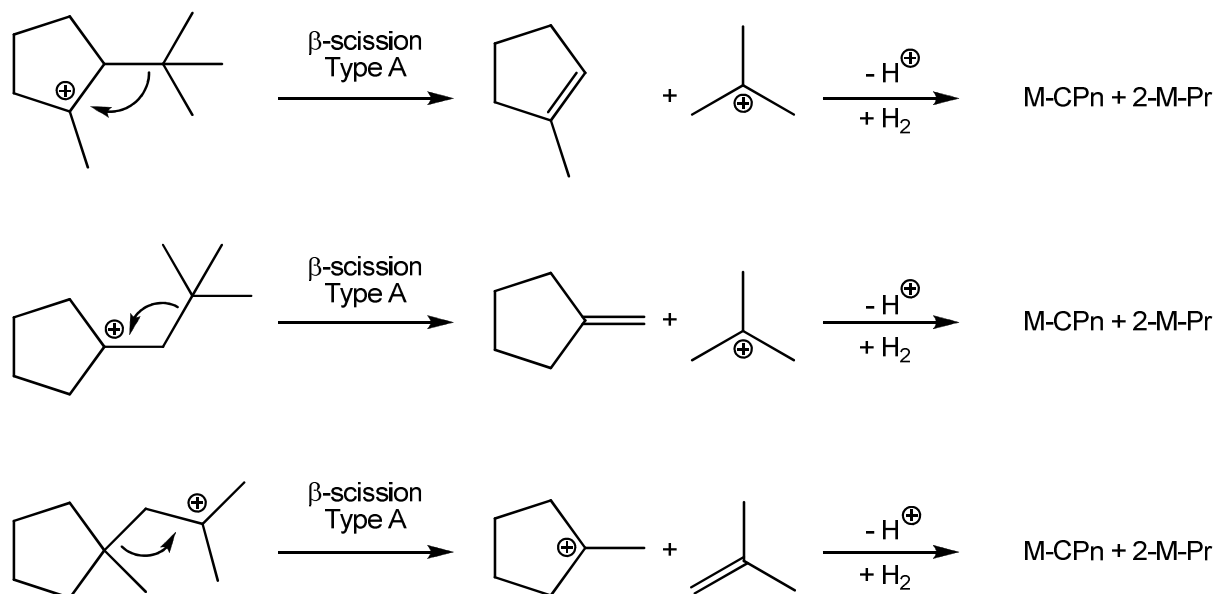


Figure 4.19: The three possible C_{10} cycloalkylcarbenium ions that can undergo exocyclic type A β -scission. M-CPn: methylcyclopentane, 2-M-Pr: 2-methylpropane (iso-butane). From Ref. [3].

A consequence of this limitation is the selective formation of methylcyclopentane and iso-butane in the bifunctional hydrocracking of C_{10} naphthenes. This reaction was observed at first by Chevron researchers [57, 58] who named it paring reaction. In this reaction, a series of type A and B isomerizations results in the formation of one out of the three precursors that allow an exocyclic β -scission of type A, see Figure 4.19. After β -scission, followed by deprotonation and hydrogenation, the only products are methylcyclopentane and iso-butane.

In the ring opening of multi-ring aromatics, naphthenoaromatics and multi-ring naphthenes most researchers used typical bifunctional catalysts with a relatively high concentration and/or strength of Brønsted acid sites [50, 59, 60]. Due to the usage of this type of catalyst but probably also due to the lack of sophisticated product analysis, reports about the formation of open-chain alkanes with the same carbon number as the feed hydrocarbon are scarce [61, 62]. Until recently, only one publication reported

quantitatively on their formation [63] with a maximal yield of open-chain decanes of 4 % in the hydroconversion of decalin on a 1.5Ir,0.75Pt/H-Y zeolite catalyst at a total pressure of 5.0 MPa.

In a study about the hydroconversion of tetralin on physical mixtures and two-bed arrangements of a non-acidic platinum catalyst and a monofunctional acidic H-Y zeolite, platinum was active only in the hydrogenation of aromatics, according to the authors [59]. In another work [64] the proximity of the metal and acid sites was varied in order to study its influence on the ring opening of tetralin. A maximal distance was realized by separating the 1.0Pt/ γ -alumina catalyst in the first catalyst bed from the H-USY zeolite in the second catalyst bed with quartz wool. A higher proximity was reached by physically mixing both catalysts (particle size of 0.25 to 0.42 mm). A minimal average distance of the noble metal and the Brønsted acid sites was obtained by impregnation of H-USY with a platinum salt. With increasing proximity of the platinum and acid sites the yields of skeletal isomers of decalin and ring-opening products increased. Hence, a bifunctional mechanism that requires a small distance between the metal and acid sites is beneficial for obtaining high yields of ring-opening products compared to a separation of both types of active sites. However, only one naphthenic ring was opened and no formation of open-chain decanes was observed.

One single publication is available about the influence of hydrogen pressure on the ring opening of decalin on a bifunctional catalyst [65]. In a batch reactor on 1.0Ir/H-[Al]Beta in the range of $p_{\text{H}_2} = 2.0$ to 6.0 MPa longer reaction times had to be applied to obtain the same decalin conversion at higher pressures. Moreover, at higher hydrogen pressures the selectivity of ROPs increased more strongly with the conversion and reached higher final values at higher hydrogen pressures. At $p_{\text{H}_2} = 6.0$ MPa also slightly lower selectivities of hydrocracked products with less than ten carbon atoms were obtained than in experiments at lower values of p_{H_2} . Hence, the hydrogen pressure has a negative influence on the decalin conversion but a positive influence on the selectivity of ring-opening products on this particular catalyst. Since a detailed product distribution was not shown, it is unclear if hydrocracking occurred mainly by hydrogenolysis on iridium or *via* bifunctional hydrocracking.

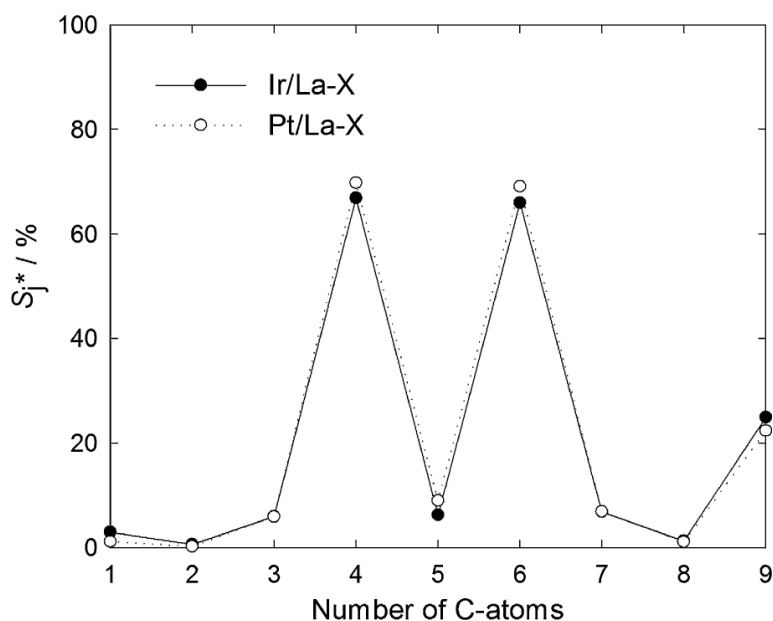


Figure 4.20: Distribution of the hydrocracked products on catalysts $0.85\text{Ir}/\text{La}_{0.30},\text{H}_{0.06},\text{Na}_{0.04}\text{-X}$ and $1.0\text{Pt}/\text{La}_{0.30},\text{H}_{0.06},\text{Na}_{0.04}\text{-X}$ in the hydroconversion of decalin. From Ref. [52].

In recent publications [52, 66] about the hydroconversion of decalin on bifunctional $0.85\text{Ir}/\text{La}_{0.30},\text{H}_{0.06},\text{Na}_{0.04}\text{-X}$, $1.0\text{Pt}/\text{La}_{0.30},\text{H}_{0.06},\text{Na}_{0.04}\text{-X}$ and $5.0\text{Rh}/\text{H}_{0.99},\text{Na}_{0.01}\text{-[Al]Beta}$ catalysts it was reported on the formation of open-chain decanes with maximal yields of 12 to 14 %. The authors emphasized that these values are not the result of improved catalysts or reaction conditions but rather a result of an enhanced product analysis. In the group of hydrocracked products with less than ten carbon atoms iso-butane and methylcyclopentane were the major products. This is a strong indication for the bifunctional properties of all three catalysts. The corresponding carbon number distribution curve of the hydrocracked products was denoted as “M-shaped” due to the maxima at C_4 and C_6 (see Figure 4.20).

4.2.3 Ring Opening of Naphthenes *via* Skeletal Isomerization and Subsequent Hydrogenolysis

One strategy for the hydrodecyclization of naphthenes with six-membered rings is the combination of a bifunctional isomerization catalyst and a hydrogenolysis catalyst. In such a configuration, the bifunctional catalyst isomerizes the six-membered ring, which is relatively difficult to open by hydrogenolysis (see Section 4.2.1.4), into a five-membered ring. Subsequently, the hydrogenolytically active noble metal, preferentially iridium, is expected to open the five-membered ring relatively fast. With $0.9\text{Pt}/\text{H-USY}$ and $2.0\text{Ir}/\gamma\text{-alumina}$ as isomerization and hydrogenolysis catalyst, respectively, higher yields of skeletal isomers and ring-opening products compared to

the experiments with the single catalysts were obtained in the ring opening of methylcyclohexane [4]. There was no noticeable change of the product composition observed when both catalysts were physically mixed and when 0.9Pt/H-USY was staged upstream of the hydrogenolysis catalyst.

Also Santikunaporn *et al.* [49] studied the hydroconversion of methylcyclohexane with 1.0Pt/H-Y as isomerization catalyst and 1.0Ir/silica as hydrogenolysis catalyst. They measured a *ca.* 15 % higher conversions at the same reaction temperatures when both catalysts were physically mixed instead of being packed in two separate catalyst beds. In the physical mixture, the yields of ring-opening products but also of hydrocracked products with less than seven carbon atoms were higher while smaller amounts of skeletal isomers were formed. By analyzing the detailed distribution of the ring-opening products the authors concluded that in the two-bed arrangement methylcyclohexane is isomerized to a large extent into substituted cyclopentanes, which can be opened by hydrogenolysis on iridium very fast. By contrast, in the physical mixture of both catalysts a larger fraction of unreacted methylcyclohexane comes into contact with the iridium catalyst. Due to the relatively slow endocyclic hydrogenolysis of six-membered rings, in the two-bed arrangement the extent of methane abstraction from methylcyclohexane is increased. Also the hydrogenolysis of alkanes leads to a higher amount of hydrocracked products with less than seven carbon atoms. By applying a 20 °C higher reaction temperature in the first catalyst bed (1.0Pt/H-Y) than in the second bed (1.0Ir/silica) the extent of multiple hydrogenolysis on iridium was lowered and higher yields of ring-opening products were obtained.

McVicker *et al.* [4] studied also the ring opening of butylcyclohexane. *Inter alia*, they tested a bifunctional 0.9Ir/H-USY catalyst, on which the acidic and hydrogenolytic functions were combined. The ring-opening yield was lower compared to the hydroconversion on a physical mixture of 0.9Pt/H-USY and 2.0Ir/ γ -alumina, according to the authors due to a lower metal dispersion when iridium is supported on H-USY. A similar product distribution was obtained in the hydroconversion of pentylcyclopentane on 2.0Ir/ γ -alumina and in the hydroconversion of butylcyclohexane on 0.9Ir/H-USY or a mixture of 0.9Pt/H-USY and 2.0Ir/ γ -alumina. The product composition, moreover, differed strongly from that of the hydrogenolysis of butylcyclohexane on 2.0Ir/ γ -alumina. It was concluded that, in the hydroconversion of butylcyclohexane, the main skeletal isomer that is formed and further opened by hydrogenolysis on iridium is probably pentylcyclopentane. A similar reaction path was also described by Santikunaporn *et al.* [59] in the hydroconversion of decalin on 1.0Pt/H-Y: They found 1-methylbicyclo[4.3.0]nonane as skeletal isomer at low

conversion and increasing amounts of the ring-opening product butylcyclohexane at higher conversions.

Recently, a new class of iridium- or platinum-containing catalysts for the selective hydrodecyclization of bicyclic naphthenes was introduced, so-called “high-performance ring-opening catalysts” (HIPEROCS) [5, 67]. These Na-Y zeolites with a metal content of *ca.* 3 wt.-% contain a small concentration of relatively weak Brønsted acid sites which are generated during reduction of the noble metal only. In the hydroconversion of decalin at $p_{\text{H}_2} = 5.2$ MPa maximal yields of open-chain decanes of 31 and 41 % were obtained on 2.9Ir/Na_{0.90}H_{0.10}-Y and 3.0Pt/Na_{0.88}H_{0.12}-Y, respectively [5]. They catalyze the skeletal isomerization *via* bifunctional catalysis, but a bifunctional hydrocracking pathway that would result in the paring reaction (see Section 4.2.2.3) is inhibited by the mild acidic properties of these catalysts. Moreover, the catalytic results strongly suggest that the ring-opening reaction to ring-opening products and open-chain decanes proceeds mainly by hydrogenolysis of endocyclic C-C bonds in decalin and, presumably more importantly, its skeletal isomers. Again, spiro[4.5]decane was identified as skeletal isomer of decalin with high selectivities at low conversions.

In the same study [5] also the strength of the Brønsted acid sites was varied by incorporating different alkali cations instead of sodium. On the three most weakly acidic iridium-containing catalysts with K⁺, Rb⁺ or Cs⁺ as alkali cations the ring-opening products were composed mainly of butylcyclohexane, 1-methyl-2-propylcyclohexane and 1,2-diethylcyclohexane. This is a strong indication for a direct ring-opening mechanism by hydrogenolysis on the noble metal.

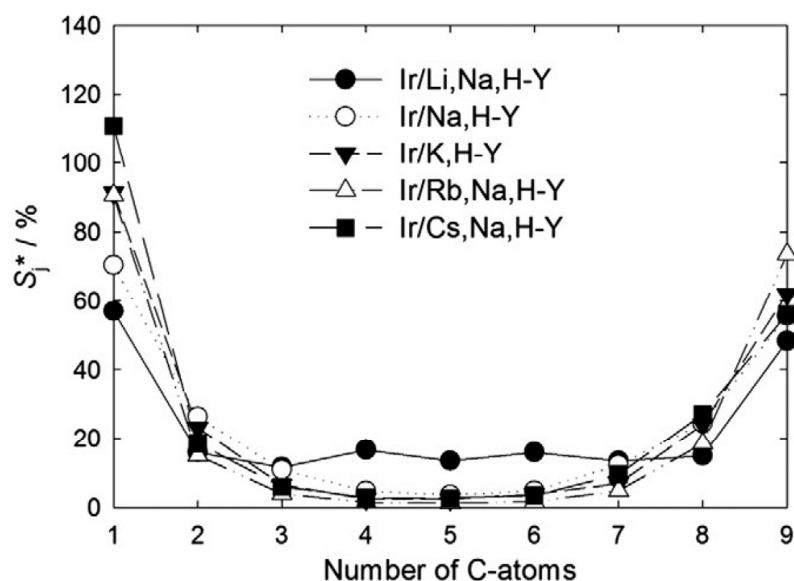


Figure 4.21: Distribution of the hydrocracked products on iridium-containing Y zeolites with different charge-compensating cations in the hydroconversion of decalin. From Ref. [5].

Moreover, it turned out that plotting the carbon number distribution of the hydrocracked products is a valuable tool for understanding the underlying hydrocracking mechanisms. Except for the Li-containing and, hence, the most strongly acidic catalyst all other iridium catalysts showed a near-symmetrical so-called “hammock-shaped” curve, see Figure 4.21. Its characteristics are large amounts of methane and C₉ products, smaller amounts of ethane and C₈ products and very small amounts of products with three to seven carbon atoms. Such a curve seems to be indicative for a hydrocracking mechanism that is dominated by hydrogenolysis on iridium. As a consequence of an increased strength of the Brønsted acid sites on the iridium catalyst with Li⁺ as cation, higher amounts of C₄ and C₆ products were observed due to the paring reaction.

In the same study [5] similar catalysts loaded with platinum instead of iridium were tested. A mainly metal-catalyzed mechanism on platinum catalysts results in a distribution of the hydrocracked products with much methane and relatively low amounts of C₂, C₃, C₄, C₆, C₇ and C₈ hydrocarbons. C₅ and C₉ products are almost absent. With an increasing strength of Brønsted acid sites, the amounts of C₄ and C₆ products increase due to the paring reaction.

As conclusion, a detailed evaluation of the hydrogenolytic pathways in the hydroconversion of decalin is required. Also the mechanistic origin of the distribution curves of the hydrocracked products on weakly or non-acidic metal catalysts is not sufficiently understood. Another important question is: Does the cleavage of

endocyclic C-C bonds on HIPEROs occur by hydrogenolysis on the noble metal or by bifunctional hydrocracking on the Brønsted acid sites?

5 Experimental Section

All chemicals that were used in this work are summarized in Table 5.1. No further purification was applied.

Table 5.1: Chemicals used in this work.

Chemical	Producer, Purity / Composition
Aerosil 380	Evonik Degussa GmbH, silica, ≥ 99.8 wt.-%
γ-Aluminum oxide	Alfa Aesar, activated, neutral, 99.9 wt.-%
Ammonia, aqueous solution	unknown, 30 wt.-% NH ₃
Black Pearls 2000	Cabot, carbon black
Butylcyclohexane	Alfa Aesar, 99.30 wt.-%
Chromosorb	Merck, particle size 0.25-0.60 mm, P/AW
cis-Decalin	Merck, 98.39 wt.-%
n-Decane	Sigma Aldrich, 99.70 wt.-%
Ethylcyclohexane	Aldrich, 99.55 wt.-%
Helium 4.6	Westfalen AG, 99.996 vol.-%
Hydrochloric acid	unknown, 37 wt.-%
Hydrogen 5.0	Westfalen AG, 99.999 vol.-%
Methyldecalin	Wako Chemicals, mixture of isomers (see Section 5.5.1.8), 99.30 wt.-%
Mixture of argon 5.0 / hydrogen 5.0	Westfalen AG, 90 vol.-% Argon, 10 vol.-% hydrogen, purity each 99.999 vol.-%
Nitrogen 5.0	Westfalen AG, 99.999 vol.-%
n-Nonane	Merck, > 99 wt.-%
n-Octane	Fluka, 99.32 wt.-%
Pentaamminechloroiridium(III) chloride	Aldrich, 50.01 wt.-% Ir and Colonial Metals, 49.86 wt.-% Ir
Pentaamminechlororhodium(III) chloride	Alfa Aesar, ≥ 34.5 wt.-% Rh
Perhydroindan	kindly provided by Eni S.p.A., 96.70 wt.-%
Pyridine	Aldrich, ≥ 99 wt.-%

Table 5.1 (continued).

Rhodium(III) chloride hydrate	Alfa Aesar, 99.99 wt.-% Rh on metals basis
Sodium nitrate	Merck, > 99 wt.-%
Spiro[4.5]decane	se ma GmbH, 98.17 wt.-%
Tetraamminepalladium(II) chloride	ChemPur, 40.62 wt.-% Pd
Tetraammineplatinum(II) chloride hydrate	ChemPur, 55.63 wt.-% Pt
Tetraethyl orthosilicate	Acros Organics, ≥ 98 %
Titania	Degussa P 25
Triblock copolymer	Aldrich, EO ₂₀ PO ₇₀ EO ₂₀ , typically $M = 5800 \text{ g}\cdot\text{mol}^{-1}$
n-Undecane	EGA-Chemie, 99 wt.-%
Zeolite Na-Y	Strem Chemicals, lot No. 148 960

Spiro[4.5]decane was purchased along with its ^1H , ^{13}C and ^{13}C DEPT NMR spectra which proved the identity of the compound.

5.1 Preparation of the Catalysts

The preparation of some catalysts was conducted by Dipl.-Chem. Yvonne Krämer, Julia Kreis, Dipl.-Chem. Melanie Mechler, Dipl.-Chem. Nelli Pfaff and Dipl.-Chem. Simon Schulze.

5.1.1 Preparation of [Si]SBA-15

The synthesis of the mesoporous catalyst support [Si]SBA-15 is analogous to the method in Ref. [68]. 12 g triblock copolymer were dissolved in a solution of 58.8 g hydrochloric acid in 184 g demineralized water. After the addition of 26.4 g tetraethyl orthosilicate the mixture was stirred for 10 min at room temperature and 24 h at 40 °C. Afterwards, crystallization was carried out at 100 °C for 24 h in a polypropylene bottle. The white solid was filtered, washed with 2 dm³ of demineralized water and dried in an air oven at 80 °C for 24 h. To remove the template the material was calcined in a muffle oven. Under a nitrogen flow of 43 dm³·h⁻¹ the material was first heated from room temperature to 540 °C with a heating rate of 2 K·min⁻¹. After 10 h at 540 °C the gas flow was slowly changed to air with the same flow rate, and the temperature was held for 10 h.

5.1.2 Ion Exchange with Ammonium Ions

To ensure that all exchangeable cations in zeolite Na-Y are sodium cations the following procedure was applied: Per 1 g of dry zeolite Na-Y the material was stirred two times for 4 h at 80 °C in 40 cm³ of a 1 mol·dm⁻³ aqueous solution of NaNO₃. After 4 h each time the zeolite was filtered and washed with demineralized water until no nitrate ions could be detected in the filtrate by a nitrate test strip anymore and dried for at least 12 h at 80 °C in an air oven.

To form a partially exchanged zeolite Na,NH₄-Y, the first modification step consisted in an ion exchange of Na-Y with ammonium nitrate in an aqueous suspension. Zeolite Na-Y was suspended in 8.3 g of a 0.17 mol·dm⁻³ aqueous solution of NH₄NO₃ per gram of dry catalyst and stirred for 4 h at 80 °C. The resulting zeolite was filtered, washed with demineralized water and dried for 12 h at 80 °C in an air oven. A zeolite Na_{0.69},(NH₄)_{0.31}-Y with an ammonium exchange degree of 31 % was obtained.

5.1.3 Incorporation of the Noble Metals

5.1.3.1 Ion Exchange

Palladium was introduced into zeolite Na_{0.69},(NH₄)_{0.31}-Y by ion exchange with [Pd(NH₃)₄]Cl₂. A dry mass of 3.71 g of this zeolite was suspended in 60 g demineralized water. An aqueous solution of 61.5 mg of [Pd(NH₃)₄]Cl₂ in 50 g demineralized water was slowly added by means of a dropping funnel within 20 min under stirring. After stirring at 80 °C for 24 h the resulting solid was filtered off, washed with 200 cm³ demineralized water and dried at 80 °C for 12 h in an air oven.

5.1.3.2 Strong Electrostatic Adsorption

All noble-metal-containing catalysts that were prepared by strong electrostatic adsorption (SEA) [13, 14] of the respective metal salt on silica (Aerosil 380) or [Si]SBA-15 are listed in Table 5.2.

Table 5.2: Catalysts that were prepared by strong electrostatic adsorption and masses of catalyst support and metal salt.

Catalyst	$m_{\text{support}} / \text{g}$	$m_{\text{metal salt}} / \text{mg}$
0.73Ir/[Si]SBA-15	8	160
0.77Ir/silica	8	206
1.02Ir/silica	8	203
2.59Ir/silica	4	300
2.73Ir/silica	8	600
0.60Pd/silica	8	112
0.92Pt/[Si]SBA-15	8	152
0.91Pt/silica	8	137
0.93Pt/silica	8	145
2.68Pt/silica	4	215
2.69Pt/silica	8	432
0.96Rh/silica	8	231

The general procedure was as follows: A dry mass of silica or [Si]SBA-15 (m_{support} , see Table 5.2) was suspended in 10 to 13 g of demineralized water per gram of dry catalyst support. This suspension was vigorously stirred for 2 h, and during that time the pH was adjusted to 10 by dropwise addition of a 1 molar aqueous ammonia solution. Subsequently, a solution of the respective noble metal salt ($m_{\text{metal salt}}$, see Table 5.2) in 20 to 40 cm³ of demineralized water was added dropwise under ongoing stirring. The metal complexes were [Ir(NH₃)₅Cl]Cl₂, [Pd(NH₃)₄]Cl₂, [Pt(NH₃)₄]Cl₂ and [Rh(NH₃)₅Cl]Cl₂. After stirring for another 18 h the solid was filtered off, washed with demineralized water and dried at 80 °C.

5.1.3.3 Impregnation

Three different catalyst supports, *viz.* γ -alumina, carbon black and titania, were impregnated with [Ir(NH₃)₅Cl]Cl₂ or [Pt(NH₃)₄]Cl₂ to form the respective six catalysts shown in Table 5.3. Due to the low solubility of [Ir(NH₃)₅Cl]Cl₂, wetness impregnation was used to load iridium onto the catalysts. For this purpose, a solution of 20.0 mg of [Ir(NH₃)₅Cl]Cl₂ in *ca.* 3.5 cm³ of demineralized water was added dropwise per gram of catalyst support. Platinum was introduced *via* incipient wetness impregnation. For this purpose, a solution of 18.0 mg of [Pt(NH₃)₄]Cl₂ in 1.9 cm³ of

demineralized water was added dropwise per gram of catalyst support. All six catalyst precursors were dried by rotary evaporation under vacuum at $T = 40\text{ }^{\circ}\text{C}$ and thereafter in an air oven at $80\text{ }^{\circ}\text{C}$ for 24 h.

Table 5.3: Catalysts that were prepared by impregnation.

0.93Ir/ γ -alumina	0.81Pt/ γ -alumina
0.91Ir/carbon black	0.91Pt/carbon black
1.05Ir/titania	1.06Pt/titania
1.03Rh/silica	

Catalyst 1.03Rh/silica was prepared by wetness impregnation of RhCl_3 on silica. A solution of 228 mg RhCl_3 in 80 cm^3 of demineralized water was impregnated on silica with a dry mass of 8.0 g. Drying was carried out in a rotary evaporator under vacuum at $T = 70\text{ }^{\circ}\text{C}$ and subsequently in an air oven at $80\text{ }^{\circ}\text{C}$ for 12 h.

5.1.4 Calcination of Catalyst Precursors

After ion exchange, the palladium-containing zeolite Y was calcined in air to obtain a good metal dispersion. It was heated from room temperature to $300\text{ }^{\circ}\text{C}$ with a heating rate of $0.5\text{ K}\cdot\text{min}^{-1}$ and held at the end temperature for 3 h in an oven under a synthetic air flow rate of $58\text{ cm}^3\cdot\text{min}^{-1}$. At lower oxidation temperatures Pd^{2+} ions would migrate into supercages where they form larger metal clusters after reduction with hydrogen [69]. When oxidation temperatures are sufficiently high, *i.e.* $300\text{ }^{\circ}\text{C}$ and above, the Pd^{2+} ions are situated in the sodalite cages where they form highly dispersed palladium particles during reduction.

In order to investigate the influence of the metal particle size, the precursor of catalyst 1.03Rh/silica was calcined after impregnation according to Ref. [70] under harsh conditions to obtain a low-dispersed metal phase. Calcination was conducted in an oven under a synthetic air flow rate of $13\text{ dm}^3\cdot\text{h}^{-1}$. After heating from room temperature to $450\text{ }^{\circ}\text{C}$ with a heating rate of $7\text{ K}\cdot\text{min}^{-1}$, this temperature was held for 1 h. Subsequently, it was heated to $700\text{ }^{\circ}\text{C}$ with a heating rate of $4\text{ K}\cdot\text{min}^{-1}$ and held at this temperature for 1 h.

5.1.5 Forming of the Catalyst Powder

The catalyst powders were pressed without a binder at 127 MPa for 15 min, and the tablets thereby formed were crushed. The size fraction of $0.20 \text{ mm} < d_{\text{cat}} < 0.32 \text{ mm}$ was used for the catalytic experiments.

5.1.6 Oxidative Treatment

All metal-containing catalyst precursors that were loaded by SEA (see Section 5.1.3.2) were calcined in a synthetic air stream with a volumetric flow rate of $\dot{V}_{\text{air}} = 200 \text{ cm}^3 \cdot \text{min}^{-1}$ at atmospheric pressure in the catalytic flow-type apparatus that was used for the subsequent catalytic experiments. Calcination was conducted for 3 h after heating to $T = 150 \text{ }^\circ\text{C}$ with a heating rate of $1 \text{ K} \cdot \text{min}^{-1}$. Oxidation at $T > 150 \text{ }^\circ\text{C}$ is expected to result in a reduced metal dispersion as demonstrated with silica and [Si]SBA-15 loaded *via* SEA with $[\text{Pt}(\text{NH}_3)_4]\text{Cl}_2$ due to the oxidation of Pt^{2+} to more mobile Pt^{4+} species [13].

Both γ -alumina-supported catalyst precursors were calcined at atmospheric pressure with air [71]. Oxidation was conducted in the catalytic flow-type apparatus that was used for the subsequent hydroconversion of n-octane with $\dot{V}_{\text{air}} = 50 \text{ cm}^3 \cdot \text{min}^{-1}$ for 4 h after heating to $T = 400 \text{ }^\circ\text{C}$ with a heating rate of $1 \text{ K} \cdot \text{min}^{-1}$. The same experimental conditions were applied for the titania-supported catalysts [72] but the final temperature of $T = 400 \text{ }^\circ\text{C}$ was held for 3 h.

5.1.7 Reduction of the Noble Metals

To obtain catalyst $0.52\text{Pd}/\text{Na}_{0.69},\text{H}_{0.31}\text{-Y}$, the ammonium-exchanged, palladium-loaded and calcined zeolite Y precursor was reduced in a flow of hydrogen with a volumetric flow rate of $\dot{V}_{\text{H}_2} = 100 \text{ cm}^3 \cdot \text{min}^{-1}$ at atmospheric pressure in the catalytic flow-type apparatus that was used for the subsequent hydroconversion of n-octane. Reduction was conducted for 2 h after heating to $T = 350 \text{ }^\circ\text{C}$ with a heating rate of $5 \text{ K} \cdot \text{min}^{-1}$.

All silica- and [Si]SBA-15-supported catalysts were reduced in a flow of hydrogen with a volumetric flow rate of $\dot{V}_{\text{H}_2} = 200 \text{ cm}^3 \cdot \text{min}^{-1}$ at atmospheric pressure in the catalytic flow-type apparatus that was used for the subsequent catalytic experiments. Reduction was conducted for 120 min after heating to $T = 400 \text{ }^\circ\text{C}$ with a heating rate of $5 \text{ K} \cdot \text{min}^{-1}$. As exceptions, and only prior to the hydroconversion of n-octane, catalysts $0.77\text{Ir}/\text{silica}$ and $0.93\text{Pt}/\text{silica}$ were reduced at $T = 250 \text{ }^\circ\text{C}$.

On the γ -alumina-supported catalysts the noble metals were reduced with $\dot{V}_{\text{H}_2} = 50 \text{ cm}^3 \cdot \text{min}^{-1}$ for 1 h after heating to $T = 400 \text{ }^\circ\text{C}$ with a heating rate of $2 \text{ K} \cdot \text{min}^{-1}$. Reduction of the noble metals on the titania-supported catalysts was conducted with $\dot{V}_{\text{H}_2} = 50 \text{ cm}^3 \cdot \text{min}^{-1}$ for 2 h after heating to $T = 400 \text{ }^\circ\text{C}$ with a heating rate of $5 \text{ K} \cdot \text{min}^{-1}$. A stepwise reduction [73] with $\dot{V}_{\text{H}_2} = 20 \text{ cm}^3 \text{ min}^{-1}$ was applied for the noble metals supported on carbon black. After heating from room temperature to $150 \text{ }^\circ\text{C}$ with a heating rate of $3 \text{ K} \cdot \text{min}^{-1}$, this temperature was held for 1 h. Subsequently, it was heated to $400 \text{ }^\circ\text{C}$ with a heating rate of $4 \text{ K} \cdot \text{min}^{-1}$ and held at this temperature for 1 h.

Table 5.4: Catalysts that have been provided by others and hydrocarbons these have been tested with.

Catalyst	Provided by	Studied in the Hydroconversion of
2.9Ir/Na _{0.90} H _{0.10} -Y	Dr. Sandra Rabl	n-Decane, butylcyclohexane
1.1Pd/Na _{0.93} H _{0.07} -Y	Dipl.-Chem. Dominic Santi	n-Decane, butylcyclohexane
3.0Pt/Na _{0.88} H _{0.12} -Y	Dr. Sandra Rabl	n-Decane, butylcyclohexane
1.0Pd/Na _{0.70} H _{0.30} -[Al]Beta-14.0	Dipl.-Chem. Dominic Santi	Perhydroindan
3.3Ir/H _{0.58} CS _{0.42} -[Al]Beta-14.0	Dipl.-Chem. Dominic Santi	Spiro[4.5]decane
1.0Pd/Na _{0.93} H _{0.07} -Y	Dipl.-Chem. Dominic Santi	Spiro[4.5]decane
3.3Pt/Na _{0.85} H _{0.15} -Y	Dipl.-Chem. Tobias Holl	Spiro[4.5]decane

For the hydroconversion of n-decane, butylcyclohexane, perhydroindan and spiro[4.5]decane also catalysts were used that have been provided by others, see Table 5.4. The catalysts for the hydroconversion of n-decane, butylcyclohexane and perhydroindan were reduced as described for the silica catalysts (*vide supra*). The reduction of the three catalysts, that were provided by others and were tested in the

hydroconversion of spiro[4.5]decane, was conducted similarly, but with a heating rate of $2 \text{ K}\cdot\text{min}^{-1}$ as done by others prior to the hydroconversion of cis-decalin [74].

5.2 Characterization of the Starting Materials and Catalysts

5.2.1 X-Ray Diffraction

Powder X-ray diffractometry (XRD) was applied to verify that zeolite Y and [Si]SBA-15 were phase-pure and had retained their structure after each synthesis and modification step. A Bruker D8 Advance diffractometer with $\text{CuK}\alpha$ radiation ($\lambda = 0.154 \text{ nm}$) was used. An excitation voltage of 35 kV and a current intensity of 40 mA were applied. Diffractograms of zeolite Y were collected between 2θ values of 3 and 50° with a step width of 0.02° and a step time of 1.5 s. The mesoporous material [Si]SBA-15 was characterized between 2θ values of 0.5 and 10° with a step width of 0.01° and a step time of 5 s. Some of these experiments were conducted by Dipl.-Chem. Simon Schulze.

5.2.2 Chemical and Thermogravimetric Analysis

To analyze the chemical composition of the catalyst precursors and catalysts, a Varian optical emission spectrometer Vista-MPX CCD with an inductively coupled plasma (ICP-OES) was used. Silicon, aluminum, sodium, iridium, palladium, platinum and rhodium were determined by ICP-OES. For that purpose, *ca.* 100 mg of the sample were dissolved in 3 cm^3 of diluted hydrofluoric acid (10 wt.-% HF in doubly distilled water) and 6 cm^3 of nitrohydrochloric acid. This mixture was filled up to 250 cm^3 with doubly distilled water and was then analyzed. To determine the content of iridium, palladium, platinum and rhodium, the samples of the catalyst precursor were analyzed after the loading with the metal salts and drying at 80°C prior to the oxidative treatment, calcination and/or reduction because after these thermal treatments some samples cannot be dissolved completely with the procedure described above. ICP-OES analyses were conducted by Heike Fingerle and Dipl.-Chem. Charalambos Freed.

The metal content of all samples is defined as the mass of the metal per dry mass of the catalyst. By storing the catalyst in a desiccator over a saturated aqueous solution of calcium nitrate for at least 24 h, a constant water content was obtained. Subsequently, in a Setaram Thermogravimetric Analyzer (TGA) Setsys TG-16/18, the precise water

content of the catalysts was determined by heating the sample in a nitrogen flow from room temperature to 600 °C with a heating rate of 20 K·min⁻¹. TGA analyses were conducted by Barbara Gehring, Dipl.-Chem. Ines Kley and Dr. Frank Salzbauer.

5.2.3 Scanning Electron Microscopy

With a scanning electron microscope (SEM) Cam Scan 44 the morphology and the size of the crystals was determined. The samples were coated with an ultrathin coating of gold by a sputter coating equipment K550 of Emitech. An excitation voltage of 5 kV was used to achieve a high resolution. SEM images were prepared by Dipl.-Chem. Ines Kley.

5.2.4 FT-Infrared Spectroscopy

Fourier transform infrared (FT-IR) spectroscopic measurements with pyridine as probe molecule were applied to determine the acidic properties of silica and one noble-metal-loaded silica sample. A spectrometer Vector 22 from Bruker with a high-vacuum sample cell was used. Prior to the measurements, the samples were ground in a vibration mill to fine powders and pressed into very thin, rectangular self-supporting wafers with edge lengths of 10 mm and *ca.* 20 mm. The wafers were placed in a metal IR cell with CaF₂ windows, a vacuum system and a separated oven. All samples were treated in an air flow of 200 cm³·min⁻¹ while heating to $T = 150$ °C with a heating rate of 1 K·min⁻¹ and holding the temperature for 3 h. Subsequently, reduction was performed in a flow of 100 cm³·min⁻¹ of hydrogen with a heating rate of 2 K·min⁻¹ up to 500 °C and holding for 2 h in the oven. After the reduction, the sample cell and the oven were evacuated for 4 h at 100 °C with a vacuum of $2.0 \cdot 10^{-6}$ Pa. After that, pyridine vapor was introduced into the cell for 1 h. The physically adsorbed pyridine was removed by evacuating for 1 h at 200 °C. Subsequently, the wafer was placed into the measurement cell, and a spectrum was recorded at 80 °C. FT-IR analyses were conducted by Dipl.-Chem. Dominic Santi.

5.2.5 Nitrogen Physisorption and Hydrogen Chemisorption

Nitrogen physisorption was conducted in a Quantachrome Autosorb-1-C instrument to measure the porous properties of the catalyst supports. The sample was evacuated for 16 h at 350 °C prior to the N₂ physisorption experiment at liquid-nitrogen temperature. For the calculation of the specific surface area A_{BET} according to Brunauer, Emmett

and Teller (BET) [75], values of $0.1 \leq p / p_0 \leq 0.3$ were chosen to obtain a linear BET plot and a positive C-value.

Hydrogen chemisorption was conducted in the same instrument by static volumetry. An adsorption stoichiometry of $n_{\text{H}} / n_{\text{noble metal}} = 1$ was assumed. After the reduction treatment with the same temperature program as used in the reactor of the catalytic flow-type apparatus, two isotherms were measured at $T = 40$ °C. Adsorption isotherms were recorded in a pressure range of 11 to 107 kPa for the noble-metal-containing catalysts, except for 0.60Pd/silica. To exclude the formation of a β -hydride phase on palladium, adsorption isotherms for this palladium catalyst were measured at lower pressures in the range of 0.3 to 2.7 kPa [76]. The first isotherm is considered to be a combination of physis- and chemisorption, and the second isotherm, measured after evacuating the sample, is interpreted as physisorption only. The difference of these two isotherms, originating from irreversibly and strongly adsorbed hydrogen, is applied for calculating the noble metal dispersion.

Nitrogen physisorption and hydrogen chemisorption were in part conducted by Matthias Scheibe.

5.3 Procedures of the Catalytic Experiments

Some of the catalytic experiments were conducted by Dipl.-Chem. Yvonne Krämer, Julia Kreis, Dipl.-Chem. Melanie Mechler, Dipl.-Chem. Nelli Pfaff and Dipl.-Chem. Simon Schulze.

5.3.1 Hydroconversion of n-Octane as Test Reaction

In order to study pure metal catalysis it is essential to find a catalyst support which does not possess catalytically active Brønsted acid sites. Hence, with five different materials, *viz.* silica, [Si]SBA-15, γ -alumina, carbon black and titania, loaded with iridium or platinum, the hydroconversion of n-octane was performed as catalytic test reaction. In addition, the zeolitic catalyst 0.52Pd/Na_{0.69}H_{0.31}-Y was tested as typical bifunctional reference catalyst.

5.3.1.1 Experimental Set-Up of the Flow Apparatus

A catalytic flow-type apparatus was used for the hydroconversion of n-octane at atmospheric pressure. The experimental set-up was similar to that used for the catalytic experiments at higher hydrogen pressures, which is depicted in Figure 5.1. The main components were (i) a saturator made of glass that was filled with Chromosorb, (ii) a fixed-bed reactor made of quartz glass and (iii) a six-port gas sampling valve that allowed the analysis of the product mixture in a gas chromatograph equipped with a capillary column and a flame-ionization detector (FID) (see Section 5.4.1).

The saturator was heated by a water jacket that was connected to a thermostat. Chromosorb was impregnated with liquid n-octane to generate the desired n-octane/hydrogen gaseous mixture. All parts downstream the saturator were held at $T = 130\text{ }^{\circ}\text{C}$ to avoid condensation of the reactant and products. The build-up of the reactor was similar to that used for the high-pressure experiments (see Figure 5.2) but all parts were made of quartz glass, except for the sealing which was made of plastic.

5.3.1.2 Conditions in the Catalytic Experiments

In all experiments the feed hydrocarbon was n-octane (purity 99.32 wt.-%; impurities: C_8 naphthenes 0.34 wt.-%; 3-methylheptane 0.12 wt.-%; n-heptane 0.04 wt.-%; other hydrocarbons 0.18 wt.-%). The mass of dry catalyst was always 0.5 g, and reactions were conducted at temperatures between 212 and 429 $^{\circ}\text{C}$. An n-octane partial pressure of 3 kPa was established by setting a saturator temperature of 33 to 34 $^{\circ}\text{C}$. The modified residence time $m_{\text{cat}} \cdot \dot{n}_{\text{reactant}}^{-1}$ amounted to 110 to 135 $\text{g}\cdot\text{h}\cdot\text{mol}^{-1}$, corresponding to *LHSV* values of 0.2 and 1.2 h^{-1} .

5.3.2 Isomerization of n-Nonane and n-Undecane

n-Nonane was isomerized on the bifunctional catalyst 0.52Pd/Na_{0.69}H_{0.31}-Y with a dry mass of 0.37 g. These experiments were done at ambient pressure in the flow-type apparatus described in Section 5.3.1.1. For metal reduction, the catalyst was heated in a hydrogen flow of 100 $\text{cm}^3\cdot\text{min}^{-1}$ from room temperature to 350 $^{\circ}\text{C}$ with a rate of 5 $\text{K}\cdot\text{min}^{-1}$, the temperature was held for 2 h. For the catalytic experiment, the reactor temperature, the total gas flow rate, the n-nonane partial pressure and the hydrogen partial pressure were 325 $^{\circ}\text{C}$, 70 $\text{cm}^3\cdot\text{min}^{-1}$, 2.9 kPa and 98.4 kPa, respectively (the

saturation temperature amounted to 54 °C). The isomerization product was collected in a cooling trap at -10 °C.

n-Undecane was isomerized on the same catalyst under identical conditions. To obtain an n-undecane partial pressure of 2.9 kPa the saturation temperature was increased to 98 °C.

5.3.3 Hydroconversion of n-Decane, Ethylcyclohexane, Butylcyclohexane, Perhydroindan, cis-Decalin, Spiro[4.5]decane and Methyl-decalin

5.3.3.1 Experimental Set-Up of the High-Pressure Flow-Type Apparatuses

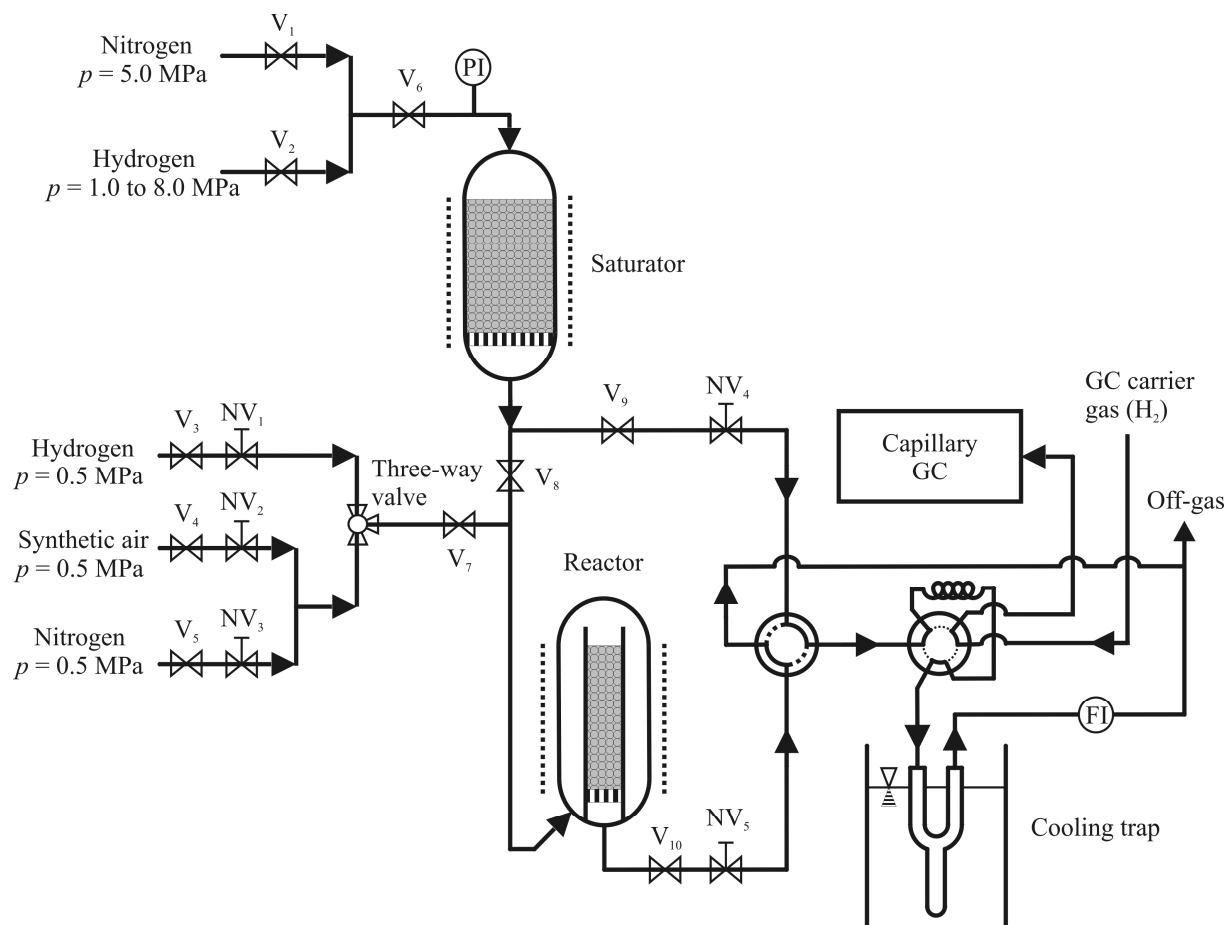


Figure 5.1: Scheme of the high-pressure flow-type apparatus used for the catalytic hydroconversion of n-decane, ethylcyclohexane, butylcyclohexane, perhydroindan, cis-decalin and methyldecalin (FI: flow indicator; GC: gas chromatograph; NV: needle valve; PI: pressure indicator).

The catalytic hydroconversion of n-decane, ethylcyclohexane, butylcyclohexane, perhydroindan, cis-decalin and methyldecalin was performed in a high-pressure flow-type apparatus which is shown in Figure 5.1 schematically. The main components were a saturator for the generation of a hydrogen/hydrocarbon mixture, a fixed-bed reactor and a gas sampling valve for the injection of a product sample into the capillary gas chromatograph. The saturator and the reactor were heated electrically and kept at a constant temperature by temperature controllers. To avoid condensation of

hydrocarbons, all pipes and valves downstream the saturator were heated electrically at *ca.* 180 °C, *i.e.* V₇ to V₁₀, NV₄, NV₅, the 4-port-2-position valve and the 6-port-2-position valve.

Hydrogen with a maximal pressure of 8.0 MPa was taken from a pressurized cylinder, equipped with a pressure regulator. *Via* valves V₂ and V₆, the hydrogen flow could be routed to the saturator. In the saturator, a fix-bed of Chromosorb was impregnated with the liquid hydrocarbon that was used in the respective catalytic experiment. In the fixed-bed, a thermocouple was mounted axially to measure the temperature in the saturator. The hydrogen flowing through the saturator was loaded with the hydrocarbon vapor. More details about the functionality of this type of saturator can be found in Ref. [77]. The hydrocarbon-loaded hydrogen could be routed either *via* V₉ to NV₄ where it was expanded to atmospheric pressure or through V₈ to the reactor. After the reactor the product mixture flowed through V₁₀ to NV₅ where it was expanded. In the 4-port-2-position valve either the stream coming directly from the saturator or the product stream coming from the reactor was routed to the 6-port-2-position gas sampling valve for GC analysis (see Section 5.4.1).

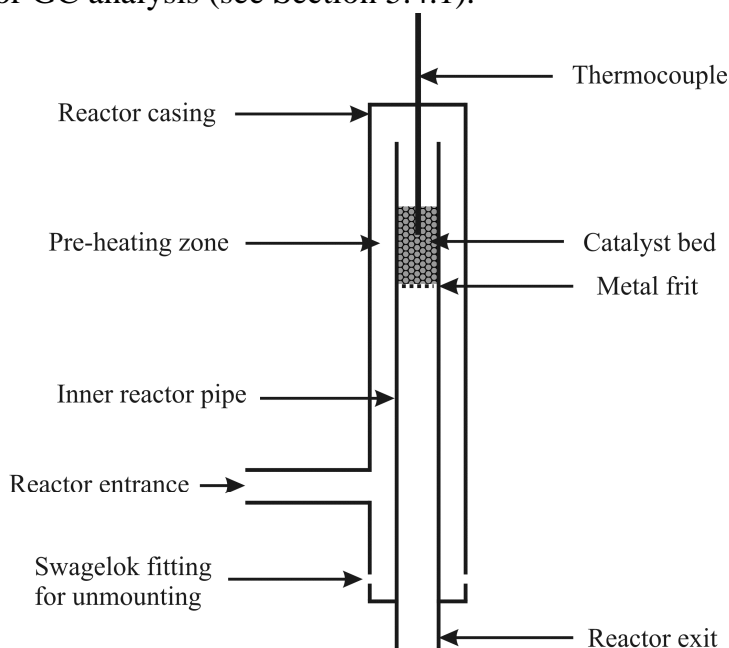


Figure 5.2: Schematic drawing of the fixed-bed reactor.

A schematic drawing of the fixed-bed reactor is shown in Figure 5.2. It was made from stainless steel and fittings purchased from Swagelok, allowing a maximal temperature of 500 °C and a maximal pressure of up to 10 MPa. The feed gas entered the reactor in the lower part and was preheated to the reaction temperature while flowing upwards. At the top, the reactant flow was routed downwards through the catalyst bed. By routing the exit gas from this gas sampling valve to a cooling trap at -10 °C, liquid

product samples were collected. These samples were used for qualitative product identification, while all quantitative evaluations were based on analyses of the gaseous samples which were injected into the GC by actuating the 6-port-2-position gas sampling valve.

For oxidative treatment of the catalyst or reduction of the noble metal on the catalyst, also synthetic air or hydrogen of lower pressure could be routed directly to the reactor. With valves V_3 or V_4 and the three-way valve the gas was selected and the flow rate was set with NV_1 or NV_2 . Nitrogen was routed through V_1 or V_5 for flushing the apparatus prior to experiments with hydrogen.

The catalytic apparatus was used for the following purposes:

- (i) Oxidative treatment of the catalyst precursor (Section 5.1.6): Valves V_4 , V_7 , V_{10} open; V_5 and V_8 closed; three-way valve open between synthetic air and reactor; flow rate was set with NV_2 while NV_5 was fully open.
- (ii) Reduction of the noble metal on the catalyst (Section 5.1.7): Valves V_3 , V_7 , V_{10} open; V_8 closed; three-way valve open between hydrogen and reactor; flow rate was set with NV_1 while NV_5 was fully open.
- (iii) Adjustment of the saturator temperature for the desired $n_{H_2} / n_{hydrocarbon}$ ratio: Valves V_2 , V_6 and V_9 open; V_1 and V_8 closed; flow rate was set with NV_4 .
- (iv) Hydroconversion of gaseous hydrogen/hydrocarbon mixtures in the fixed-bed reactor: Valves V_2 , V_6 , V_8 and V_{10} open; V_1 , V_7 and V_9 closed; flow rate was set with NV_5 .

5.3.3.2 Conditions in the Catalytic Experiments with n-Decane

In the catalytic experiments with n-decane (purity 99.70 wt.-%; impurities: other hydrocarbons 0.30 wt.-%) as feed hydrocarbon, the bulk volume of catalyst was 0.4 cm^3 corresponding to a dry mass of 0.17 to 0.20 g. The reaction temperature was varied between 230 and 430 °C. The total pressure was 5.0 MPa throughout, while the n-decane partial pressure at the reactor entrance was 15 kPa corresponding to a saturator temperature of 110 °C. An *LHSV* of 0.4 h^{-1} was applied. Two samples of the products were analyzed with the capillary gas chromatograph at each reaction temperature. The first sample was injected after 45 min time-on-stream and another

after 175 min time-on-stream. Usually, the integration results of the second analysis were used for the evaluation of the catalytic experiments.

In order to study the hydrogenolysis of branched decane isomers, a two-bed arrangement of an isomerization catalyst in the first catalyst bed and a hydrogenolysis catalyst in the second bed was applied. The two catalysts were separated by quartz glass wool and sea sand. The volumetric ratio of the bulk volumes was 1:1, and the *LHSV* of 0.4 h^{-1} was calculated for the combined bulk volume.

5.3.3.3 Conditions in the Catalytic Experiments with Ethylcyclohexane

In the experiments with ethylcyclohexane (purity 99.55 wt.-%; impurities: cyclohexane 0.11 wt.-%; methylcyclohexane 0.19 wt.-%; different C_7 - and C_8 -hydrocarbons 0.15 wt.-%) as feed hydrocarbon, the bulk volume of catalyst was 0.4 cm^3 corresponding to a dry mass of 0.17 g. The reaction temperature was varied between 270 and 410 °C. The total pressure was 5.2 MPa throughout, while the ethylcyclohexane partial pressure at the reactor entrance was 18 kPa corresponding to a saturator temperature of 86 °C. An *LHSV* of 0.4 h^{-1} was applied. Two samples of the products were analyzed with the capillary gas chromatograph at each reaction temperature. The first sample was injected after 45 min time-on-stream and another after 155 min time-on-stream. Usually, the integration results of the second analysis were used for the evaluation of the catalytic experiments.

5.3.3.4 Conditions in the Catalytic Experiments with Butylcyclohexane

In the catalytic experiments with butylcyclohexane (purity 99.30 wt.-%; impurities: tert-butylcyclohexane 0.18 wt.-%, 1-methyl-2-propylcyclohexane 0.15 wt.-%, other hydrocarbons, mainly C_{10} 0.37 wt.-%) as feed hydrocarbon, the bulk volume of catalyst was 0.4 cm^3 corresponding to a dry mass of 0.17 to 0.21 g. The reaction temperature was varied between 230 and 410 °C. The total pressure was 5.0 MPa throughout, while the butylcyclohexane partial pressure at the reactor entrance was 16 kPa corresponding to a saturator temperature of 117 °C. An *LHSV* of 0.4 h^{-1} was applied. Two samples of the products were analyzed with the capillary gas chromatograph at each reaction temperature. The first sample was injected after 45 min time-on-stream and another after 205 min time-on-stream. Usually, the integration results of the second analysis were used for the evaluation of the catalytic experiments.

Also the hydrogenolysis of skeletal isomers of butylcyclohexane was studied. A two-bed arrangement of an isomerization catalyst in the first catalyst bed and a hydrogenolysis catalyst in the second bed was applied. The two catalysts were separated by quartz glass wool and sea sand. The volumetric ratio of the bulk volumes was 1:1, and the *LHSV* of 0.4 h^{-1} was calculated for the combined bulk volume.

5.3.3.5 Conditions in the Catalytic Experiments with Perhydroindan

In the experiments with perhydroindan (purity 96.70 wt.-%; cis-isomer 67.40 wt.-%; trans-isomer 29.30 wt.-%; impurities: C_7 , C_8 and C_9 hydrocarbons 0.70 wt.-%; C_{10} and C_{11} hydrocarbons 2.60 wt.-%) as feed hydrocarbon, the bulk volume of catalyst was 0.4 cm^3 corresponding to a dry mass of 0.17 g. Except for the experiments at different hydrogen pressures (see Section 9.8.1), the total pressure was 5.2 MPa, while the perhydroindan partial pressure at the reactor entrance was 18 kPa corresponding to a saturator temperature of $116 \text{ }^\circ\text{C}$. In these experiments the reaction temperature was varied between 210 and $430 \text{ }^\circ\text{C}$. An *LHSV* of 0.4 to 0.5 h^{-1} was applied. Two samples of the products were analyzed with the capillary gas chromatograph at each reaction temperature. The first sample was injected after 45 min time-on-stream and another after 205 min time-on-stream. Usually, the integration results of the second analysis were used for the evaluation of the catalytic experiments.

In addition, with catalyst 2.69Pt/silica experiments at different hydrogen pressures were conducted. In order to identify the influence of the hydrogen partial pressure only, all other experimental parameters were kept constant. Therefore, the partial pressure of perhydroindan and the *LHSV* were kept constant at 20 kPa and 0.4 h^{-1} , respectively. The mass of dry catalyst was always 0.17 g and the mass flow rate of perhydroindan was adjusted to $0.139 \text{ g}\cdot\text{h}^{-1}$. According to the Poynting correction [78], an increase of the total pressure in a system leads to an increased partial pressure of a liquid phase at a given temperature. To realize a constant partial pressure of perhydroindan at varying hydrogen pressure, the saturator temperature had to be increased with decreasing hydrogen pressure in the range of 115 to $120 \text{ }^\circ\text{C}$. The reaction temperature was varied between 290 and $410 \text{ }^\circ\text{C}$, and the total pressure was varied between 1.0 and 8.0 MPa.

5.3.3.6 Conditions in the Catalytic Experiments with cis-Decalin

In the experiments with cis-decalin (purity 98.39 wt.-%; impurities: trans-decalin 1.14 wt.-%; skeletal isomers of decalin and hydrocarbons with more than ten carbon

atoms 0.47 wt.-%) as feed hydrocarbon, the bulk volume of catalyst was 0.4 cm³ corresponding to a dry mass of 0.17 g. Except for the experiments at different hydrogen pressures (see Section 9.8.2), the total pressure was 5.2 MPa throughout. In these experiments the reaction temperature was varied between 290 and 410 °C while the cis-decalin partial pressure at the reactor entrance was 16 kPa corresponding to a saturator temperature of 136 °C. An *LHSV* of 0.4 h⁻¹ was applied. Two samples of the products were analyzed with the capillary gas chromatograph at each reaction temperature. The first sample was injected after 45 min time-on-stream and another after 205 min time-on-stream. Usually, the integration results of the second analysis were used for the evaluation of the catalytic experiments. In separate time-on-stream experiments with catalysts 2.73Ir/silica and 2.69Pt/silica the first sample was injected after 4 h time-on-stream and the last one after ca. 70 h.

In addition, with catalyst 2.73Ir/silica experiments at different hydrogen pressures were conducted. In order to identify the influence of the hydrogen partial pressure only, all other experimental parameters were kept constant. Therefore, the partial pressure of cis-decalin and the *LHSV* were kept constant at 18 kPa and 0.4 h⁻¹, respectively. The mass of dry catalyst was always 0.17 g and the mass flow rate of cis-decalin was adjusted to 0.140 g·h⁻¹. As described for perhydroindan in Section 5.3.3.5, also the partial pressure of cis-decalin vapors over a liquid phase depends on the total pressure [78]. To realize a constant partial pressure of cis-decalin at varying hydrogen pressure, the saturator temperature had to be increased with decreasing hydrogen pressure in the range of 133 to 140 °C. The reaction temperature was varied between 200 and 350 °C, and the total pressure was varied between 1.0 and 8.0 MPa.

5.3.3.7 Conditions in the Catalytic Experiments with Spiro[4.5]decane

In the experiments with spiro[4.5]decane (purity 98.17 wt.-%; impurities: spiro[4.5]decan-6-on 1.13 wt.-%, 1-cyclohexylcyclohexene 0.27 wt.-%, toluene 0.23 wt.-%, C₁₀ naphthenes 0.20 wt.-%) as feed hydrocarbon, the bulk volume of catalyst was 0.4 cm³ corresponding to a dry mass of 0.16 to 0.18 g. The reaction temperature was varied between 200 and 360 °C. The total pressure was 5.0 MPa throughout, while the spiro[4.5]decane partial pressure at the reactor entrance was 16 kPa corresponding to a saturator temperature of 121 °C. An *LHSV* of 0.4 h⁻¹ was applied. One product sample was analyzed with the capillary gas chromatograph at each reaction temperature after at least 45 min time-on-stream and used for the evaluation of the catalytic experiments.

5.3.3.8 Conditions in the Catalytic Experiments with Methyldecalin

In the catalytic experiments with methyldecalin (purity 99.30 wt.-%; impurities: mainly C₁₀- and C₁₁-hydrocarbons 0.70 wt.-%) as feed hydrocarbon, the bulk volume of catalyst was 0.4 cm³ corresponding to a dry mass of 0.17 g. The reaction temperature was varied between 270 and 410 °C. The total pressure was 5.2 MPa throughout, while the methyldecalin partial pressure at the reactor entrance was 16 kPa corresponding to a saturator temperature of 148 °C. An *LHSV* of 0.4 h⁻¹ was applied. Two samples of the products were analyzed with the capillary gas chromatograph at each reaction temperature. The first sample was injected after 45 min time-on-stream and another after 275 min time-on-stream. Usually, the integration results of the second analysis were used for the evaluation of the catalytic experiments. More details concerning the different isomers of methyldecalin in the feed hydrocarbon will be given in Section 5.5.1.8.

5.4 Product Analysis by Capillary Gas Chromatography

5.4.1 On-line Gas Chromatography

The entire quantitative evaluation of the catalytic experiments was based on the on-line GC analyses of the full product samples that were injected *via* a gas sampling valve. The products obtained in the n-octane hydroconversion were analyzed in a Hewlett-Packard 5890 Series II instrument equipped with an HP/Agilent Chemstation. Details of the analytical conditions are shown in Table 5.5.

Table 5.5: Conditions in the capillary gas chromatograph used for the analysis of products obtained in the hydroconversion of n-octane.

Column	SGE BP1-PONA
Stationary phase	Dimethyl polysiloxane
Length	50 m
Internal diameter	0.15 mm
Film thickness	0.5 μm
Temperature program	5 min at 35 °C; heating with 1 K·min ⁻¹ to 70 °C
Carrier gas	Hydrogen
Pressure at column entrance	200 kPa
Flow through column	0.56 cm ³ min ⁻¹
Injection	<i>via</i> gas sampling loop
Volume of sampling loop	250 mm ³
Split ratio	26 : 1
Injector temperature	180 °C
Detector	Flame ionization detector (FID)
Temperature	400 °C
\dot{V}_{H_2} to FID	47 cm ³ ·min ⁻¹
\dot{V}_{air} to FID	350 cm ³ ·min ⁻¹

The products obtained in the hydroconversion of n-decane, ethylcyclohexane, butylcyclohexane, perhydroindan, cis-decalin (except for the time-on-stream experiments) and methyldecalin were analyzed in a Hewlett-Packard HP 6890N instrument equipped with an Agilent Chemstation. Details of the analytical conditions are shown in Table 5.6.

Table 5.6: Conditions in the capillary gas chromatograph used for the analysis of products obtained in the hydroconversion of n-decane, ethylcyclohexane, butylcyclohexane, perhydroindan, cis-decalin (except for the time-on-stream experiments) and methyldecalin.

Column	Petrocol DH 150
Stationary phase	Dimethyl polysiloxane
Length	150 m
Internal diameter	0.25 mm
Film thickness	1.0 μm
Carrier gas	Hydrogen
Pressure at column entrance	193 kPa
Flow through column	1.5 $\text{cm}^3 \cdot \text{min}^{-1}$
Injection	<i>via</i> gas sampling loop
Volume of sampling loop	250 mm^3
Split ratio	5 : 1
Injector temperature	250 $^{\circ}\text{C}$
Detector	Flame ionization detector (FID)
Temperature	250 $^{\circ}\text{C}$
\dot{V}_{H_2} to FID	40 $\text{cm}^3 \cdot \text{min}^{-1}$
\dot{V}_{air} to FID	450 $\text{cm}^3 \cdot \text{min}^{-1}$

In the hydroconversion of perhydroindan and cis-decalin at $p_{\text{H}_2} = 1.0$ and 2.0 MPa a split ratio of 40 : 1 was set.

In Table 5.7 the different temperature programs are listed that were applied for the different feed hydrocarbons.

Table 5.7: Temperature programs of the capillary gas chromatograph that were applied for the different feed hydrocarbons.

Feed Hydrocarbon	Temperature Program
n-Decane	10 min at 35 °C; heating with 1 K·min ⁻¹ to 100 °C; heating with 0.5 K·min ⁻¹ to 125 °C
Ethylcyclohexane	10 min at 35 °C; heating with 1 K·min ⁻¹ to 100 °C; heating with 0.5 K·min ⁻¹ to 115 °C
Perhydroindan, butylcyclohexane, cis-decalin, spiro[4.5]decane	10 min at 35 °C; heating with 1 K·min ⁻¹ to 100 °C; heating with 0.5 K·min ⁻¹ to 140 °C; holding for 1 min
Methyldecalin	10 min at 35 °C; heating with 1·K·min ⁻¹ to 100 °C; heating with 0.5 K·min ⁻¹ to 140 °C; holding for 15 min; heating with 1 K·min ⁻¹ to 200 °C

The products obtained in the time-on-stream experiments with cis-decalin and in the hydroconversion of spiro[4.5]decane were analyzed in an Agilent 7890A instrument equipped with an Agilent Chemstation. In this GC identical analytical conditions as shown in Table 5.6 were applied, except for the gas flow rates in the FID which were $\dot{V}_{\text{H}_2} = 40 \text{ cm}^3 \cdot \text{min}^{-1}$ and $\dot{V}_{\text{air}} = 450 \text{ cm}^3 \cdot \text{min}^{-1}$.

5.4.2 Off-line Gas Chromatography / Mass Spectrometry

The integral liquid product samples collected in the cooling trap were used for qualitative peak assignment *via* ancillary off-line GC/MS analyses. A second gas chromatograph (Agilent 6890N) which was also equipped with a Supelco Petrocol DH 150 capillary column and coupled to a mass spectrometer (Agilent 5876B inert XL MSD) was used for this purpose. Details of the analytical conditions are shown in Table 5.8.

Table 5.8: Conditions in the ancillary capillary gas chromatograph coupled with mass spectrometry.

Column	Petrocol DH 150
Stationary phase	Dimethyl polysiloxane
Length	150 m
Internal diameter	0.25 mm
Film thickness	1.0 μm
Temperature program	10 min at 35 °C; heating with 1 K·min ⁻¹ to 100 °C; heating with 0.5 K·min ⁻¹ to 180 °C; holding for 100 min
Carrier gas	Helium
Pressure at column entrance	177 kPa
Flow through column	1.5 cm ³ ·min ⁻¹
Injection	liquid sample <i>via</i> syringe
Injected volume	0.1 mm ³
Split ratio	5 : 1
Injector temperature	250 °C
Detector	Flame ionization detector (FID)
Temperature	250 °C
\dot{V}_{H_2} to FID	35 cm ³ ·min ⁻¹
\dot{V}_{air} to FID	450 cm ³ ·min ⁻¹
Mass spectrometer	Electron ionization
Acceleration voltage	70 eV
Temperature of ion source	230 °C
Temperature of quadrupole analyzer	150 °C

5.5 Evaluation of the Catalytic Experiments

5.5.1 Terminology of the Reactions and Products

With an increasing number of carbon atoms and rings in a feed hydrocarbon the reaction network of its hydroconversion can become more and more complex. Hence, the reactions and products obtained with different feed hydrocarbons were classified as described in the following subsections. In some experiments, especially at high reaction temperatures, small amounts of unsaturated products were formed which are

not described by the product groups C₈ aromatics, E-Bz, B-Bz or DHPs (*vide infra*). They were treated like the corresponding saturated hydrocarbons. Benzene or Pentylbenzene, for example, were treated as cyclohexane or pentylcyclopentane, respectively.

5.5.1.1 Hydroconversion of n-Octane

In the n-octane hydroconversion at the given reaction conditions four different kinds of reactions can occur. These are listed in Table 5.9 together with the products and designations of the product groups.

Table 5.9: Reactions and products occurring in the catalytic hydroconversion of n-octane (n-Oc).

Reaction	Products	Formula	Short Designation
Isomerization	Skeletal isomers	C ₈ H ₁₈	sk-Isos
Dehydrocyclization	One-ring naphthenes with 8 carbon atoms (ring closure products)	C ₈ H ₁₆	RCPs
Aromatization	Aromatic hydrocarbons with 8 carbon atoms	C ₈ H ₁₀	C ₈ aromatics
Hydrocracking	Hydrocarbons with less than 8 carbon atoms		C ₇ -

5.5.1.2 Hydroconversion of n-Decane

Three different kinds of reactions can occur in the n-decane hydroconversion at the given reaction conditions. No aromatic hydrocarbons were detected due to the high hydrogen pressure of 5.0 MPa. In Table 5.10 the reactions are listed together with the products and designations of the product groups.

Table 5.10: Reactions and products occurring in the catalytic hydroconversion of n-decane (n-De).

Reaction	Products	Formula	Short Designation
Isomerization	Skeletal isomers	$C_{10}H_{22}$	sk-Isos
Dehydrocyclization	One-ring naphthenes with 10 carbon atoms (ring closure products)	$C_{10}H_{20}$	RCPs
Hydrocracking	Hydrocarbons with less than 10 carbon atoms		C ₉ -

5.5.1.3 Hydroconversion of Ethylcyclohexane

In the hydroconversion of ethylcyclohexane four different kinds of reactions can occur at the given reaction conditions. These are listed in Table 5.11 together with the products and designations of the product groups.

Table 5.11: Reactions and products occurring in the catalytic hydroconversion of ethylcyclohexane (E-CHx).

Reaction	Products	Formula	Short Designation
Isomerization	Skeletal isomers	C_8H_{16}	sk-Isos
Ring opening	Open-chain octanes	C_8H_{18}	OCOs
Dehydrogenation	Ethylbenzene	C_8H_{10}	E-Bz
Hydrocracking	Hydrocarbons with less than 8 carbon atoms		C ₇ -

5.5.1.4 Hydroconversion of Butylcyclohexane

Also in the hydroconversion of butylcyclohexane four different kinds of reactions can occur. They are listed in Table 5.12 together with the products and designations of the product groups.

Table 5.12: Reactions and products occurring in the catalytic hydroconversion of butylcyclohexane (B-CHx).

Reaction	Products	Formula	Short Designation
Isomerization	Skeletal isomers	$C_{10}H_{20}$	sk-Isos
Ring opening	Open-chain decanes	$C_{10}H_{22}$	OCDs
Dehydrogenation	Butylbenzene	$C_{10}H_{14}$	B-Bz
Hydrocracking	Hydrocarbons with less than 10 carbon atoms		C_9-

5.5.1.5 Hydroconversion of Perhydroindan

The feed hydrocarbon perhydroindan (bicyclo[4.3.0]nonane) was a mixture of cis-(c-PHI) and trans-perhydroindan (tr-PHI) which were lumped to a single pseudo-reactant perhydroindan (PHI). In its hydroconversion five different kinds of reactions can occur at the given reaction conditions. They are listed in Table 5.13 together with the products and designations of the product groups.

Table 5.13: Reactions and products occurring in the catalytic hydroconversion of perhydroindan (PHI).

Reaction	Products	Formula	Short Designation
Isomerization	Skeletal isomers	C_9H_{16}	sk-Isos
Ring opening	Ring-opening products (i) alkylcyclohexanes (ii) alkylcyclopentanes	C_9H_{18}	ROPs CHx-ROPs CPn-ROPs
Double ring opening	Open-chain nonanes	C_9H_{20}	OCNs
Dehydrogenation	Dehydrogenated products (i) indan (ii) indene	C_9H_{10} C_9H_8	DHPs
Hydrocracking	Hydrocarbons with less than 9 carbon atoms		C_8-

Hydrocarbons with more than nine carbon atoms are impurities in the reactant and not formed by catalytic conversion. Hence, selectivities and yields of products are calculated without incorporating these hydrocarbons.

5.5.1.6 Hydroconversion of cis-Decalin

Five different kinds of reactions can occur in the hydroconversion of cis-decalin (cis-bicyclo[4.4.0]decane). In Table 5.14 the reactions that occur at the given reaction conditions are listed, together with the products and designations of product groups. The isomerization to trans-decalin was very fast, hence, this stereoisomer of the reactant was classified as unconverted decalin. In this work, a mixture of cis- and trans-decalin is always lumped as decalin (Dec).

Table 5.14: Reactions and products occurring in the catalytic hydroconversion of cis-decalin (c-Dec).

Reaction	Products	Formula	Short Designation
Isomerization	Isomers	$C_{10}H_{18}$	
	(i) trans-decalin		
Ring opening	(ii) skeletal isomers	$C_{10}H_{20}$	sk-Isos
	Ring-opening products		
Double ring opening	(i) alkylcyclohexanes	$C_{10}H_{22}$	OCDs
	(ii) alkylcyclopentanes		
Dehydrogenation	Open-chain decanes	$C_{10}H_{12}$	DHPs
	Dehydrogenated products		
Hydrocracking	(i) tetralin	$C_{10}H_{12}$	C_9-
	(ii) naphthalene	$C_{10}H_8$	
	Hydrocarbons with less than 10 carbon atoms		

5.5.1.7 Hydroconversion of Spiro[4.5]decane

Four different kinds of reactions can occur in the hydroconversion of spiro[4.5]decane at the given reaction conditions. These are listed in Table 5.15 together with the products and designations of the product groups.

Table 5.15: Reactions and products occurring in the catalytic hydroconversion of spiro[4.5]decane (spiro).

Reaction	Products	Formula	Short Designation
Isomerization	Skeletal isomers	C ₁₀ H ₁₈	sk-Isos
Ring opening	Ring-opening products (i) alkylcyclohexanes (ii) alkylcyclopentanes	C ₁₀ H ₂₀	ROPs
Double ring opening	Open-chain decanes	C ₁₀ H ₂₂	OCDs
Hydrocracking	Hydrocarbons with less than 10 carbon atoms		C ₉ -

5.5.1.8 Hydroconversion of Methyldecalin

Besides 0.70 wt.-% impurities (see Section 5.3.3.8), the feed hydrocarbon methyldecalin was a mixture of ten different diastereoisomeric and constitutional isomers. By GC/MS the signals of these compounds could not be assigned to specific isomers. Theoretically, three different positions of the methyl group are possible, *viz.* 1-methyldecalin, 2-methyldecalin and 4a-methyldecalin. When considering all possible diastereoisomers, as shown in Figure 5.3, ten different isomers result which could be separable by gas chromatography.

By GC/MS, in addition, two other compounds of the product mixture that were not contained in the feed hydrocarbon have been assigned to methyldecalin. Hence, all 12 signals that were assigned to 1-, 2- and 4a-methyldecalin and its diastereomers were lumped as methyldecalin (M-Dec). The five different reactions and products that occur in the hydroconversion of methyldecalin at the given reaction conditions are listed in Table 5.16 together with the designation of product groups.

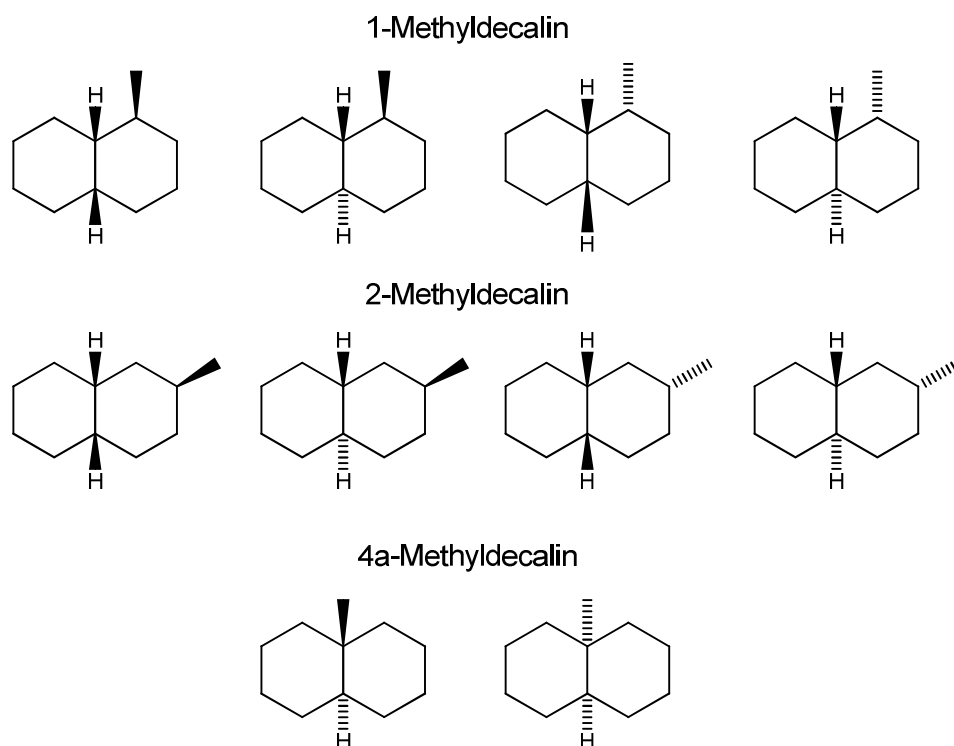


Figure 5.3: All ten possible diastereomers of 1-methyldecalin, 2-methyldecalin and 4a-methyldecalin.

Table 5.16: Reactions and products occurring in the catalytic hydroconversion of methyldecalin (M-Dec).

Reaction	Products	Formula	Short Designation
Isomerization	Skeletal isomers	$C_{11}H_{20}$	sk-Isos
Ring opening	Ring-opening products (i) alkylcyclohexanes (ii) alkylcyclopentanes	$C_{11}H_{22}$	ROPs
Double ring opening	Open-chain undecanes	$C_{11}H_{24}$	OCUs
Dehydrogenation	Dehydrogenated products (i) methyltetralin (ii) methylnaphthalene	$C_{11}H_{14}$ $C_{11}H_{10}$	DHPs
Hydrocracking	Hydrocarbons with less than 11 carbon atoms		C_{10}^-

5.5.2 Assignment of the GC Signals

The main method for peak assignment in chromatograms was the GC/MS analysis of the liquid products of the catalytic experiments collected in the cooling trap. Some product signals could not be assigned to a specific hydrocarbon but it was possible to identify the molar mass. This molar mass allowed an assignment of the products to the different product groups that are given in Section 5.5.1.

Moreover, when a hydrocarbon was commercially available, it was co-injected with the liquid product of the cooling trap. Iso-alkanes that were obtained in the hydroconversion of the respective n-alkanes were also co-injected with the liquid product mixture of the catalytic experiments. The isomerization of n-octane, n-nonane, n-decane and n-undecane is described in Section 5.3.1, Section 5.3.2, Ref. [74] and Section 5.3.2, respectively.

The peak assignments for the products obtained in the experiments with the different feed hydrocarbons are tabulated in the Appendix 12.1.

5.5.3 Conversions, Yields and Selectivities

The general equations for the calculation of the conversion of a feed hydrocarbon X_{feed} , yields of products Y_j and selectivities of products S_j in a continuously operated fix-bed reactor are shown in Eqs. (5.1) to (5.3):

$$X_{\text{feed}} = \frac{(\dot{n}_{\text{feed}})_{\text{in}} - (\dot{n}_{\text{feed}})_{\text{out}}}{(\dot{n}_{\text{feed}})_{\text{in}}} \quad (5.1)$$

$$Y_{\text{feed}} = \frac{(\dot{n}_j)_{\text{out}} - (\dot{n}_j)_{\text{in}}}{(\dot{n}_{\text{feed}})_{\text{in}}} \cdot \frac{|\nu_{\text{feed}}|}{\nu_j} \quad (5.2)$$

$$S_{\text{feed}} = \frac{(\dot{n}_j)_{\text{out}} - (\dot{n}_j)_{\text{in}}}{(\dot{n}_{\text{feed}})_{\text{in}} - (\dot{n}_{\text{feed}})_{\text{out}}} \cdot \frac{|\nu_{\text{feed}}|}{\nu_j} \quad (5.3)$$

The molar fluxes $(\dot{n}_{\text{feed}})_{\text{out}}$ and $(\dot{n}_j)_{\text{out}}$ can be calculated directly from the areas of the respective signals in the gas chromatogram under incorporation of the compound-specific FID correction factors f of the respective feed hydrocarbon or products (see Appendix 12.2.2.2). More details on the calculation of X_{feed} , Y_j and S_j are given in the Appendix 12.1. Finally, in Eqs. (5.4) to (5.6) the resulting equations are presented.

$$X_{\text{feed}} = \frac{\sum_j \frac{|v_{\text{feed}}|}{v_j} \cdot \frac{M_{\text{feed}}}{M_j} \cdot f_j \cdot A_j}{f_{\text{feed}} \cdot A_{\text{feed}} + \sum_j \frac{|v_{\text{feed}}|}{v_j} \cdot \frac{M_{\text{feed}}}{M_j} \cdot f_j \cdot A_j} \quad (5.4)$$

$$Y_j = \frac{f_j \cdot A_j}{f_{\text{feed}} \cdot A_{\text{feed}} + \sum_j \frac{|v_{\text{feed}}|}{v_j} \cdot \frac{M_{\text{feed}}}{M_j} \cdot f_j \cdot A_j} \cdot \frac{|v_{\text{feed}}|}{v_j} \cdot \frac{M_{\text{feed}}}{M_j} \quad (5.5)$$

$$S_j = \frac{f_j \cdot A_j}{\sum_j \frac{|v_{\text{feed}}|}{v_j} \cdot \frac{M_{\text{feed}}}{M_j} \cdot f_j \cdot A_j} \cdot \frac{|v_{\text{feed}}|}{v_j} \cdot \frac{M_{\text{feed}}}{M_j} \quad (5.6)$$

Although hydrocracked products, *i.e.* hydrocarbons with a smaller number of carbon atoms than the reactant, are undesired in the ring opening of naphthenes, their composition can furnish valuable mechanistic information. Of particular interest were the quantitative carbon-number distribution and also the detailed composition of these products. For this purpose, the modified hydrocracking selectivity is defined as the molar amount of hydrocarbons with *j* carbon atoms formed divided by the molar amount of reactant converted into hydrocracked products. In Eq. (5.7) the final equation for S_j^* is given while a detailed calculation is described in the Appendix 12.2.5.

$$S_j^* = \frac{(\dot{n}_j)_{\text{out}}}{(\dot{n}_{\text{feed}})_{\text{converted into hydrocracked products}}} = \frac{f_j \cdot A_j}{\sum_j \frac{|v_{\text{feed}}|}{v_j} \cdot \frac{M_{\text{feed}}}{M_j} \cdot f_j \cdot A_j} \cdot \frac{M_{\text{feed}}}{M_j} \quad (5.7)$$

5.5.4 Liquid Hourly Space Velocity

The liquid hourly space velocity (*LHSV*, see Eq. (5.8)) is defined as the volumetric hourly flow rate of the liquid reactant at room temperature and 0.10 MPa divided by the bulk volume of the catalyst $V_{\text{cat, bulk}}$.

$$LHSV = \frac{\dot{V}_{\text{feed, liquid, RT}}}{V_{\text{cat, bulk}}} \quad (5.8)$$

In all catalytic experiments with n-decane, ethylcyclohexane, butylcyclohexane, perhydroindan, cis-decalin, spiro[4.5]decane and methyldecalin a constant *LHSV* of *ca.* 0.4 h^{-1} was set. The bulk volume of the catalyst was always 0.4 cm^3 . For the determination of the volumetric flow rate of the feed hydrocarbon, the mass of the hydrocarbon collected in the cooling trap during one hour was measured, while the hydrogen flow-rate, the hydrogen pressure and the saturator temperature were constant (see Section 5.3.3.1). With the density of the hydrocarbon, $\dot{V}_{\text{feed,liquid,RT}}$ was calculated and assumed values of *ca.* $0.16 \text{ cm}^3 \cdot \text{h}^{-1}$.

6 Characterization of the Catalyst Precursors and Catalysts

6.1 Zeolite Y

Powder X-ray diffractograms of zeolite Na-Y (not shown) prior to the ion exchange with NH_4NO_3 were in agreement with simulated spectra [79]. After the ion exchange with NH_4NO_3 and $[\text{Pd}(\text{NH}_3)_4]\text{Cl}_2$, followed by calcination, the same reflexes were again observed and no additional ones were found. Hence, the zeolite hat retained its structure.

6.2 Silica

In Figure 6.1 the SEM images of silica are depicted. There, agglomerates of diameters up to *ca.* 20 μm are visible. They seem to be comprised of smaller particles that cannot be resolved with the available equipment. According to the manufacturer the average primary particle size assumes a value of 7 nm.

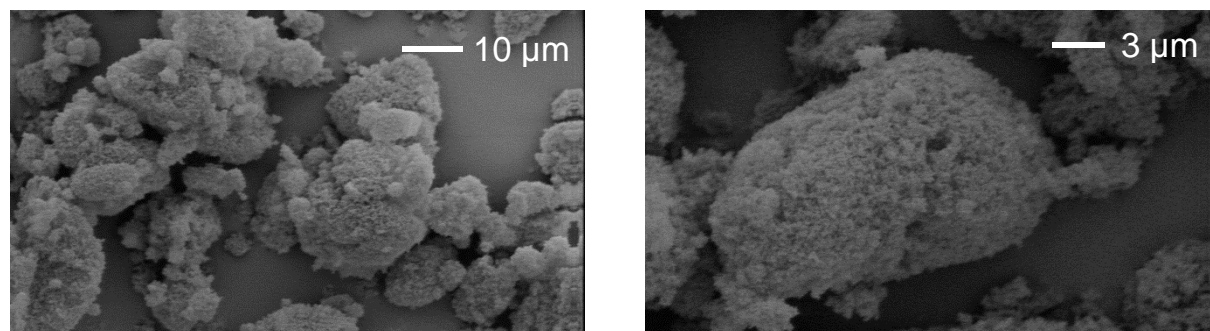


Figure 6.1: SEM images of silica.

Due to the high dispersion of silica, the material had to be pelletized (see Section 5.1.5) prior to nitrogen physisorption. A high specific surface area of $A_{\text{BET}} = 391 \text{ m}^2 \cdot \text{g}^{-1}$ and a pore volume of $1.07 \text{ cm}^3 \cdot \text{g}^{-1}$ were obtained for this amorphous material.

An adsorption of pyridine on a Brønsted acid site results in a characteristic ring vibration mode which corresponds to an adsorption at 1545 cm^{-1} . By FT-IR measurements with pyridine as probe molecule no absorption band at 1545 cm^{-1} was detected, neither on the silica support without noble metal, nor on 2.68Pt/silica. Hence, no Brønsted acid sites of sufficient strength for the protonation of pyridine exist on this catalyst as consequently on all other silica-supported catalysts.

6.3 [Si]SBA-15

The powder X-ray diffractograms of [Si]SBA-15 (a) before and (b) after removal of the template are shown in Figure 6.2. They correspond to the diffractograms from literature [10] with a shift of the reflexes to higher 2θ values after the calcination. This shift indicates a reduction of the cell parameters according to Bragg's law.

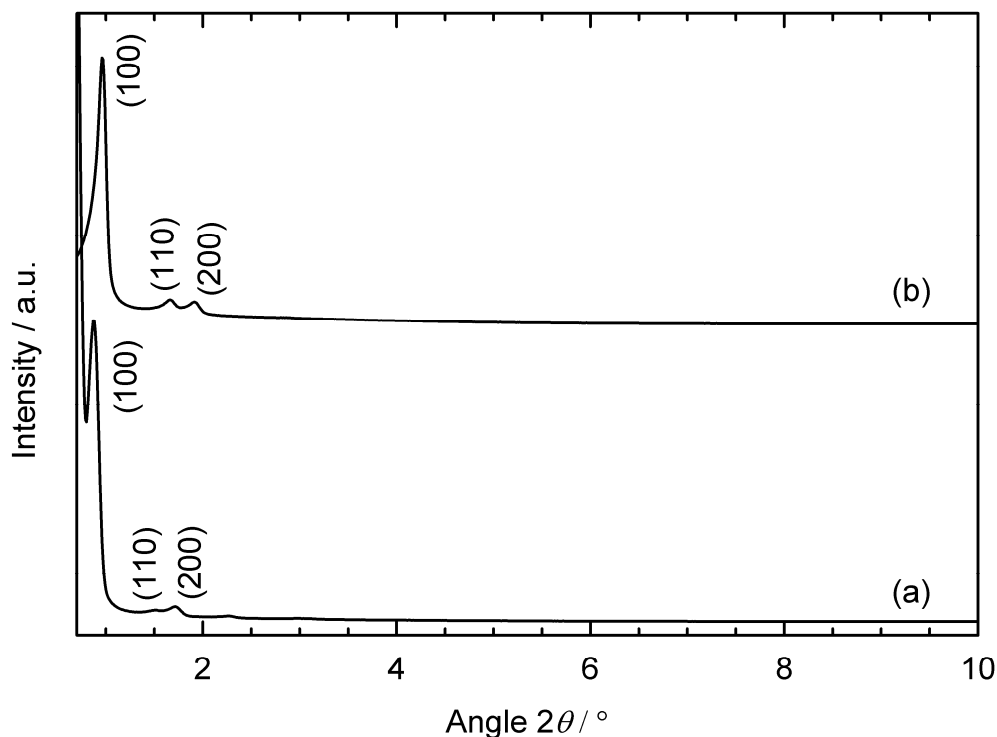


Figure 6.2: X-ray diffractograms of [Si]SBA-15 (a) as synthesized and (b) after removal of the template by calcination together with the assignment of reflexes according to Ref. [10].

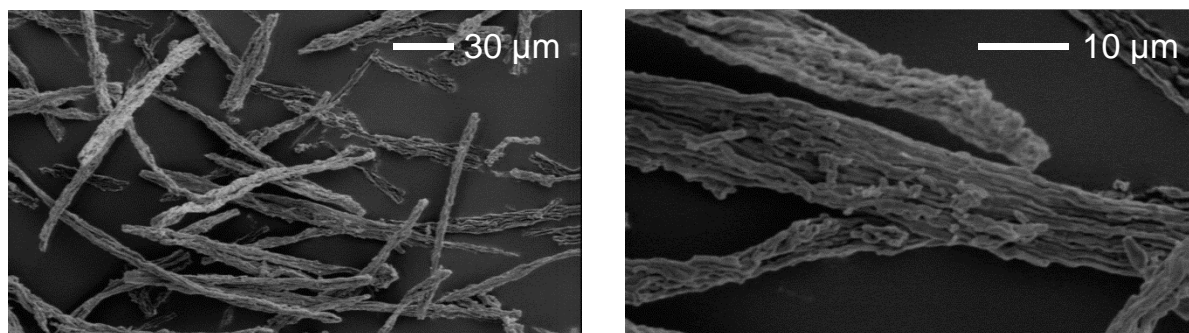


Figure 6.3: SEM images of [Si]SBA-15 after calcination.

In Figure 6.3 the SEM images of [Si]SBA-15 after calcination show stick-shaped crystallites with a length of *ca.* 90 μm and a diameter of *ca.* 10 μm . There is no further solid phase observable, proving phase purity of the sample. The morphology is

roughly the same as reported in Ref. [10]. Nitrogen physisorption experiments proved that a highly porous material was obtained with $A_{\text{BET}} = 740 \text{ m}^2 \cdot \text{g}^{-1}$ and a pore volume of $0.96 \text{ cm}^3 \cdot \text{g}^{-1}$.

6.4 Metal Dispersions of the Catalysts

In Table 6.1 the dispersions of the noble metals and particle size of the metal clusters on all silica- and [Si]SBA-15-supported catalysts are listed as determined by hydrogen chemisorption. A general trend of an increase of dispersion in the order $\text{Pd} < \text{Rh} < \text{Pt} < \text{Ir}$ can be observed, in qualitative accordance with literature data [80-82]. The values for the iridium dispersion above unity could have their origin in a real adsorption stoichiometry higher than the anticipated one, i.e. $n_{\text{H}} / n_{\text{Ir}} > 1$ [80].

Table 6.1: Metal dispersion and metal particle size of the silica- and [Si]SBA-15-supported catalysts as determined by hydrogen chemisorption.

Catalyst	Metal Dispersion	Metal Particle Size / nm
0.73Ir/[Si]SBA-15	1.41	0.70
0.77Ir/silica	1.52	0.65
1.02Ir/silica	1.09	0.91
2.59Ir/silica	1.02	0.97
2.73Ir/silica	1.18	0.84
0.92Pt/[Si]SBA-15	0.84	1.34
0.91Pt/silica	0.76	1.50
0.93Pt/silica	0.99	1.14
2.68Pt/silica	0.64	1.77
2.69Pt/silica	0.68	1.68
0.60Pd/silica	0.15	7.66
0.96Rh/silica	0.57	1.93
1.03Rh/silica	0.17	6.38

Differences in the noble metal dispersions on the two rhodium catalysts of similar metal content stem from differing preparation methods. The 0.96Rh/silica catalyst was prepared by SEA and a mild oxidative treatment at $T = 150 \text{ }^\circ\text{C}$, to obtain a high dispersion as recommended for Pt/silica [13]. In contrast, to form catalyst

1.03Rh/silica with a low metal dispersion, rhodium was loaded *via* impregnation, and calcination was done at $T = 700$ °C.

7 Preliminary Experiments

7.1 Co-Injection of n-Alkane Isomers

In the catalytic conversion of hydrocarbons with hydrogen, the product mixture becomes more and more complex with increasing number of carbon atoms and naphthenic rings in the feed hydrocarbon. From an applicative point of view, open-chain alkanes with the same number of carbon atoms as the reactant are the most desirable products in the hydroconversion of naphthenes due to their high cetane numbers. One method for the peak assignment of these open-chain alkanes in the gas chromatogram is the co-injection of a liquid mixture of iso-alkanes with the liquid product mixture obtained in the hydroconversion of a naphthene. Such mixtures of iso-alkanes were generated in the test reaction with n-octane on the bifunctional reference catalyst $0.52\text{Pd}/\text{Na}_{0.69},\text{H}_{0.31}\text{-Y}$ (see Section 8.1) and by isomerization of n-nonane and n-undecane on the same catalyst (see Section 5.3.2). Moreover, also iso-decanes generated by others [74] were co-injected. The isomerization products were analyzed by GC/MS and, in addition, the peak assignment was improved by the knowledge obtained in prior work of the group [47, 83]. Below, the results obtained with iso-nonanes and iso-undecanes are shown.

In Figure 7.1, exemplarily the results of the co-injection of the liquid products gained by isomerization of n-nonane and by the hydroconversion of perhydroindan on $0.93\text{Pt}/\text{silica}$ at $T_r = 430\text{ }^\circ\text{C}$ are depicted in the relevant range of retention times. In the pertinent literature, the GC analysis of the products is often unsatisfactory. For example, in the work of McVicker *et al.* [71] the authors reported that they were not able to resolve 2,5- and 3,5-dimethylheptane on their ID DB-1 capillary column with a length of 30 m. By contrast and as seen in Figure 7.1, using the capillary column Petrocol DH 150 with a length of 150 m does allow the separation of these two nonane isomers, even the two diastereomers of 3,5-dimethylheptane are separated.

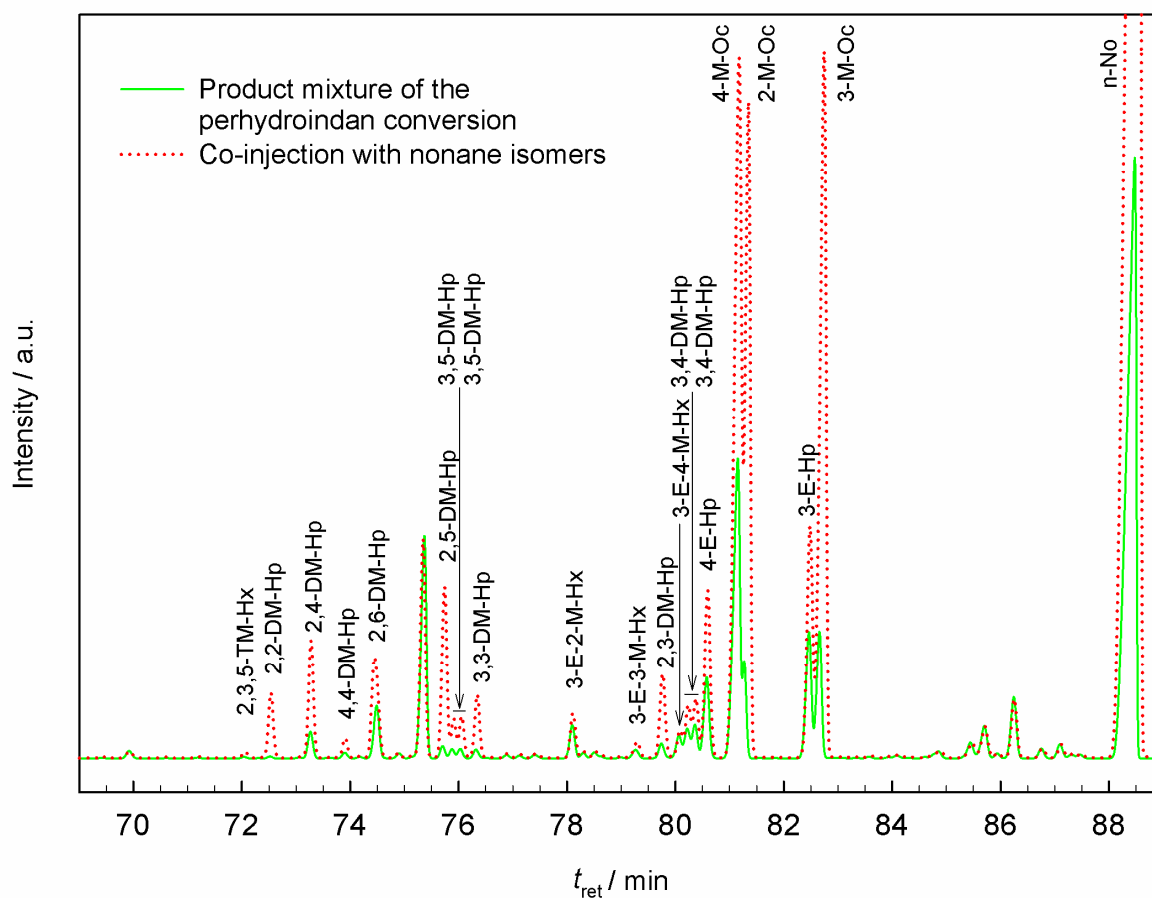


Figure 7.1: Gas chromatograms of the liquid product gained by the hydroconversion of perhydroindan on 0.93Pt/silica at $T_r = 430\text{ }^\circ\text{C}$ (solid line) and the same product co-injected with the product of the n-nonane isomerization on 0.52Pd/Na_{0.69}H_{0.31}-Y (dotted line).

In the range of retention times between $t_{\text{ret}} = 72$ and 83 min many signals are identical and their areas increase upon co-injection. In contrast, the areas of peaks between $t_{\text{ret}} = 83$ and 88 min, where no nonane isomers elute, did not increase upon co-injection. Hence, open-chain nonanes were formed from perhydroindan on 0.93Pt/silica.

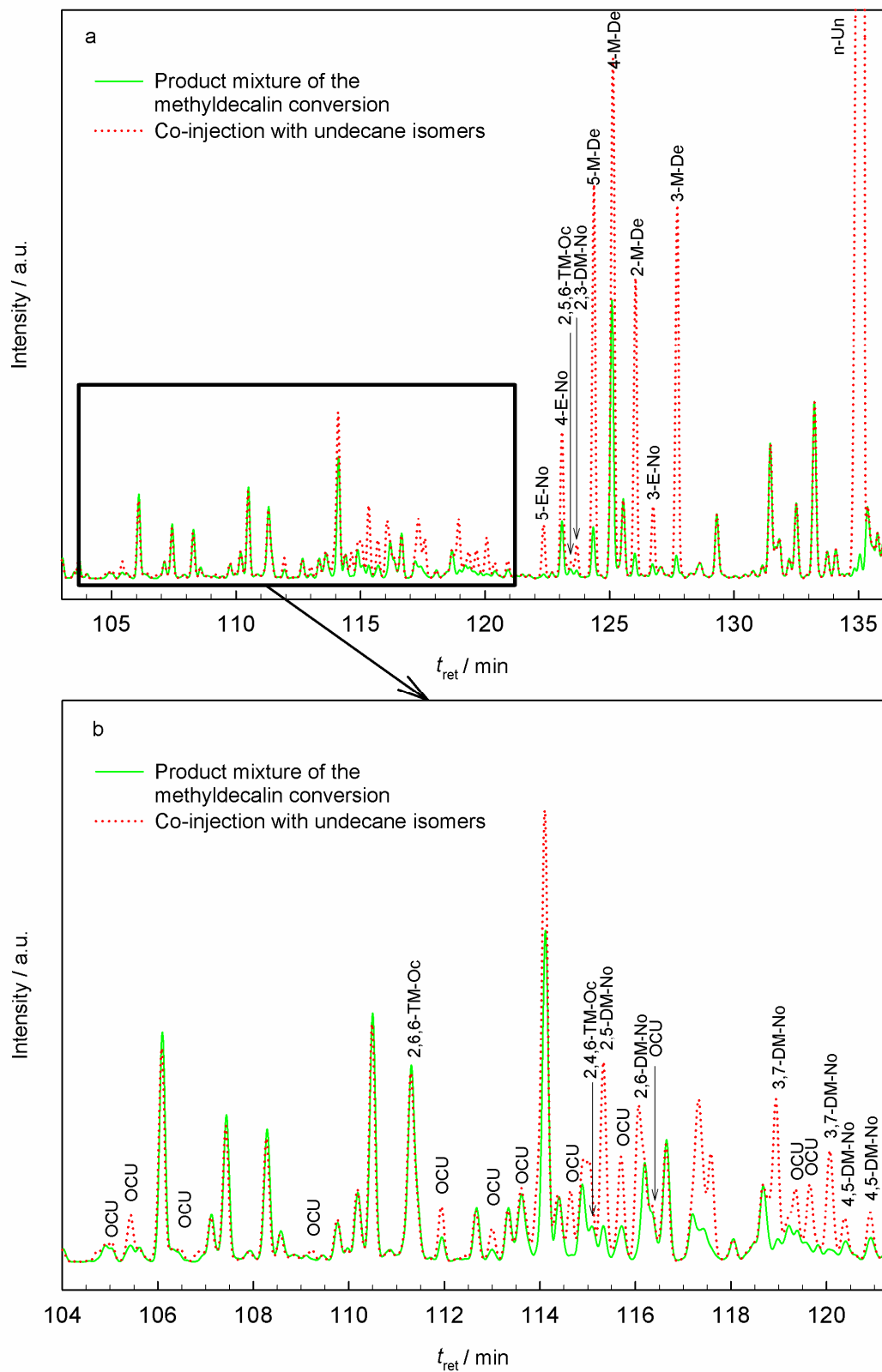


Figure 7.2: Gas chromatograms of the liquid product gained by the hydroconversion of methyldecalin on 0.77Ir/silica at $T_r = 370$ °C (solid line) and the same product co-injected with the product of the n-undecane isomerization on 0.52Pd/Na_{0.69}H_{0.31}-Y (dotted line).

In Figure 7.2, the results of the co-injection of the liquid products gained by isomerization of n-undecane and by the hydroconversion of methyldecalin on 0.77Ir/silica at $T_r = 370$ °C are depicted in the relevant range of retention times. Between $t_{ret} = 105$ and 128 min many signals are identical and their areas increase upon co-injection. Some signals could not be assigned to a specific undecane isomer but due to their molecular ion signal of $m/z = 156$ in the mass spectrogram an assignment to the group of open-chain undecanes OCUs was possible. Other signals that increase upon co-injection were assigned to other product groups like C_{10} - due to the absence of the molecular ion signal at $m/z = 156$. In contrast, the areas of peaks between $t_{ret} = 128$ and 134 min where no undecane isomers elute did not increase upon co-injection. Hence, OCUs were formed from methyldecalin on 0.77Ir/silica.

It can be concluded that the co-injection of iso-alkanes is a valuable method of peak assignment. Especially for complex mixtures of hydrocarbons with up to eleven carbon atoms GC/MS analyses are insufficient and require an additional method of peak assignment, *e.g.* co-injection of iso-alkanes. However, limitations of this method are (i) not every possible isomer is formed in a bifunctional isomerization of an n-alkane and (ii) peak overlaps with signals of other products can occur.

7.2 Blank Tests

In order to exclude a catalytic activity of the experimental set-up or of the catalyst support silica or the occurrence of thermal hydrocracking, blank tests with cis-decalin as feed hydrocarbon were conducted. In one experiment the reactor was empty and in the second one the reactor was filled with silica. The same experimental conditions as in the catalytic experiments with cis-decalin and metal-containing catalysts were applied (see Section 5.3.3.6)

Table 7.1: Conversion of decalin and selectivities of different groups of products at different reaction temperatures in the blank tests.

Reactor filling	T_r / °C	X_{Dec} / %	$S_{sk-Isos}$ / %	S_{ROPs} / %	S_{OCDs} / %	S_{C_9} / %	S_{DHPs} / %
Empty	390	9.7	12	4.5	0.8	0.5	83
Empty	430	15	10	2.7	0.4	1.8	85
Silica	390	8.4	17	3.7	0.4	0.6	78
Silica	430	28	27	1.2	0.1	0.5	72

In Table 7.1 the results of the blank tests show that at $T_r = 390$ °C conversions of about 9 % are obtained in the empty reactor and with silica as catalyst. When applying the definition of conversion (see Section 5.5.3) to a sample of the liquid reactant, a seeming conversion of 0.5 % would have been indicated from impurities in the feed hydrocarbon. Small amounts of ROPs and C₉-, and negligible amounts of OCDs indicate that a small extent of hydrocracking occurred, since these products were absent in the liquid feed hydrocarbon (see Section 5.3.3.6). Also the yields of sk-Isos around 1.3 % were slightly higher compared to the mass fraction of these impurities in the reactant. As expected by thermodynamic calculations [84], the main reaction was the dehydrogenation to DHPs which were comprised mainly of tetralin. At $T_r = 430$ °C the conversion increased more strongly on silica and higher amounts of sk-Isos were formed. Perhaps, at this very high reaction temperature very weak Brønsted acid sites on silica become catalytically active.

Hence, at temperatures up to 390 °C the contribution of thermal cracking or catalysis on silica is negligible. Higher temperatures might bring about a very weak catalytic activity of Brønsted acid sites on silica or thermal hydrocracking. The main reactions at high temperatures were always the dehydrogenation to tetralin and naphthalene according to the thermodynamic equilibrium.

8 Hydroconversion of n-Octane as Test Reaction

For studying catalysis on a dispersed and supported noble metal it is essential to identify a catalyst support that does not contribute to catalysis. Of utmost importance is the absence of bifunctional catalysis *via* carbocations which are usually generated on Brønsted acid sites. At least eight carbon atoms are required in a hydrocarbon to allow the fastest type of β -scission in a corresponding carbocation, as shown in Figure 4.18, page 32. Hence, the hydroconversion of n-octane was chosen as test reaction to identify a catalyst support which does not show a contribution of bifunctional catalysis. After loading with iridium or platinum, the following support materials were examined: amorphous silica, mesoporous [Si]SBA-15, titania, γ -alumina, carbon black.

In the hydroconversion of n-octane at $p_{\text{H}_2} = 0.1$ MPa all catalysts deactivated as proved by a control experiment at the end of a series of catalysis experiments at a temperature that was used earlier with the same catalyst. No deactivation of the silica-supported catalysts was observed in the conversion of n-decane at $p_{\text{H}_2} = 5.0$ MPa (see Section 9.1). Hence, the low hydrogen pressure leads to the build-up of coke and, consequently, to deactivation. This sometimes leads to kinks in the conversion patterns. As a general tendency, the iridium-containing catalysts showed higher conversions than the platinum-containing ones, but due to the occurrence of deactivation, a detailed discussion of relative catalyst activities is omitted.

8.1 Palladium-Containing Y Zeolite as Bifunctional Reference Catalyst

As a reference catalyst for bifunctional catalysis 0.52Pd/Na_{0.69}H_{0.31}-Y was tested. In Figure 8.1 the results of the temperature behavior of the n-octane conversion and selectivities at atmospheric pressure are shown. At low n-octane conversions up to *ca.* 20 %, skeletal isomers are the dominating products with a selectivity of 90 % or more. Increasing the reaction temperature and conversion brings about a decrease of the selectivity for skeletal isomers and an increase of the selectivity for hydrocracked products. The selectivities for RCPs and C₈ aromatics are small (sum < 8 %) in the entire range of temperatures applied.

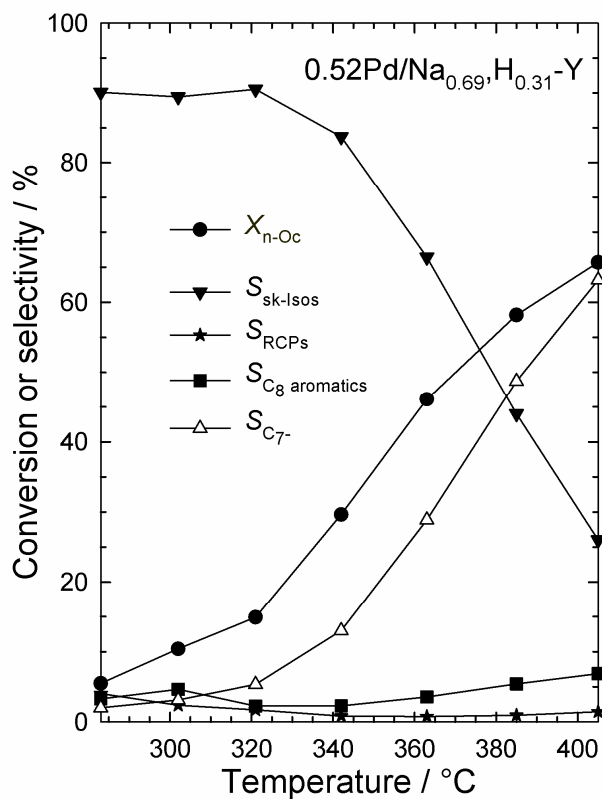


Figure 8.1: Conversion of n-octane and selectivities of different groups of products at different temperatures on the bifunctional reference catalyst.

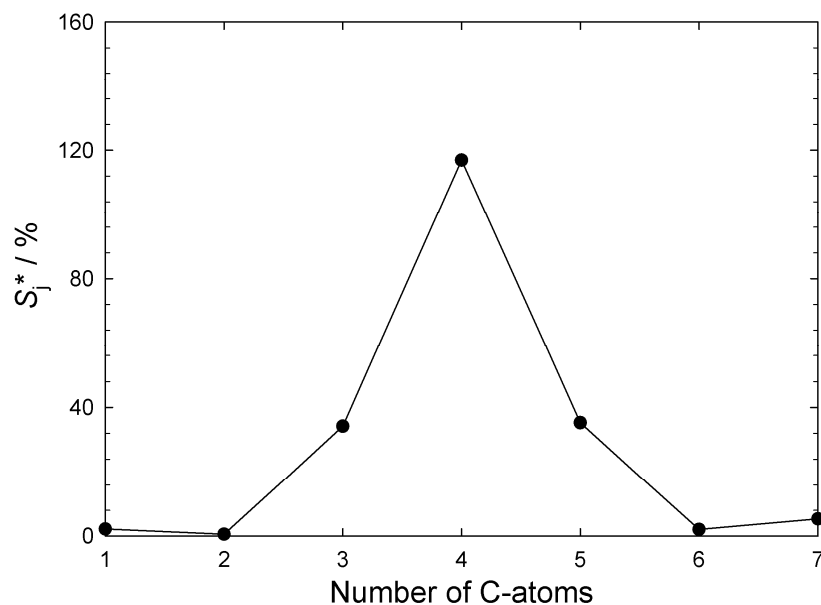


Figure 8.2: Modified hydrocracking selectivities S_j^* on the bifunctional reference catalyst $0.52Pd/Na_{0.69},H_{0.31}-Y$ in the hydroconversion of n-octane: $T_r = 321 \text{ }^\circ\text{C}$; $X_{n-Oc} = 15 \text{ } \%$; $Y_{C_7-} = 1 \text{ } \%$; $\sum S_j^* = 197 \text{ } \%$.

The distribution of the hydrocracked products (see Figure 8.2) shows a volcano shape with a strong maximum at C_4 , much less C_3 and C_5 and negligible amounts of C_1 , C_2 , C_6 and C_7 . The molar distribution curve is symmetrical around C_4 which indicates a pure primary hydrocracking selectivity [83]. This pure primary hydrocracking selectivity is also reflected by $\Sigma S_j^* \approx 200\%$. The occurrence of very small amounts of C_1 and C_7 is probably due to some hydrogenolysis on palladium superimposed to the main bifunctional hydrocracking.

8.2 Iridium- or Platinum-Containing Catalysts Supported on Silica or [Si]SBA-15

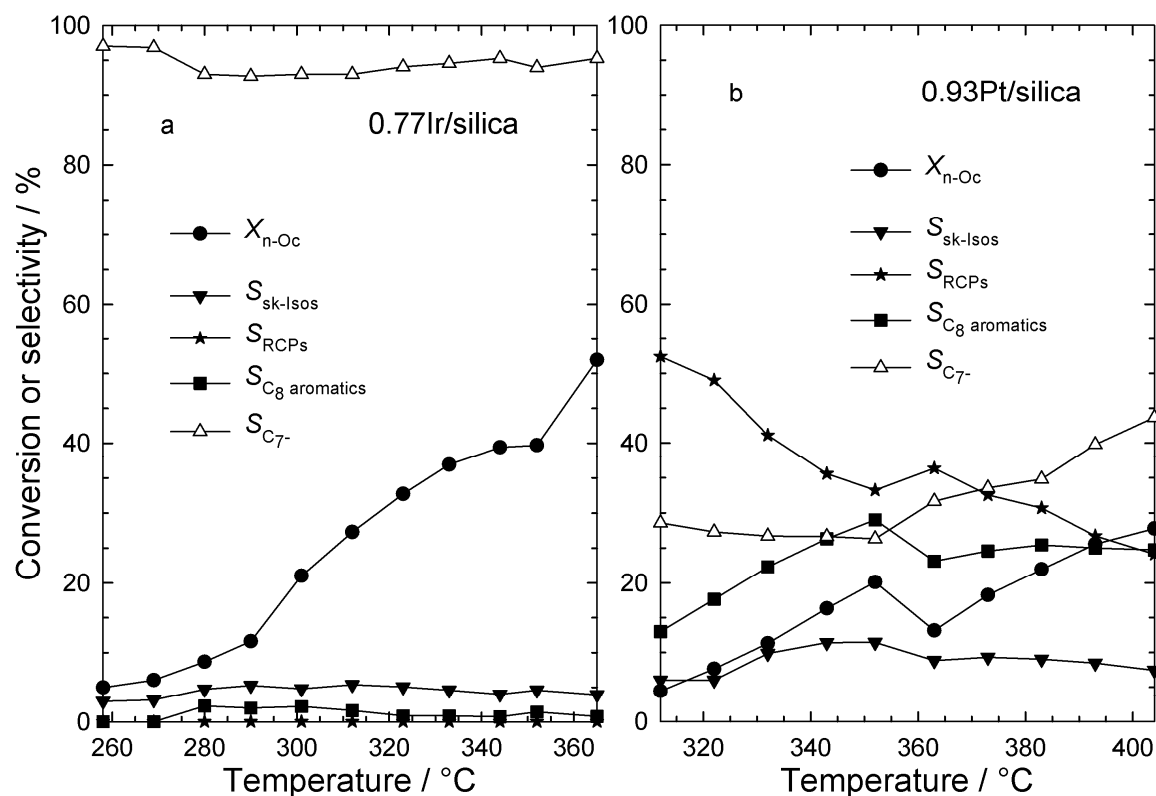


Figure 8.3: Conversion of n-octane and selectivities of different groups of products at different temperatures on two silica-supported catalysts.

Compared to the bifunctional palladium-containing catalyst completely different product selectivities are obtained with the silica-supported catalysts 0.77Ir/silica and 0.93Pt/silica, see Figure 8.3. The decrease of conversion between $T_r = 352\text{ }^\circ\text{C}$ and $363\text{ }^\circ\text{C}$ on Pt/silica is due to catalyst deactivation (*vide supra*). On both catalysts, the extent of isomerization remains below $S_{sk-Isos} = 12\%$ in contrast to the abundant isomerization found on 0.52Pd/Na_{0.69}H_{0.31}-Y (see Figure 8.1) at moderate conversions. In Figure 8.3a the selectivity pattern of the iridium-containing catalyst shows $S_{C_7-} \geq$

93 % at all temperatures, accompanied by small amounts of skeletal isomers with $S_{sk-Isos}$ between 3 and 5 %. As shown in Figure 8.3b, on the platinum-containing one dehydrocyclization to RCPs and hydrocracking are the main reactions with an increasing trend of aromatization with increasing temperature.

A very similar catalytic behavior was found for the two corresponding [Si]SBA-15-supported catalysts (not shown). In Figure 8.4 the distribution curves of the hydrocracked products for the four silica- and [Si]SBA-15-supported catalysts are shown. On both iridium catalysts the curves tend to monotonously increase from C_7 to C_1 . Compared to the almost horizontal curve shape on unsupported iridium particles [31] (see Figure 4.8, page 20) this is a very similar result. On the supported catalysts it is superimposed by multiple hydrogenolysis as indicated by $\Sigma S_j^* > 200$ % resulting in the increasing modified selectivities with decreasing number of carbon atoms.

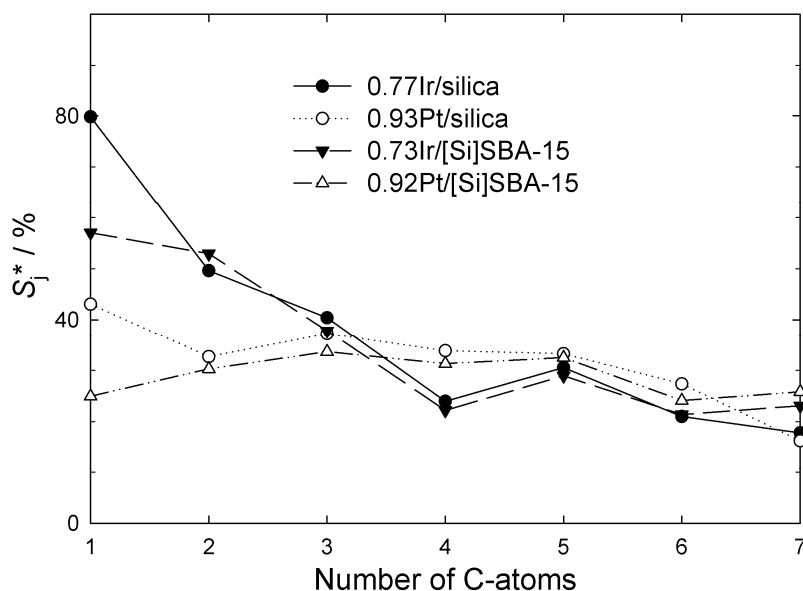


Figure 8.4: Modified hydrocracking selectivities S_j^* on the silica- and [Si]SBA-15-supported catalysts in the hydroconversion of n-octane:

- 0.77Ir/silica: $T_r = 280$ °C; $X_{n-Oc} = 9$ %; $Y_{C_7-} = 8$ %; $\Sigma S_j^* = 263$ %.
- 0.93Pt/silica: $T_r = 332$ °C; $X_{n-Oc} = 14$ %; $Y_{C_7-} = 4$ %; $\Sigma S_j^* = 224$ %.
- 0.73Ir/[Si]SBA-15: $T_r = 280$ °C; $X_{n-Oc} = 12$ %; $Y_{C_7-} = 11$ %; $\Sigma S_j^* = 243$ %.
- 0.92Pt/[Si]SBA-15: $T_r = 320$ °C; $X_{n-Oc} = 10$ %; $Y_{C_7-} = 3$ %; $\Sigma S_j^* = 203$ %.

Beside small deviations in the relative amounts of methane formed, both platinum catalysts show a very similar almost horizontal curve. Also on unsupported platinum particles [31] (see Figure 4.8, page 20) a roughly horizontal curve was obtained in the hydroconversion of n-heptane. There, the mole fraction of C_1 was relatively high. Presumably, multiple hydrogenolysis of n-heptane occurred on the unsupported

platinum particles as indicated by the lower value at C₆ compared to C₁. As a conclusion, both modifications of silicon dioxide lead to a very similar catalytic behavior of the respective deposited noble metal.

Due to the above-mentioned similar influence of both supports on catalysis, the following detailed discussion of the product distribution is conducted exemplarily only for one type of catalyst, *viz.* the [Si]SBA-15-supported ones. For a comparison of the mechanisms occurring on the bifunctional catalyst 0.52Pd/Na_{0.69}H_{0.31}-Y and on the [Si]SBA-15-supported catalysts the distributions of the skeletal isomers in the product mixture are listed in Table 8.1.

Table 8.1: Composition of the skeletal isomers obtained from n-octane on the [Si]SBA-15-supported catalysts and on the bifunctional zeolite catalyst.

Catalyst	0.73Ir/[Si]SBA-15		0.92Pt/[Si]SBA-15		0.52Pd/Na _{0.69} H _{0.31} -Y	
$T_r / ^\circ\text{C}$	241	321	299	361	283	342
$X_{n\text{-Oc}} / \%$	5	31	3	34	5	30
$S_{\text{sk-Isos}} / \%$	6	2	12	34	90	84
Skeletal isomer	$S / S_{\text{sk-Isos}} / \%$					
2-M-Hp	21.4	25.3	20.6	13.2	29.3	28.7
3-M-Hp	6.8	8.9	22.1	8.2	42.4	34.8
4-M-Hp	21.6	31.6	32.7	41.8	17.5	13.6
3-E-Hx	16.0	16.8	16.0	18.9	6.4	4.9
3-E-2-M-Pn	10.6	5.4	3.2	6.7	0.1	0.4
2,2-DM-Hx	0	0	0	0	0.9	2.5
2,3-DM-Hx	3.2	2.3	2.1	1.0	0.9	3.6
2,4-DM-Hx	13.6	3.5	3.4	1.8	1.2	4.8
2,5-DM-Hx	0	0	0	0	0.6	3.1
3,3-DM-Hx	0	0	0	0	0.6	2.0
3,4-DM-Hx	6.9	6.4	0	8.4	0.2	1.7

It can be seen that on the bifunctional catalyst much higher amounts of 3-methylheptane (3-M-Hp) are generated, and isomerization to the dibranched octane isomers 2,2-, 2,5- and 3,3-dimethylhexane (2,2-, 2,5-, 3,3-DM-Hx) occurs. These dibranched isomers are not formed on the [Si]SBA-15-supported catalysts. Another characteristic difference is shown by the low fractions of the isomers 4-methylheptane (4-M-Hp), 3-ethylhexane (3-E-Hx), 3,4-dimethylhexane (3,4-DM-Hx) and 3-ethyl-2-

methylpentane (3-E-2-M-Pn) occurring on the bifunctional catalyst. The relatively high amounts of 4-methylheptane, 3-ethylhexane, 3,4-dimethylhexane and 3-ethyl-2-methylpentane on the [Si]SBA-15-supported catalysts can be explained by a cyclic isomerization mechanism *via* substituted cyclopentanes [22, 23] occurring solely on the metal sites (see Section 4.2.1.2).

More information is obtained from the hydrocracked products with five carbon atoms. In Figure 8.6c the distribution of the pentane isomers n-pentane and 2-methylbutane that were formed on the bifunctional zeolite catalyst is depicted. On this catalyst, at low conversions mainly 2-methylbutane is formed, with an increasing selectivity of n-pentane with increasing temperature. Comparing this with the selectivity pattern of the pentane isomers on 0.73Ir/[Si]SBA-15 (see Figure 8.6a) and 0.92Pt/[Si]SBA-15 (see Figure 8.6b) the difference is obvious. These monofunctional catalysts produce mainly n-pentane with only low amounts of 2-methylbutane.

The formation of 2-methylbutane on the bifunctional catalyst can be rationalized by applying the relatively fast β -scissions of type B₁, B₂ and C (see Figure 4.18) to all carbocations of the octane isomers that are tabulated in Table 8.1. Exactly two of these reactions can result in the formation of 2-methylbutane, *viz.* the β -scission of type B₂ or B₁ in carbenium ions of 2,4-dimethylhexane or 3,3-dimethylhexane, respectively (see Figure 8.5). The fastest β -scission of type A in a C₈ carbocation can only result in the formation of two iso-butane molecules [48]. Indeed, also iso-butane is formed in large amounts on 0.52Pd/Na_{0.69}H_{0.31}-Y (not shown).

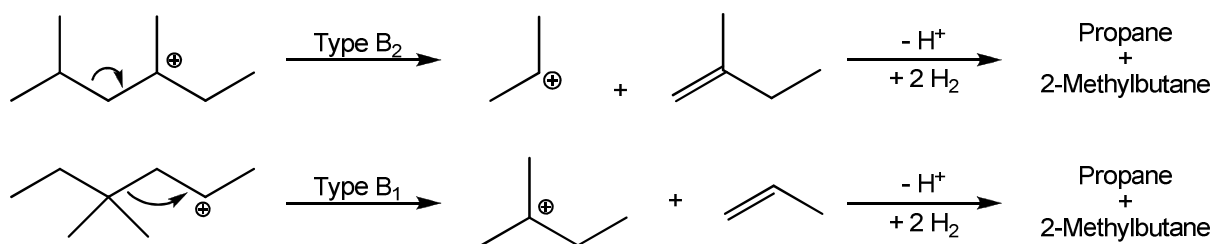


Figure 8.5: β -Scission of cations of 2,4-dimethylhexane and 3,3-dimethylhexane.

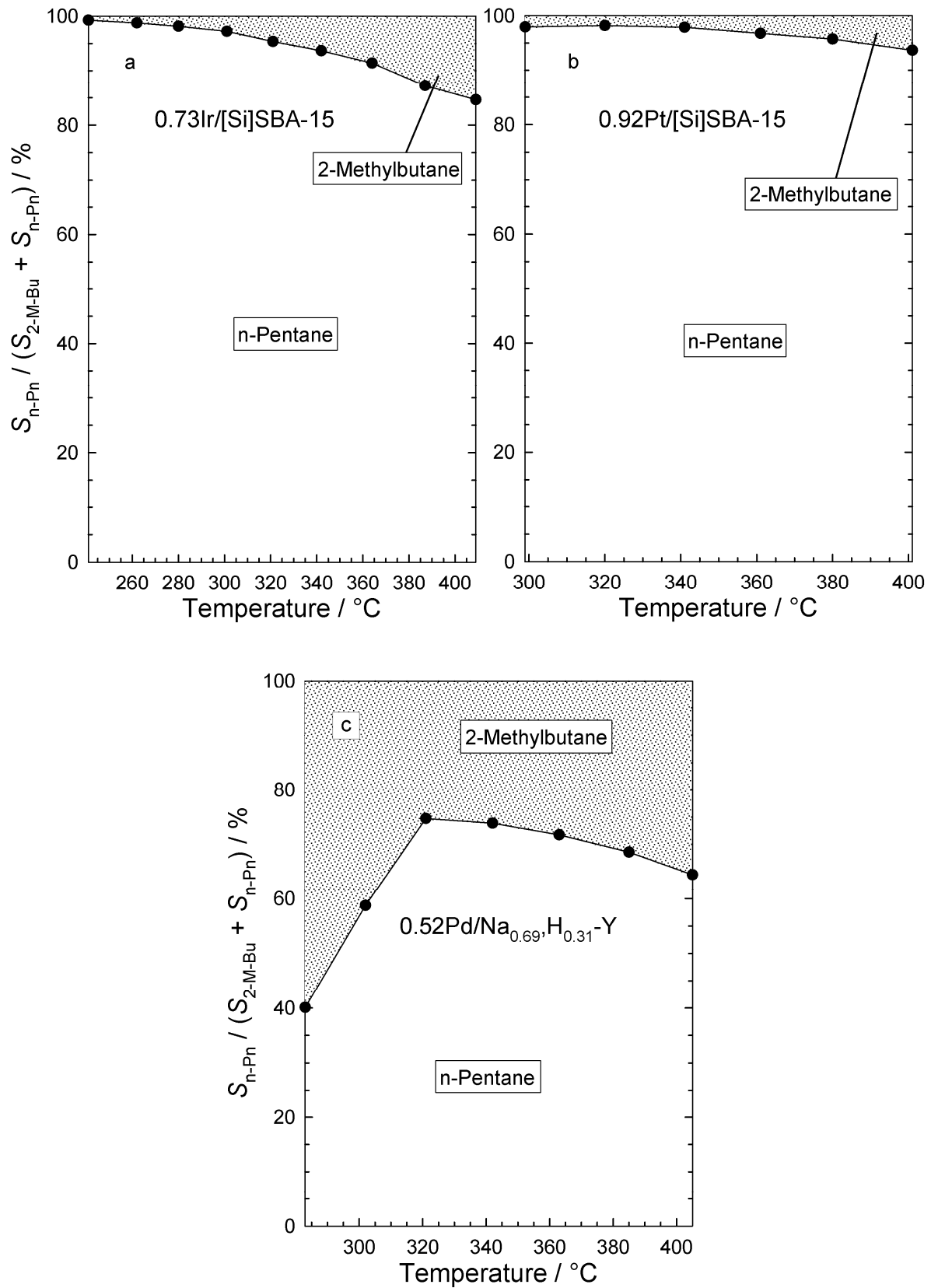


Figure 8.6: Relative selectivities of the pentane isomers 2-methylbutane and n-pentane in the hydroconversion of n-octane on both [Si]SBA-15-supported catalysts and on the bifunctional zeolite catalyst.

8.3 Iridium- or Platinum-Containing Catalysts Supported on γ -Alumina, Titania or Carbon Black

On both titania-supported catalysts, the product distribution is very similar to the silica- and [Si]SBA-15-supported ones with the same noble metal. A *ca.* 10 % higher selectivity of sk-Isos and a *ca.* 10 % lower selectivity of C₈ aromatics is obtained on 1.06Pt/titania compared to the silicon-dioxide-supported iridium catalysts (see Figure 8.3b). As depicted in Figure 8.7, the C₇- products on 1.05Ir/titania show a similar carbon number distribution as the respective silicon-dioxide-supported platinum catalysts (see Figure 8.4) with a smaller amount of methane. Also on 1.06Pt/titania the distribution resembles that obtained on the silicon-dioxide-supported platinum catalysts. However, the slightly increasing values from C₁ and C₇ towards C₄ as observed on 0.52Pd/Na_{0.69}H_{0.31}-Y could point to a contribution of bifunctional catalysis on 1.06Pt/titania.

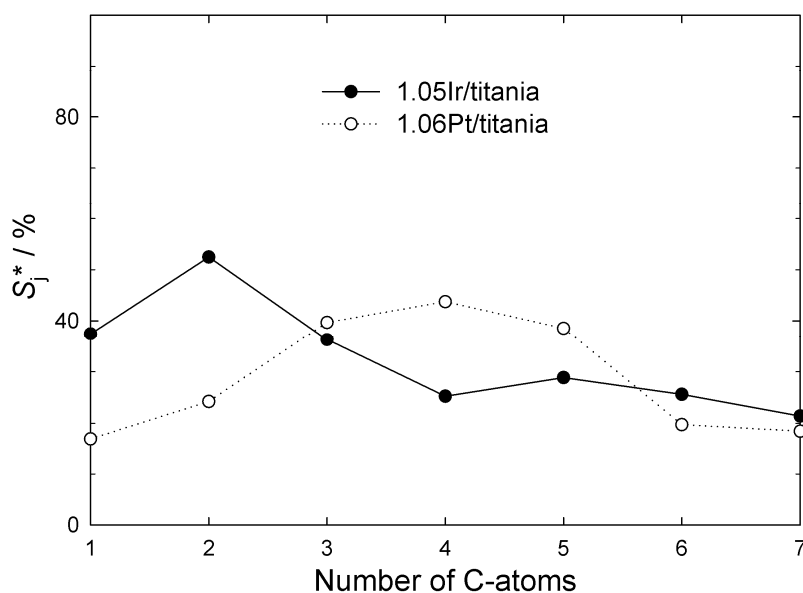


Figure 8.7: Modified hydrocracking selectivities S_j^* on the titania-supported catalysts in the hydroconversion of n-octane:

1.05Ir/titania: $T_r = 279\text{ }^\circ\text{C}$; $X_{n\text{-Oc}} = 14\text{ }%$; $Y_{C_{7-}} = 14\text{ }%$; $\Sigma S_j^* = 227\text{ }%$.

1.06Pt/titania: $T_r = 389\text{ }^\circ\text{C}$; $X_{n\text{-Oc}} = 15\text{ }%$; $Y_{C_{7-}} = 5\text{ }%$; $\Sigma S_j^* = 201\text{ }%$.

On 0.93Ir/ γ -alumina slightly higher selectivities of sk-Isos and RCPs were formed compared to the iridium-containing catalysts that are supported on silica and [Si]SBA-15. A totally different product mixture was formed on 0.91Ir/carbon black with high selectivities of sk-Isos between 24 and 48 % and low $S_{C_{7-}}$ values of maximal 33 %.

On the γ -alumina- and carbon-black-supported platinum catalysts the selectivities of sk-Isos and C_{7-} products are higher and S_{RCPs} are lower in comparison with the platinum-containing silicon-dioxide-supported catalysts. This could point to a contribution of Brønsted acid sites which facilitate skeletal isomerization and hydrocracking while the contribution of metal-catalyzed reactions like dehydrocyclization is reduced.

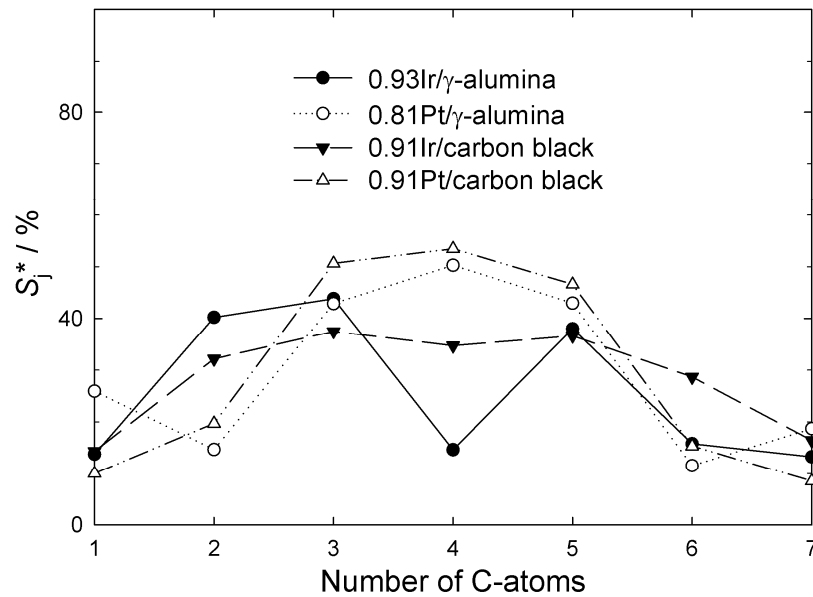


Figure 8.8: Modified hydrocracking selectivities S_j^* on the γ -alumina- and carbon black-supported catalysts in the hydroconversion of n-octane:

0.93Ir/ γ -alumina: $T_r = 256$ °C; $X_{n-Oc} = 16$ %; $Y_{C_{7-}} = 13$ %; $\Sigma S_j^* = 180$ %.

0.81Pt/ γ -alumina: $T_r = 311$ °C; $X_{n-Oc} = 14$ %; $Y_{C_{7-}} = 6$ %; $\Sigma S_j^* = 207$ %.

0.91Ir/carbon black: $T_r = 342$ °C; $X_{n-Oc} = 21$ %; $Y_{C_{7-}} = 10$ %; $\Sigma S_j^* = 204$ %.

0.91Pt/carbon black: $T_r = 372$ °C; $X_{n-Oc} = 20$ %; $Y_{C_{7-}} = 6$ %; $\Sigma S_j^* = 200$ %.

In Figure 8.8 the modified hydrocracking selectivities of the γ -alumina- and carbon-black-supported catalysts are shown. They deviate from those described for the corresponding silica- and [Si]SBA-15-supported ones. On the iridium-containing catalysts the values at C_1 and C_7 are lower compared to the silicon dioxide-supported ones. Since at these reaction temperatures methane can only be formed by hydrogenolysis on the metal, an interpretation is that on 0.93Ir/ γ -alumina and 0.91Ir/carbon black hydrogenolysis on the metal is superimposed by bifunctional hydrocracking on Brønsted acid sites. Also on the corresponding platinum-containing catalysts Brønsted acid sites seem to be active as suggested by the relatively high amounts of C_3 , C_4 and C_5 as found on the bifunctional reference catalyst as well (see Figure 8.2).

8.4 Conclusions

Several indications were obtained which demonstrate that silica and [Si]SBA-15 are the most appropriate support materials for studying the metal function alone with a minimal contribution of Brønsted acid sites: (i) The distribution curves of the hydrocracked products resemble those of the unsupported metals [31]. (ii) Much smaller selectivities of skeletal isomers are formed compared to the bifunctional zeolite catalyst and also their composition is different. (iii) Especially at low conversions, the formation of 2-methylbutane is negligible while on the bifunctional reference catalyst 60 % of the C₅ fraction is composed of 2-methylbutane. (iv) By FT-IR spectroscopy with pyridine as probe molecule no Brønsted acid sites of sufficient strength were detected on silica (see Section 6.2).

On the other support materials titania, γ -alumina and carbon black essentially two catalytic properties demonstrated a possible contribution of Brønsted acid sites: (i) Higher selectivities of sk-Isos compared to silica- and [Si]SBA-15-supported catalysts and (ii) distribution curves of the hydrocracked products that can be interpreted by a superimposition of a volcano shape as typical for bifunctional hydrocracking with the distribution curve known from unsupported metal catalysts [31].

9 Hydrogenolysis on Monofunctional Noble Metal Catalysts

For all experiments about the hydrogenolysis of hydrocarbons the noble metal was supported on silica due to the absence of pyridine adsorption (see Section 6.2) and due to its non-acidic character in the test reaction with n-octane (see Section 8). In addition, for the hydroconversion of cis-decalin also two [Si]SBA-15-supported catalysts were tested. In a control experiment at the end of each series of measurements with a specific catalyst and reactant no catalyst deactivation has been observed after *ca.* 40 h of time-on-stream. Mild deactivation was observed in specific time-on-stream experiments with cis-decalin as reactant at high reaction temperatures after *ca.* 70 h (see Sections 9.5.2 and 9.5.3).

9.1 n-Decane

In Sections 9.3, 9.5 and 9.6 the hydrogenolysis of mono- and bicyclic naphthenes with ten carbon atoms on Ir/silica and Pt/silica will be examined. There, open-chain decanes (OCDs) are the most important group of products concerning the improvement of diesel fuel by ring opening of naphthenes. With these reactants it is often unclear to what extent hydrogenolysis of OCDs leads to a degradation of the number of carbon atoms, *i.e.* the formation of hydrocracked products. In order to learn about the precursors of C₉- products in the conversion of these naphthenes it seems worthwhile to study the hydroconversion of a decane isomer under similar experimental conditions. Since n-decane is the only commercially available decane isomer it is used as a representative OCD in the hydroconversion on 2.73Ir/silica and 2.69Pt/silica.

The iridium catalyst is much more active than the platinum catalyst (see Figure 9.1). With the latter, *ca.* 80 °C higher temperatures have to be applied to obtain similar conversions. On both catalysts hydrogenolysis to C₉- products is the main reaction. Skeletal isomers are formed on 2.73Ir/silica and 2.69Pt/silica with $S_{\text{sk-Isos}} \leq 3$ and 5 %, respectively. On both catalysts and all temperatures at least 86 % of all sk-Isos are mono-branched (methylnonanes and ethyloctanes). Dehydrocyclization occurs to a negligible extent, most likely due to the high hydrogen pressure of 5.0 MPa in contrast to high selectivities of RCPs and C₈ aromatics in the n-octane conversion at $p_{\text{H}_2} = 0.1$ MPa on 0.93Pt/silica (see Figure 8.3b, page 83).

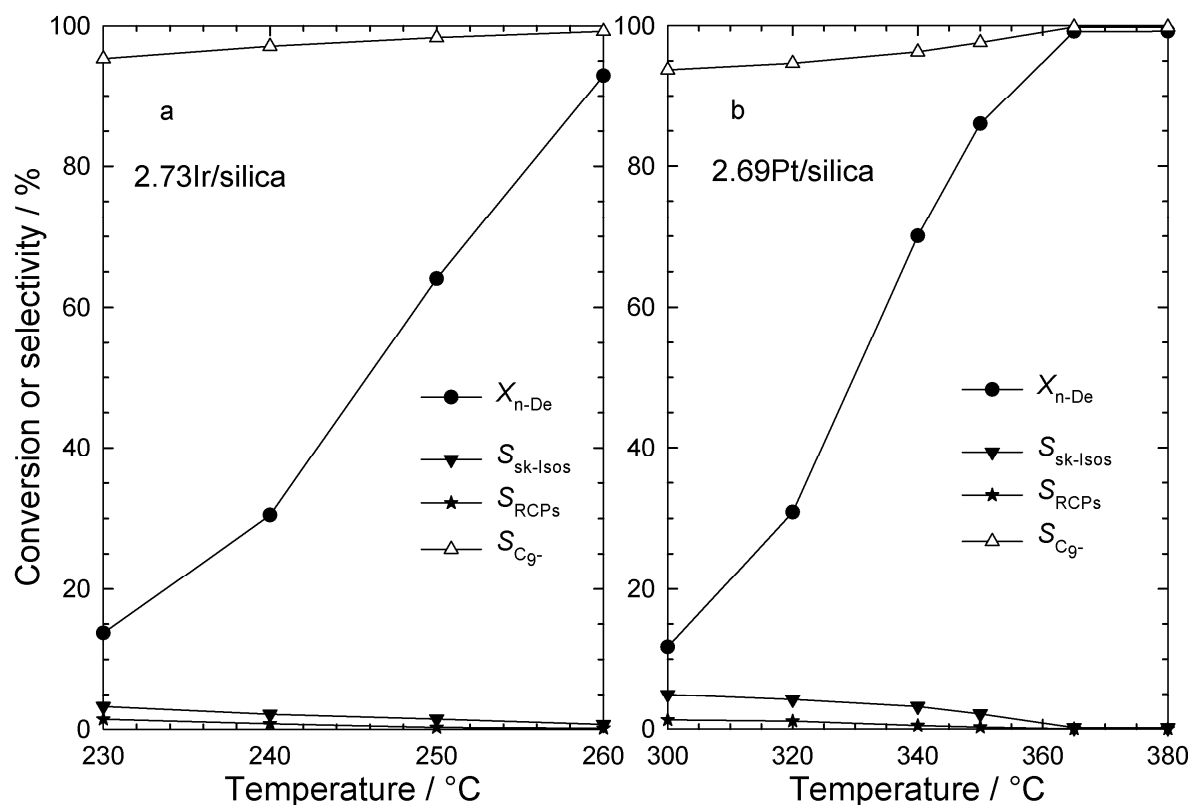


Figure 9.1: Conversion of n-decane and selectivities of different groups of products at different temperatures on two silica-supported catalysts.

In the distribution curves of the hydrocracked products (see Figures 9.2 and 9.3) also the fractions of n-alkanes (primary hydrogenolysis products) are given as black bars at carbon numbers at which this discrimination is possible. No bars are shown for the coproducts methane, ethane and propane. Since in the corresponding carbon number fractions these are the only products, no differentiation between products which can stem from a direct hydrogenolysis of n-decane and products which are formed in the course of other reaction paths would be possible. On the iridium catalyst the hydrocracked products are comprised only of n-alkanes (see Figure 9.2). Hence, neither n-decane nor the C₉- products undergo isomerization on this catalyst. Together with $\sum S_j^* \approx 200\%$ this is a strong indication that in every n-decane molecule that is converted into C₉- products one single C-C bond is cleaved. Moreover, the curve shape demonstrates that the cleavage of internal bonds in the alkane chain is preferred whereas hydrogenolysis between C₁ and C₂ or C₂ and C₃ in the decane molecule is slower.

A similar carbon number distribution curve is obtained for 2.69Pt/silica (see Figure 9.3). Again hydrogenolysis between central carbon atoms is faster in qualitative accordance with results of the n-decane hydroconversion on 2.0Pt/alumina [23] at

$p_{H_2} = 2.0$ MPa. Platinum, as already demonstrated by the slightly higher $S_{sk-Isos}$ (see Figure 9.1), exhibits a mild isomerization activity what is now also reflected in the occurrence of some very small amounts of iso-alkanes in the hydrocracked products.

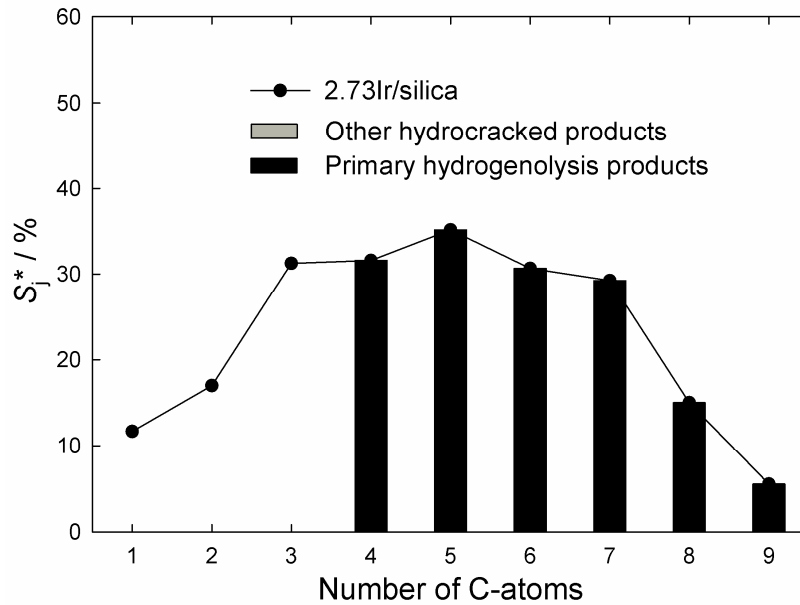


Figure 9.2: Modified hydrocracking selectivities S_j^* on 2.73Ir/silica in the hydroconversion of n-decane and fraction of primary hydrogenolysis products:

$T_r = 240$ °C; $X_{n-De} = 30$ %; $Y_{C_9^-} = 30$ %; $\Sigma S_j^* = 207$ %.

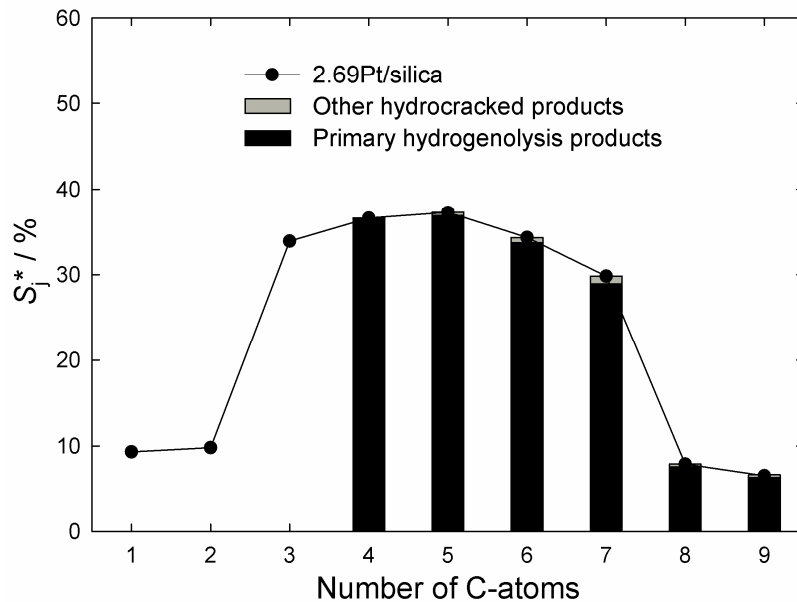


Figure 9.3: Modified hydrocracking selectivities S_j^* on 2.69Pt/silica in the hydroconversion of n-decane and fraction of primary hydrogenolysis products:

$T_r = 320$ °C; $X_{n-De} = 31$ %; $Y_{C_9^-} = 29$ %; $\Sigma S_j^* = 205$ %.

9.2 Ethylcyclohexane

To study the general catalytic behavior of iridium or platinum in the hydroconversion of six-membered rings ethylcyclohexane was chosen as feed hydrocarbon. The expected not too complex product distribution should facilitate a mechanistic interpretation. Dehydrogenation to ethylbenzene occurred to a negligible extent with maximal selectivities of 0.3 %. Hence these selectivities are not plotted in Figure 9.4.

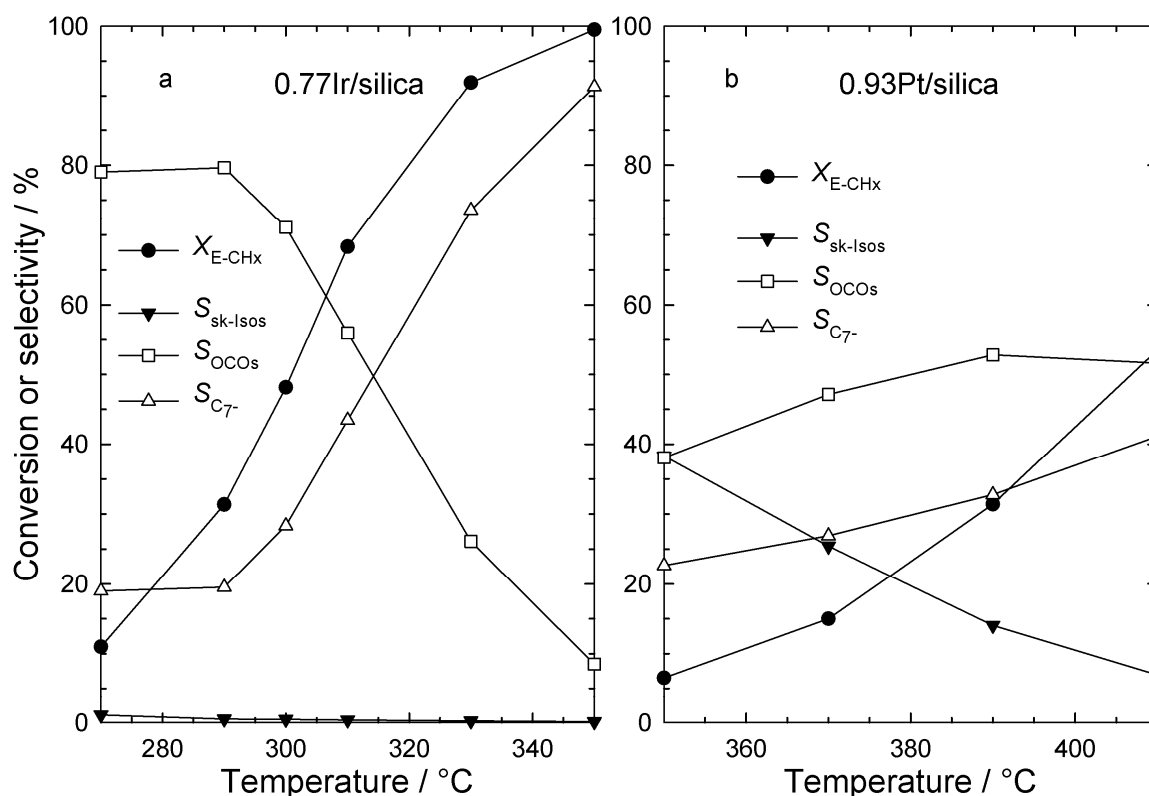


Figure 9.4: Conversion of ethylcyclohexane and selectivities of different groups of products at different temperatures on two silica-supported catalysts.

As also observed in the hydroconversion of n-decane (see Figure 9.1), the iridium catalyst is much more active than the corresponding platinum catalyst with a comparable metal loading (see Figure 9.4). Similar conversions are reached at *ca.* 100 °C higher reaction temperatures on 0.93Pt/silica. As shown in Figure 9.4a the formation of sk-Isos is negligible on 0.77Ir/silica. Up to intermediate conversions open-chain octanes (OCOs) are the main products with a maximal yield of $Y_{OCOs} = 38\%$ at $T_r = 310\text{ °C}$ and $X_{E-CHx} = 68\%$. With increasing temperature the selectivity of C₇- products increases strongly, except for the lowest temperature which is a consequence of impurities in the reactant.

As observed with n-decane (see Figure 9.1b), the platinum catalyst is active in the formation of skeletal isomers. On 0.93Pt/silica (see Figure 9.4b) the selectivity of sk-Isos decreases from 38 to 7 % with increasing temperature and conversion. Simultaneously, the selectivity of OCOs increases slightly and a maximal $Y_{\text{OCO}_s} = 28 \%$ is reached at $T_r = 410 \text{ }^\circ\text{C}$ and $X_{\text{E-CH}_x} = 53 \%$. Within the temperature range applied, the selectivity of C₇- increases with increasing temperature up to 41 %.

Propylcyclopentane is the most abundant skeletal isomer that is formed on the platinum catalyst with $S_{\text{P-CPn}} / S_{\text{sk-Isos}} = 44 \%$ at the lowest conversion and a decreasing relative selectivity with increasing conversion to $S_{\text{P-CPn}} / S_{\text{sk-Isos}} = 26 \%$ at $X_{\text{E-CH}_x} = 53 \%$. Other skeletal isomers are different substituted cyclopentanes and cyclohexanes with eight carbon atoms but also methylcycloheptane is formed with a maximal $S = 1.3 \%$ at $T_r = 350 \text{ }^\circ\text{C}$. Since the results of FT-IR measurements (see Section 6.2) and of the n-octane hydroconversion (see Section 8) gave no indications for Brønsted acid sites on Pt/silica a metal-catalyzed isomerization mechanism has to be envisaged.

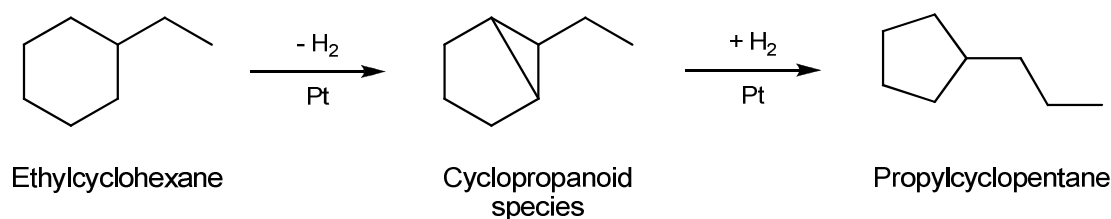


Figure 9.5: Isomerization of ethylcyclohexane to propylcyclopentane on platinum according to the bond-shift mechanism.

To understand the formation of propylcyclopentane the bond-shift mechanism [24, 27, 28] (see Section 4.2.1.2) is tentatively applied to ethylcyclohexane, see Figure 9.5. A cleavage of a C-C bond in the three-membered ring other than the new one formed can result in the formation of propylcyclopentane. It was observed to be the predominant type of metal-catalyzed isomerization of n-octane when the hydrogen pressure was increased from 0.5 to 2.0 MPa [23]. Alternatively, also a 1,5-dehydrocyclization of the major OCO n-octane (see Figure 9.8b) to a five-membered ring could furnish propylcyclopentane, see Figure 9.6.

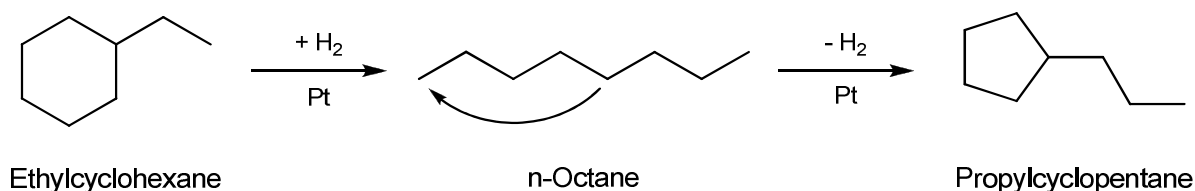


Figure 9.6: Isomerization of ethylcyclohexane to propylcyclopentane on platinum *via* ring opening to n-octane followed by 1,5-dehydrocyclization.

Since propylcyclopentane is a primary product with the highest selectivity at the lowest conversion, while the selectivity of n-octane increases from $T_r = 350$ over 370 to 390 °C, its formation occurs most probably *via* the bond-shift mechanism. By applying the bond-shift mechanism, in addition the skeletal isomers 1-ethyl-1-methylcyclopentane, cis- and trans 1-ethyl-2-methylcyclopentane and cis- and trans 1-ethyl-3-methylcyclopentane are expected. Indeed these sk-Isos are formed with a total relative selectivity $S / S_{\text{sk-Isos}}$ of 27 to 31 %. A rationale for the preferred formation of propylcyclopentane cannot be given. Perhaps, ethylcyclohexane is adsorbed on platinum preferentially in such a manner that the cyclopropanoid species shown in Figure 9.5 is formed.

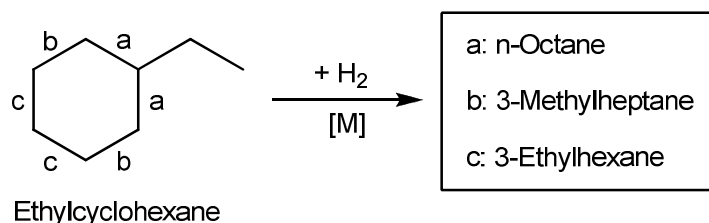


Figure 9.7: Labeling of the endocyclic bonds in ethylcyclohexane with the respective hydrogenolysis products (direct OCOs).

On the iridium catalyst in the whole temperature range at least 96 % of all OCOs are these three OCOs that originate from a direct hydrogenolytic ring opening (direct OCOs, see Figure 9.7), *viz.* n-octane, 3-methylheptane and 3-ethylhexane. Due to the isomerization activity of the platinum catalyst this value is slightly lower on 0.93Pt/silica with values ≤ 92 % in the whole range of temperatures applied. In Figure 9.8 the relative selectivities of the three direct OCOs are plotted versus conversion.

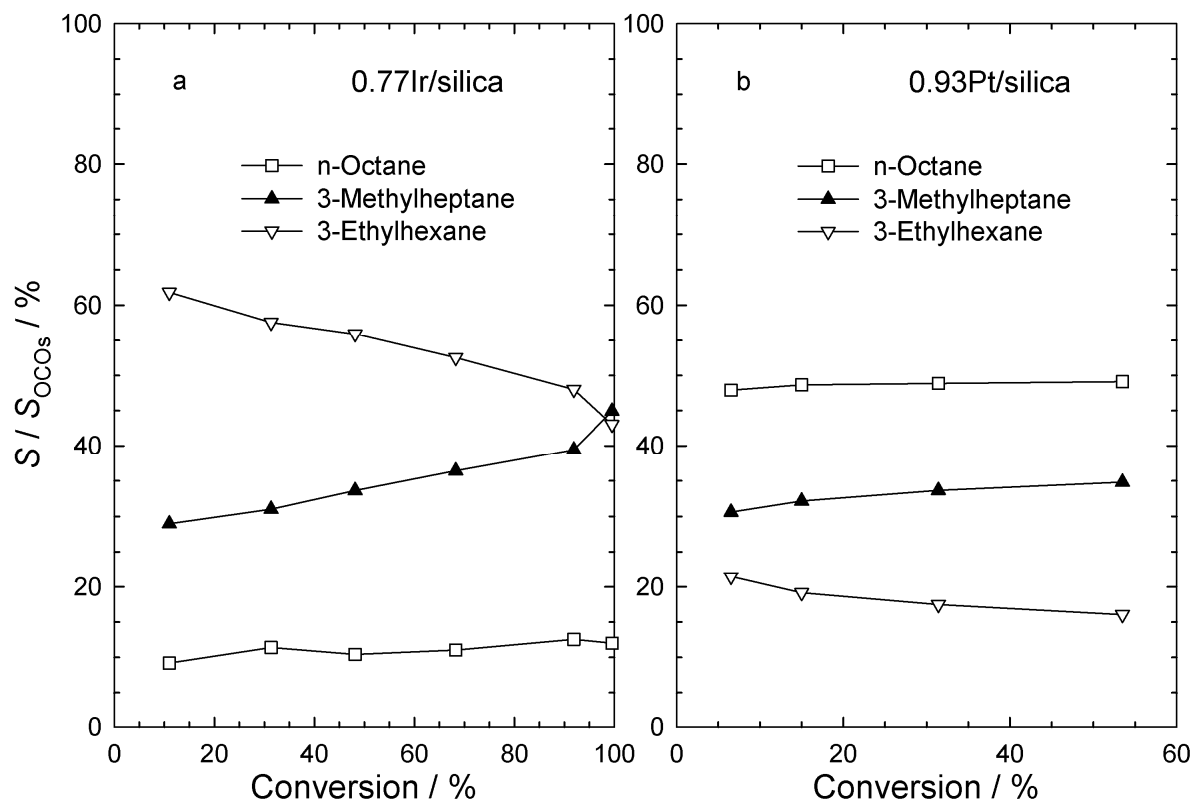


Figure 9.8: Selectivities of the three direct OCOs originating from a direct ring opening of ethylcyclohexane on two silica-supported catalysts.

For the iridium catalyst the probability of breaking the bonds a : b : c is about 0.2 : 0.5 : 1.0 at the lowest conversion and changes with increasing conversion to 0.3 : 1.0 : 1.0 at the highest conversion. This can be explained with a dominating selective mechanism (see Section 4.2.1.4), which opens the unsubstituted bonds b and c. This mechanism is accompanied by another ring-opening mechanism, presumably the non-selective mechanism or the partially selective mechanism, leading to n-octane by cleaving bond a. A similar regioselectivity with a ratio a : b : c of 0.1 : 0.6 : 1.0 was also found in the ring opening of methylcyclohexane on 0.9Ir/ γ -alumina at a conversion of 15 % [4], see Table 4.1, page 25 and in the ring opening of butylcyclohexane on the same catalyst [4]. It is unknown why the cleavage of the bissecondary bond c is preferred over that of the other bissecondary bond b at low conversions. Perhaps, bond c, which is situated more distant from the alkyl group, is adsorbed on iridium more easily due to sterical reasons. At higher conversions, and accordingly at higher temperatures, the ring is vibrating more intensively and it seems, that the adsorption at bonds b and c occurs to a similar extent.

On the platinum catalyst the relative selectivities of direct OCOs remain nearly constant over the whole temperature range with a ratio of breaking the bonds a : b : c

of about 3 : 2 : 1, far away from the non-selective mechanism observed in the ring opening of methylcyclopentane on platinum [33]. A preference for breaking the substituted bond was also found in the ring opening of methylcyclohexane on 0.6Pt/silica [4] (see Table 4.1, page 25) with a ratio a : b : c of about 2 : 1 : 0. There, in contrast to the results shown in Figure 9.8, the rupture of bond c occurred only to a negligible extent. Perhaps, the small differences of the reactant, methyl vs. ethyl group, are responsible for the different regioselectivities. Also different metal dispersions could be the reason, since platinum can exhibit particle size effects in the ring opening of methylcyclopentane [33] (see Section 4.2.1.4).

An additional reaction path for the n-octane formation on 0.93Pt/silica is the ring opening of the major sk-Iso propylcyclopentane at the substituted endocyclic C-C bond. Also in the ring opening of ethylcyclopentane on 0.6Pt/silica others [4] found that 54 % of the ring-opening products were n-heptane, formed by hydrogenolysis of the substituted C-C bond.

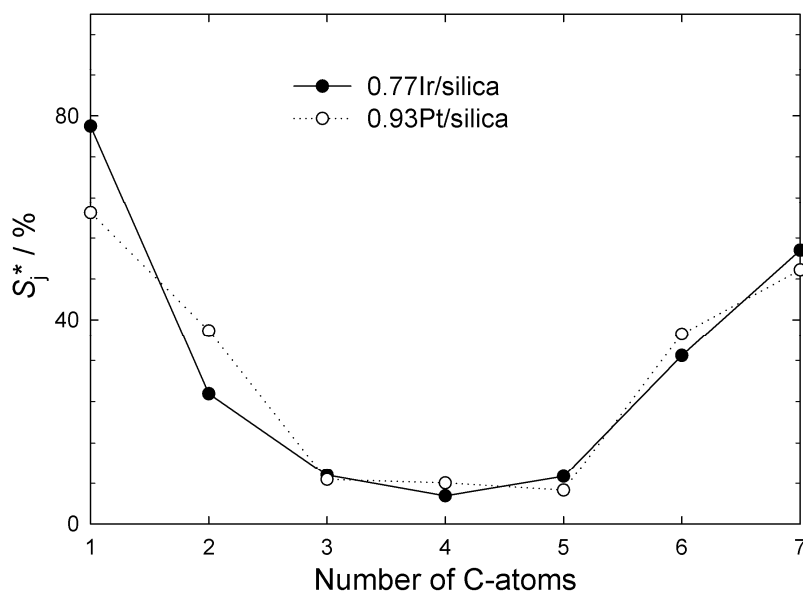


Figure 9.9: Modified hydrocracking selectivities S_j^* on two silica-supported catalysts in the hydroconversion of ethylcyclohexane:

0.77Ir/silica: $T_r = 290\text{ }^\circ\text{C}$; $X_{\text{E-CH}_x} = 31\text{ \%}$; $Y_{\text{C}_7} = 6\text{ \%}$; $\Sigma S_j^* = 215\text{ \%}$.

0.93Pt/silica: $T_r = 390\text{ }^\circ\text{C}$; $X_{\text{E-CH}_x} = 31\text{ \%}$; $Y_{\text{C}_7} = 10\text{ \%}$; $\Sigma S_j^* = 209\text{ \%}$.

For both catalysts the curves of the carbon number distributions of the hydrocracked products (see Figure 9.9) are symmetrical and very similar with large amounts of C_1 and C_7 , much C_2 and C_6 and small amounts of C_3 to C_5 . A similar curve was obtained

in the hydroconversion of decalin on weakly acidic iridium catalysts for which the term “hammock-type curve” was coined [52] (see Figure 4.21, page 38).

A large fraction of the C₆ and C₇ products are comprised of cyclohexane and methylcyclohexane, respectively. On the iridium catalyst at the lowest conversion a mole fraction of 86 % of the C₆ and 52 % of the C₇ fraction are cyclohexane and methylcyclohexane, respectively. These values decrease strongly with increasing conversion. On the platinum catalyst at the lowest conversion mole fractions of 91 % of the C₆ and of the C₇ fraction are cyclohexane and methylcyclohexane, respectively. On Pt/silica these values decrease only moderately with increasing conversion.

Hence, on iridium the high amounts of C₁, C₂, C₆ and C₇ stem at low conversions mainly from the exocyclic hydrogenolysis in the alkyl side-chain of ethylcyclohexane. However, at high conversions these products are formed to a larger extent by cleaving of C-C bonds in OCOs and by ring opening of cyclohexane and methylcyclohexane. On the platinum catalyst further additional reaction paths are possible due to its isomerization activity. One reason for the fast exocyclic hydrogenolysis in the alkyl side-chain on platinum could be the slow ring opening of six-membered rings on this metal [4].

In the hydrogenolysis of n-decane on Pt/silica at similar reaction conditions relatively small amounts of C₁ and C₉ are formed by cleaving the primary-secondary C-C bond in the alkyl chain (see Figure 9.3). Assuming a similar regioselectivity in the hydrogenolysis of the major OCO that is formed in the ring opening of ethylcyclohexane on Pt/silica, *viz.* n-octane, (see Figure 9.8b) relatively small amounts of C₁ and C₇ would be expected. However, since high amounts of C₁ and C₇ are formed this is an additional indication that n-octane is not the main precursor of hydrocracked products.

At the lowest conversion the ratio n_{M-CH_x} / n_{CH_x} equals 1.0 on the iridium and 1.5 on the platinum catalyst. With increasing conversion this ratio increases on the iridium catalyst to 1.8 at $X_{E-CH_x} = 68\%$, at higher conversions multiple hydrogenolysis occurs as indicated by $\sum S_j^* \gg 200\%$. In contrast, on the platinum catalysts this ratio decreases with increasing conversion to 1.1 at the maximal conversion of $X_{E-CH_x} = 53\%$ without multiple hydrogenolysis. Hence, on iridium both C-C bonds in the ethyl side-chain of ethylcyclohexane are cleaved with the same probability at low conversions, whereas at higher conversions the hydrogenolysis of the exocyclic primary-secondary C-C bond is preferred. On platinum this trend occurs with decreasing conversion.

9.3 Butylcyclohexane

Butylcyclohexane is the only commercially available direct ring-opening product of decalin, and it is formed on all Ir/silica and Pt/silica catalysts by a direct hydrogenolytic ring opening of cis-decalin (see Section 9.5). Hence, it was chosen as feed hydrocarbon to investigate the consecutive reaction steps of this intermediate in the formation of OCDs from decalin on 2.73Ir/silica and 2.69Pt/silica. For example, the distribution of the hydrocracked products formed from butylcyclohexane could give hints about the precursors of the hydrocracked products in the hydroconversion of decalin.

Again the iridium catalyst is much more active than the corresponding platinum catalyst with a similar metal loading (see Figure 9.10). To obtain similar conversions *ca.* 100 °C higher reaction temperatures have to be applied on 2.69Pt/silica.

On 2.73Ir/silica the hydrogenolysis of endo- and exocyclic C-C bonds in butylcyclohexane to OCDs and C₉-, respectively, are the main reactions at low conversions. A maximal Y_{OCDs} of 30 % is obtained at $T_r = 250$ °C. With increasing conversion, OCDs are hydrocracked to C₉-. Skeletal isomers and butylbenzene are formed in negligible amounts.

By contrast, on 2.69Pt/silica a maximal $S_{\text{sk-Isos}} = 27$ % at the lowest conversion shows that platinum alone is active in isomerization, possibly together with some very weak acid sites of silica at the high reaction temperatures of $T_r \geq 320$ °C. At the lowest conversions of 10 and 16 %, the fraction of pentylcyclopentane in the product group of sk-Isos amounts to 38 and 36 % respectively, and decreases with increasing conversion. As described for the isomerization of ethylcyclohexane to propylcyclopentane on 0.93Pt/silica (see Figures 9.5 and 9.6, page 95), metal-catalyzed isomerization mechanisms can explain its formation.

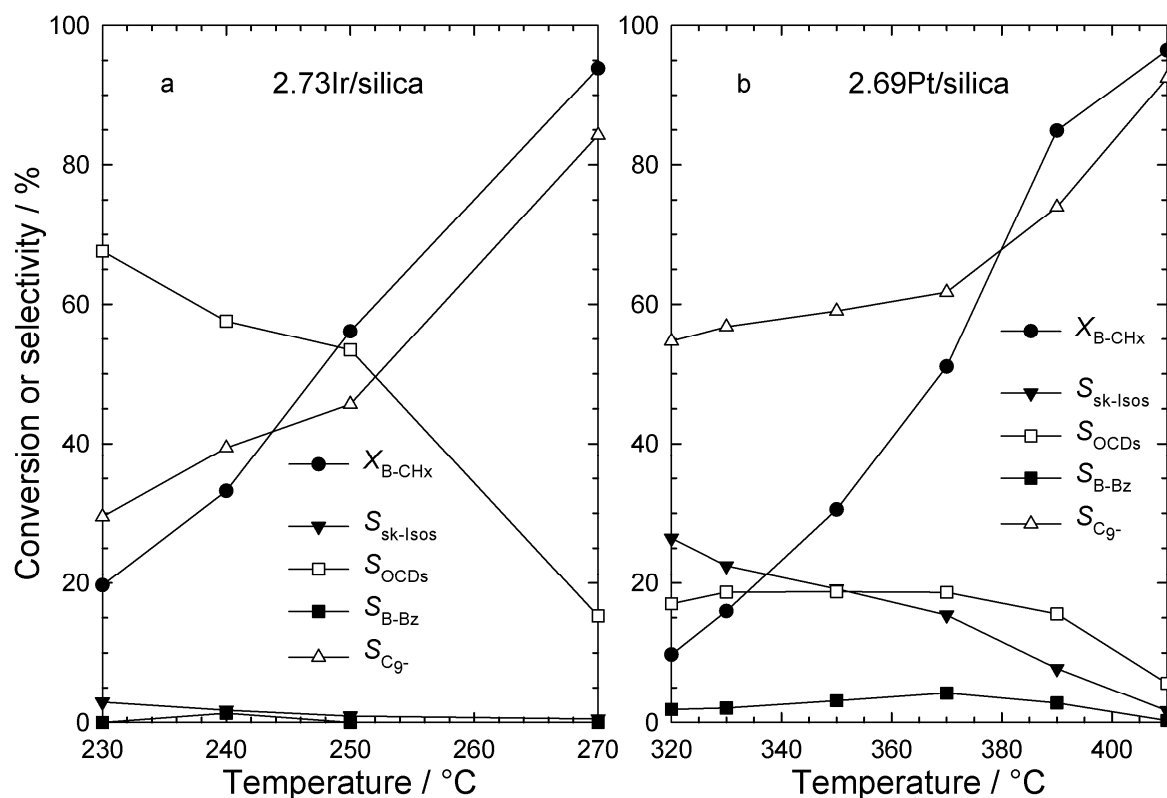


Figure 9.10: Conversion of butylcyclohexane and selectivities of different groups of products at different temperatures on two silica-supported catalysts.

On 2.69Pt/silica the strong preference of exocyclic instead of endocyclic hydrogenolysis is the reason for the low amounts of OCDs with a maximal $Y_{OCDs} = 13\%$ at $T_r = 390\text{ °C}$ and high amounts of C_9- formed (*vide infra*). Small amounts of butylbenzene with $S_{B-Bz} \leq 4\%$ were formed at the relatively high reaction temperatures.

For a detailed look at the direct hydrogenolysis products, the different C-C bonds in butylcyclohexane are designated as a to g, as shown in Figure 9.11. On both catalysts the summed up selectivities of the direct hydrogenolysis products methane, ethane, propane, n-butane, cyclohexane, methylcyclohexane, ethylcyclohexane, propylcyclohexane, n-decane, 5-methylnonane and 4-ethyloctane are $\geq 68\%$ at low conversions, see Table 9.1.

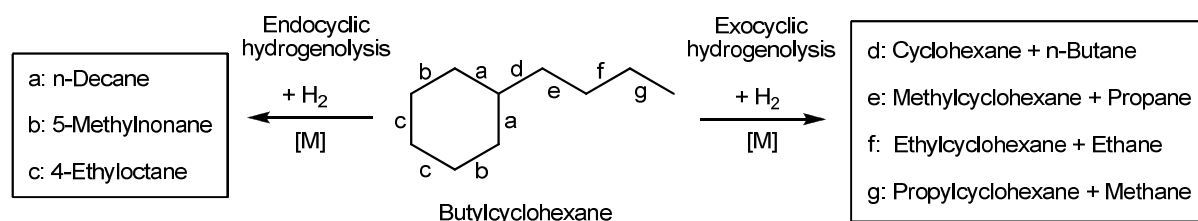


Figure 9.11: Labeling of the different C-C bonds in butylcyclohexane with the respective hydrogenolysis products.

Table 9.1: Direct hydrogenolysis products of butylcyclohexane on two silica-supported catalysts at low conversions.

	Catalyst		Theoretical Distribution		
	2.73Ir /silica	2.69Pt /silica	Selective mechanism	Non-selective mechanism	
$T_r / ^\circ\text{C}$	230	330			
$X_{\text{B-CH}_x} / \%$	20	16			
Selectivity of direct hydrogenolysis products / %	91	68	100	100	
$\Sigma S_j^* / \%$	198	205	200	200	
Molar Distribution of the Direct Hydrogenolysis Products with 6 to 10 Carbon Atoms / %					
Bond	Product				
a	n-Decane	5	11	0	20
b	5-Methylnonane	20	8	29	20
c	4-Ethyl-octane	49	6	29	20
d	Cyclohexane	2	19	0	10
e	Methylcyclohexane	19	43	14	10
f	Ethylcyclohexane	3	6	14	10
g	Propylcyclohexane	2	7	14	10

Moreover, the molar composition of the direct hydrogenolysis products with 6 to 10 carbon atoms is shown in Table 9.1 at mild reaction temperatures of negligible multiple hydrogenolysis ($\Sigma S_j^* \approx 200\%$). Interestingly, on 2.73Ir/silica the endocyclic bonds in butylcyclohexane are cleaved faster than the exocyclic bonds with a preference for the hydrogenolysis of the bisecundary C-C bonds b, c, e and f. A very similar distribution of the OCDs formed on 0.9Ir/ γ -alumina was detected by McVicker *et al.* [4]. Surprisingly, the exocyclic bisecundary bond e is opened about six times faster than the other exocyclic bisecundary bond f. Also in the hydrogenolysis of

n-decane on the same catalyst, the cleavage of the bonds between the third and the fourth carbon atom in the alkyl-chain was preferred. Perhaps, the adsorption of these carbon atoms is geometrically favored on iridium.

On Pt/silica the hydrogenolysis of exocyclic C-C bonds is faster and, as on Ir/silica, in the butyl side-chain a preference for the cleavage of bond e is found. Neither the selective nor the non-selective mechanism alone can explain the regioselectivities observed in the hydrogenolysis of butylcyclohexane on the two catalysts of Table 9.1.

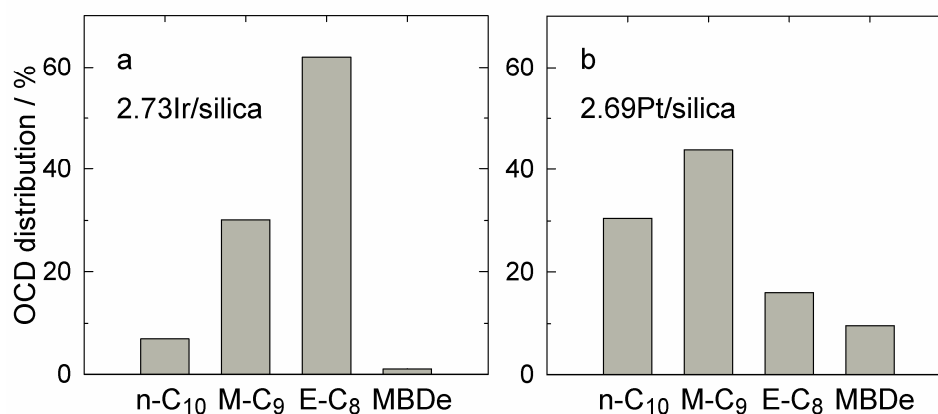


Figure 9.12: Breakdown of the selectivities of OCDs formed from butylcyclohexane into differently branched decanes on two silica-supported catalysts (MBDe: Multiply branched decanes):

2.73Ir/silica: $T_r = 250\text{ }^\circ\text{C}$; $X_{\text{B-CH}_x} = 56\%$; $Y_{\text{OCDs}} = 30\%$; $S_{\text{OCDs}} = 53\%$.

2.69Pt/silica: $T_r = 390\text{ }^\circ\text{C}$; $X_{\text{B-CH}_x} = 85\%$; $Y_{\text{OCDs}} = 13\%$; $S_{\text{OCDs}} = 16\%$.

From a practical viewpoint, the alkanes produced by ring opening should not have a too high degree of branching because this has a negative influence on the cetane number. In Figure 9.12 the distribution of OCDs classified into n-decane (n-C₁₀), methylnonanes (M-C₉), ethyloctanes (E-C₈) and multiply branched iso-decanes (MBDe) is given for 2.73Ir/silica and 2.69Pt/silica at conditions where maximal OCD yields were obtained. No propylheptane was formed. Since MBDe can only be formed from butylcyclohexane by isomerization prior to or after ring opening, these are virtually absent on the iridium catalyst, but they are formed on the mildly isomerization-active platinum catalyst. It is important to notice that, when at least two rings are present in the reactant, a significantly different distribution of open-chain alkanes is observed (see Sections 9.4 to 9.7).

A new type of distribution curves for the C₉- products was found with butylcyclohexane on 2.73Ir/silica (see Figure 9.13): Their features are very high amounts of C₃ and C₇, smaller amounts of C₁ and C₉, low amounts of C₂, C₄, C₆ and

C₈, and only traces of C₅. The black bars stand for the modified hydrocracking selectivities of the primary hydrogenolysis products which one would expect for a hydrogenolytic cleavage of one C-C bond in the butyl side-chain of butylcyclohexane, *i.e.* n-butane, cyclohexane, methylcyclohexane, ethylcyclohexane and propylcyclohexane. In the C₁ to C₃ fraction no differentiation between different products is possible.

As shown in Figure 9.13 at reaction conditions of maximal $Y_{\text{OCDs}} = 30\%$, 87 mol-% of the C₇ fraction consist of methylcyclohexane, formed by the hydrogenolytic abstraction of propane from butylcyclohexane. The remaining 13 mol-% are the respective ring-opening products n-heptane, 2-methylhexane and 3-methylhexane. In the C₈ products a mole fraction of 53 % is ethylcyclohexane, formed by ethane abstraction from butylcyclohexane, the remaining 47 % are virtually only the respective ring-opening products n-octane, 3-methylheptane and 3-ethylhexane. A small fraction of 19 mol-% of the C₉ products is propylcyclohexane, the remaining C₉ hydrocarbons are open-chain nonanes (OCNs) which can either be formed by a ring opening to OCDs and subsequent methane abstraction or by the ring opening of propylcyclohexane.

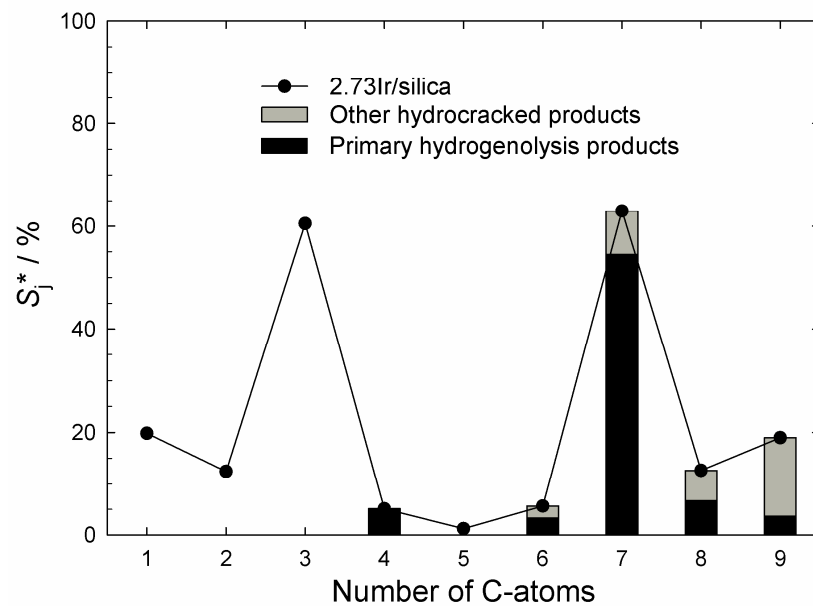


Figure 9.13: Modified hydrocracking selectivities S_j^* on 2.73Ir/silica in the hydroconversion of butylcyclohexane and fraction of primary hydrogenolysis products:

$$T_r = 250\text{ }^\circ\text{C}; X_{\text{B-CHx}} = 56\%; Y_{\text{C}_0^-} = 26\%; \Sigma S_j^* = 199\%.$$

From the fact that the fraction of primary hydrogenolysis products decreases from C₇ (87 mol-%) over C₈ (53 mol-%) to C₉ (19 mol-%) the following conclusion can be

drawn: With increasing molecular weight, the direct hydrogenolysis products methylcyclohexane, ethylcyclohexane and propylcyclohexane become adsorbed on iridium more preferentially, leading to a higher probability of ring opening in the same order. It is not surprising that C_5 products are virtually absent, as there is no C-C bond in butylcyclohexane the direct hydrogenolytic rupture of which would lead to a C_5 hydrocarbon (see Figure 9.11).

The carbon number distribution of the hydrocracked products on 2.69Pt/silica (see Figure 9.14) is qualitatively similar to the distribution obtained on the iridium catalyst. The higher amounts of C_4 and C_6 consisting, respectively, mainly of n-butane and cyclohexane, reflect the higher tendency of platinum to cleave substituted C-C bonds. Again, the C_7 fraction contains mainly methylcyclohexane formed by propane abstraction from butylcyclohexane.

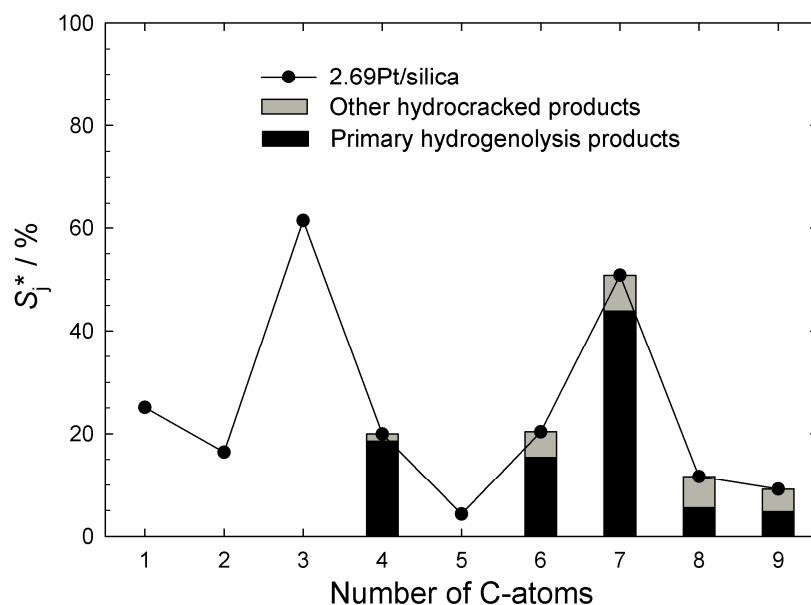


Figure 9.14: Modified hydrocracking selectivities S_j^* on 2.69Pt/silica in the hydroconversion of butylcyclohexane and fraction of primary hydrogenolysis products:

$$T_r = 390 \text{ }^\circ\text{C}; X_{\text{B-CH}_x} = 85 \text{ } \%; Y_{\text{C}_0^-} = 63 \text{ } \%; \sum S_j^* = 219 \text{ } \%.$$

With increasing reaction temperature and, hence, increasing conversion and increasing extent of multiple hydrogenolysis, the values of C_7 and C_9 decrease and those of C_1 , C_2 and C_6 increase on the platinum catalyst, see Figure 9.15. Since C_7 products are largely composed of methylcyclohexane, their smaller amounts at higher reaction temperatures can be explained by the abstraction of methane under the formation of the C_6 product cyclohexane. A similar hydrogenolysis reaction seems to occur in the alkyl side-chain of propylcyclohexane at high reaction temperatures. From $T_r = 370$ to

410 °C the mole fraction of propylcyclohexane in the C₉ products decreases from 73 to 16 %, presumably due to exocyclic hydrogenolysis under the formation of ethane and methylcyclohexane.

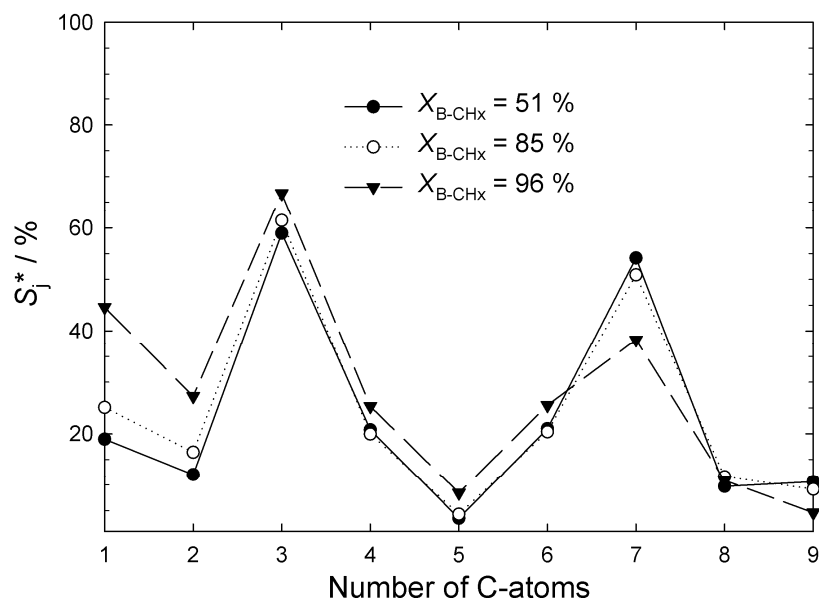


Figure 9.15: Modified hydrocracking selectivities S_j^* on 2.69Pt/silica in the hydroconversion of butylcyclohexane at different temperatures:

$T_r = 370$ °C; $X_{B-CHx} = 51$ %; $Y_{C_9} = 32$ %; $\Sigma S_j^* = 210$ %.

$T_r = 390$ °C; $X_{B-CHx} = 85$ %; $Y_{C_9} = 63$ %; $\Sigma S_j^* = 219$ %.

$T_r = 410$ °C; $X_{B-CHx} = 96$ %; $Y_{C_9} = 89$ %; $\Sigma S_j^* = 252$ %.

A more detailed discussion of possible ring-opening mechanisms in the butylcyclohexane conversion is conducted in Section 10.2.

9.4 Perhydroindan

In the ring opening of bicyclic naphthenes like decalin on catalysts containing Brønsted acid sites an isomerization of six- to five-membered rings was frequently reported as reaction step that precedes the ring-opening [5, 59]. Since perhydroindan contains both a five- and a six-membered ring in one molecule, it is a particularly interesting reactant for ring-opening studies on non-acidic metal catalysts, *viz.* 0.77Ir/silica, 0.93Pt/silica and 0.60Pd/silica.

A mixture of both stereoisomers consisting of 70 % cis- and 30 % trans-perhydroindan was used as feed in all catalytic experiments. In the products of the catalytic

hydroconversion the mole fraction of cis-perhydroindan assumed values between 47 and 61 %, regardless of the catalyst used and the perhydroindan conversion attained in a very broad range from a few percent to *ca.* 90 %. Also on the bifunctional catalyst 1.0Pd/Na_{0.70}H_{0.30}-[Al]Beta-14.0 this mole fraction assumed values of 50 to 51 % (catalytic results in Section 10.3). Moreover, these values resemble the results of Frye and Weitkamp [85] and of Allinger and Coke [86] who converted indene or perhydroindan, respectively, on Pd/carbon catalysts and found mole fractions of cis-perhydroindan ranging from 53 to 57 % and 50 to 58 %, respectively.

Hence, it can be concluded that equilibrium is rapidly established between the two stereoisomers, in analogy to the very rapid equilibration of cis- and trans-decalin observed in recent studies with zeolitic iridium- and platinum-containing catalysts [5, 52]. For the equilibration of the stereoisomers, mechanisms at the Brønsted acid sites *via* carbocations or at the noble metal sites *via* olefins can be invoked [87]. From the fact that the cis/trans-stereoisomerization occurs as the fastest reaction on the three monofunctional silica catalysts and also on the bifunctional zeolite catalyst (see Section 10.3) it can be concluded that the stereoisomerization proceeds on the noble metals.

On the three silica catalysts, that were tested with perhydroindan (see Figure 9.16) the metal contents of Ir, Pt and Pd are approximately the same. So the following activity sequence can be deduced for perhydroindan hydroconversion: Ir > Pt > Pd. This is in accordance with literature data, *e.g.* for the hydrogenolysis of n-heptane [31]. Although the metal content on a molar basis is higher on 0.60Pd/silica, the low metal dispersion (see Table 6.1, page 74) could be an additional explanation for the low activity of this catalyst.

On 0.77Ir/silica ROPs are the sole products at low conversions. At higher conversions endocyclic hydrogenolysis of ROPs leads to OCN formation with a maximal $Y_{\text{OCNs}} = 30\%$ at $T_r = 310\text{ }^\circ\text{C}$. At still higher temperatures exocyclic hydrogenolysis of ROPs and hydrogenolysis of OCNs result in the formation of C₈- products. A similar selectivity pattern is observed for 0.93Pt/silica, however, as observed already with other hydrocarbons skeletal isomerization occurs to a small extent with the highest selectivity $S_{\text{sk-Isos}} = 8\%$ at the lowest conversion and $T_r = 300\text{ }^\circ\text{C}$. A maximal $Y_{\text{OCNs}} = 19\%$ at $T_r = 410$ was attained, see Table 9.2.

Table 9.2: Maximum yields of open-chain nonanes obtained in the hydroconversion of perhydroindan.

Catalyst	$T_r / ^\circ\text{C}$	$X_{\text{PHI}} / \%$	$S_{\text{OCNs}} / \%$	$Y_{\text{OCNs, max.}} / \%$
0.77Ir/silica	310	98	31	30
0.93Pt/silica	410	93	21	19
0.60Pd/silica	410	37	0.1	0.0

0.60Pd/silica is hardly active in skeletal isomerization and ring opening of perhydroindan (see Figure 9.16c). It is, however, an efficient catalyst for its dehydrogenation to indan with a maximal mole fraction $n_{\text{indan}} / (n_{\text{PHI}} + n_{\text{indan}}) = 32 \%$ and traces of indene at the maximal reaction temperature of 410 °C. This is probably not far from the position of the dehydrogenation/hydrogenation equilibrium and in the same order of magnitude as data published by Nylén *et al.* [88]. These authors converted indan on an Ir,Pt/boehmite catalyst at a hydrogen pressure of 4.0 MPa.

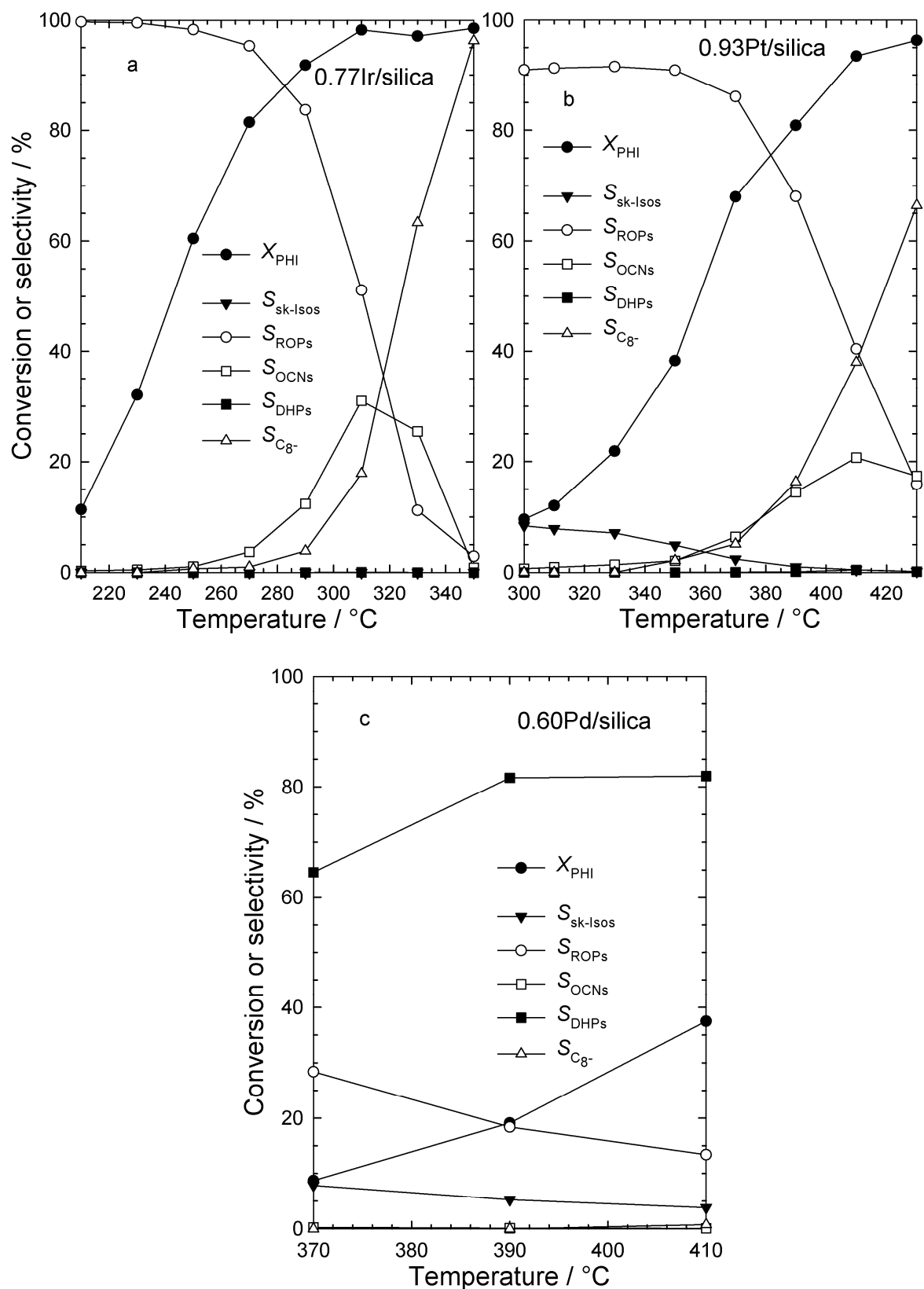


Figure 9.16: Conversion of perhydroindan and selectivities of different groups of products at different temperatures on three silica-supported catalysts.

A closer look at the ring-opening products formed on the three metals (see Figure 9.17) shows that endocyclic hydrogenolysis of the five-membered ring is clearly preferred. This is particularly true for iridium where the ring-opening results almost exclusively in C₉ naphthenes with a remaining six-membered ring (CH_x-ROPs). The reasons for the peculiar behavior of the data points at the two highest temperatures in Figure 9.17a are unknown. This extreme preference for opening the five-membered ring is usually interpreted in terms of a higher ring strain in five-membered compared to six-membered rings [4, 38]. On platinum this preference is less pronounced than on iridium, up to 11 % of all ROPs contain a five-membered ring (CP_n-ROPs). It might also be that the higher temperatures that had to be applied with the platinum catalyst facilitate opening of the six-membered ring.

Only small selectivities of ROPs between 13 and 28 % were reached on 0.60Pd/silica. They are composed mainly of ROPs with a remaining saturated six-membered ring (Figure 9.17c) and the corresponding aromatics which are formed in substantial amounts and make up 33 mol-% of all ROPs at 410 °C. No aromatic ROPs were formed on the other two silica-supported catalysts. This is in accordance with the low activity of the catalyst in general together with the high reaction temperatures that led also to large amounts of the DHPs indan and indene, see Figure 9.16c. Also some ROPs are formed on all three catalysts which cannot be assigned to particular molecules but were assigned to the product group of ROPs by GC/MS due to their molecular ion signal (unknown ROPs) but they contribute only to a very small extent on Ir/silica and Pt/silica. On Pd/silica up to 10 % of all ROPs are unidentified, but due to the small ring-opening selectivity the total amount of these products is unimportant.

As depicted in Figure 9.18, opening of the five-membered ring in perhydroindan can principally result in three C₉ ROPs, *viz.* 1-ethyl-2-methylcyclohexane (*cis*- and *trans*-isomer) or propylcyclohexane and cyclononane. The first-mentioned hydrocarbon forms by hydrogenolysis *via* the selective ring-opening mechanism whereas hydrogenolysis *via* the non-selective or partially selective mechanism would be expected to give 1-ethyl-2-methylcyclohexane, propylcyclohexane, and, perhaps, cyclononane. No cyclononane was found in the products of all three catalysts by GC/MS analysis, but it cannot be ruled out that traces of the compound have been formed. Propylcyclohexane did occur, but only in very small amounts ($S_{P-CH_3} \ll S_{1-E-2-M-CH_3}$). Unfortunately, on the Supelco Petrocol DH 150 capillary column, the peak for propylcyclohexane appears very shortly after that of *cis*-1-ethyl-2-methylcyclohexane, hence small amounts of propylcyclohexane cannot be reliably quantified, if the peak of *cis*-1-ethyl-2-methylcyclohexane is large. Exactly this was the case in the chromatograms of the products on Ir/silica, confirming the expectation

[4, 33] that hydrogenolytic ring cleavage of perhydroindan on that catalyst proceeds *via* the selective mechanism.

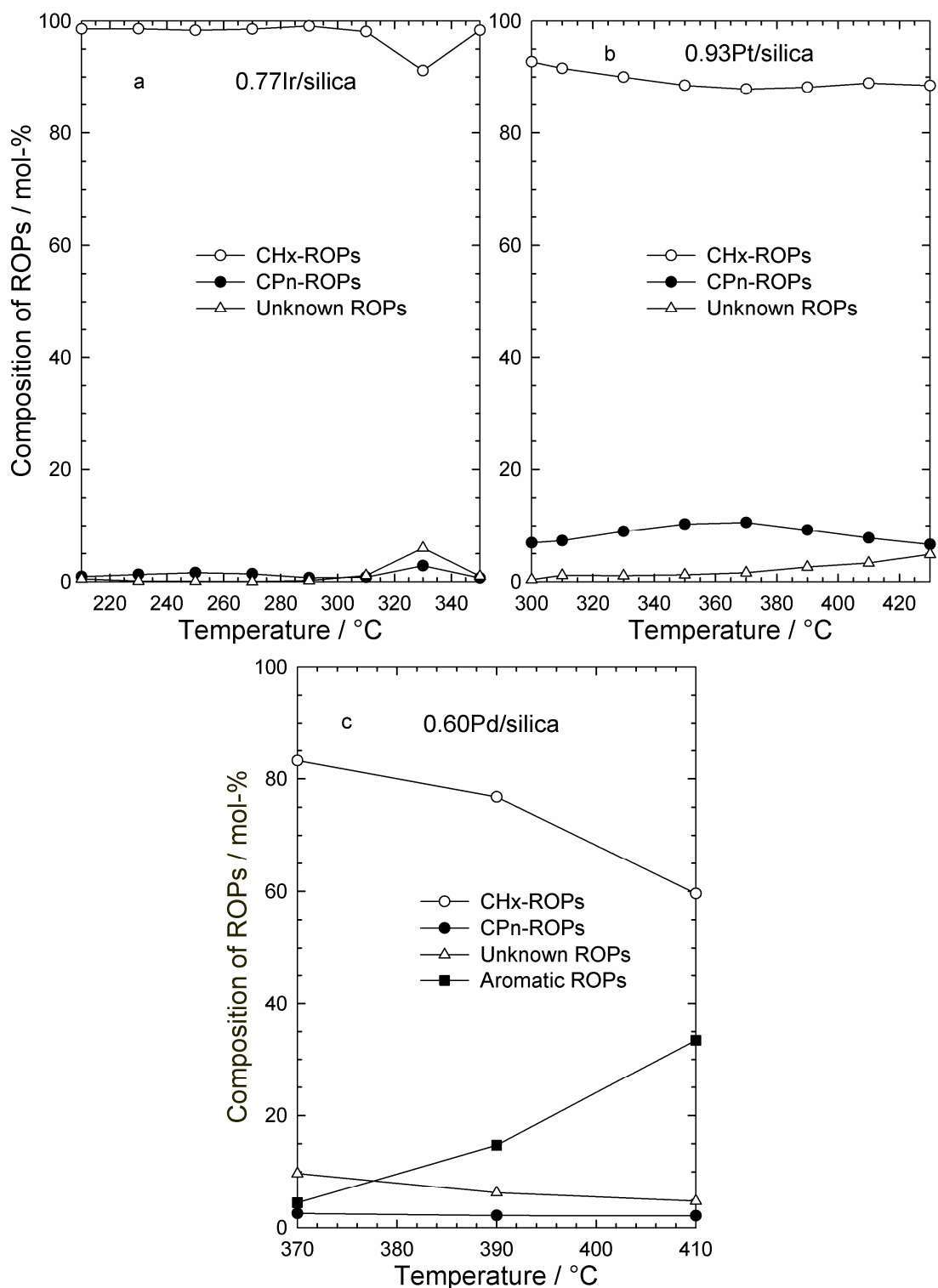


Figure 9.17: Breakdown of the ring-opening products into ROPs with a remaining six-membered ring (CHx-ROPs), with a remaining five-membered ring (CPn-ROPs), into ROPs that have been identified by the molar mass of $M = 126 \text{ g} \cdot \text{mol}^{-1}$ only (unknown ROPs) and into ROPs with an aromatic ring (aromatic ROPs).

On Ir/silica within the temperature range from 210 to 310 °C the mole fraction of cis- and trans-1-ethyl-2-methylcyclohexane in the total ring-opening products amounted to values between 96 and 100 %. Using Pt/silica and Pd/silica, this mole fraction assumed values between 34 and 61 % only. This is partly due to the opening of the six-membered ring in perhydroindan, partly to the occurrence of hydrogenolysis at substituted carbon-carbon bonds according to the non-selective mechanism which is well-known to operate on highly dispersed platinum [33], and partly to the mild skeletal isomerization activity of platinum and palladium.

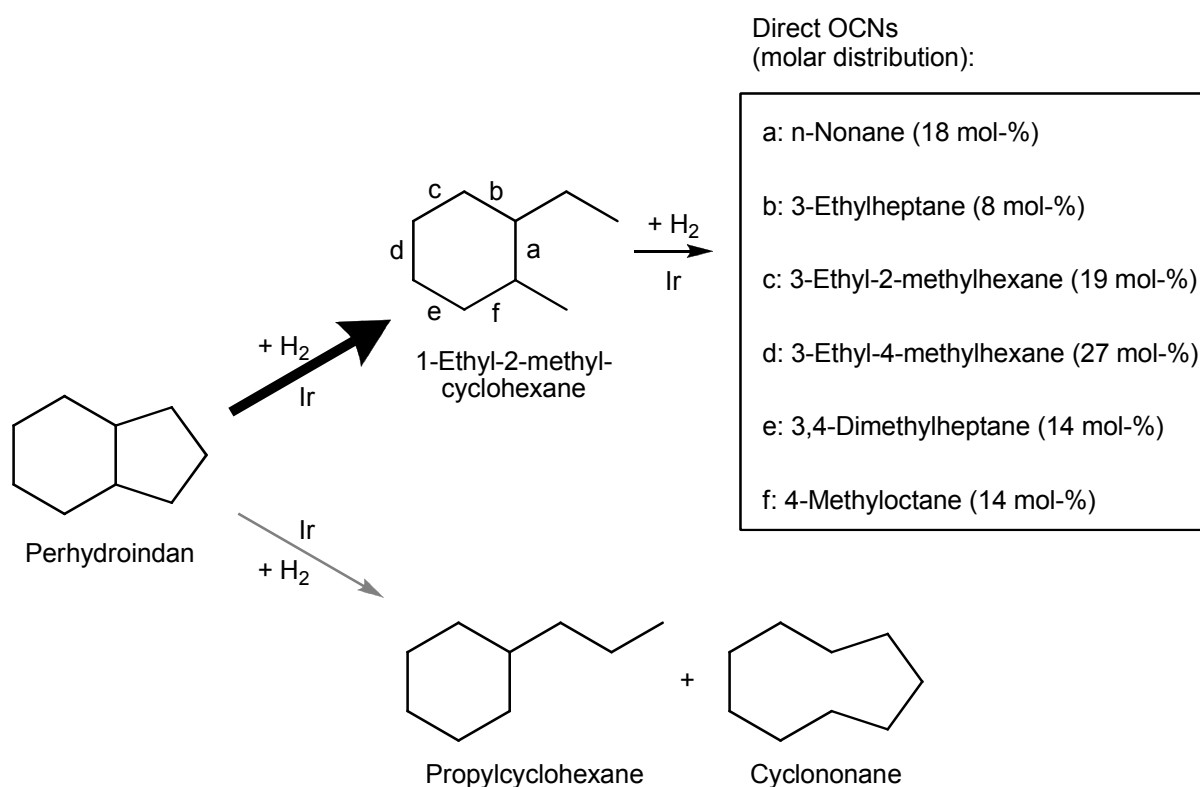


Figure 9.18: Ring opening of perhydroindan on 0.77Ir/silica. The molar distribution of direct OCNs was obtained at $T_r = 310$ °C.

Given the extremely high selectivity for the ring-opening products cis- and trans-1-ethyl-2-methylcyclohexane on Ir/silica, one expects the formation of open-chain nonanes to occur by a second hydrogenolysis step starting from this particular C₉ naphthene. The six predicted open-chain nonane isomers (direct OCNs) are listed in Figure 9.18 together with their molar distribution. Indeed, at reaction conditions of maximal Y_{OCNs} , *i.e.*, at $T_r = 310$ °C these direct OCNs account for 92 % of all OCNs formed. Since only 60 % of the direct OCNs were formed *via* cleavage of the unsubstituted bonds c, d and e, a pure selective ring-opening mechanism cannot account for their formation. A ring cleavage of bonds between substituted carbon atoms is best accounted for by the partially selective mechanism [33]. It is known to

become operative at the higher temperatures required for the more demanding hydrogenolysis of six-membered naphthenic rings, especially if the number of alkyl substituents increases, and it was also invoked by McVicker *et al.* [4] for the hydrogenolysis of 1,2,4-trimethylcyclohexane on an Ir/ γ -alumina catalyst.

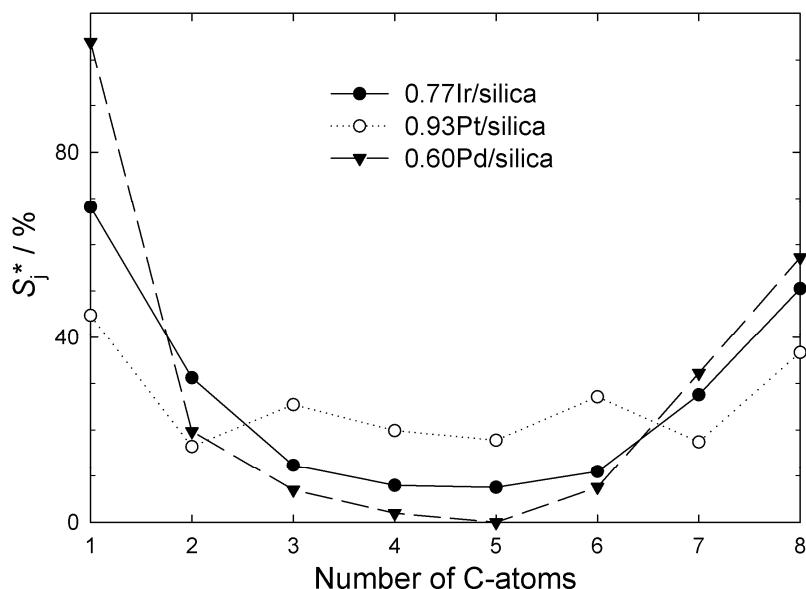


Figure 9.19: Modified hydrocracking selectivities S_j^* on three silica-supported catalysts in the hydroconversion of perhydroindan:

0.77Ir/silica: $T_r = 310\text{ }^\circ\text{C}$; $X_{\text{PHI}} = 98\%$; $Y_{\text{C}_8^-} = 18\%$; $\Sigma S_j^* = 217\%$.

0.93Pt/silica: $T_r = 410\text{ }^\circ\text{C}$; $X_{\text{PHI}} = 93\%$; $Y_{\text{C}_8^-} = 35\%$; $\Sigma S_j^* = 205\%$.

0.60Pd/silica: $T_r = 410\text{ }^\circ\text{C}$; $X_{\text{PHI}} = 37\%$; $Y_{\text{C}_8^-} = 0.3\%$; $\Sigma S_j^* = 229\%$.

Figure 9.19 displays the carbon number distributions of the C_8^- products. For Ir/silica and Pt/silica, the experiments with maximal selectivities of open-chain nonanes and moderate selectivities of hydrocracked products were chosen. A typical hammock-type distribution curve is obtained on Ir/silica as also described for Ir/Na,H-Y in the perhydroindan conversion [67]. It is obvious that on both iridium catalysts the C_8^- hydrocarbons are formed *via* hydrogenolysis on the metal. Essentially the same hammock-type curve results on Pd/silica, hydrogenolysis seems to be the pathway for C_8^- formation on this catalyst as well. The distribution curve for Pt/silica (Figure 9.19) is almost identical to the one for Pt/Na,H-Y zeolite in the perhydroindan conversion [67].

In Figure 9.20 the distribution of OCNs classified into n-nonane (n- C_9), methyloctanes (M- C_8), ethylheptanes (E- C_7) and multiply branched iso-nonanes (MBNo) is given for 0.77Ir/silica and 0.93Pt/silica at conditions where maximal OCN yields were obtained. It is obvious that the iridium catalyst tends to produce much larger amounts of

multiply branched nonanes compared to Pt/silica. From the viewpoint of the diesel fuel ignition characteristics the latter catalyst is more favorable.

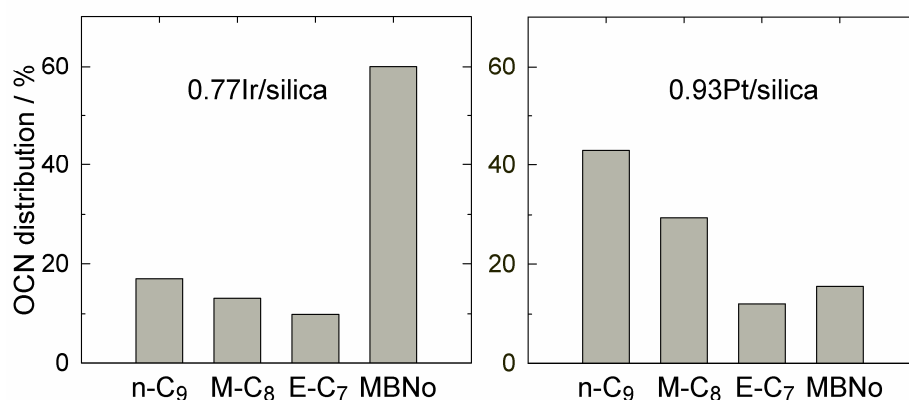


Figure 9.20: Breakdown of the selectivities of OCNs into differently branched nonanes on two silica-supported catalysts:

0.77Ir/silica: $T_r = 310\text{ }^\circ\text{C}$; $X_{\text{PHI}} = 98\%$; $Y_{\text{OCNs}} = 30\%$; $S_{\text{OCNs}} = 31\%$.

0.93Pt/silica: $T_r = 410\text{ }^\circ\text{C}$; $X_{\text{PHI}} = 93\%$; $Y_{\text{OCNs}} = 19\%$; $S_{\text{OCNs}} = 21\%$.

9.5 cis-Decalin

On iridium- or platinum-containing zeolite catalysts with a low concentration of relatively weak Brønsted acid sites typical metal-catalyzed reactions were observed in the hydroconversion of cis-decalin [5, 74]. Now, the deliberately non-acidic support silica is used, for which the absence of catalytically active Brønsted acid sites was evidenced by FT-IR spectroscopy (see Section 6.2) and the test reaction with n-octane (see Section 8). To examine the influence of a higher surface area of the support material, also iridium- or platinum-containing catalysts supported on [Si]SBA-15 were tested, *viz.* 0.77Ir/silica, 2.59Ir/silica, 0.73Ir[Si]SBA-15, 0.93Pt/silica, 2.68Pt/silica and 0.92Pt/[Si]SBA-15. Since little is known about a particle size effect of rhodium, two Rh/silica catalysts, *viz.* 1.03Rh/silica and 0.96Rh/silica, with different metal dispersions of $D = 0.17$ and 0.57 , respectively, were tested.

9.5.1 Stereoisomerization of cis- and trans-Decalin

On all eight catalysts with the noble metals iridium, platinum or rhodium the fastest reaction is the stereoisomerization of cis- to trans-decalin. The mole fraction $n_{\text{tr-Dec}} / (n_{\text{c-Dec}} + n_{\text{tr-Dec}})$ assumed values from 0.83 to 0.92 at reaction temperatures from 250 to 410 °C and conversions in the range from 8 to 90 %. As discussed previously [52], the extent of isomerization corresponds nicely to the values calculated from

compiled thermodynamic data [84, 89]. Accordingly, this stereoisomerization is very likely to occur on these catalysts *via* dehydrogenation to 1,9- or 9,10-octalins (mono-unsaturated decalin) and re-hydrogenation to trans-decalin as proposed by Weitkamp [87]. This is in agreement with a finding reported by Lai and Song [90] that decalin stereoisomerization proceeds readily on metal-containing H-mordenites, but much more slowly on metal-free H-mordenite. Also the stereoisomerization of cis- and trans-perhydroindan occurs most likely on the noble metals (see Section 9.4). Since this stereoisomerization is very fast, cis- and trans-decalin are lumped as a pseudo-reactant “decalin”.

9.5.2 Hydroconversion on Ir/Silica and Ir/[Si]SBA-15 Catalysts

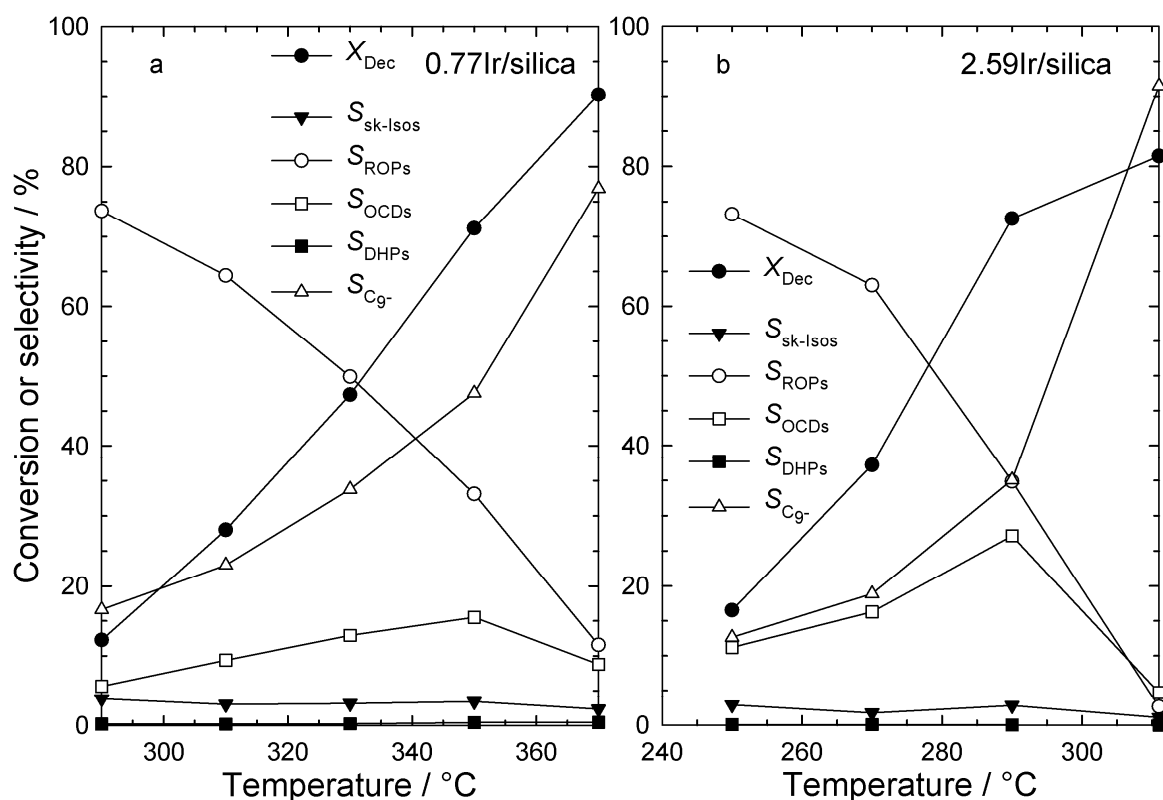


Figure 9.21: Conversion of decalin and selectivities of different groups of products at different temperatures on two Ir/silica catalysts.

As primary group of products, ROPs are formed with $S_{ROPs} > 70\%$ at the lowest conversions on both Ir/silica catalysts, see Figure 9.21. Further, the S_{OCDs} go through maxima with a $Y_{OCDs} = 11\%$ at $T_r = 350\text{ °C}$ on 0.77Ir/silica and $Y_{OCDs} = 20\%$ at $T_r = 290\text{ °C}$ on 2.59Ir/silica. The results suggest that one reason for the very small amounts of OCDs formed on 0.9Ir/ γ -alumina from decalin in the work of McVicker *et al.* [4] was a too mild reaction condition ($T_r = 275\text{ °C}$, $LHSV = 1.6\text{ h}^{-1}$). At higher

temperatures, as seen in Figure 9.21, most hydrocarbons are hydrocracked to C₉-. Skeletal isomers are formed with low selectivities ≤ 4 %, indicating that isomerization on the noble metal plays an almost negligible role. Dehydrogenation to tetralin and naphthalene with S_{DHPs} < 1 % is practically absent. An increase of the iridium content from 0.77Ir/silica to 2.59Ir/silica leads to a similar conversion at an about 40 °C lower reaction temperature.

In separate experiments using 2.73Ir/silica as catalyst in a second high-pressure flow-type apparatus at long times-on-stream and T_r = 290 °C a decrease of conversion from 64 to 52 % was observed after 70 h. Meanwhile, the yield of OCDs decreased from 12 to 7 %. If deactivation had originated from coke formation on the metal clusters most probably DHPs or products with more than ten carbons would have been observed in the product mixture [91]. Since at these reaction temperatures such products were absent, most probably deactivation did not originate from coke formation but rather from sintering of iridium. A determination of the metal dispersion on the used catalyst by hydrogen chemisorption was not conducted since the adsorbed hydrocarbons on the catalyst are known to interfere with such measurements. 0.73Ir/[Si]SBA-15 showed a similar activity and product distribution like 0.77Ir/silica, see Table 9.3. Hence, this mesoporous support with a higher specific surface area does not show advantageous catalytic properties in comparison with amorphous silica.

Table 9.3: Maximum yields of open-chain decanes and selectivities of open-chain nonanes obtained in the hydroconversion of decalin.

Catalyst	T _r / °C	X _{Dec} / %	S _{OCDs} / %	Y _{OCDs, max.} / %	S _{OCDs} / %
0.77Ir/silica	350	71	16	11	8
2.59Ir/silica	290	73	28	20	8
0.73Ir/[Si]SBA-15	350	61	12	7	7

As summarized in Table 9.3, the highest yield of OCDs was obtained on 2.59Ir/silica with Y_{OCDs, max.} = 20 % at T_r = 290 °C. In the order of their abundance, the seven OCDs with highest selectivities were: an unidentified OCD, 4-ethyloctane, 3,4-diethylhexane, n-decane, an unidentified OCD, 5-methylnonane, 4,5-dimethyloctane (both diastereoisomers). Unidentified OCDs are decane isomers that cannot be assigned to a specific molecule but to the group of OCDs by GC/MS (*vide infra*). For the hydroconversion of a real feedstock into a blending component for diesel fuel a ring opening that is accompanied by a degradation of the carbon number by one can still furnish useful products with good cetane numbers and boiling points in the diesel range. On the

iridium catalysts OCNs with a selectivity of 8 % at the maximal yield of OCDs on 2.59Ir/silica were formed. Hence, a combined $Y_{\text{OCDs}} + Y_{\text{OCNs}} = 26\%$ was attained at $T_r = 290\text{ }^\circ\text{C}$.

For a more concise discussion and due to the similar catalytic behavior of the silica- and the [Si]SBA-15-supported catalysts with a metal loading of 0.77 and 0.73 wt.-%, respectively, only the results of the silica-supported one will be discussed in detail.

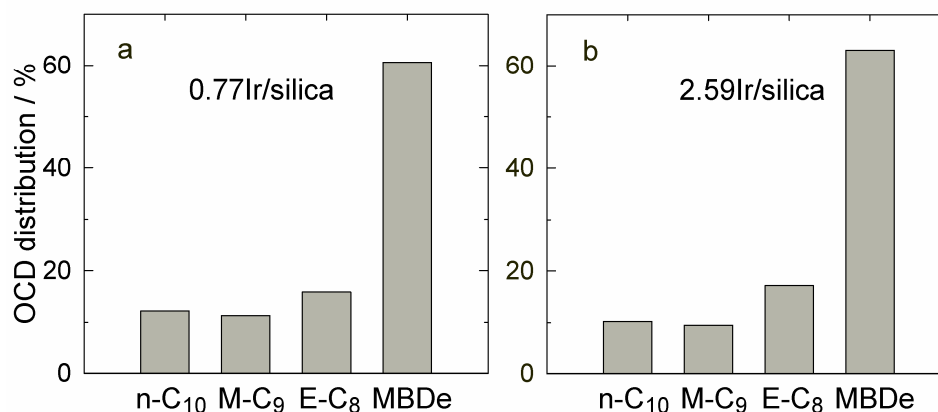


Figure 9.22: Breakdown of the selectivities of OCDs into differently branched decanes on two Ir/silica catalysts:

0.77Ir/silica: $T_r = 350\text{ }^\circ\text{C}$; $X_{\text{Dec}} = 71\%$; $Y_{\text{OCDs}} = 11\%$; $S_{\text{OCDs}} = 16\%$.

2.59Ir/silica: $T_r = 290\text{ }^\circ\text{C}$; $X_{\text{Dec}} = 73\%$; $Y_{\text{OCDs}} = 20\%$; $S_{\text{OCDs}} = 28\%$.

For the upgrading of diesel fuel the degree of branching in the formed decane isomers has a strong influence on the cold-flow properties and also on the cetane number [92]. In Figure 9.22 the selectivities of the differently branched decanes formed on the catalysts are summarized, no propylheptane was detected on any of these catalysts. On both catalysts very similar distributions of the differently branched OCDs are generated. Multiply branched decanes dominate the distribution with relative selectivities of 61 and 63 % on 0.77Ir/silica and 2.59Ir/silica, respectively. The relative selectivities of n-decane, methylnonanes and ethyloctanes are between 10 and 17 %. Iridium is well-known to open preferentially unsubstituted C-C bonds by the selective ring-opening mechanism, so the high fraction of multiply branched decanes can be rationalized by a hydrogenolytic rupture of one endocyclic bissecondary C-C bond in each of both rings of one decalin molecule. In a hydrocracking of such bonds, the branchings in the reactant molecules survive.

Hammock-shaped curves for the distributions of the hydrocracked products on both Ir/silica catalysts are obtained, as shown in Figure 9.23 for comparable conversions. High amounts of methane and C₉, smaller amounts of C₂ and C₈ and further decreasing

modified selectivities towards C_5 are formed, as reported also in the decalin conversion on weakly acidic zeolite Y catalysts (see Figure 4.21, page 38) [5]. The curves are almost symmetrical, with slightly higher values at C_1 to C_4 , indicating, together with $\Sigma S_j^* > 200\%$, that some hydrocracked products stem from secondary hydrogenolysis of primary C_9 - products. Methane and ethane are not formed in bifunctional catalysis *via* carbocations, hence it can be concluded that, on Ir/silica, noble metal catalyzed hydrogenolysis is the main hydrocracking pathway. Also the hydroconversion of the bicyclic C_9 naphthene perhydroindan on 0.77Ir/silica and 0.60Pd/silica results in such a curve type with high amounts of C_1 and C_8 (see Figure 9.19, page 113).

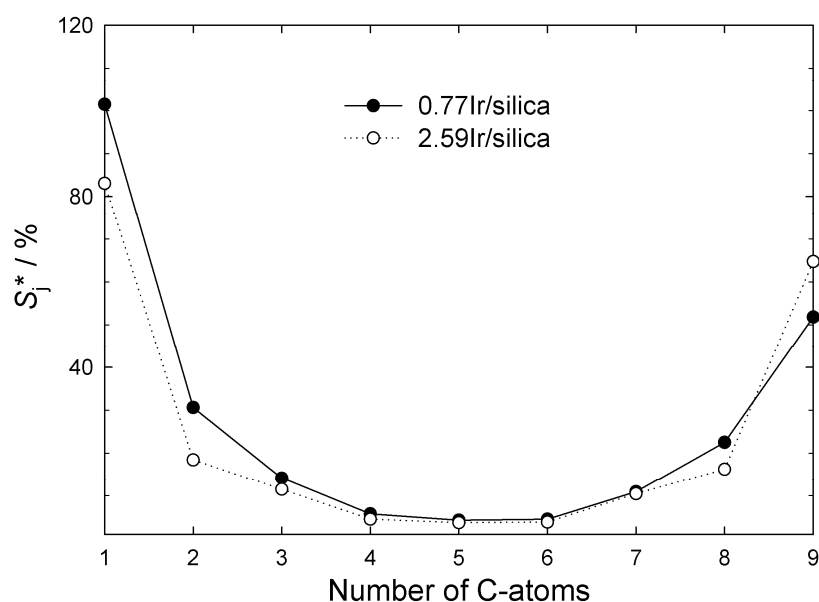


Figure 9.23: Modified hydrocracking selectivities S_j^* on two Ir/silica catalysts in the hydroconversion of decalin:

0.77Ir/silica: $T_r = 330\text{ }^\circ\text{C}$; $X_{\text{Dec}} = 47\%$; $Y_{C_9^-} = 16\%$; $\Sigma S_j^* = 246\%$.

2.59Ir/silica: $T_r = 270\text{ }^\circ\text{C}$; $X_{\text{Dec}} = 43\%$; $Y_{C_9^-} = 3\%$; $\Sigma S_j^* = 217\%$.

In comparison to the large number of products on 2.68Pt/silica (91 signals at $X_{\text{Dec}} = 9\%$, catalytic results in Section 9.5.3), a slightly less complex product distribution was formed on 2.59Ir/silica (77 signals at $X_{\text{Dec}} = 17\%$) with a few strong signals dominating the product mixture at low conversions. In Figure 9.24 the gas chromatogram of the product of decalin hydroconversion on catalyst 2.59Ir/silica at a low conversion of 17% is depicted. Beside cis- and trans-decalin, the most intense peaks stem from the five direct ring-opening products (direct ROPs) butylcyclohexane (B-CHx), cis- and trans-1-methyl-2-propylcyclohexane (1-M-2-P-CHx) and cis- and trans-1,2-diethylcyclohexane (1,2-DE-CHx). Moreover, the direct C_9 ring-opening

products (direct C₉ ROPs) cis- and trans-1-ethyl-2-methylcyclohexane (1-E-2-M-CHx), which are expected to be formed by the abstraction of methane from direct ROPs, can be identified as important signals. The signal of the third expected direct C₉ ROP, *i.e.* propylcyclohexane, overlaps with the signal of an unknown OCD. By co-injection of propylcyclohexane with the product mixture it was verified that this signal originates mainly from the OCD, hence, the small amounts of propylcyclohexane could not be reliably determined.

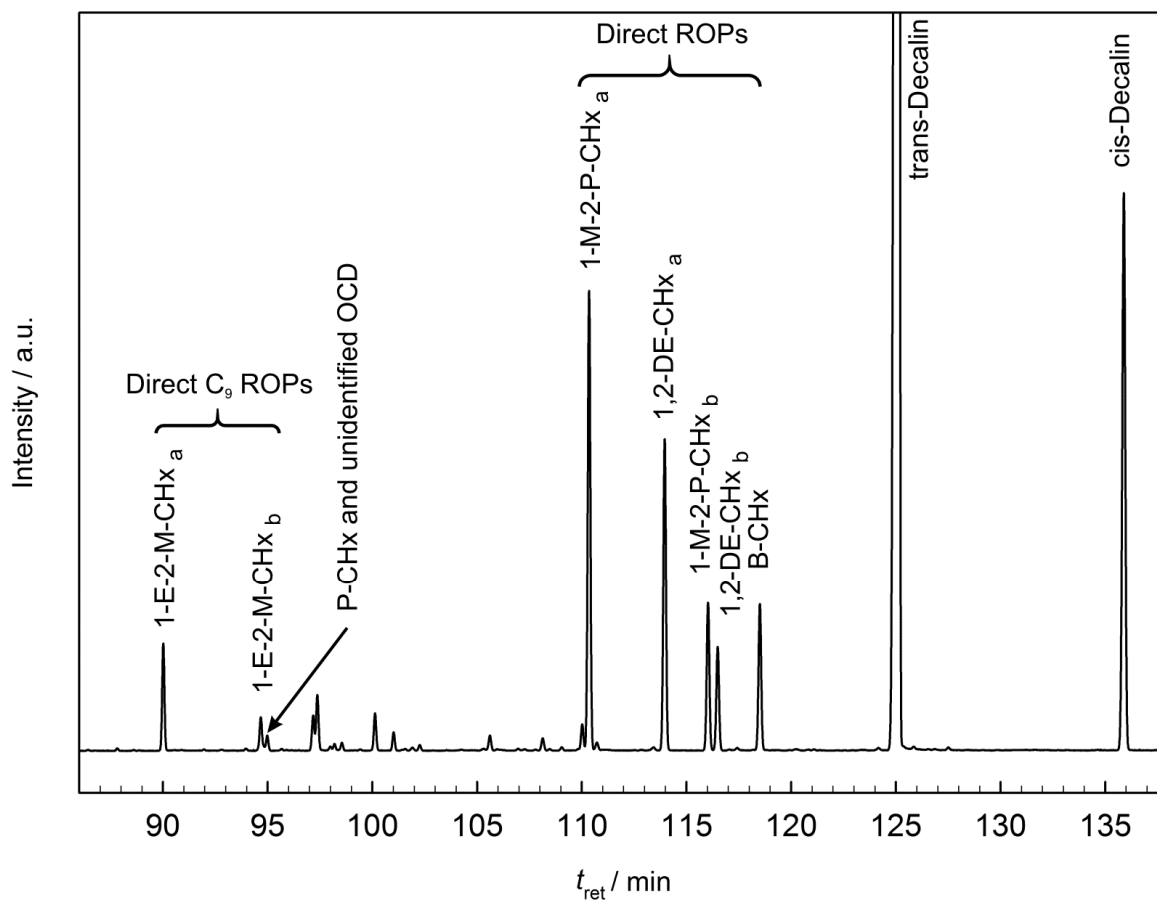


Figure 9.24: Section of the gas chromatogram of the product of the decalin hydroconversion on the 2.59Ir/silica catalyst at $X_{Dec} = 17\%$. Direct ring-opening products (direct ROPs): butylcyclohexane (B-CHx), cis- and trans-1-methyl-2-propylcyclohexane (1-M-2-P-CHx) and cis- and trans-1,2-diethylcyclohexane (1,2-DE-CHx). Direct C₉ ring-opening products (direct C₉ ROPs): cis- and trans-1-ethyl-2-methylcyclohexane (1-E-2-M-CHx) and propylcyclohexane (P-CHx). *a* and *b* denote the two stereoisomers.

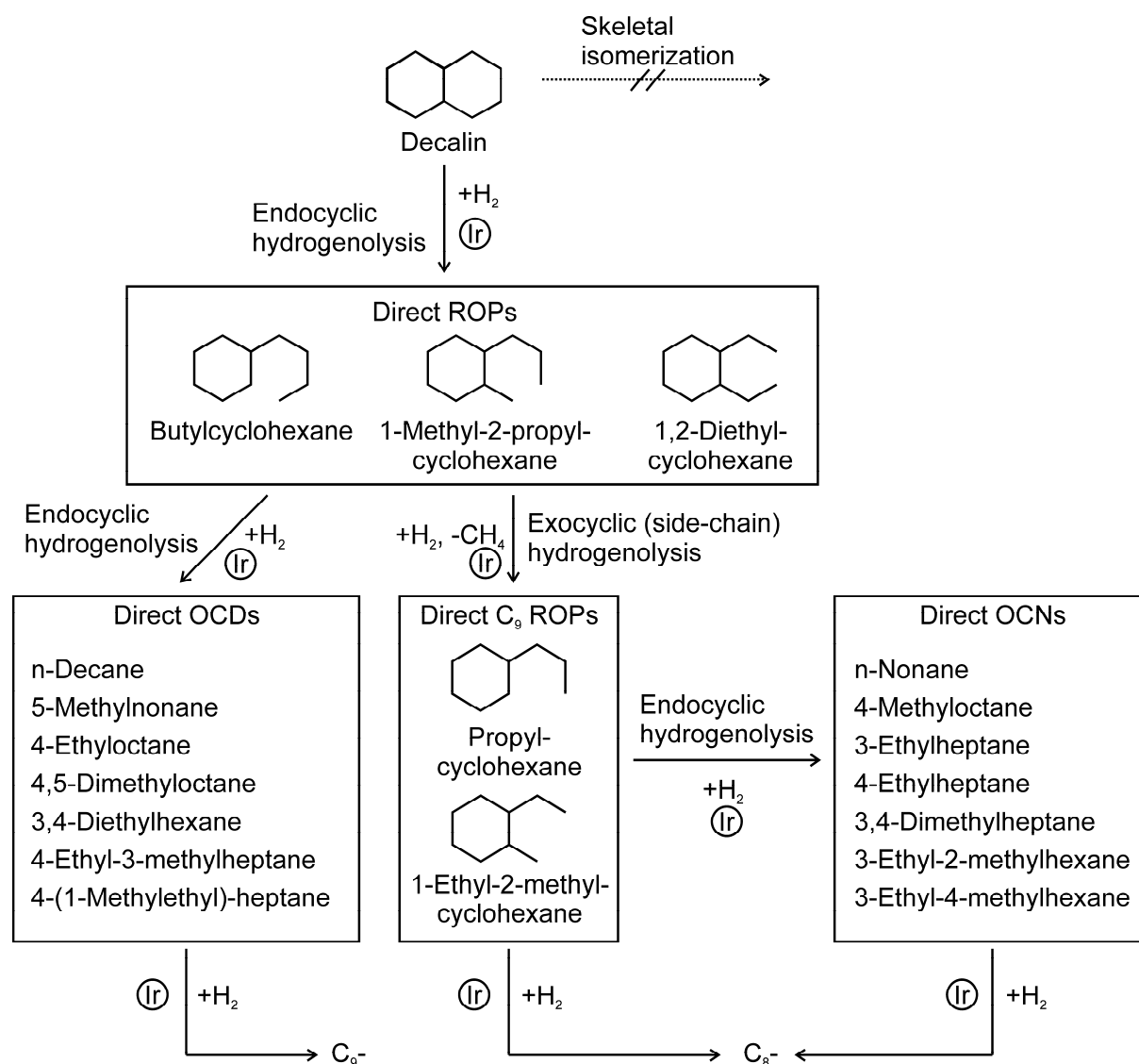


Figure 9.25: Hydrogenolytic pathways in the ring opening of decalin on non-acidic iridium catalysts.

The product group direct ROPs is introduced since these five C₁₀ naphthenes can be formed by a hydrogenolytic cleavage of one endocyclic carbon-carbon bond without prior isomerization of decalin as depicted in Figure 9.25. A similar reaction network was presented recently for the decalin conversion on very weakly acidic iridium-containing zeolite catalysts [74]. Cyclodecane, which could be formed by a cleavage of the bridging carbon-carbon bond was not detected on both Ir/silica catalysts, as ascertained by co-injection of cyclodecane to the liquid product mixture. By opening of the remaining cyclohexane ring, these can be further transformed into OCDs, or, by hydrogenolytic abstraction of methane, into direct C₉ ROPs and further into open-chain nonanes by endocyclic hydrogenolysis. An endocyclic ring opening of the five direct ROPs mentioned before would lead to the following seven direct OCDs: n-decane, 5-methylnonane, 4-ethyl-octane, 4,5-dimethyl-octane, 3,4-diethyl-hexane, 4-ethyl-3-methyl-heptane and 4-(1-methylethyl)-heptane. In fact, five of these seven

OCDs make up a large fraction of the OCDs formed on 2.59Ir/silica. Moreover, two unknown OCDs, one of them identified by GC/MS and by co-injection of decane isomers, the other one identified by GC/MS only, are formed in large amounts. Presumably, the one identified by co-injection and GC/MS is 4-ethyl-3-methylheptane which is expected to be formed *via* bifunctional isomerization [48]. The OCD identified by GC/MS only could be the highly-branched 4-(1-methylethyl)-heptane. Under these assumptions 95 % of all OCDs are direct OCDs at $T_r = 290$ °C.

In Figure 9.26 the temperature dependence of the selectivities of direct ROPs, OCDs, direct C₉ ROPs and direct OCNs for catalyst 2.59Ir/silica is plotted. Qualitatively, the consecutive reaction pathway which is presented in Figure 9.25 can be found: The main product group direct ROPs is either ring-opened at higher temperatures to OCDs or an abstraction of methane leads to the formation of direct C₉ ROPs which are subsequently ring-opened to direct OCNs.

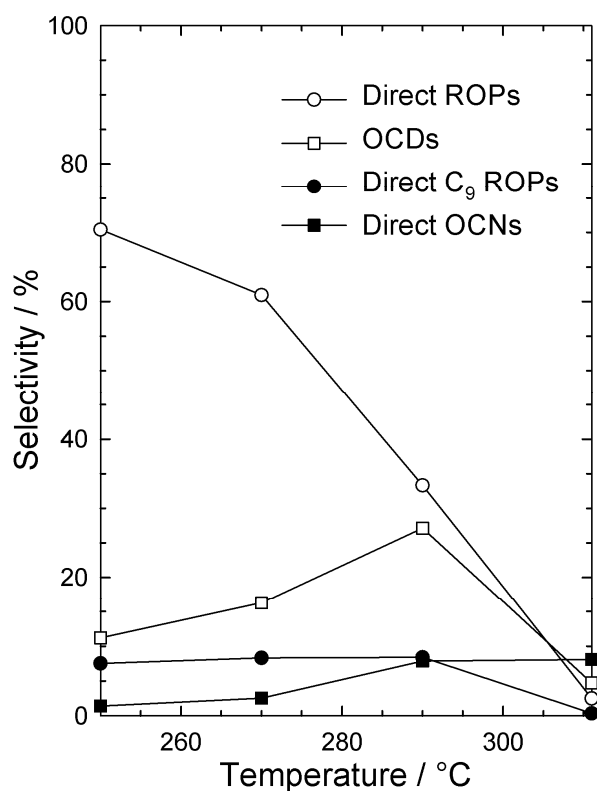


Figure 9.26: Temperature dependence of the selectivities of direct ROPs, OCDs, direct C₉ ROPs and direct OCNs in the decalin hydroconversion on catalyst 2.59Ir/silica.

On the Ir/silica catalysts at low conversions, 96 % of the ring-opening products from decalin are direct ROPs (see Table 9.4). Compared to the distribution of direct ROPs theoretically obtained *via* a non-selective or a selective ring-opening mechanism,

neither a pure selective nor a pure non-selective mechanism takes place on Ir/silica. Rather a mixture of both mechanisms occurs as also found in the ring opening of perhydroindan on 0.77Ir/silica (see Section 9.4).

At the lowest conversions of 12 and 17 % on 0.77Ir/silica and 2.59Ir/silica, respectively, the ratio $S_{\text{direct OCNs}} / S_{\text{OCNs}}$ assumes a value of 100 %. The detailed distribution of these direct OCNs (n-nonane, 4-methyloctane, 3-ethylheptane, 4-ethylheptane, 3,4-dimethylheptane, 3-ethyl-2-methylhexane, 3-ethyl-4-methylhexane) on the Ir/silica catalysts is shown in Table 9.5. Further, the theoretical distribution of direct OCNs that would be obtained by a ring opening of 1-ethyl-2-methylcyclohexane is shown, under the assumption of a non-selective and of a selective ring-opening mechanism. When comparing the experimental and the theoretical values it is evident that neither the non-selective nor the selective mechanism can account for the distributions obtained. However, direct OCNs can also be formed by methane abstraction from OCDs. Although this reaction path seems to contribute only to a small extent (*vide supra*) it cannot be ruled out that some direct OCNs stem from the hydrogenolysis of OCDs.

Table 9.4: Details on the ring-opening products obtained on both Ir/silica catalysts at low decalin conversions and theoretical product distribution.

Catalyst	T_r / °C	X_{Dec} / %	$\frac{S_{\text{direct ROPs}}}{S_{\text{ROPs}}}$ / %	$\frac{S_{\text{B-CHx}}}{S_{\text{direct ROPs}}}$ / %	$\frac{S_{\text{1-M-2-P-CHx}}}{S_{\text{direct ROPs}}}$ / %	$\frac{S_{\text{1,2-DE-CHx}}}{S_{\text{direct ROPs}}}$ / %
0.77Ir/silica	290	12	96	13	52	35
2.59Ir/silica	250	17	96	13	51	36
Assumed Non-Selective Ring Opening of Decalin						
			100	40	40	20
Assumed Selective Ring Opening of Decalin						
			100	0	67	33

Also in the ring opening of the intermediate product 1-ethyl-2-methylcyclohexane in the hydroconversion of perhydroindan (see Figure 9.18, page 112) on Ir/silica, a distribution of OCNs was obtained that cannot be explained by the two above mentioned mechanisms. The compositions of OCNs are roughly similar with a higher amount of n-nonane in the perhydroindan conversion due to the higher temperature of 310 °C. At the same $T_r = 290$ °C $S_{\text{n-No}} / S_{\text{direct OCNs}}$ assumes a more similar value of 13 % in the perhydroindan conversion. This could be due to a smaller contribution of

the partially selective mechanism which is known to become operative at relatively high temperatures [33].

Table 9.5: Composition of direct OCNs in the hydroconversion of decalin on 0.77Ir/silica and 2.59Ir/silica at $X_{\text{Dec}} = 12\%$ and 17% , respectively.

Direct OCN	Distribution of Direct OCNs / %			
	Catalyst		Predicted Ring Opening of 1-Ethyl-2-Methylcyclohexane	
	0.77Ir/silica	2.59Ir/silica	Non-selective	Selective
n-Nonane	8	8	17	0
4-Methyloctane	14	12	17	0
3-Ethylheptane	11	9	17	0
4-Ethylheptane	0	3	0	0
3,4-Dimethylheptane	9	13	17	33
3-Ethyl-2-methylhexane	22	20	17	33
3-Ethyl-4-methylhexane	36	35	17	33

Due to the absence of skeletal isomerization and a direct hydrogenolysis of decalin an attempt has been made to simulate the distribution of the hydrocracked products with the method described in the Appendix 12.3. For the best-fit of the experimental and simulated results, a hydrogenolysis of the real mixture of direct ROPs obtained at low conversions with a preferred cleavage of unsubstituted C-C bonds (factor $\alpha_{\text{unsubst.}} = 0.87$) is assumed. As shown in Figure 9.27 a reasonably good correlation is obtained.

Qualitatively, the high amounts of C_1 and C_9 can be rationalized by the high degree of branching that remains conserved due to the preference for hydrogenolysis of unsubstituted C-C bonds in decalin: In the major direct ROPs 1-methyl-2-propylcyclohexane and 1,2-diethylcyclohexane most exocyclic unsubstituted C-C bonds are of the primary-secondary type, and their hydrogenolysis on iridium leads to the formation of C_1 and C_9 . In the major OCDs the two tertiary carbon atoms remain from the reactant cis-decalin and several alkyl chains are present. Hence, again many C-C bonds are substituted and a large fraction of the unsubstituted C-C bonds are primary-secondary ones resulting in C_1 and C_9 after hydrogenolysis.

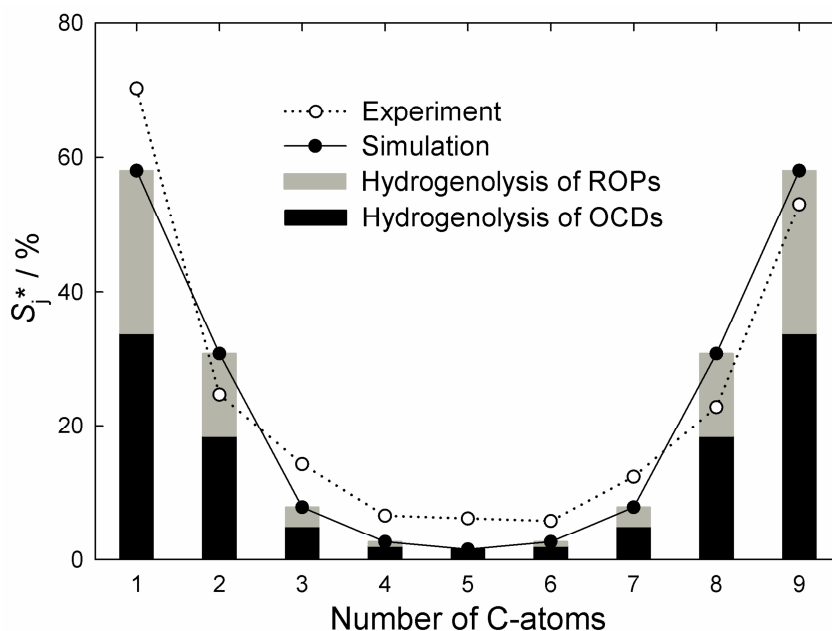


Figure 9.27: Distribution of the hydrocracked products in the catalytic experiment on 2.59Ir/silica and by the best-fit simulation. Bars: composition of the precursors of the hydrocracked products according to the simulation.

The grey and black bars in Figure 9.27 indicate to what extent C₉- products were formed by hydrogenolysis in the alkyl side-chain of direct ROPs (route 1 in Figure 12.1, page 207) or by hydrogenolysis of direct OCDs (route 2 in Figure 12.1, page 207), respectively. The results of the simulation based on the underlying assumptions suggest that slightly more than 50 % (black bars) of the hydrocracked products are formed *via* route 2, *i.e.*, by hydrogenolysis of direct OCDs.

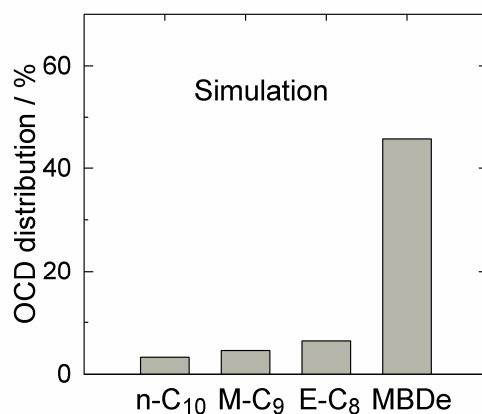


Figure 9.28: Breakdown of the selectivities of OCDs into differently branched decanes according to the best-fit simulation.

In the best-fit simulation an endocyclic hydrogenolysis of direct ROPs results in the formation of a mixture of direct OCDs. In Figure 9.28 this theoretical distribution of OCDs is shown. Qualitatively, an analogous distribution as obtained in the

experiments with 2.59Ir/silica (see Figure 9.22b) results, although the mechanistic input for the simulation was taken from the catalytic experiment at $T_r = 250$ °C, whereas the measured OCD distribution on Ir/silica holds for $T_r = 290$ °C. Even though 76 % of all OCDs are predicted to be multi-branched by the simulation, whereas a lower value of 63 % was obtained in the experiment, the qualitative similarity of both distributions can be looked upon as supporting the underlying mechanistic assumptions.

As summary, the assumption of hydrogenolytic C-C bond cleavage in decalin, direct ROPs and direct OCDs with a preference of unsubstituted bonds seems to be appropriate. Moreover, now the hammock-type curve of the distribution of the hydrocracked products on non-acidic iridium catalysts can be understood.

9.5.3 Hydroconversion on Pt/Silica and Pt/[Si]SBA-15 Catalysts

On catalysts 0.93Pt/silica and 2.68Pt/silica, an increase of the platinum content raises the decalin conversion only slightly, see Figure 9.29. Perhaps the larger platinum particles on 2.68Pt/silica (see Section 6.4) contain only slightly more crystallographic sites that are catalytically active [93]. At low conversions sk-Isos and ROPs are the main product groups with selectivities around 40 % each. With increasing temperatures large amounts of DHPs are formed as expected by thermodynamics [84, 89] and also formed in the empty and in the silica-filled reactor (see Section 7.2). OCDs are the product group formed with the lowest selectivity over nearly the whole temperature range with $Y_{\text{OCDs}} \leq 2$ %. Some cracking to C₉- occurs with maximal selectivities of 13 % but no OCNs are formed. In a separate time-on-stream experiment at $T_r = 390$ °C a small decrease of conversion from 46 to 42 % after 70 h is observed but the product selectivities remain virtually constant.

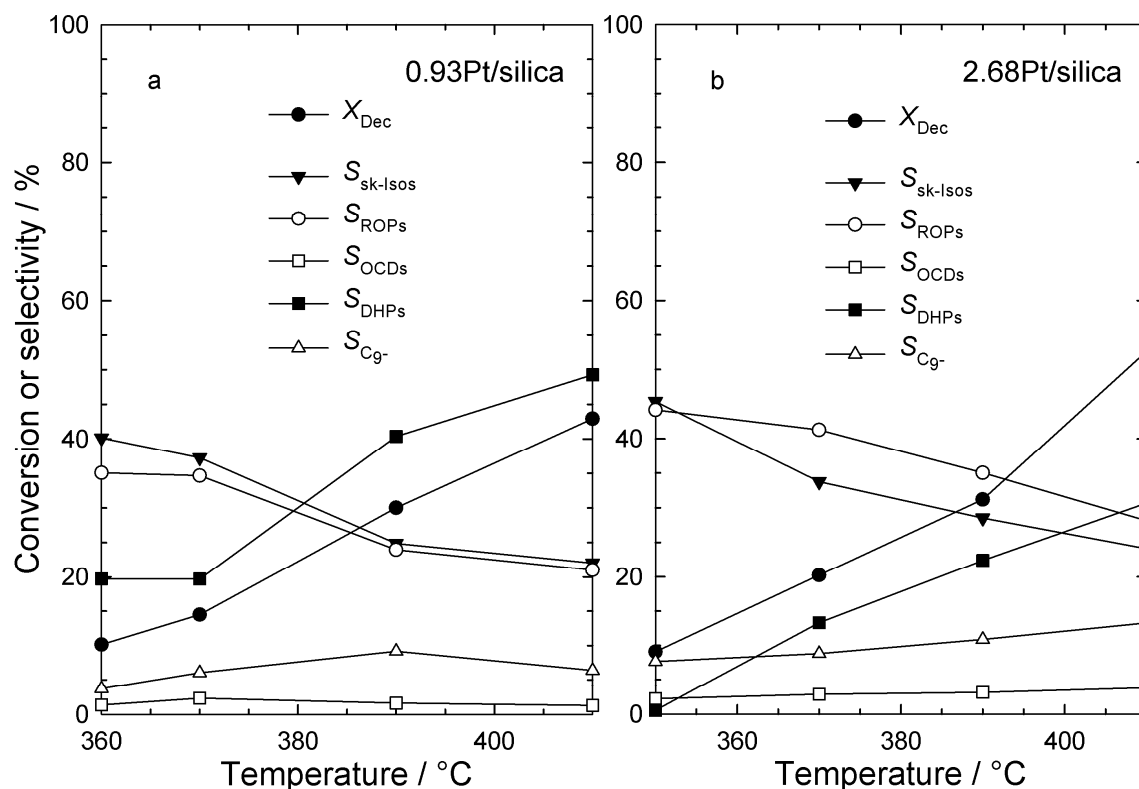


Figure 9.29: Conversion of decalin and selectivities of different groups of products at different temperatures on two Pt/silica catalysts.

On 0.92Pt/[Si]SBA-15 an identical catalytic behavior as on 0.93Pt/silica was found, see Table 9.6. Hence, as for the iridium catalysts in Section 9.5.2 the detailed discussion will be limited to the silica-supported ones.

Table 9.6: Maximum yields of open-chain decanes and selectivities of open-chain nonanes obtained in the hydroconversion of decalin.

Catalyst	$T_r / ^\circ\text{C}$	$X_{\text{Dec}} / \%$	$S_{\text{OCDs}} / \%$	$Y_{\text{OCDs, max.}} / \%$	$S_{\text{OCNs}} / \%$
0.93Pt/silica	410	43	2	1	0
2.68Pt/silica	410	53	4	2	0
0.92Pt/[Si]SBA-15	410	44	2	1	0

In Figure 9.30 the distribution of the differently branched decanes formed on 2.68Pt/silica is shown, no propylheptane was detected. Due to the very small S_{OCDs} on 0.93Pt/silica, this distribution is not depicted, n-decane (n-C₁₀) and ethyloctanes (E-C₈) occur with selectivities below 1%. On 2.68Pt/silica high selectivities of methylnonanes (M-C₉) and multiply branched decanes (MBDe) are formed. In comparison to Ir/silica (see Figure 9.22, page 117) the fraction of methylnonanes is

strongly increased. This lower degree of branching on Pt/silica compared to Ir/silica was also observed in the ring opening of perhydroindan (see Figure 9.20, page 114) and can be explained by the preference of platinum to cleave substituted C-C bonds in six-membered rings [4].

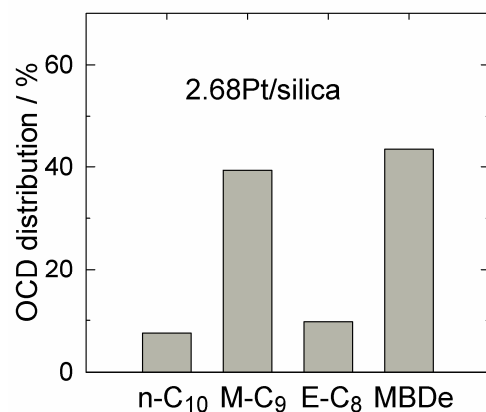


Figure 9.30: Hydroconversion of decalin on 2.68Pt/silica. Breakdown of the selectivities of OCDs into differently branched isomers:

$T_r = 410\text{ }^\circ\text{C}$; $X_{\text{Dec}} = 53\%$; $Y_{\text{OCDs}} = 2\%$; $S_{\text{OCDs}} = 4\%$.

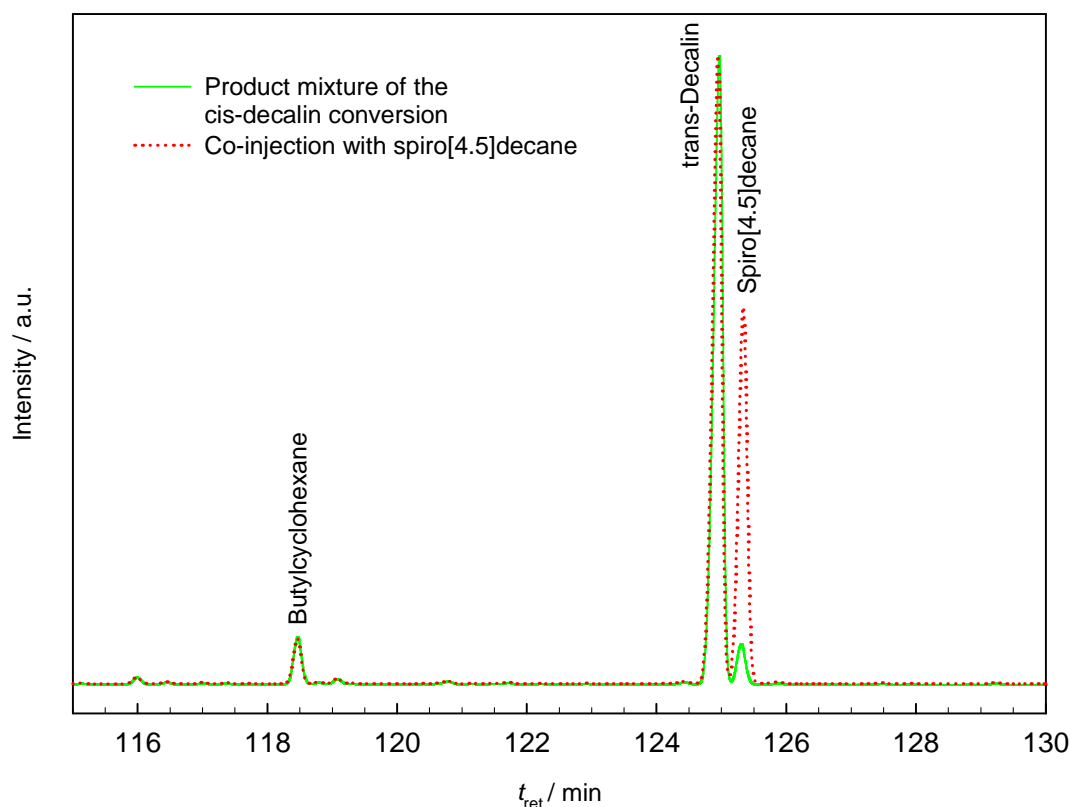


Figure 9.31: Gas chromatograms of the liquid product gained by the hydroconversion of cis-decalin on 0.93Pt/silica at $T_r = 390\text{ }^\circ\text{C}$ (solid line) and the same product co-injected with spiro[4.5]decane (dotted line).

For the identification of a major signal in the gas chromatogram next to trans-decalin at $t_{\text{ret}} = 125.3$ min, the assignment to spiro[4.5]decane that was obtained by GC/MS was verified by co-injection of the pure compound in the gas chromatograph. As depicted in Figure 9.31 the signal in question increases strongly upon co-injection whereas the signals of cis- and trans-decalin remain constant. Hence, the assignment of this signal to spiro[4.5]decane is reasonably safe.

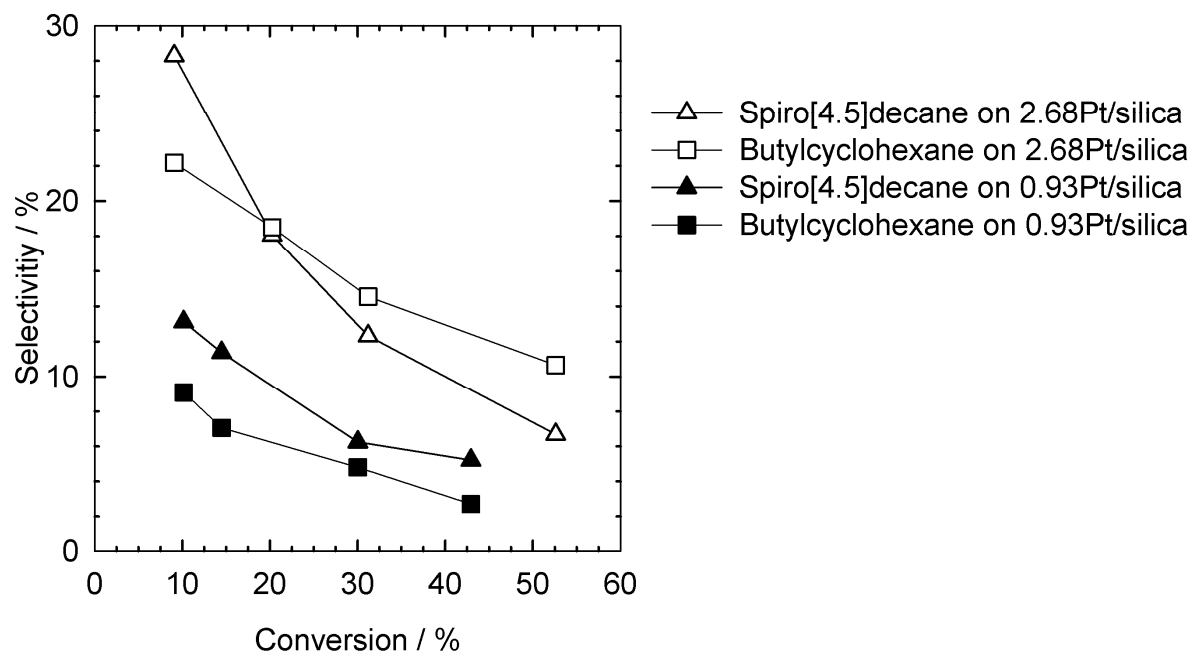


Figure 9.32: Selectivities of spiro[4.5]decane and butylcyclohexane in the hydroconversion of decalin on 0.93Pt/silica and 2.68Pt/silica at different conversions.

Beside tetralin, on both platinum catalysts and at all conversions the products formed with the highest selectivities are butylcyclohexane and spiro[4.5]decane. As seen in Figure 9.32, at the lowest conversions the highest selectivities of butylcyclohexane and spiro[4.5]decane are formed. 50 % of all ROPs consist of butylcyclohexane and 62 % of all sk-Isos consist of spiro[4.5]decane on 2.68Pt/silica at the lowest conversion of 9 %. This indicates that both products are formed in an early stage of the reaction network.

For the formation of spiro[4.5]decane, two completely different mechanisms can be envisaged. Recently, a carbocationic isomerization of type A was proposed for the isomerization of decalin to spiro[4.5]decane on a bifunctional Pt/La-X catalyst [52]. However, as shown by FT-IR spectroscopy (see Section 5.2.4) and the n-octane hydroconversion (see Section 8.2), no acid sites are active on Pt/silica. Hence, as already described for the skeletal isomerization of ethylcyclohexane (see Section 9.2)

and butylcyclohexane (see Section 9.3) on Pt/silica, two purely metal-catalyzed isomerization mechanisms are considered which can furnish spiro[4.5]decane as well.

The capability of platinum to induce skeletal isomerization of light alkanes is well established as the so-called bond-shift mechanism [24, 27, 28]. It is generally believed to proceed via cyclopropanoid species and was observed to be the predominant type of metal-catalyzed isomerization of n-octane when the hydrogen pressure was increased from 0.5 to 2.0 MPa [23]. As shown in Figure 9.33, applying the bond-shift mechanism to decalin leads one to predict spiro[4.5]decane as a primary product:

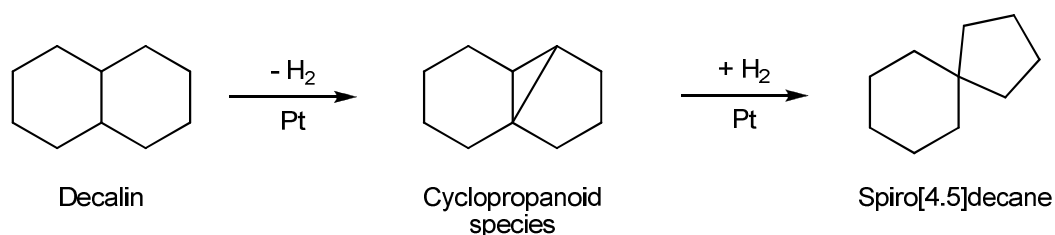


Figure 9.33: Possible platinum-catalyzed formation of spiro[4.5]decane *via* the bond-shift mechanism.

By GC/MS two other skeletal isomers which can be formed by the bond-shift mechanism can be assigned, *viz.* cis- and trans-bicyclo[5.3.0]decane, with a maximal total selectivity of 2 %. However, one would expect also eight other skeletal isomers (cis- and trans-isomers of 1-, 2- and 3a-methylperhydroindan and bicyclo[4.3.1]decane) instead of the strong preponderance of this spiro compound. Moreover, according to GC/MS analyses also the skeletal isomer bicyclopentyl is formed with a selectivity of maximal 3 %. An explanation could be the isomerization of spiro[4.5]decane *via* the bond-shift mechanism which is described in the context of its hydroconversion in Figure 9.40, page 140. An alternative pathway would start from the main ring-opening product butylcyclohexane which undergoes 1,5-dehydrocyclization [22, 23, 26, 29], furnishing spiro[4.5]decane as shown in Figure 9.34.

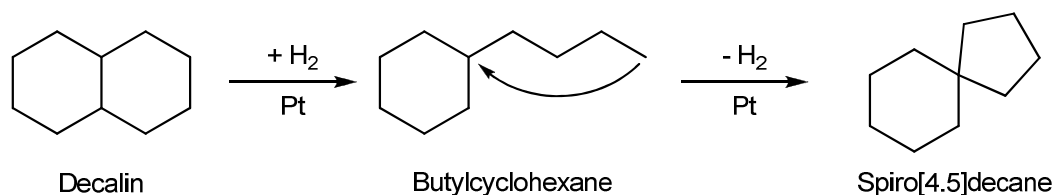


Figure 9.34: Hypothetical platinum-catalyzed isomerization of decalin *via* ring opening to butylcyclohexane followed by 1,5-dehydrocyclization.

Such a mechanism seems less probable since spiro[4.5]decane would be expected to be a secondary product formed from the primary product butylcyclohexane, whereas Figure 9.32 suggests that spiro[4.5]decane is rather a primary product.

In general, due to the isomerization activity of Pt/silica the ratio $S_{\text{direct ROPs}} / S_{\text{ROPs}}$ equals 65 and 79 % at low conversions on 0.93Pt/silica and 2.68Pt/silica, respectively (see Table 9.7). The butylcyclohexane formation can easily be rationalized by a preferred hydrogenolytic rupture of the secondary-tertiary carbon-carbon bond in decalin and spiro[4.5]decane as also found for the endocyclic hydrogenolysis in ethylcyclohexane (see Section 9.2) or butylcyclohexane (see Section 9.3) on Pt/silica. A cleavage of the bisecondary bonds in decalin occurs to a low extent as indicated by the lower selectivities of the direct ROPs cis- and trans-1-methyl-2-propylcyclohexane and cis- and trans-1,2-diethylcyclohexane (see Table 9.7). Also in spiro[4.5]decane the unsubstituted C-C bonds in the five-membered ring are cleaved only with a very low total selectivity of the respective ring-opening products with $S \leq 1.6$ % (see Section 9.6). A cleavage of the bridging C-C bond between the two tertiary carbon atoms in decalin is strongly hindered, but small amounts of the respective product cyclodecane were detected with a maximal selectivity of 0.5 % at a reaction temperature of 410 °C on 2.68Pt/silica. Hence, ring opening occurs on the Pt/silica catalysts most probably by a mixture of the non-selective and the partially selective ring-opening mechanism.

Table 9.7: Details on the ring-opening products obtained on both Pt/silica catalysts at low decalin conversions and theoretical product distribution.

Catalyst	T_r / °C	X_{Dec} / %	$\frac{S_{\text{direct ROPs}}}{S_{\text{ROPs}}}$ / %	$\frac{S_{\text{B-CHx}}}{S_{\text{direct ROPs}}}$ / %	$\frac{S_{\text{1-M-2-P-CHx}}}{S_{\text{direct ROPs}}}$ / %	$\frac{S_{\text{1,2-DE-CHx}}}{S_{\text{direct ROPs}}}$ / %
0.93Pt/silica	370	15	65	54	34	12
2.68Pt/silica	370	20	79	64	28	8
Assumed Non-Selective Ring Opening of Decalin						
			100	40	40	20
Assumed Partially Selective Ring Opening of Decalin						
			100	100	0	0

On 2.69Pt/silica the ring opening of butylcyclohexane to OCDs occurs with selectivities up to 19 % (see Section 9.3) whereas the ring opening of butylcyclohexane as intermediate product in the decalin conversion on 2.68Pt/silica is hindered (maximal $S_{\text{OCDs}} = 4$ %). A rationale can be given by the *ca.* 40 °C higher

reaction temperatures that have to be applied with decalin to reach similar conversions, which results in exocyclic hydrogenolysis of butylcyclohexane (*vide infra*).

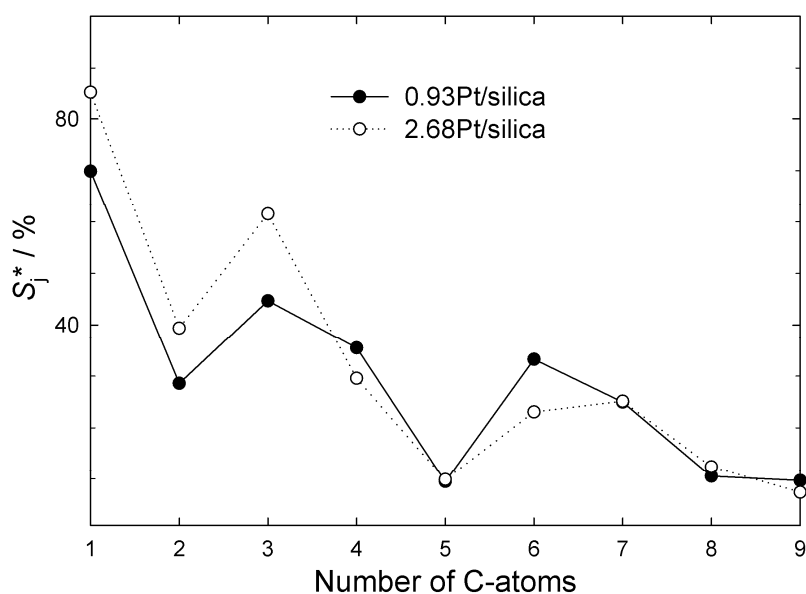


Figure 9.35: Modified hydrocracking selectivities S_j^* on two Pt/silica catalysts in the hydroconversion of decalin:

0.93Pt/silica: $T_r = 410\text{ }^\circ\text{C}$; $X_{\text{Dec}} = 43\text{ }%$; $Y_{\text{C}_{9-}} = 3\text{ }%$; $\Sigma S_j^* = 274\text{ }%$.
 2.68Pt/silica: $T_r = 410\text{ }^\circ\text{C}$; $X_{\text{Dec}} = 53\text{ }%$; $Y_{\text{C}_{9-}} = 7\text{ }%$; $\Sigma S_j^* = 294\text{ }%$.

When the noble metal is supported on silica, the distributions of the hydrocracked products, shown in Figure 9.35 for comparable conversions, differ substantially from the distributions obtained on bifunctional catalysts in the hydroconversion of decalin [52]. They rather resemble those obtained on catalysts with very weak Brønsted acid sites like Pt/Cs,Na,H-Y [5]. Large amounts of C_1 to C_4 , C_6 and C_7 are formed. Methane and ethane cannot be the product of a carbocationic mechanism, hence, monofunctional metal catalysis must be operative. Since C_8 and C_9 are formed in smaller amounts, the precursors cannot be C_{10} hydrocarbons but rather C_9 - products, which is also reflected in the $\Sigma S_j^* > 270\text{ }%$ on both Pt/silica catalysts.

On 0.93Pt/silica and 2.68Pt/silica, 38 and 53 %, respectively, of the C_6 fraction consist of cyclohexane which could be formed by hydrogenolytic abstraction of the C_4 hydrocarbon n-butane from the main ring-opening product butylcyclohexane. A similar explanation can be found for C_3 and C_7 . On these catalysts 75 and 81 % of the C_7 fraction consist of methylcyclohexane, which can also be formed by side-chain hydrogenolysis in butylcyclohexane forming propane as co-product. Indeed, in the butylcyclohexane hydroconversion on Pt/silica exocyclic hydrogenolysis occurred preferentially in bond e (see Figure 9.11, page 102) under the formation of propane

and methylcyclohexane. An explanation for the high amounts of C₆ consisting to a large extent of cyclohexane together with the high amounts of methane and multiple hydrogenolysis ($\Sigma S_j^* > 270\%$) could be the methane abstraction in methylcyclohexane. An increased formation of C₁ and C₆ accompanied by lowered amounts of C₇ is observed in the hydroconversion of butylcyclohexane on 2.69Pt/silica at the highest conversion of $X_{B-CHx} = 96\%$ when multiple hydrogenolysis occurs with $\Sigma S_j^* = 252\%$ (see Figure 9.15, page 106). Also higher amounts of ethane are formed from butylcyclohexane under these conditions. This similarity of the distributions of the hydrocracked products from the reactants butylcyclohexane and decalin indicates that butylcyclohexane is the main precursor for the formation of hydrocracked products from decalin on Pt/silica.

9.5.4 Hydroconversion on Rh/Silica Catalysts

In Figure 9.36 the catalytic results of two Rh/silica catalysts with a metal loading of ca. 1 wt.-% and metal dispersions D of 0.17 and 0.57 are shown. The higher dispersion and accordingly the lower particle size and smaller specific metal surface area have no influence on the overall conversion. However, the product selectivities are influenced. On 1.03Rh/silica with a low dispersion of $D = 0.17$ higher $S_{sk-Isos}$ and lower S_{ROPs} are obtained, compared to 0.96Rh/silica with $D = 0.57$. The formation of spiro[4.5]decane occurs on 1.03Rh/silica with the highest selectivity of 5% at the lowest conversion, whereas on 0.96Rh/silica only traces with $S \leq 0.1\%$ are formed. Perhaps, special crystallographic sites on the larger metal clusters are isomerization-active, or, conversely, the smaller clusters are more active in hydrogenolysis. A higher isomerization activity of larger rhodium clusters was also observed in the conversion of n-hexane on Rh/alumina with $D = 0.18$ and 0.57 [94].

In accordance with the higher isomerization activity of 1.03Rh/silica the ratio $S_{direct\ ROPs} / S_{ROPs}$ assumes values of 61 to 64% in comparison to higher values of 91 to 95% on 0.96Rh/silica over the whole range of temperatures applied. On the latter catalyst the ring is opened essentially at the bissecondary C-C bonds since a fraction of 96 to 97% of all direct ROPs are the corresponding products 1-methyl-2-propylcyclohexane and 1,2-diethylcyclohexane. In spite of this similar regioselectivity as on Ir/silica (see Table 9.4, page 122) the subsequent opening of the six-membered ring is strongly hindered on 0.96Rh/silica resulting in $S_{OCDs} \leq 2\%$. On 1.03Rh/silica slightly higher amounts with S_{OCDs} up to 4% are formed. Presumably, the mild isomerization activity facilitates the ring opening as observed with other catalysts [5].

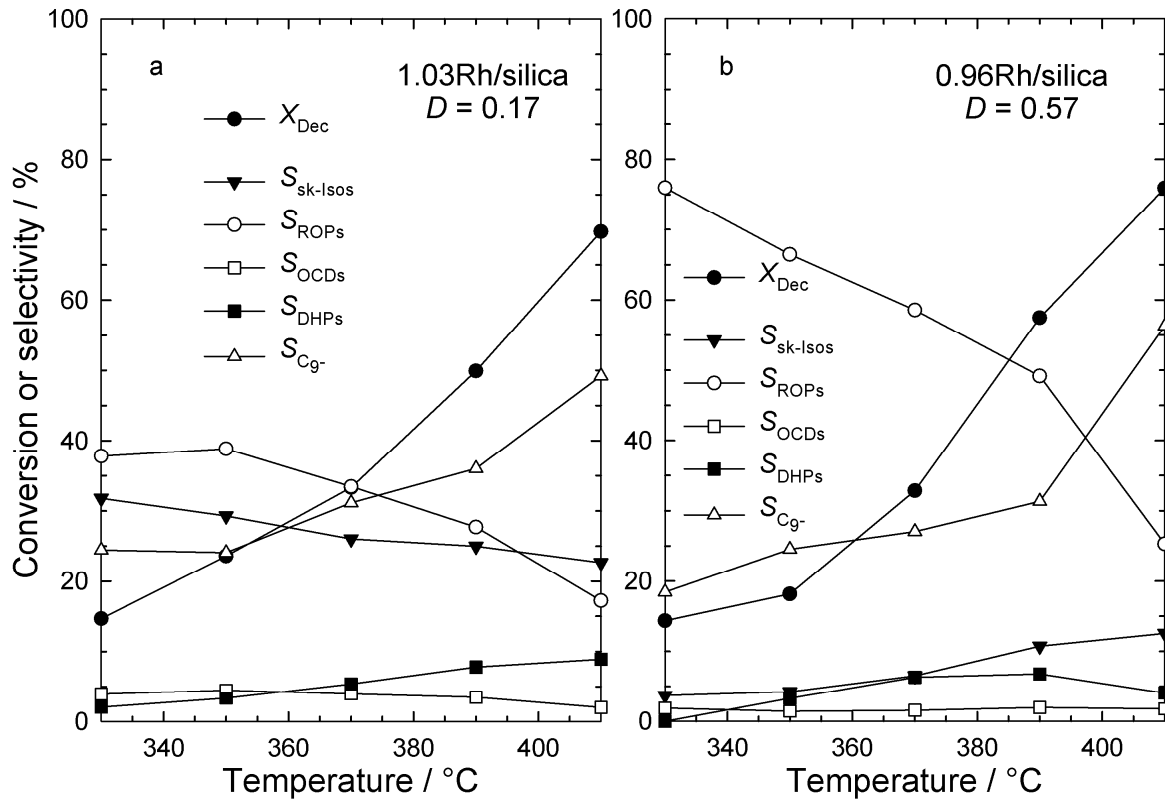


Figure 9.36: Conversion of decalin and selectivities of different groups of products at different temperatures on two Rh/silica catalysts of different metal dispersions D .

The low amounts of OCDs on both Rh/silica catalysts compared to 0.77Ir/silica can be explained by the *ca.* 50 °C higher reaction temperatures that have to be applied to reach the same conversion. In Figure 9.37 the carbon number distribution curves of the hydrocracked products at similar conversions as shown in Figure 9.23, page 118, for Ir/silica are plotted. The higher reaction temperatures favor multiple hydrogenolysis as indicated by the strong asymmetry with high amounts of methane and $\Sigma S_j^* > 200$ %. Both curves are essentially hammock-shaped indicating hydrogenolysis on a metal that prefers the cleavage of bisecondary C-C bonds, but for 1.03Rh/silica weak maxima at C_4 and C_6 are superimposed. A mole fraction of iso-butane in the C_4 fraction of 74 % and of methylcyclopentane in the C_6 fraction of 58 % at $T_r = 390$ °C could be an indication of the paring reaction. However, iso-butane can also be formed by multiple hydrogenolysis of bisecondary C-C bonds and the formation of methylcyclopentane can also be a consequence of the isomerization activity of large rhodium particles [94].

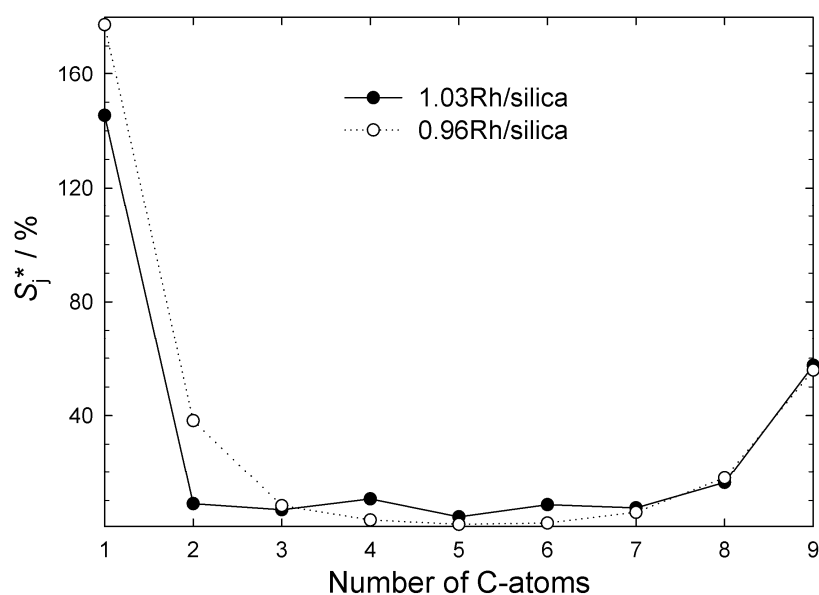


Figure 9.37: Modified hydrocracking selectivities S_j^* on two Rh/silica catalysts in the hydroconversion of decalin:

1.03Rh/silica: $T_r = 390\text{ }^\circ\text{C}$; $X_{\text{Dec}} = 50\%$; $Y_{\text{C}_9} = 34\%$; $\Sigma S_j^* = 266\%$.

0.96Rh/silica: $T_r = 390\text{ }^\circ\text{C}$; $X_{\text{Dec}} = 57\%$; $Y_{\text{C}_9} = 18\%$; $\Sigma S_j^* = 311\%$.

9.6 Spiro[4.5]decane

In the hydroconversion of decalin on Pt/silica (see Section 9.5.3) and bifunctional catalysts [5, 52], spiro[4.5]decane was identified as an important skeletal isomer formed by isomerization on platinum or by bifunctional isomerization, mainly at low conversions. It seems that the isomerization of decalin to spiro[4.5]decane is crucial for obtaining high OCD selectivities, due to the relatively fast hydrogenolytic ring opening of five-membered rings as demonstrated with perhydroindan (see Section 9.4). However, in these studies the only detected ring-opening product of a direct hydrogenolysis of spiro[4.5]decane was butylcyclohexane. Hence, the hydroconversion of this spiro compound on 2.73Ir/silica and 2.69Pt/silica seems worthwhile for a better understanding of the hydrogenolytic reaction steps that are possible after the isomerization to spiro[4.5]decane.

In Table 9.8 the results of the spiro[4.5]decane conversion on 2.73Ir/silica show that spiro[4.5]decane is much more reactive than decalin on the very similar catalyst 2.59Ir/silica (see Figure 9.21b, page 115). Although only three different reaction temperatures have been measured with spiro[4.5]decane, the maximal $S_{\text{OCDs}} = 49\%$ is much higher than the maximal value of 28% with decalin as reactant. One reason

could be the fast ring opening of the five-membered ring in spiro[4.5]decane as also found with perhydroindan (see Section 9.4).

Table 9.8: Conversion of spiro[4.5]decane and selectivities of different groups of products on catalyst 2.73Ir/silica at different temperatures.

$T_r / ^\circ\text{C}$	$X_{\text{spiro}} / \%$	$S_{\text{sk-Isos}} / \%$	$S_{\text{ROPs}} / \%$	$S_{\text{OCDs}} / \%$	$S_{\text{C}_9} / \%$
200	40	1.9	97	0.2	0.6
240	100	1.0	91	6.7	0.9
280	100	0.4	32	49	19

An additional explanation for the higher OCD selectivity in the hydroconversion of spiro[4.5]decane could be the higher number of endocyclic bisecundary C-C bonds in the direct ring-opening products of spiro[4.5]decane which are cleaved preferentially on iridium. Also McVicker *et al.* [4] observed a decreased ring-opening selectivity on Ir/ γ -alumina when more alkyl substituents are attached to the cyclohexane ring. On 0.77Ir/silica two ROPs are expected to be formed in high amounts by cleavage of an unsubstituted C-C bond in both naphthenic rings of spiro[4.5]decane, *viz.* 1-methyl-1-propylcyclohexane and 1,1-diethylcyclohexane, see Figure 9.39. Both ROPs contain four endocyclic unsubstituted C-C bonds, whereas the main ROPs obtained from decalin (1-methyl-2-propylcyclohexane and 1,2-diethylcyclohexane) contain only three bonds of that type.

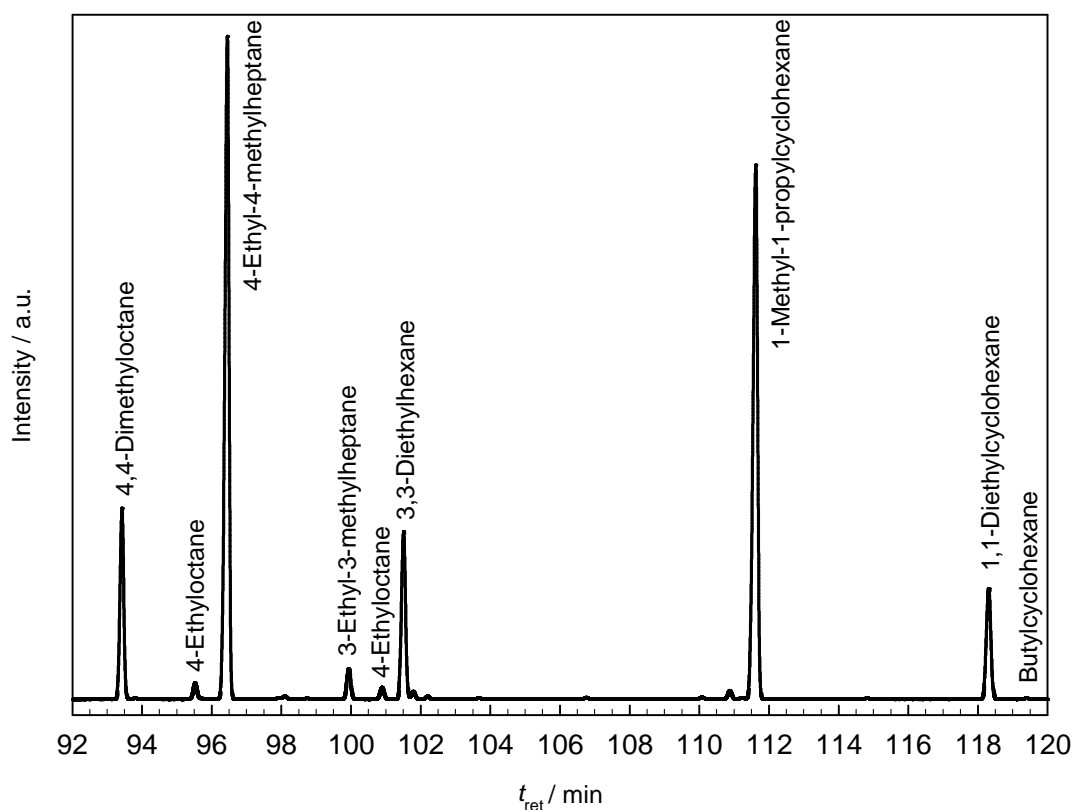


Figure 9.38: Gas chromatogram of the products obtained in the hydroconversion of spiro[4.5]decane on 2.73Ir/silica at $T_r = 280$ °C.

Unfortunately, the two main ring-opening products (see Figure 9.38) derived from spiro[4.5]decane can be assigned to this product group only due to a molar mass of $M = 140 \text{ g} \cdot \text{mol}^{-1}$ as detected by GC/MS but not to a specific molecule. However, the knowledge obtained with perhydroindan makes it reasonable to assume that these two ROPs are 1-methyl-1-propylcyclohexane (1-M-1-P-CHx) and 1,1-diethylcyclohexane (1,1-DE-CHx) which are expected by the fast ring opening of the five-membered ring by hydrogenolysis at the bissecondary C-C bonds b and c (see Figure 9.39). Both products occur in a molar ratio of *ca.* 4 : 1, comparable to a molar ratio of 1-methyl-1-propylcyclohexane to 1,1-diethylcyclohexane of 2 : 1 if a statistical ring opening of the two bissecondary C-C bonds b and c is assumed. According to these considerations the larger peak at $t_{\text{ret}} = 111.60$ min is tentatively assigned to 1-methyl-1-propylcyclohexane and the smaller one at $t_{\text{ret}} = 118.30$ min to 1,1-diethylcyclohexane.

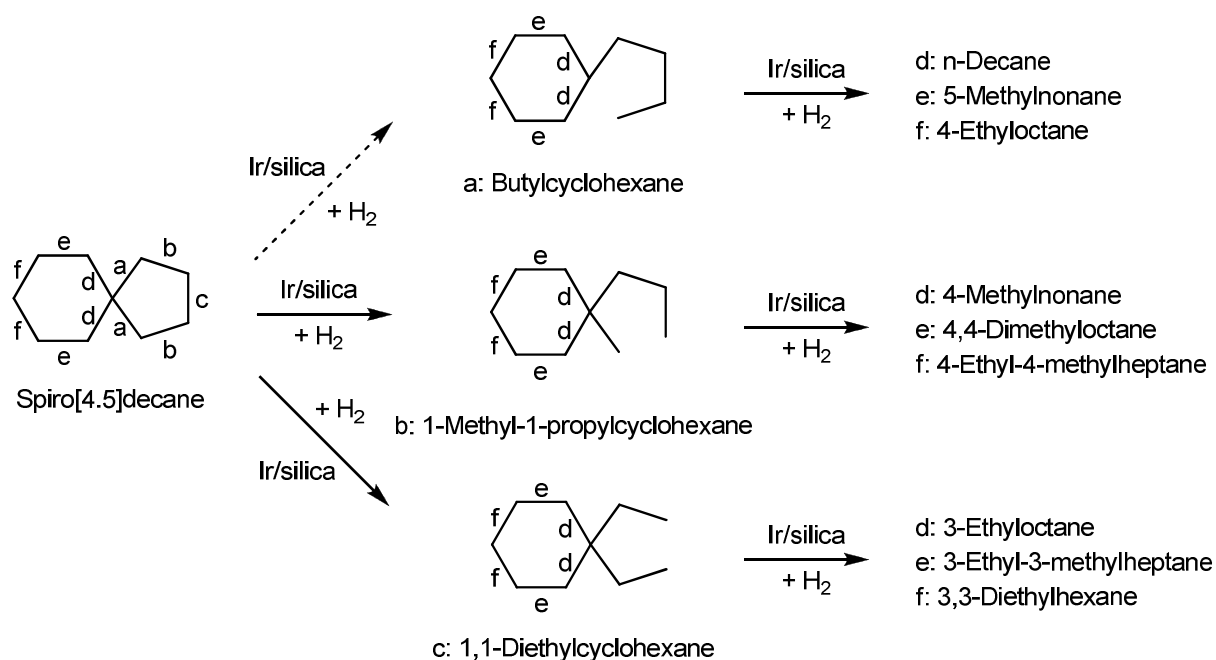


Figure 9.39: Reaction paths in the endocyclic hydrogenolysis of spiro[4.5]decane on Ir/silica.

With this peak assignment the distribution of ring-opening products that was obtained on 2.73Ir/silica is shown in Table 9.9. Obviously, in all three runs and even at conversions of 100 %, 98 % of all ROPs are the two ones formed by cleaving bonds b or c in spiro[4.5]decane, see Figure 9.39.

Table 9.9: Distribution of ring-opening products from spiro[4.5]decane on catalyst 2.73Ir/silica at different temperatures.

$T_r / ^\circ\text{C}$	$X_{\text{spiro}} / \%$	$S_{\text{B-CH}_x} / S_{\text{ROPs}} \%$	$S_{\text{1-M-1-P-CH}_x} / S_{\text{ROPs}} \%$	$S_{\text{1,1-DE-CH}_x} / S_{\text{ROPs}} \%$	$S_{\text{other ROPs}} / S_{\text{ROPs}} \%$
200	40	1.9	76	22	0.1
240	100	1.7	77	21	0.3
280	100	0.2	81	17	1.8

In the gas chromatogram (see Figure 9.38) one large signal at $t_{\text{ret}} = 96.45$ min could be assigned by GC/MS to 4-ethyl-4-methylheptane, an OCD that can be formed by cleaving bond f in the main ROP 1-methyl-1-propylcyclohexane (see Figure 9.39). Some other signals in the gas chromatogram were difficult to assign by GC/MS to specific OCDs, and the signal of the molecular ion with $m/z = 142$ was very weak. This could be explained by the expected formation of OCDs with a quaternary carbon atom that remains when the main ROPs 1-methyl-1-propylcyclohexane and 1,1-

diethylcyclohexane undergo endocyclic hydrogenolysis at the bisecondary C-C bonds e and f, as shown in Figure 9.39. In the GC/MS analysis, radical cations that possess a quaternary carbon atom are prone to a fast decomposition because tertiary radicals or cations can result which are relatively stable.

A comparison of the retention times of the signals in question and the boiling points [95] of (i) the OCDs resulting from a direct endocyclic hydrogenolysis of 1-methyl-1-propylcyclohexane and 1,1-diethylcyclohexane, that were not assigned previously, *i.e.*, 3-ethyl-3-methylheptane and 3,3-diethylhexane, with (ii) those of the OCDs that were assigned safely by co-injection of decane isomers and (iii) that of 4-ethyl-4-methylheptane which was assigned by GC/MS only was conducted. A good correlation of the products identified by GC/MS and the molar mass only with the known OCDs allowed a tentative assignment of the signals.

At $T_r = 280$ °C and $S_{\text{OCDs}} = 49$ %, 95 % of all OCDs are these four OCDs which can be formed by cleaving the bisecondary C-C bonds a and b in spiro[4.5]decane and further e and f in the resulting ROPs: 4,4-dimethyloctane, 4-ethyl-4-methylheptane, 3-ethyl-3-methylheptane and 3,3-diethylhexane. This regioselectivity is in accordance with the selective ring-opening mechanism as observed also in the ring opening of ethylcyclohexane, butylcyclohexane, perhydroindan and cis-decalin.

On 2.69Pt/silica skeletal isomers are the main products at all reaction temperatures. Ring-opening products are formed with selectivities of 11 to 22 % whereas hydrocracking to OCDs and C_9 - occurs to a negligible extent only. The slight increase in $S_{\text{sk-Isos}}$ with increasing temperature is due to an increased formation of many products in small amounts which are assigned to sk-Isos mainly due to their range of retention times. Perhaps some of these compounds are unsaturated hydrocarbons since also tetralin (sk-Iso) is formed with a selectivity of 2 % at $T_r = 360$ °C.

Table 9.10: Conversion of spiro[4.5]decane and selectivities of different groups of products on catalyst 2.69Pt/silica at different temperatures.

$T_r / \text{°C}$	$X_{\text{spiro}} / \%$	$S_{\text{sk-Isos}} / \%$	$S_{\text{ROPs}} / \%$	$S_{\text{OCDs}} / \%$	$S_{C_9-} / \%$
260	5.0	77	22	0.0	0.7
300	21	84	16	0.0	0.2
360	62	88	11	0.7	0.8

On the similar catalyst 2.68Pt/silica decalin was less reactive (see Figure 9.29b, page 126). To find out if a faster ring opening of the five-membered ring in spiro[4.5]decane is the reason for the higher reactivity of spiro[4.5]decane compared to decalin, the yields of ROPs on both catalysts at the same temperature will be compared. At $T_r = 360\text{ }^\circ\text{C}$ with decalin as reactant, $Y_{\text{ROPs}} = 6.3\%$ is obtained by interpolation of the values at $T_r = 350$ and $370\text{ }^\circ\text{C}$. At the same temperature and with spiro[4.5]decane as reactant a very similar value of $Y_{\text{ROPs}} = 6.8\%$ was reached. Such a comparison with OCDs or C_9 - products is not possible, due to the small amounts on both catalysts. The high selectivity of sk-Isos with spiro[4.5]decane and the similar Y_{ROPs} values with both reactants at the same temperatures suggest that the higher reactivity of spiro[4.5]decane stems mainly from the isomerization of spiro[4.5]decane to decalin (see Table 9.11). Hence, the formation of ROPs starts from a similar mixture of bicyclic C_{10} naphthenes with spiro[4.5]decane and with decalin as reactant.

Table 9.11: Composition of skeletal isomers formed from spiro[4.5]decane on catalyst 2.69Pt/silica at different temperatures.

$T_r / ^\circ\text{C}$	X_{spiro} / %	$S_{\text{sk-Isos}}$ / %	S_{Dec} / $S_{\text{sk-Isos}}$ / %	$S_{\text{bicyclo[5.3.0]decane}}$ / $S_{\text{sk-Isos}}$ / %	$S_{\text{bicyclopentyl}}$ / $S_{\text{sk-Isos}}$ / %	$S_{\text{other sk-Isos}}$ / $S_{\text{sk-Isos}}$ / %
260	5.0	77	88	8.7	2.0	0.8
300	21	84	91	4.6	1.3	3.5
360	62	88	83	1.3	1.6	14.2

A more detailed insight into the composition of sk-Isos formed from spiro[4.5]decane is given in Table 9.11. Decalin is by far the main skeletal isomer, and a mole fraction of $n_{\text{tr-Dec}} / (n_{\text{tr-Dec}} + n_{\text{c-Dec}}) = 0.86$ to 0.88 is in the range of values that are also observed in the hydroconversion of decalin on the same catalyst (see Section 9.5.1). By GC/MS two signals can be assigned to bicyclo[5.3.0]decane (cis- and trans-isomer) and one signal to bicyclopentyl. Most probably, the formation of all these sk-Isos can be explained by metal-catalyzed isomerization.

To account for the formation of the skeletal isomers bicyclo[5.3.0]decane, decalin and bicyclopentyl, the platinum-catalyzed bond-shift mechanism is applied in Figure 9.40. The first step would be the formation of two different cyclopropanoid species. After cleavage of a C-C bond in the cyclopropane ring other than the new one formed, the skeletal isomers bicyclo[5.3.0]decane, decalin and bicyclopentyl would result.

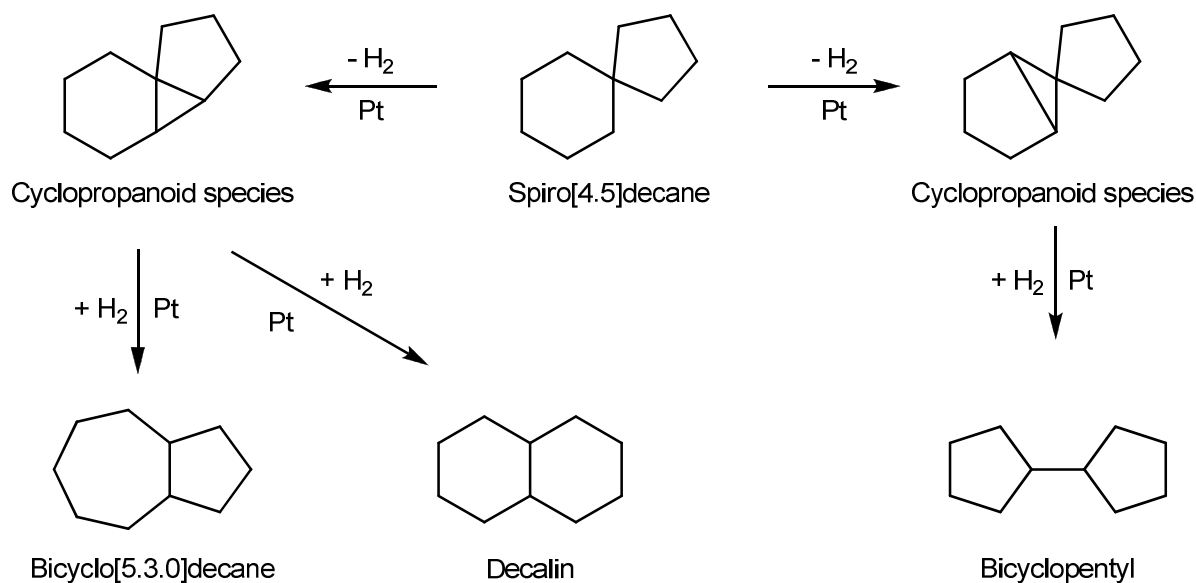


Figure 9.40: Skeletal isomerization of spiro[4.5]decane on platinum *via* the bond-shift mechanism.

An alternative reaction path for the formation of bicyclopentyl is depicted in Figure 9.41. The first step would be a ring opening to pentylcyclopentane which is formed in very small amounts with a maximal selectivity of 1.1 % at $T_r = 360^\circ\text{C}$. After 1,5-dehydrocyclization [22, 23, 26, 29] bicyclopentyl would be obtained.

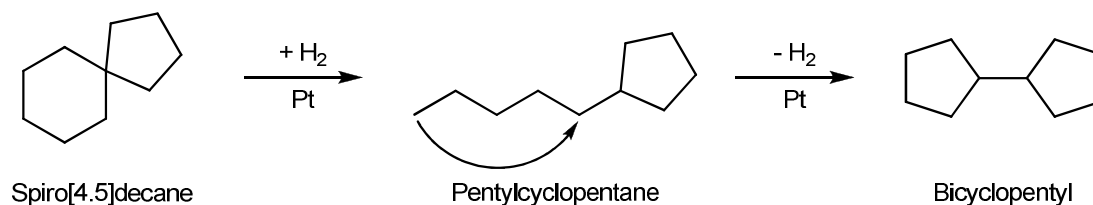


Figure 9.41: Skeletal isomerization of spiro[4.5]decane on platinum *via* ring opening to pentylcyclopentane and subsequent 1,5-dehydrocyclization to bicyclopentyl.

However, at the high hydrogen pressure of 5.0 MPa, the bond-shift mechanism is known to be prevailing [23], as already discussed for the skeletal isomerization of decalin on Pt/silica in Section 9.5.3. Moreover, the mechanism described in Figure 9.41 seems hardly probable as the intermediate product pentylcyclopentane is formed only in very small amounts on Pt/silica (*vide supra*).

At $T_r = 260$ and 300°C on Pt/silica, a fraction of *ca.* 95 % of all ROPs are the products of a direct hydrogenolytic ring opening of the five-membered ring, *i.e.*, butylcyclohexane, 1-methyl-1-propylcyclohexane and 1,1-diethylcyclohexane (direct ROPs). The molar ratios of these three ROPs are *ca.* 8 : 3 : 1, indicating a strong

preference of platinum for the cleavage at the secondary-quaternary carbon-carbon bond a in Figure 9.39, as also observed by McVicker *et al.* [4] in the ring opening of methylcyclohexane on 0.6Pt/silica, see Table 4.1, page 25. However, butylcyclohexane can also stem from the ring opening of the major sk-Iso decalin, since it was the main ROP in the hydroconversion of cis-decalin on the similar catalyst 2.68Pt/silica (see Table 9.7, page 130). The peak assignment for the products 1-methyl-1-propylcyclohexane and 1,1-diethylcyclohexane was also transferred to the product mixture obtained in the hydroconversion of cis-decalin on Pt/silica. A low total selectivity of these products of $\leq 1.6\%$ demonstrates that, although spiro[4.5]decane is formed on that catalyst, ring opening does virtually not occur at the unsubstituted C-C bonds in the five-membered ring.

At a higher temperature of 360 °C only 71 % of all ROPs are direct ROPs. Several explanations are possible for the formation of these ROPs that cannot stem from direct hydrogenolysis of the five-membered ring in spiro[4.5]decane: (i) Ring opening of the six-membered ring in spiro[4.5]decane, (ii) ring opening of sk-Isos, and (iii) isomerization of direct ROPs.

A distribution curve of the hydrocracked products will be shown only for Ir/silica, on Pt/silica the amount of C₉- products is too low. The curve obtained from spiro[4.5]decane on Ir/silica (see Figure 9.42) differs to some extent from the hammock-shaped one that is typically found for non-acidic iridium catalysts in the hydroconversion of decalin (see Figure 9.23, page 118). In the conversion of spiro[4.5]decane higher amounts of C₃ and C₇ were formed in comparison with the hydroconversion of decalin. Most probably, the origin of these differences is the different structure of ROPs and OCDs which are formed from the two bicyclic naphthenes. Due to the preference of iridium for cleaving unsubstituted C-C bonds and the conservation of C-C bonds between a quaternary and a secondary carbon atom this is expected to result in a different distribution of hydrocracked products. The higher amounts of C₇ than of C₈ cannot be explained so far, although the peak assignment was re-examined.

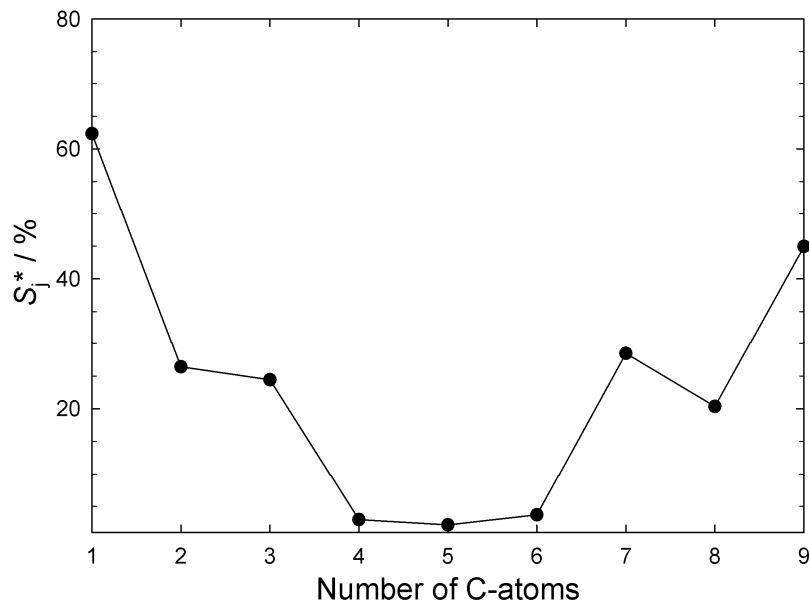


Figure 9.42: Modified hydrocracking selectivities S_j^* on 2.73Ir/silica catalyst in the hydroconversion of spiro[4.5]decane:
 $T_r = 280\text{ }^\circ\text{C}$; $X_{\text{spiro}} = 100\text{ }%$; $Y_{\text{C}_9^-} = 19\text{ }%$; $\Sigma S_j^* = 216\text{ }%$.

9.7 Methyldecalin

Methyldecalin was chosen as reactant to find out whether the knowledge about hydrogenolytic ring opening of C_8 to C_{10} naphthenes can be transferred to a bicyclic C_{11} naphthene. Concerning real diesel fuel this is a more appropriate model compound due to its higher boiling point compared to, *e.g.*, *cis*-decalin. This feed hydrocarbon is a mixture of ten different diastereoisomeric and constitutional isomers (see Figure 5.3, page 68).

Catalyst 0.77Ir/silica is much more active than 0.93Pt/silica (see Figure 9.43a), for which *ca.* $60\text{ }^\circ\text{C}$ higher reaction temperatures have to be applied to reach a similar conversion. Beside an apparently varying behavior at the lowest reaction temperature which is due to impurities in the feed hydrocarbon, ROPs and C_{10^-} are the main products at low conversions. With increasing conversion the selectivity of ring-opening products decreases, and $S_{\text{C}_{10^-}}$ increases. A maximal yield of open-chain undecanes of 6.9 % is reached at $T_r = 350\text{ }^\circ\text{C}$ and $X_{\text{M-Dec}} = 65\text{ }%$ with the following composition: 0 % *n*-undecane, 19 % methyldecane, 14 % ethylnonane, 67 % multiply branched undecanes. Only small amounts of skeletal isomers are formed and the dehydrogenation to methyltetralin and methylnaphthalene (DHPs) is negligible. In

general, a similar catalyst behavior as in the hydroconversion of cis-decalin on the same catalyst is observed (see Figure 9.21, page 115). Methyldecalin is slightly less reactive, presumably due to the availability of a smaller number of unsubstituted C-C bonds which are preferentially cleaved on iridium [4].

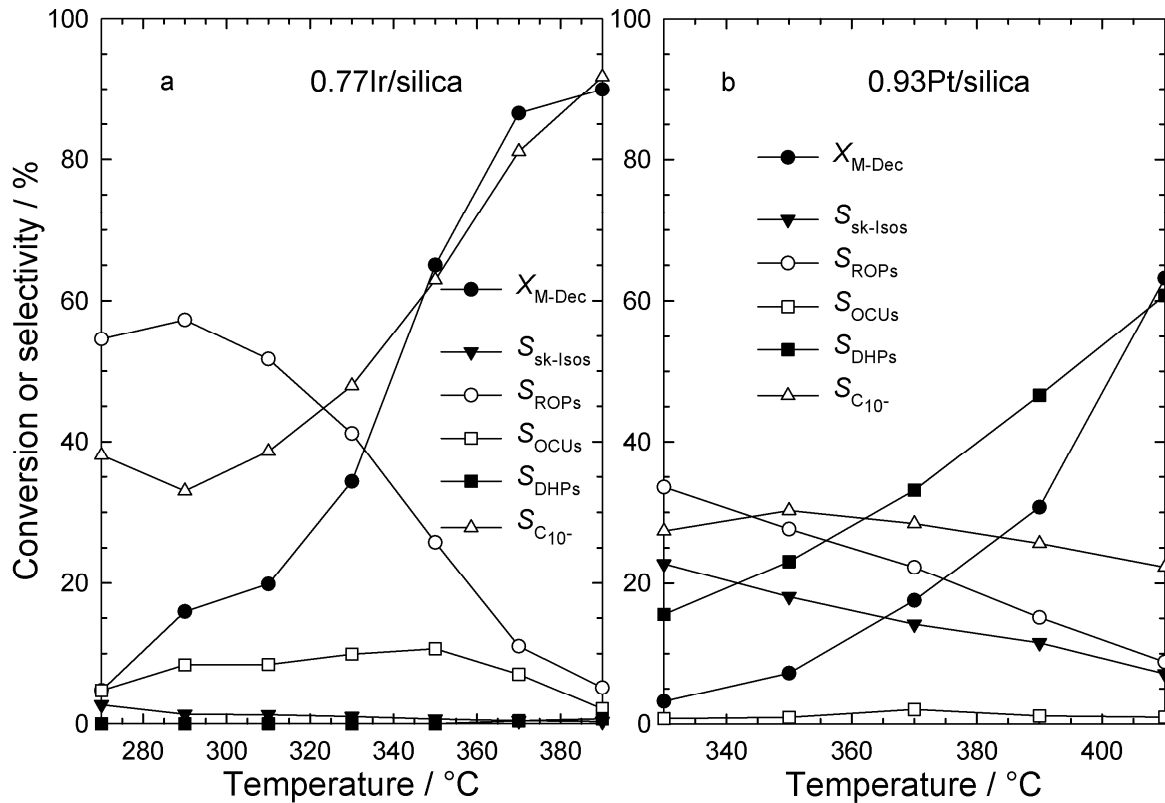


Figure 9.43: Conversion of methyldecalin and selectivities of different groups of products at different temperatures on two silica-supported catalysts.

On 0.93Pt/silica at low conversions, skeletal isomerization, ring opening, hydrocracking to C_{10}^- and dehydrogenation occur to a similar extent (see Figure 9.43b). With increasing conversion the selectivity of DHPs, consisting mainly of methyltetralin, increases up to $S_{DHPs} = 61\%$ at $T_r = 410\text{ °C}$ and $X_{M-Dec} = 63\%$. Also unsaturated hydrocarbons other than methyltetralin and methyl-naphthalene are formed with increasing selectivities at higher temperatures. On 0.93Pt/silica and 0.77Ir/silica, the maximal selectivities of those unsaturated hydrocarbons are 10.3% and 0.5%, respectively, at the highest temperatures. These products consist mainly of aromatic molecules of the product groups C_{10}^- , ROPs and sk-Isos. Open-chain undecanes are formed with a maximal $Y_{OCUs} = 0.6\%$ at $T_r = 410\text{ °C}$ and $X_{M-Dec} = 63\%$. Methyldecalin is similarly reactive as decalin on this catalyst. The product selectivities in the hydroconversion of methyldecalin correspond roughly to those observed with cis-decalin on the same catalyst, see Figure 9.29b, page 126. In the methyldecalin

conversion higher amounts of hydrocracked products with $S_{C_{10^-}} \approx 25\%$ instead of $S_{C_9^-} \approx 5\%$ with decalin are formed, due to the high tendency of cleaving the C-C bond between the bicyclic structure and the methyl group (*vide infra*).

Unfortunately, no reaction network can be drawn for the hydroconversion of methyldecalin because (i) the reactant is a mixture of up to three different constitutional isomers, (ii) numerous different products are formed and also expected when a direct hydrogenolysis mechanism as described for decalin is adopted, (iii) many signals in the gas chromatogram could be assigned only to a product group due to their molecular ion signal but not to specific molecules.

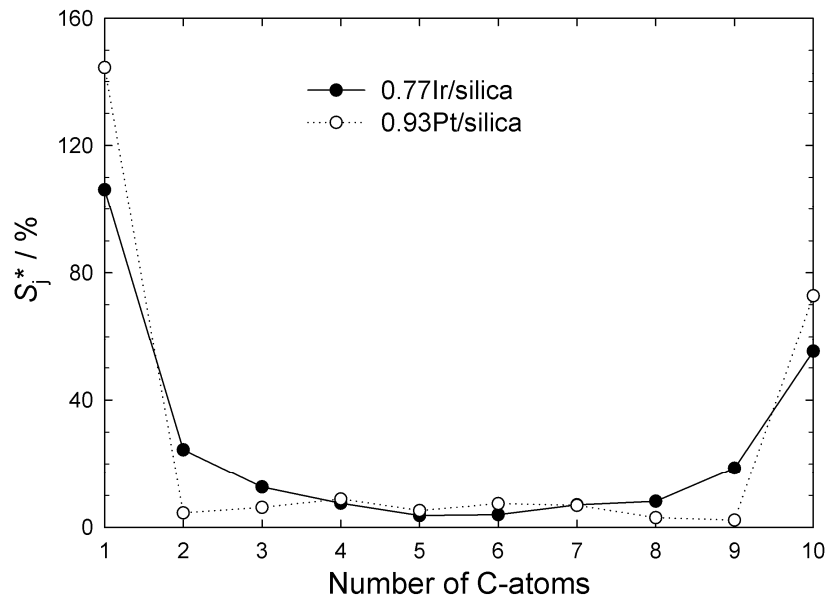


Figure 9.44: Modified hydrocracking selectivities S_j^* on two silica-supported catalysts in the hydroconversion of methyldecalin:

0.77Ir/silica: $T_r = 350\text{ }^\circ\text{C}$; $X_{M\text{-Dec}} = 65\%$; $Y_{C_{10^-}} = 41\%$; $\Sigma S_j^* = 192\%$.

0.93Pt/silica: $T_r = 410\text{ }^\circ\text{C}$; $X_{M\text{-Dec}} = 63\%$; $Y_{C_{10^-}} = 14\%$; $\Sigma S_j^* = 189\%$.

In Figure 9.44 the distribution curves of the hydrocracked products at reaction conditions of maximal OCU yields are shown. Values of $\Sigma S_j^* < 200\%$ are most probably due to an erroneous assignment of some signals in the very complex product mixture. In spite of these uncertainties a hammock-type curve is clearly obtained on the iridium catalyst with substantially higher amounts of C_1 and C_{10} compared to the other carbon number fractions. This is a similar result as in the hydroconversion of decalin (see Figure 9.23, page 118) on this catalyst. In contrast, on the platinum catalyst a completely different distribution curve is found compared to the one for decalin conversion on the same catalyst (see Figure 9.35, page 131). It resembles that

obtained on Ir/silica but the formation of C_1 and C_{10} is more pronounced. A preferred abstraction of the methyl group from methyldecalin is the reason for the high amounts of C_1 and C_{10} on 0.93Pt/silica as indicated by $n_{\text{decalin}} / n_{C_{10}} = 53 \%$. On 0.77Ir/silica this molar ratio assumes a lower value of 30 %, the other C_{10} products are a mixture of different naphthenic and aliphatic hydrocarbons.

9.8 Influence of the Hydrogen Pressure

In literature investigations about the influence of the hydrogen pressure on the pure hydrogenolytic ring opening of multi-ring naphthenes are lacking (see Section 4.2.1.4). Hence, perhydroindan and cis-decalin were chosen to be tested in the hydroconversion on 2.69Pt/silica and 2.73Ir/silica, respectively, at $p_{H_2} = 1.0$ to 8.0 MPa in order to identify the best suited hydrogen pressure for the hydrogenolytic ring opening of bicyclic naphthenes. Pt/silica is hardly active in the opening of six-membered rings (see Section 9.5) while five-membered rings can be readily opened on platinum (see Section 9.4). Hence, for studying the influence of hydrogen pressure on the hydrogenolytic ring opening of bicyclic naphthenes on a non-acidic platinum catalyst, the more reactive feed perhydroindan was chosen.

9.8.1 Hydrogenolysis of Perhydroindan on Platinum

A comparison of the perhydroindan conversion on 2.69Pt/silica in dependence of the reaction temperature at varying hydrogen pressure is shown in Figure 9.45. Under otherwise constant conditions (see Section 5.3.3.5, page 56) the conversion decreases with increasing hydrogen pressure, especially from $p_{H_2} = 1.0$ to 2.0 MPa. No catalyst deactivation occurred at any hydrogen pressure.

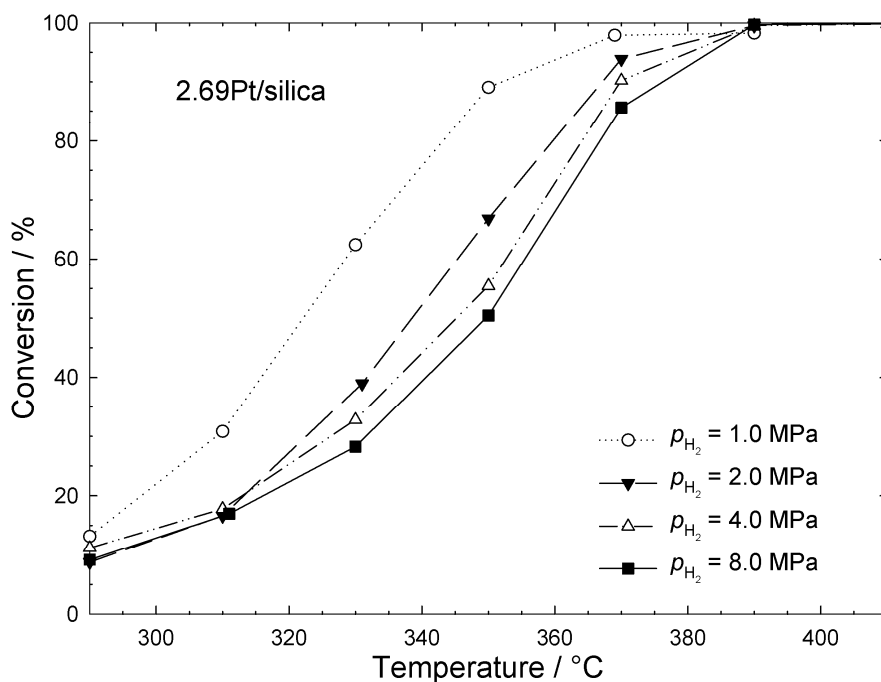


Figure 9.45: Conversion of perhydroindan on catalyst 2.69Pt/silica at different hydrogen pressures and temperatures.

In the hydroconversion of perhydroindan on 2.69Pt/silica at $p_{H_2} = 1.0$ MPa DHPs are the main products up to $X_{PHI} = 62\%$, see Figure 9.46d. A decrease of S_{DHPs} with increasing temperature and conversion was accompanied by a strong increase of the aromatics content in the product groups C_8 - and ROPs. These aromatics make up a total selectivity of 48% at $T_r = 390$ °C and consist mainly of ethylmethylbenzenes. By GC/MS the attribution to specific constitutional isomers of the ethylmethylbenzenes was not possible, but it is likely that 1-ethyl-2-methylbenzene was formed by ring opening of indan or by dehydrogenation of 1-ethyl-2-methylcyclohexane. Upon increasing the hydrogen pressure, DHPs formation is more and more suppressed, and at $p_{H_2} = 8.0$ MPa S_{DHPs} is close to zero regardless of the reaction temperature. The dehydrogenation to DHPs at $p_{H_2} = 1.0$ and 2.0 MPa is an additional reaction path and is one reason for the higher conversions at these hydrogen pressures (see Figure 9.45).

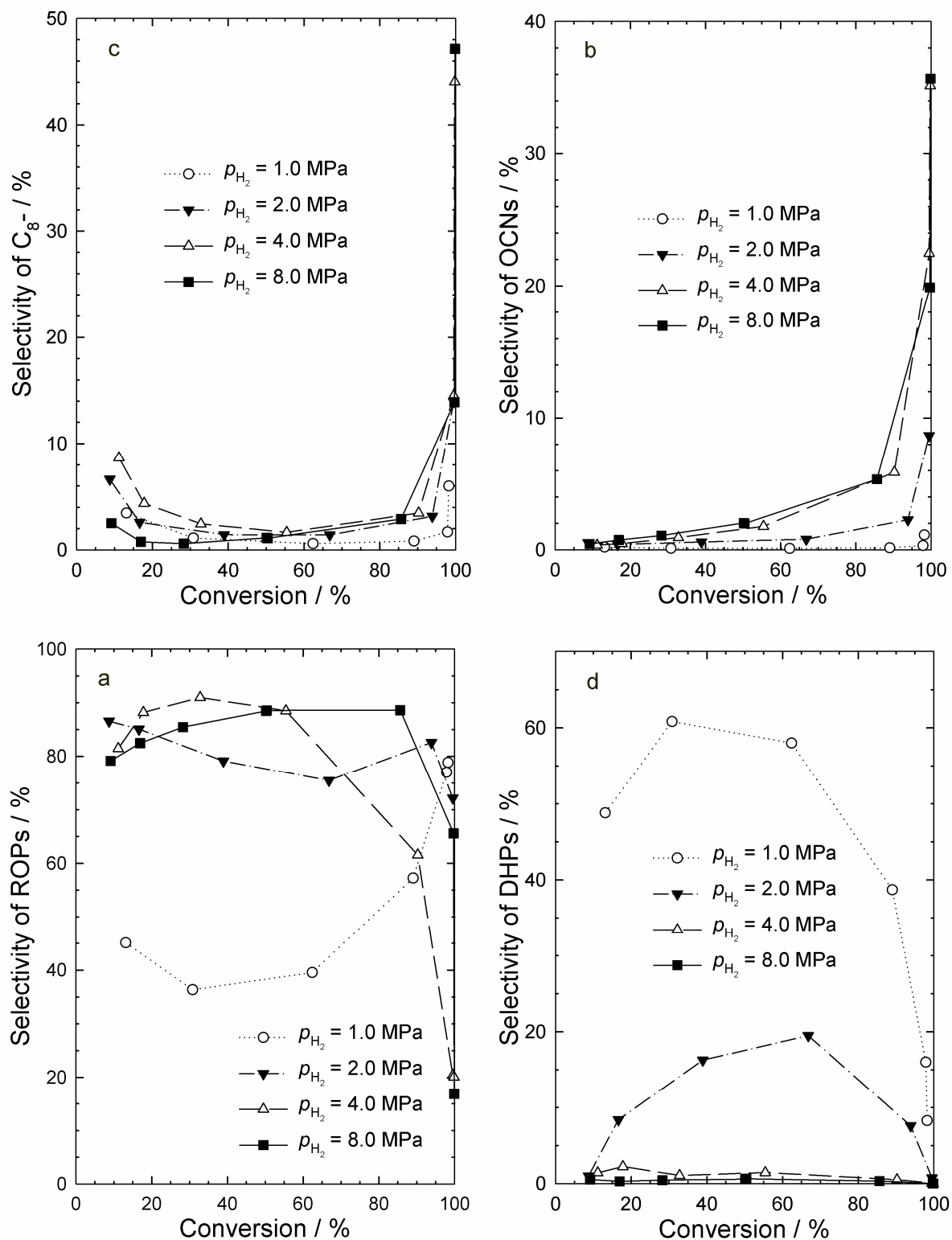


Figure 9.46: Selectivities of different groups of products on catalyst 2.69Pt/silica at different hydrogen pressures and perhydroindan conversions.

Isomerization of perhydroindan occurs to a very small extent at hydrogen pressures of 1.0 and 2.0 MPa, whereas at 4.0 and 8.0 MPa up to $S_{sk-Isos} = 17\%$ is reached at low conversions (not shown).

In Figure 9.46 comparisons of product selectivities of ROPs, OCNs, C₈- products and DHPs at different hydrogen pressures and conversions are depicted. Highest selectivities of ROPs are obtained at hydrogen pressures of 4.0 and 8.0 MPa. OCN selectivities are maximal at $p_{\text{H}_2} = 4.0$ and 8.0 MPa, and the influence of hydrogen pressure on the selectivities of C₈- is negligible. Similar OCN distributions as formed at a hydrogen pressure of 5.2 MPa (see Figure 9.20, page 114) were observed at $p_{\text{H}_2} = 2.0$ to 8.0 MPa (not shown). Hence, at a high hydrogen pressure of 4.0 to 8.0 MPa that is high enough to suppress the formation of aromatics, the hydrogenolysis of perhydroindan on platinum is hardly influenced by the hydrogen pressure leading to a maximal $Y_{\text{OCNs}} = 36\%$, see Table 9.12. One reason for the poor ring-opening performance at hydrogen pressures of 1.0 and 2.0 MPa is the strong dehydrogenation tendency at lower hydrogen pressures that leads to relatively high conversions due to the formation of DHPs.

Table 9.12: Maximum yields of open-chain nonanes obtained on catalyst 2.69Pt/silica at different hydrogen pressures in the hydroconversion of perhydroindan.

$p_{\text{H}_2} / \text{MPa}$	$T_{\text{r}} / ^\circ\text{C}$	$X_{\text{PHI}} / \%$	$S_{\text{OCNs}} / \%$	$Y_{\text{OCNs, max.}} / \%$
1.0	390	98	1.1	1.1
2.0	390	100	8.7	8.7
4.0	410	100	35	35
8.0	410	100	36	36

The distribution of the hydrocracked products in Figure 9.47 is depicted for each hydrogen pressure at a reaction temperature of maximal OCN yield. Interestingly, while $Y_{\text{OCNs, max.}}$ increases with increasing hydrogen pressure, also the distribution curve of the hydrocracked products changes gradually. With increasing hydrogen pressure the high amounts of C₁, C₂ and C₇ decrease gradually while the values of C₃ to C₆ increase slightly. Most significant is the increased formation of C₄ and C₅ hydrocarbons with increasing $Y_{\text{OCNs, max.}}$. Both fractions consist of roughly equal amounts of iso- and n-butane or 2-methylbutane and n-pentane, respectively. Hydrogenolysis of OCNs can generate C₄ and C₅ alkanes, whereas a singular hydrogenolysis of direct ROPs with a six-membered ring (1-ethyl-2-methylcyclohexane and propylcyclohexane) could not result in the formation of C₄ or C₅ products. Therefore, the altered curve shape at high OCN yields presumably stems from the hydrogenolysis of OCNs.

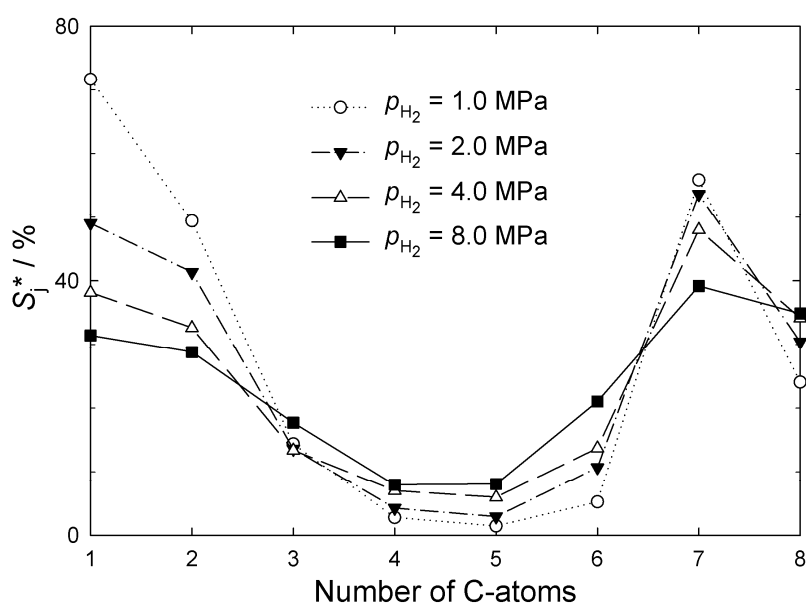


Figure 9.47: Modified hydrocracking selectivities S_j^* on 2.69Pt/silica in the hydroconversion of perhydroindan at different hydrogen pressures:

$p_{H_2} = 1.0$ MPa:	$T_r = 390$ °C;	$X_{PHI} = 98$ %;	$Y_{C_8-} = 6$ %;	$\Sigma S_j^* = 225$ %.
$p_{H_2} = 2.0$ MPa:	$T_r = 390$ °C;	$X_{PHI} = 100$ %;	$Y_{C_8-} = 14$ %;	$\Sigma S_j^* = 206$ %.
$p_{H_2} = 4.0$ MPa:	$T_r = 410$ °C;	$X_{PHI} = 100$ %;	$Y_{C_8-} = 43$ %;	$\Sigma S_j^* = 193$ %.
$p_{H_2} = 8.0$ MPa:	$T_r = 410$ °C;	$X_{PHI} = 100$ %;	$Y_{C_8-} = 47$ %;	$\Sigma S_j^* = 225$ %.

9.8.2 Hydrogenolysis of cis-Decalin on Iridium

A comparison of the decalin conversion at different reaction temperatures and varying hydrogen pressure is shown in Figure 9.48. With increasing hydrogen pressure from 1.0 to 2.0 and 4.0 MPa, the conversion increases at all reaction temperatures, with one exception at the maximal reaction temperatures of *ca.* 330 °C. At a higher hydrogen pressure of 8.0 MPa, however, the conversion is lower compared to a pressure of 4.0 MPa, again with the exception at $T_r = 330$ °C.

The hydrogen pressure dependency of the conversion of decalin on 2.73Ir/silica deviates strongly from the results with perhydroindan on 2.69Pt/silica (see Figure 9.45). It is unknown if the origin of these differences is the nature of the noble metal or the type of the reactant. In the hydrogenolytic ring opening of cyclohexane and methylcyclohexane on Ir/ γ -alumina Shi *et al.* [45] found decreasing reaction rates by increasing the hydrogen pressure from 0.3 to *ca.* 1.7 MPa. No experiments at higher pressures have been conducted, hence, the influence of hydrogen pressure on the purely metal-catalyzed conversion at p_{H_2} up to 8.0 MPa is unknown. Moreover, the

larger number of carbon atoms in the reactant decalin could change the influence of hydrogen pressure strongly, see Figure 4.9, page 21.

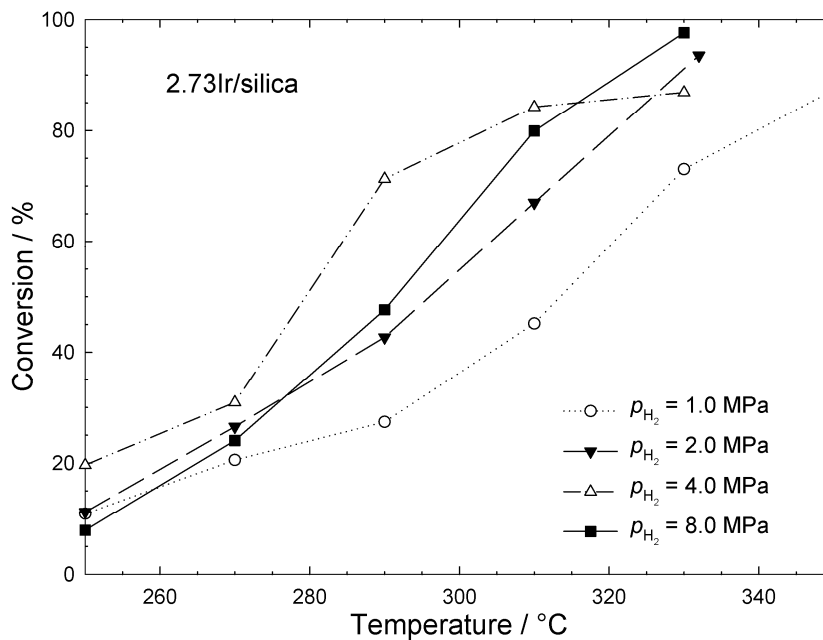


Figure 9.48: Conversion of decalin on catalyst 2.73Ir/silica at different hydrogen pressures and temperatures.

Only at the lowest pressure of $p_{H_2} = 1.0$ MPa substantial amounts of DHPs were formed with a maximal selectivity of 8 % at $T_r = 310$ °C. At a hydrogen pressure of 2.0 MPa a maximum of $S_{DHPs} = 1$ % was attained and higher pressures did not lead to the formation of DHPs (not shown). At all hydrogen pressures ROPs are the main product group at low conversions. With increasing temperature these undergo hydrogenolysis to OCDs and C_9 - products (see Figure 9.49). However, the OCD formation at 1.0 MPa is strongly hindered due to the formation of substituted benzenes with a maximal selectivity of 46 % at $T_r = 350$ °C which cannot be opened to OCDs. At $p_{H_2} = 2.0$ MPa the formation of substituted benzenes was negligible with a maximal selectivity of 1 % and, moreover, higher hydrogen pressures led to amounts below 1 %. An increase of the hydrogen pressure resulted in a continuous increase of the maximal OCD yield up to $Y_{OCDs, max.} = 22$ % at $p_{H_2} = 8.0$ MPa (see Table 9.13). At all pressures the OCD distributions are similar with the formation of mainly multiply branched decanes (not shown) as observed at $p_{H_2} = 5.2$ MPa, see Figure 9.22, page 117.

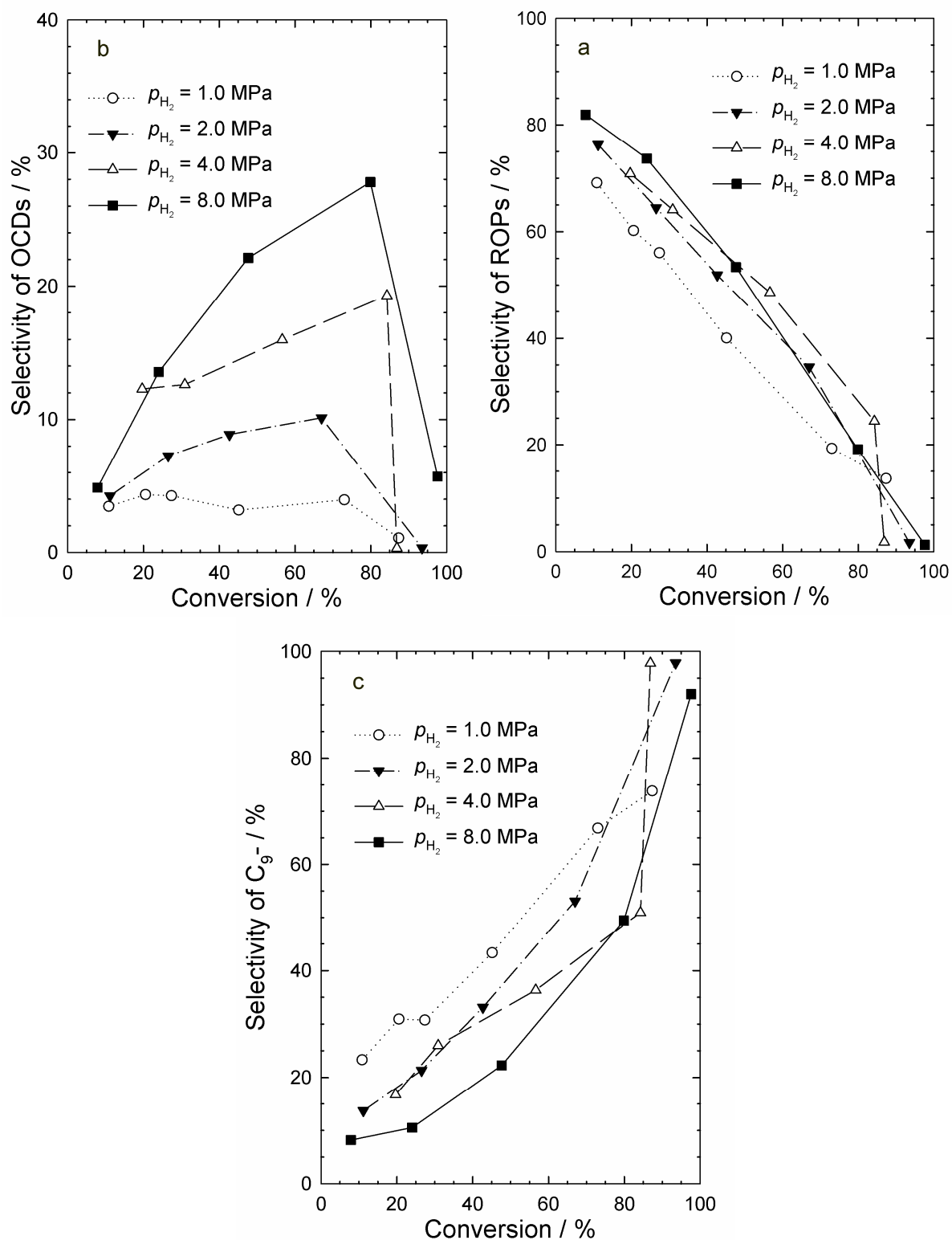


Figure 9.49: Selectivities of different groups of products on catalyst 2.73Ir/silica at different hydrogen pressures and decalin conversions.

With varying hydrogen pressures different dependencies of product selectivities on the conversion have been found, see Figure 9.49. Compared to the results obtained at higher hydrogen pressures, at $p_{H_2} = 1.0$ MPa the selectivities of ROPs and OCDs are

lower while hydrocracking to C₉- occurs with higher selectivities. In the formation of ROPs and C₉- products only small differences between $p_{\text{H}_2} = 2.0, 4.0$ and 8.0 MPa have been found. At most conversions, the extent of hydrocracking to C₉- is minimal at $p_{\text{H}_2} = 8.0$ MPa. OCD formation is strongly enhanced with each value of increased hydrogen pressure. The maximal S_{OCDs} value increased with increasing hydrogen pressure from 1.0 to 8.0 MPa in the following order: $4, 10, 19$ and 28 % (see Table 9.13). Hence, higher values of hydrogen pressure lead to a decreased extent of hydrogenolysis in the alkyl side-chain of ROPs or of OCDs while the endocyclic hydrogenolysis in ROPs to OCDs is enhanced.

Table 9.13: Maximum yields of open-chain decanes obtained on catalyst 2.73Ir/silica at different hydrogen pressures in the conversion of decalin.

$p_{\text{H}_2} / \text{MPa}$	$T_r / ^\circ\text{C}$	$X_{\text{Dec}} / \%$	$S_{\text{OCDs}} / \%$	$Y_{\text{OCDs, max.}} / \%$
1.0	330	73	4	3
2.0	310	67	10	7
4.0	310	84	19	16
8.0	310	80	28	22

At low conversions and yields of C₉- products around 30 %, the distributions of the hydrocracked products are hammock-shaped, and the amounts of C₁ and C₉ are very high (not shown). The distribution curves of the hydrocracked products at reaction temperatures of maximal OCD yield are hammock-shaped for $p_{\text{H}_2} \geq 2.0$ MPa, see Figure 9.50. At the lowest hydrogen pressure of 1.0 MPa a hammock-like curve with high values at C₁ and C₈ was obtained. With increasing hydrogen pressure, a roughly similar variation of the distribution curve was obtained as in the hydroconversion of perhydroindan on Pt/silica, see Figure 9.47, page 149. This change is characterized by an increase at C₄ and C₅ with perhydroindan as reactant or at C₄, C₅, C₆ with decalin. The second characteristic is an increase in the ratio C₈/C₇ or C₉/C₈ with perhydroindan or decalin, respectively. At low hydrogen pressures different compositions of precursors of hydrocracked products are formed compared to higher pressures. ROPs are composed to a large extent of aromatic hydrocarbons and smaller amounts of OCNs or OCDs are formed. Presumably, these different compositions of C₉-precursors are the origin of the special curve type at low hydrogen pressures.

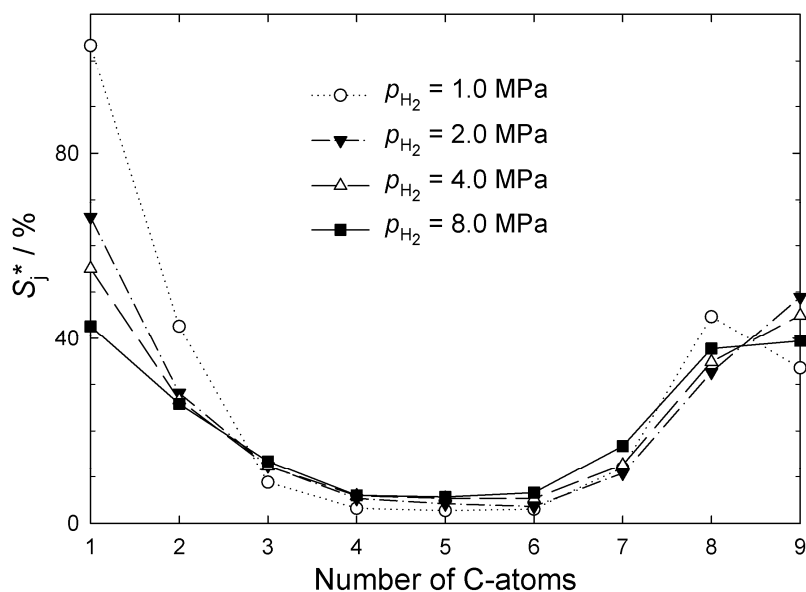


Figure 9.50: Modified hydrocracking selectivities S_j^* on 2.73Ir/silica in the hydroconversion of cis-decalin at different hydrogen pressures:

$p_{H_2} = 1.0$ MPa:	$T_r = 330$ °C;	$X_{Dec} = 73$ %;	$Y_{C_9} = 49$ %;	$\Sigma S_j^* = 254$ %.
$p_{H_2} = 2.0$ MPa:	$T_r = 310$ °C;	$X_{Dec} = 67$ %;	$Y_{C_9} = 34$ %;	$\Sigma S_j^* = 212$ %.
$p_{H_2} = 4.0$ MPa:	$T_r = 310$ °C;	$X_{Dec} = 84$ %;	$Y_{C_9} = 45$ %;	$\Sigma S_j^* = 203$ %.
$p_{H_2} = 8.0$ MPa:	$T_r = 310$ °C;	$X_{Dec} = 80$ %;	$Y_{C_9} = 40$ %;	$\Sigma S_j^* = 194$ %.

9.9 Conclusions

9.9.1 Influence of the Nature of the Noble Metal

The catalytic activity of the noble metals decreases in the order Ir > Rh > Pt > Pd. In the same order higher reaction temperatures are required which lead to an increasing tendency of aromatization due to thermodynamical reasons. All four noble metals are active in the stereoisomerization of the cis- and trans-isomers of perhydroindan and decalin. Skeletal isomerization occurs on Pd, Pt and low-dispersed Rh.

One important type of isomerization is the interconversion of five- and six-membered rings. Whether these reactions proceed *via* the bond-shift and/or the cyclic mechanism is difficult to distinguish. However, the large amounts of decalin formed on Pt/silica from spiro[4.5]decane cannot be explained with a 1,5-dehydrocyclization, which is the main reaction step in the cyclic isomerization mechanism of alkanes. Hence, at least with spiro[4.5]decane, the bond-shift mechanism that proceeds *via* cyclopropanoid species is prevailing. Although it was demonstrated by FT-IR spectroscopy (see

Section 6.2) and the n-octane test reaction (see Section 8) that no catalytically active Brønsted acid sites seem to be present it cannot be totally ruled out that at high reaction temperatures some very weak Brønsted acid sites become active and catalyze isomerization *via* the bifunctional route.

On Ir/silica hydrogenolysis is essentially the only reaction. Together with the high activity and, hence, low reaction temperatures the extent of multiple hydrogenolysis leading to $\Sigma S_j^* \gg 200\%$ is low. This facilitates the examination of reaction networks, as, *e.g.*, in the ring opening of decalin. On Pt/silica the isomerization activity and the higher extent of multiple hydrogenolysis due to the high reaction temperatures required, hamper such examinations. Pd/silica shows a very low activity in the hydrogenolysis. On Rh/silica with a high metal dispersion mainly hydrogenolysis occurs but the low activity and high reaction temperatures result in multiple hydrogenolysis and the formation of C₉- in large amounts.

As noble metal component for good ring-opening catalysts only iridium seems to be appropriate. For hydrogenolysis on Pd, Pt and Rh too high temperatures are required. However, when acid sites are present, as, *e.g.*, on Pt/Na,H-Y a high-performance ring-opening catalyst can result [5], presumably due to the isomerization of six- to five-membered rings. Indeed, in the hydroconversion of perhydroindan on Pt/silica the fast hydrogenolytic opening of the five-membered ring becomes evident.

In naphthenic rings on iridium the hydrogenolysis of unsubstituted C-C bonds (secondary-secondary) is faster than that of substituted C-C bonds (secondary-tertiary and tertiary-tertiary). This preference is known from the selective ring-opening mechanism which was proposed by Maire *et al.* for the ring opening of methylcyclopentane [33]. However, the experimentally found regioselectivities for the cleavage of endocyclic C-C bonds cannot be explained by just one of the three established ring-opening mechanisms (non-selective, selective and partially selective, see Section 4.2.1.4). Also a linear combination of them does not result in a good correlation with the experimental results. It appears that the adsorption mode of the hydrocarbon on the metal can largely depend on the geometric conformation and isomeric composition. In alkyl chains (n-decane and side-chain in butylcyclohexane) the cleavage of the primary-secondary and the adjacent secondary-secondary C-C bond is much slower than that of the other C-C bonds in the alkyl chain. However, in the hydroconversion of different naphthenes on Ir/silica hammock-type distribution curves of the hydrocracked products are obtained with large amounts of methane and ethane. As demonstrated with the simulation of the C₉- product distribution (see Section 9.8.2) this is due to the high degree of branching in ring-opening products and

open-chain alkanes, and, correspondingly, a high number of relatively short alkyl chains in which hydrogenolysis can occur. Only with butylcyclohexane a different distribution is found, the origin being the preferred hydrogenolysis in the butyl side-chain resulting in methylcyclohexane and propane.

Due to the isomerization activity of Pt/silica hydrogenolysis occurs not only in the feed hydrocarbon and its hydrogenolysis products but also in its skeletal isomers. Hence, the composition of hydrocracked products on this catalyst tends to be very complex and does only allow a limited insight into the regioselectivity of hydrogenolysis. However, it seems reasonable to assume that on platinum substituted C-C bonds, *i.e.* secondary-tertiary, are cleaved preferentially.

Different dependencies of conversion on hydrogen pressure were observed. While with Ir/silica and decalin conversion at similar temperatures was maximal at $p_{\text{H}_2} = 4.0$ MPa, in the conversion of perhydroindan on Pt/silica the highest conversions were attained at $p_{\text{H}_2} = 1.0$ MPa. Whether the origin of these different pressure effects reside in types of influence is the type of hydrocarbon or the nature of the noble metal cannot be distinguished. For the ring opening of perhydroindan on Pt/silica and of cis-decalin on Ir/silica the highest pressure of $p_{\text{H}_2} = 8.0$ MPa was beneficial for high selectivities of alkanes with the same number of carbon atoms as the reactant.

9.9.2 Influence of the Type of Hydrocarbon

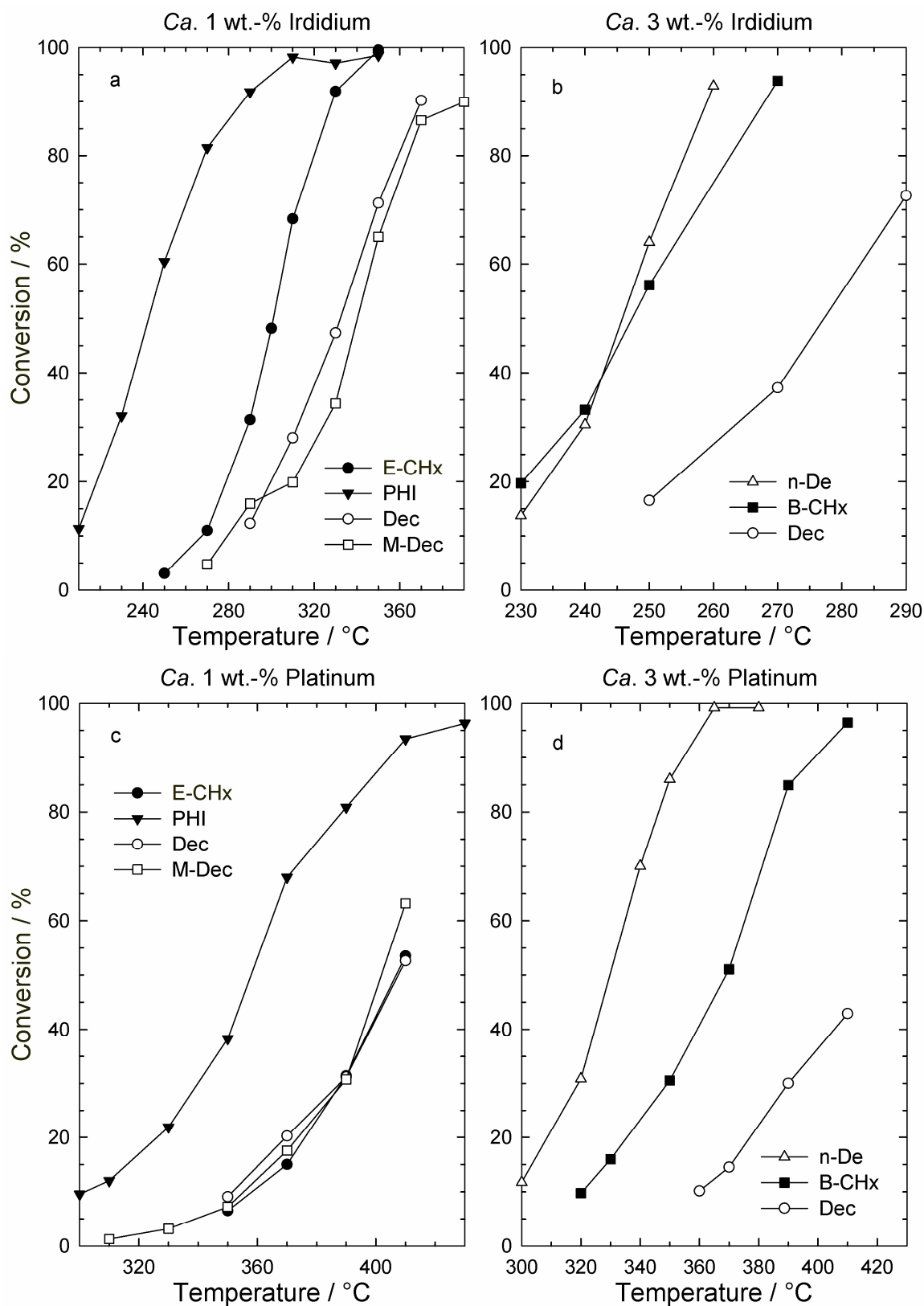


Figure 9.51: Influence of temperature on the conversion of different hydrocarbons on silica-supported catalysts loaded with ca. 1 or 3 wt.-% iridium or platinum.

For a comparison of the reactivity of the different hydrocarbons that have been studied in the hydroconversion on silica-supported iridium- or platinum-containing catalysts the conversions at different temperatures are plotted in Figure 9.51. Spiro[4.5]decane is omitted due to the small number of reaction temperatures that were applied. The following trends are observed on both noble metals:

- Perhydroindan is more reactive than ethylcyclohexane, decalin and methyldecalin. This can be explained by the faster opening of the five-membered ring compared to hydrogenolysis in alkyl side-chains or six-membered rings.
- Decalin is less reactive than n-decane and butylcyclohexane. The reason is the slow opening of the six-membered ring, both other reactants contain an alkyl chain in which hydrogenolysis is relatively fast.

Also differences in the trends of reactivity on Ir/silica vs. Pt/silica can be observed: On iridium ethylcyclohexane is more reactive than decalin and methyldecalin whereas on platinum they are of similar reactivity. To understand the difference it has to be considered that on iridium hydrogenolysis is essentially the only reaction. Due to the availability of an ethyl side-chain higher conversions at similar temperatures are obtained with ethylcyclohexane as reactant in contrast to decalin and methyldecalin.

On platinum, in addition, skeletal isomerization occurs already at low conversions with roughly similar selectivities as those of ROPs and hydrocracked products. Hence, due to the comparable conversions at the same temperatures, the reactivity concerning skeletal isomerization seems to be similar, independent of the reactant. Moreover, DHPs are formed from decalin and methyldecalin on Pt/silica but not from ethylcyclohexane. Hence, this additional reaction path adds to the conversion and perhaps a lower reactivity of decalin and methyldecalin would result if dehydrogenation were absent, as on Ir/silica. In the conversion of perhydroindan on Pt/silica hydrogenolysis is the primary reaction due to the very fast opening of the five-membered ring while the extent of skeletal isomerization is low, resulting in a much higher reactivity.

n-Decane and butylcyclohexane are similarly reactive on iridium, whereas on platinum n-decane is of higher reactivity. This difference can be understood in terms of a similar rate of hydrogenolysis in alkyl chains and six-membered rings on iridium whereas hydrogenolysis on platinum is much faster when the C-C bond is not part of a six-membered ring.

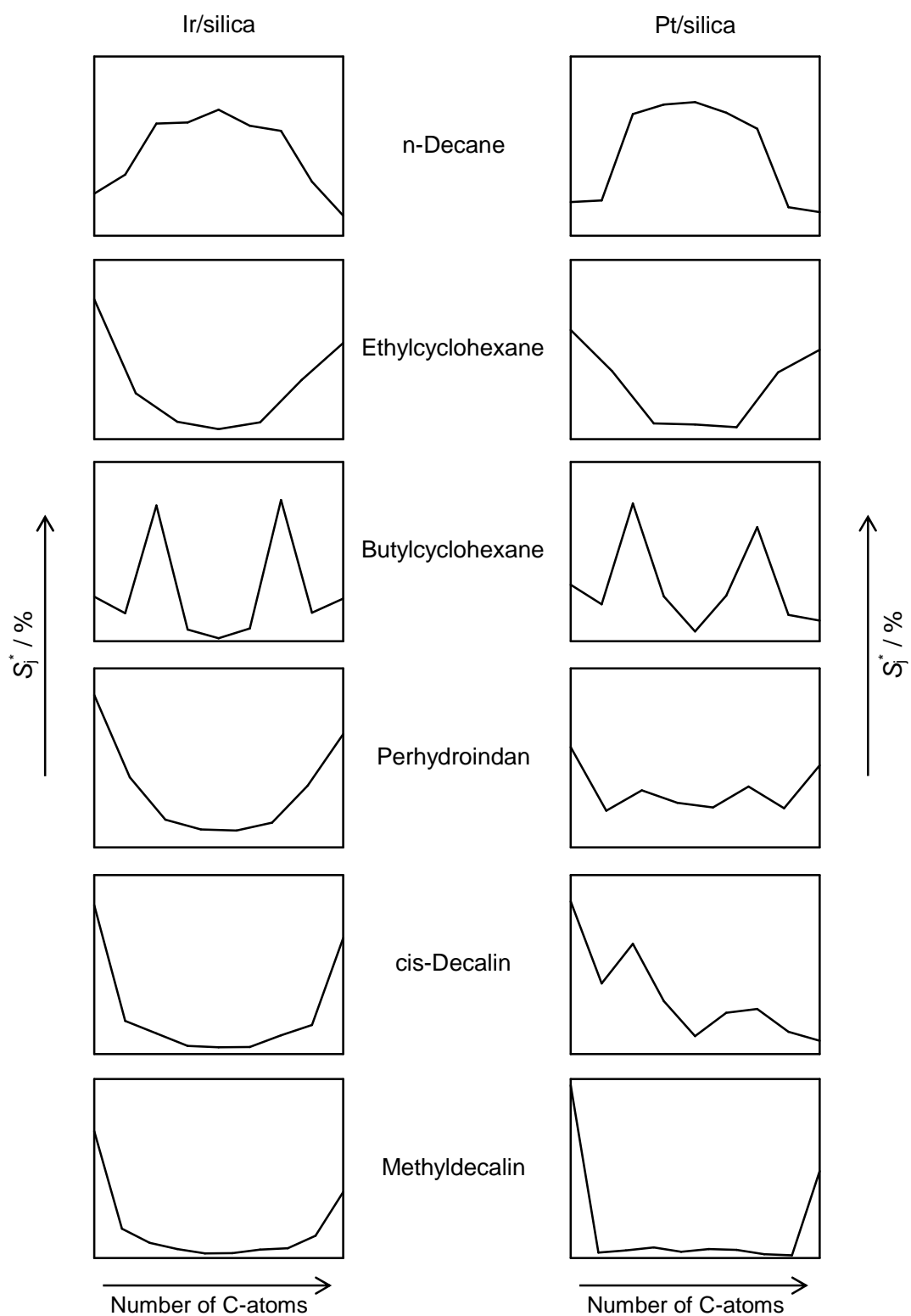


Figure 9.52: Distribution curves of the hydrocracked products obtained on Ir/silica and Pt/silica with different reactants. The metal loadings and reaction conditions can be found in Sections 9.1 to 9.7. Only cis-decalin was converted on catalysts of two different metal loadings. Here, the curves obtained on the catalysts with ca. 3 wt.-% noble metal were chosen.

An overview on the different curve types of the hydrocracked products distributions at a hydrogen pressure of 5 MPa is given in Figure 9.52 for the Ir/silica and Pt/silica catalysts. Mechanistic interpretations were given already in the previous Sections 9.1 to 9.7. However, the overview in Figure 9.52 impressively shows the large variance of the curve shapes. The main influence on the type of the distribution curve is the structure of the hydrocarbon. Although different hydrogenolysis mechanisms are thought to proceed on iridium and platinum, due to the differences in activity and selectivities, for many hydrocarbons the curve shapes formed on iridium *vs.* platinum are relatively similar.

When comparing the curves obtained with one reactant and different noble metals, the largest disparities are observed with *cis*-decalin. As discussed in Section 9.5, the differences are presumably due to different ring-opening products that undergo hydrogenolysis to C₉- products. In the hydroconversion of perhydroindan a similar explanation could be the reason for those differences. With methyldecalin the similar curves are not a consequence of analogous reaction mechanisms. Rather, the hammock-type curve on iridium is a consequence of the pure hydrogenolysis mechanism as demonstrated with decalin (see Section 9.5.2) whereas the pronounced C₁ and C₁₀ formation on platinum stems from the preferred abstraction of the methyl group attached to the bicyclic structure.

10 Hydrocracking on Metal Catalysts Containing Brønsted Acid Sites

Several zeolitic catalysts (see Table 5.4, page 46) that contained Brønsted acid sites and were loaded with the noble metals Ir, Pd or Pt were tested in the hydroconversion of n-decane, butylcyclohexane perhydroindan and spiro[4.5]decane. Most of these experiments were performed to examine reaction networks of isomerization and hydrogenolysis. In a control experiment at the end of each series of measurements with a specific catalyst and reactant it was ensured that no catalyst deactivation had taken place after times-on stream of up to 40 h.

10.1 n-Decane

In the hydroconversion of cis-decalin on high-performance ring-opening catalysts (HIPEROCs) [5], the question arose, as to whether the distribution curves of the hydrocracked products stem from hydrocracking of ring-opening products or rather from hydrocracking of open-chain decanes. Moreover, it was uncertain if the hydrocracking of open-chain decanes occurs by hydrogenolysis or by bifunctional hydrocracking on these catalysts. Hence, n-decane was also used in the hydroconversion on two HIPEROCs (2.9Ir/Na_{0.90}H_{0.10}-Y, 3.0Pt/Na_{0.88}H_{0.12}-Y) and one bifunctional isomerization catalyst (1.1Pd/Na_{0.93}H_{0.07}-Y) in addition to the non-acidic catalysts (see Section 9.1). Moreover, a two-bed arrangement comprised of 1.1Pd/Na_{0.93}H_{0.07}-Y (1st catalyst bed) as isomerization catalyst and 2.69Pt/silica (2nd bed) as non-acidic hydrogenolysis catalyst of similar activity was tested. It was expected to furnish more insight into the product distributions that are obtained by hydrogenolysis of decane isomers.

In the hydroconversion of n-decane, similar conversions were obtained at *ca.* 40 °C higher temperatures on 3.0Pt/Na_{0.88}H_{0.12}-Y compared to 2.9Ir/Na_{0.90}H_{0.10}-Y (see Figure 10.1). A similar difference of catalyst activities had been found with cis-decalin as reactant on the same catalysts [5].

As shown in Figure 10.1a the HIPEROC 2.9Ir/Na_{0.90}H_{0.10}-Y is less active in the hydroconversion of n-decane than the non-acidic catalyst 2.73Ir/silica (see Figure 9.1a). To obtain similar conversions, *ca.* 40 °C higher reaction temperatures have to be applied on the zeolite catalyst under otherwise identical reaction conditions. On both catalysts the metal loading and also the dispersion of iridium are similar with $D = 1.13$ and 1.02 on the zeolite and the silica-supported catalyst, respectively. Perhaps,

differences in the diffusion or adsorption properties due to the zeolite structure or the differing polarities of the supports, respectively, are the reasons.

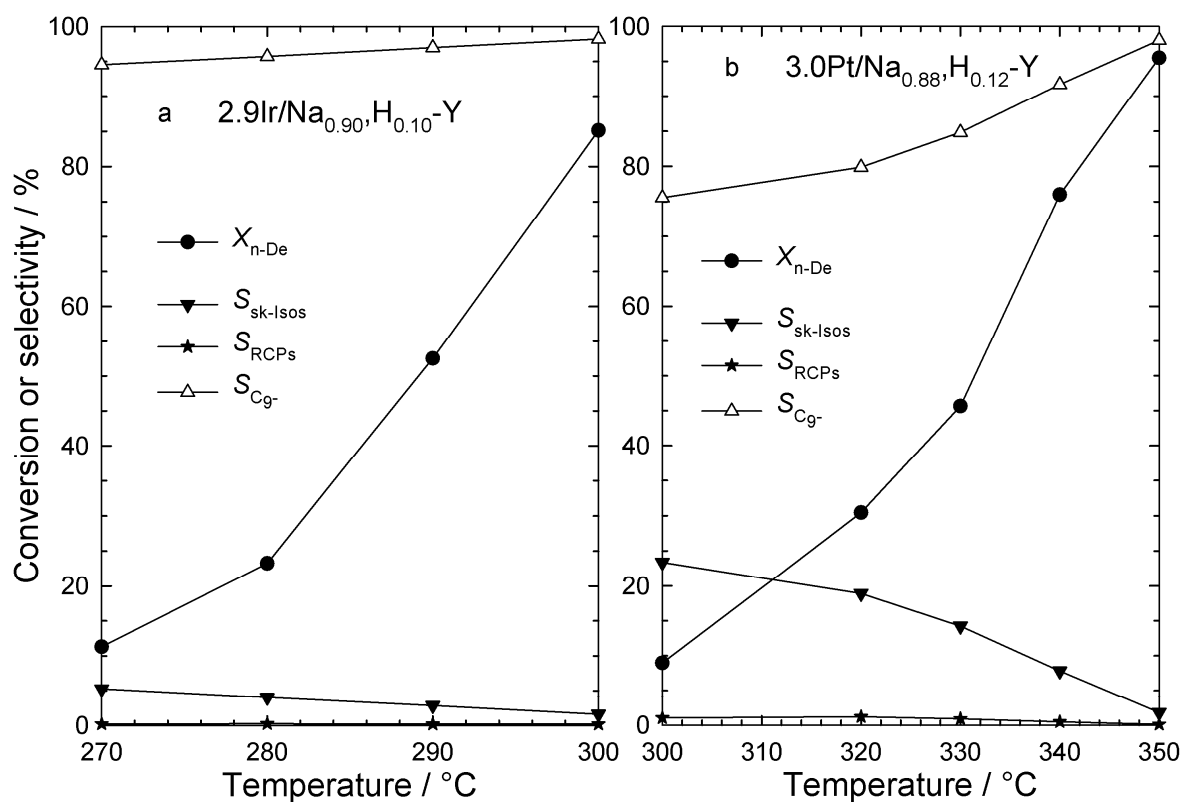


Figure 10.1: Conversion of n-decane and selectivities of different groups of products at different temperatures on two HIPEROCS.

2.9Ir/Na_{0.90}H_{0.10}-Y is essentially a hydrocracking catalyst with $S_{C9-} \geq 95\%$ and a similar selectivity of sk-Isos at low conversion ($S_{sk-Isos} = 5\%$ at $X_{n-De} = 11\%$ and $T_r = 270\text{ °C}$) compared to 2.73Ir/silica ($S_{sk-Isos} = 3\%$ at $X_{n-De} = 14\%$ and $T_r = 230\text{ °C}$). Hence, virtually no isomerization of decalin occurs due to the small concentration of Brønsted acid sites. No RCP formation was detected.

Compared to 2.69Pt/silica (see Figure 9.1b, page 92) a similar activity of the HIPEROC 3.0Pt/Na_{0.88}H_{0.12}-Y (see Figure 10.1b) was found in the n-decane hydroconversion. On both catalysts hydrocracking is the main reaction pathway at all temperatures. While on 2.69Pt/silica low amounts of skeletal isomers are formed with $S_{sk-Isos} \leq 5\%$, the formation of higher amounts with $S_{sk-Isos} \leq 23\%$ is observed on 3.0Pt/Na_{0.88}H_{0.12}-Y. A negligible formation of RCPs was detected.

Mainly mono-branched decanes were formed on both zeolite catalysts with decreasing selectivities in the following order at $X_{n-De} \approx 10\%$: 3-methylnonane, 4-methylnonane,

5-methylnonane, 2-methylnonane, 4-ethyloctane, 3-ethyloctane. A similar distribution of decane isomers was found by Weitkamp [47] in the isomerization of n-decane at low conversion on a typical bifunctional zeolite catalyst. Hence, isomerization occurs largely *via* a bifunctional isomerization mechanisms on 2.9Ir/Na_{0.90}H_{0.10}-Y and 3.0Pt/Na_{0.88}H_{0.12}-Y.

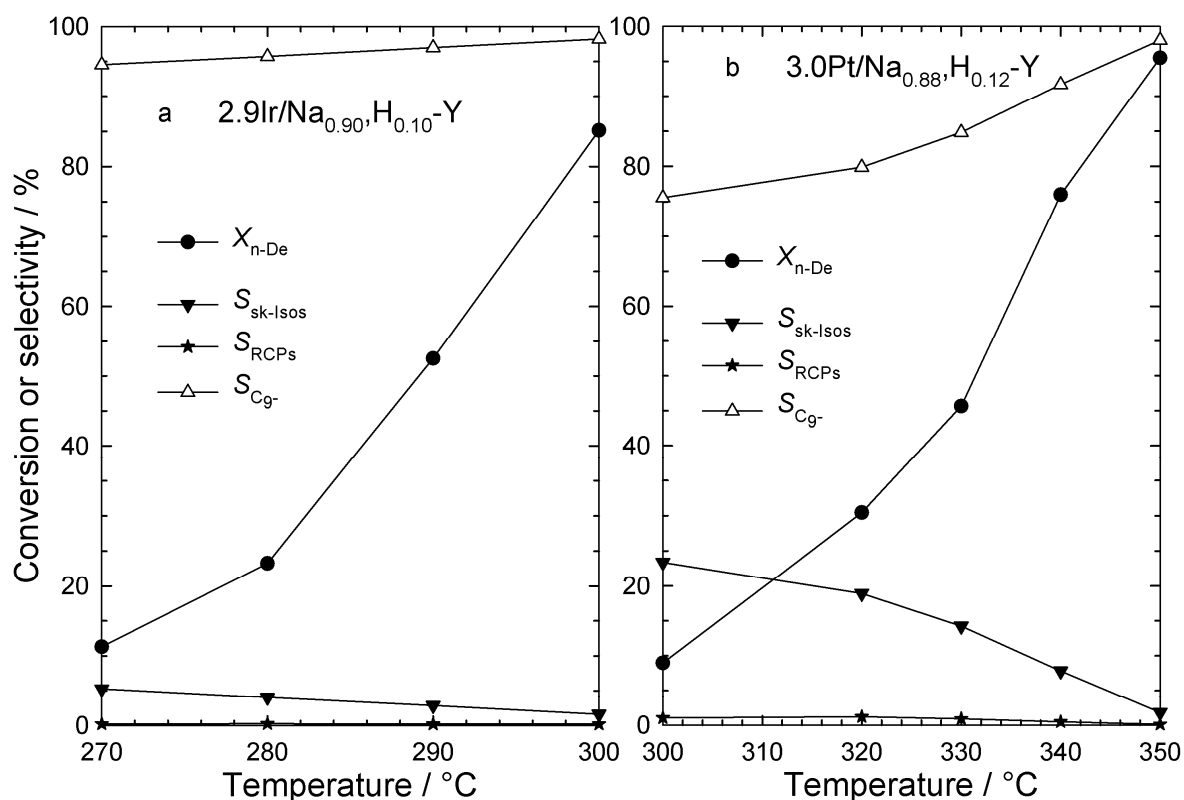


Figure 10.2: Conversion of n-decane and selectivities of different groups of products at different temperatures (a) on a bifunctional isomerization catalyst and (b) on a two-bed arrangement of catalysts 1.1Pd/Na_{0.93}H_{0.07}-Y and 2.69Pt/silica.

Up to intermediate conversions catalyst 1.1Pd/Na_{0.93}H_{0.07}-Y forms mainly skeletal isomers, see Figure 10.2a, as already known from the conversion of cis-decalin on another Pd/Y catalyst [96]. At the lowest conversion their composition is similar to that described for the two iridium- and platinum-containing catalysts (*vide supra*). At higher conversions sk-Isos are hydrocracked to C₉- which is the main product group at X_{n-De} ≥ 83 %. Also RCPs were detected with maximal selectivities of 3 %.

In the two-bed arrangement of catalysts 1.1Pd/Na_{0.93}H_{0.07}-Y and 2.69Pt/silica intermediate conversion values compared to the single-bed arrangements were obtained, see Figure 10.2b. A minimum of the selectivity of C₉- was observed at an intermediate conversion. This unusual behavior is due to a superposition of the

different activities and selectivities obtained on the two catalysts. 2.69Pt/silica is more active and forms almost exclusively C₉- products, whereas 1.1Pd/Na_{0.93}H_{0.07}-Y is less active and forms at low conversions only small amounts of hydrocracked products.

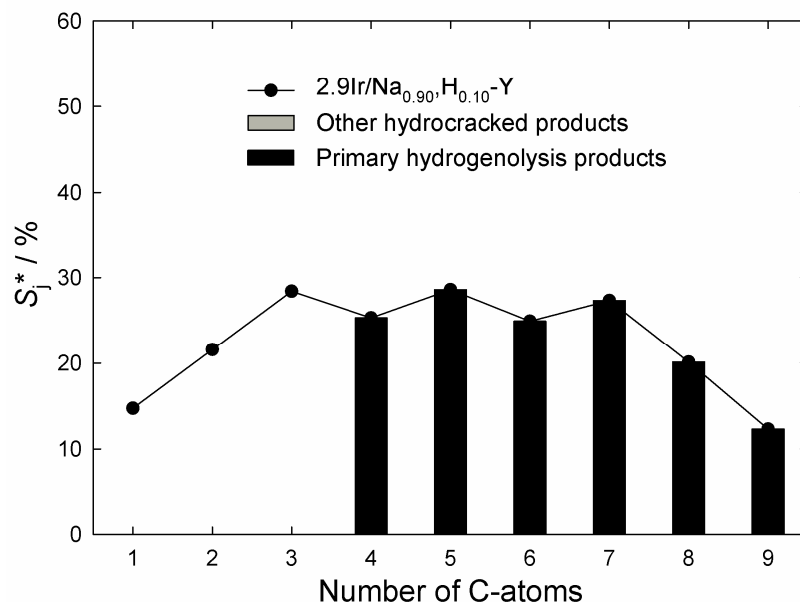


Figure 10.3: Modified hydrocracking selectivities S_j^* on 2.9Ir/Na_{0.90}H_{0.10}-Y in the hydroconversion of n-decane and fraction of primary hydrogenolysis products:

$$T_r = 280 \text{ }^\circ\text{C}; X_{n\text{-De}} = 23 \text{ } \%; Y_{C_9-} = 22 \text{ } \%; \sum S_j^* = 203 \text{ } \%$$

Both distribution curves of the hydrocracked products that were obtained on the HIPEROCS 2.9Ir/Na_{0.90}H_{0.10}-Y (see Figure 10.3) and 3.0Pt/Na_{0.88}H_{0.12}-Y (see Figure 10.4) resemble those described in Section 9.1 for the corresponding non-acidic catalysts. Moreover, on the zeolitic iridium catalyst the hydrocracked products are composed of n-alkanes exclusively and also on the zeolitic platinum catalyst nearly all C₉- products are n-alkanes. These analogous distributions irrespective of the presence or absence of Brønsted acid sites are a strong indication for pure metal-catalyzed hydrogenolysis as underlying mechanism for the cleavage of C-C bonds.

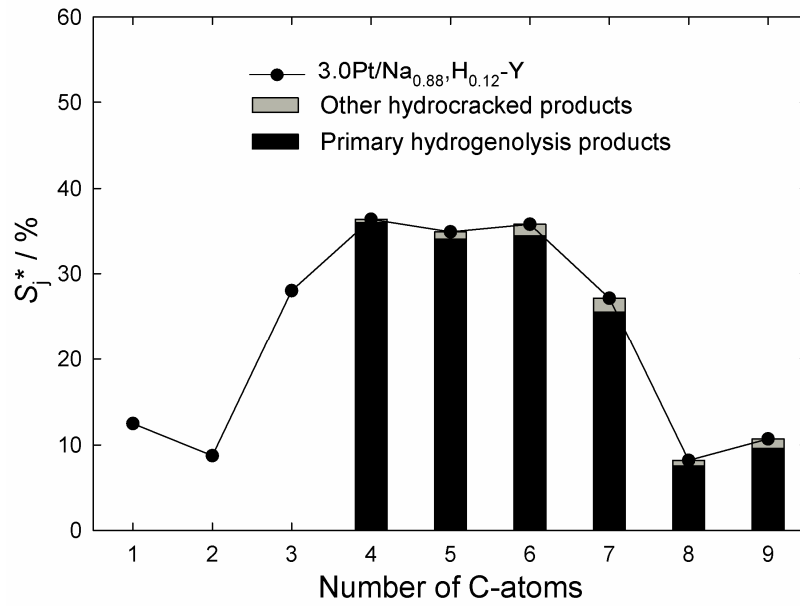


Figure 10.4: Modified hydrocracking selectivities S_j^* on 3.0Pt/Na_{0.88},H_{0.12}-Y in the hydroconversion of n-decane and fraction of primary hydrogenolysis products:

$T_r = 320\text{ }^\circ\text{C}$; $X_{n\text{-De}} = 30\%$; $Y_{C_9^-} = 24\%$; $\Sigma S_j^* = 202\%$.

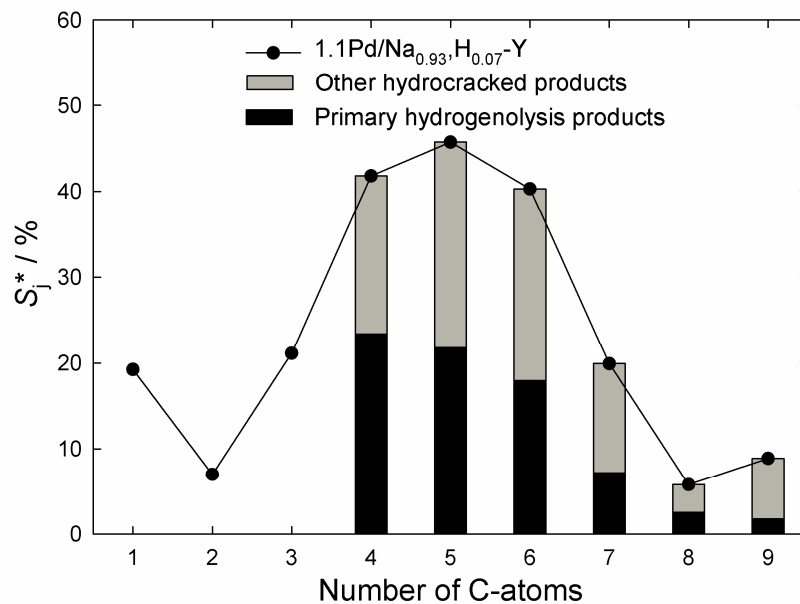


Figure 10.5: Modified hydrocracking selectivities S_j^* on 1.1Pd/Na_{0.93},H_{0.07}-Y in the hydroconversion of n-decane and fraction of primary hydrogenolysis products:

$T_r = 400\text{ }^\circ\text{C}$; $X_{n\text{-De}} = 70\%$; $Y_{C_9^-} = 22\%$; $\Sigma S_j^* = 210\%$.

In addition, the composition of the hydrocracked products formed on the bifunctional 1.1Pd/Na_{0.93}H_{0.07}-Y catalyst (see Figure 10.5) differs strongly from that obtained on the two HIPEROcs. It resembles a volcano shape with a maximum at C₅, high amounts of C₄ and C₆, smaller amounts of C₃ and C₇ as typical for bifunctional hydrocracking of n-alkanes [83]. However, as shown in the hydroconversion of perhydroindan on 0.60Pd/silica (see Figure 9.19, page 113), the formation of methane and ethane stems from the superposition of hydrogenolysis on palladium as side reaction. In case of a reactant with ten carbon atoms, C₉ and C₈ products are the coproducts. Also the large content of branched alkanes in the hydrocracked products indicates that a bifunctional mechanism is the main hydrocracking pathway.

Due to the high similarity to the curve obtained on Pt/silica (see Figure 9.3, page 93) and the prevalence of linear alkanes, it is obvious that the two-bed arrangement with catalysts 1.1Pd/Na_{0.93}H_{0.07}-Y and 2.69Pt/silica (see Figure 10.5b) furnishes C₉-products mainly *via* hydrogenolysis of n-decane on platinum.

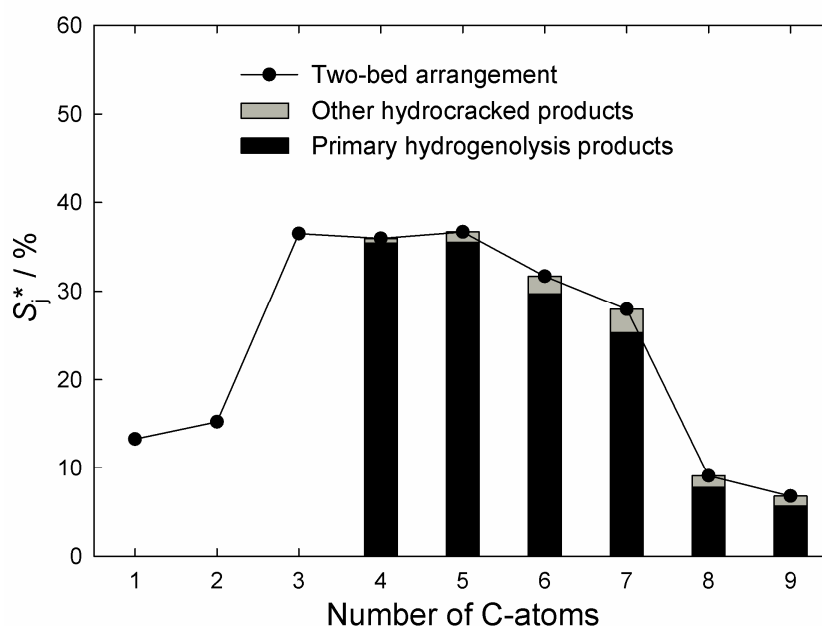


Figure 10.6: Modified hydrocracking selectivities S_j^* on a two-bed arrangement of catalysts 1.1Pd/Na_{0.93}H_{0.07}-Y and 2.69Pt/silica in the hydroconversion of n-decane and fraction of primary hydrogenolysis products: $T_r = 350\text{ }^\circ\text{C}$; $X_{n\text{-De}} = 39\%$; $Y_{C_9^-} = 31\%$; $\sum S_j^* = 213\%$.

The question about the contribution of hydrocracking of OCDs in the ring opening of decalin on HIPEROcs [5] can be answered as follows: A comparison of the distribution curves of the hydrocracked products obtained in the hydroconversion of n-decane and cis-decalin on 2.9Ir/Na_{0.90}H_{0.10}-Y reveals strong differences. No hammock-type curve (see Figure 10.3) was obtained with n-decane. Hence, hints were

obtained that the hydrogenolysis of n-decane contributes only to a small extent to the formation of C₉- products from cis-decalin. An analogous comparison for the 3.0Pt/Na_{0.88},H_{0.12}-Y catalyst reveals a higher similarity. Due to the isomerization activity of 3.0Pt/Na_{0.88},H_{0.12}-Y, most probably, a mixture of OCDs underwent hydrogenolysis. This can be interpreted by a, possibly, strong contribution of OCD hydrogenolysis in the cis-decalin hydroconversion.

However, most of the OCDs formed on both HIPEROcs are branched decane isomers, the fraction of n-decane is < 10 % [5]. A hydrogenolysis of the real mixture of OCDs could result in a different distribution of the hydrocracked products than that obtained with n-decane. Hence, it is unclear to what extent the results of the n-decane hydroconversion can be transferred to the ring opening of cis-decalin.

10.2 Butylcyclohexane

To answer the question about the origin of the precursors of the hydrocracked products from cis-decalin (see Section 10.1), butylcyclohexane was chosen as representative ring-opening product. It was hydroconverted on the same catalysts as n-decane: two HIPEROcs (2.9Ir/Na_{0.90},H_{0.10}-Y, 3.0Pt/Na_{0.88},H_{0.12}-Y), one bifunctional isomerization catalyst (1.1Pd/Na_{0.93},H_{0.07}-Y) and a two-bed arrangement (1.1Pd/Na_{0.93},H_{0.07}-Y and 2.69Pt/silica in the 1st and 2nd catalyst bed, respectively).

An important question is: Does the opening of the naphthenic ring on the best catalysts (HIPEROcs) occur *via* hydrogenolysis on the noble metal or *via* bifunctional hydrocracking? Also on a similar Pd/Na,H-Y catalyst small amounts of ROPs and OCDs were observed in the hydroconversion of cis-decalin [96] in spite of the low hydrogenolysis activity of palladium (see Section 9.4). Is the ring opening on this catalyst possible by bifunctional hydrocracking? Moreover, the distribution of the hydrocracked products that are formed by hydrogenolysis of a mixture of C₁₀ one-ring naphthenes in the two-bed arrangement could help to understand the formation of C₉-products in the decalin hydroconversion.

10.2.1 Hydroconversion on High-Performance Ring-Opening Catalysts

In the hydroconversion of butylcyclohexane, similar conversions were obtained at *ca.* 30 °C higher temperatures on 3.0Pt/Na_{0.88},H_{0.12}-Y compared to 2.9Ir/Na_{0.90},H_{0.10}-Y (see Figure 10.7). A similar difference of catalyst activities was found with n-decane (see

Figure 10.1, page 161) and cis-decalin [5] as reactants on the same catalysts. No dehydrogenation to butylbenzene occurred on both catalysts.

Again, as observed in the hydroconversion of n-decane (see Sections 9.1 and 10.1), 2.9Ir/Na_{0.90}H_{0.10}-Y is less active than the corresponding non-acidic 2.73Ir/silica catalyst. At *ca.* 50 °C higher reaction temperatures similar conversion are reached. Possible explanations were given in Section 10.1.

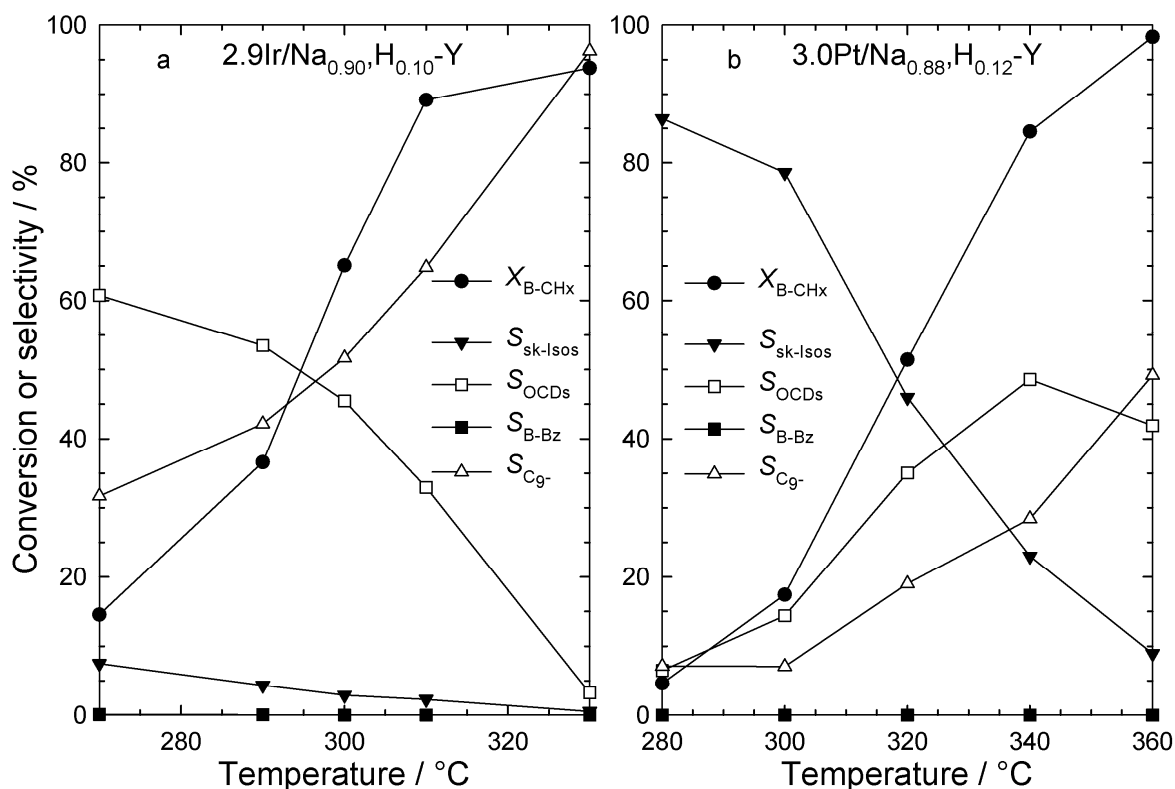


Figure 10.7: Conversion of butylcyclohexane and selectivities of different groups of products at different temperatures on two HIPEROCS.

The selectivity pattern for 2.9Ir/Na_{0.90}H_{0.10}-Y (see Figure 10.7a, page 167) resembles that for 2.73Ir/silica (see Figure 9.10a, page 101). Higher amounts of sk-Isos are formed on 2.9Ir/Na_{0.90}H_{0.10}-Y ($S_{sk-Isos} = 7\%$ at $X_{B-CHx} = 15\%$ and $T_r = 270\text{ °C}$) compared to 2.73Ir/silica ($S_{sk-Isos} = 3\%$ at $X_{B-CHx} = 20\%$ and $T_r = 230\text{ °C}$) due to bifunctional catalysis on the Brønsted acid sites. On both iridium catalysts OCDs were formed with maximal $Y_{OCDs} \approx 30\%$ (see Table 10.1, page 168).

Compared to 2.69Pt/silica (see Figure 9.10b, page 101) a higher activity of the HIPEROCS 3.0Pt/Na_{0.88}H_{0.12}-Y (see Figure 10.7b, page 167) was found in the butylcyclohexane hydroconversion. Similar conversions were obtained at *ca.* 40 °C higher reaction temperatures on the silica-supported catalyst. In contrast, with

n-decane as reactant the activity of both catalysts was similar (see Sections 9.1 and 10.1). On the zeolite catalyst in the hydroconversion of n-decane hydrogenolysis is the main reaction at all temperatures, whereas with butylcyclohexane as reactant skeletal isomerization is the main reaction up to intermediate conversions of $X_{B-CHx} = 51\%$. On 2.69Pt/silica, however, with both reactants hydrogenolysis is the major reaction path. Hence, the higher activity of the zeolite catalyst in the hydroconversion of butylcyclohexane could stem from the relatively fast bifunctional isomerization of the six-membered ring that is possible on the zeolitic catalyst only. In addition, the slow hydrogenolysis of six-membered rings on platinum can explain the low activity of the non-acidic catalyst.

Table 10.1: Maximum yields of open-chain decanes obtained in the hydroconversion of butylcyclohexane.

Catalyst	T_r / °C	X_{B-CHx} / %	S_{OCDs} / %	$Y_{OCDs, max.}$ / %
2.73Ir/silica	250	56	53	30
2.9Ir/Na _{0.90} H _{0.10} -Y	300	65	45	29
2.69Pt/silica	390	85	16	13
3.0Pt/Na _{0.88} H _{0.12} -Y	340	85	49	41
1.1Pd/Na _{0.93} H _{0.07} -Y	410	86	13	11
Two-bed arrangement of 1.1Pd/Na _{0.93} H _{0.07} -Y and 2.69Pt/silica	390	78	16	13

As shown in Table 10.1, a small concentration of relatively weak Brønsted acid sites leads to an increase of $Y_{OCDs, max.}$ from 13 to 41 % on the platinum-containing catalysts. This is the highest OCD yield of all catalysts that were tested with butylcyclohexane in the present study.

On both HIPEROCs (see Figure 10.8) very similar OCD distributions as on the corresponding silica-supported catalysts (see Figure 9.12, page 103) are obtained at maximal OCD yields. This is an indication for analogous ring-opening mechanisms *via* hydrogenolysis on the respective noble metal.

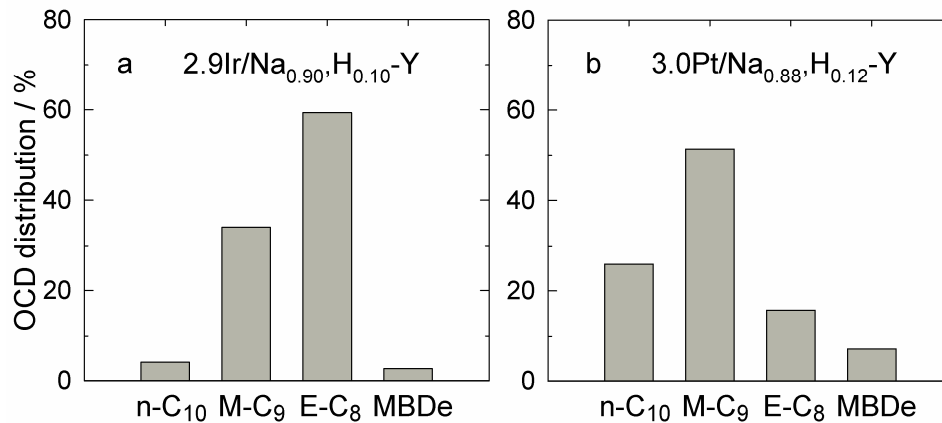


Figure 10.8: Hydroconversion of butylcyclohexane on two HIPEROCs. Breakdown of the selectivities of OCDs into differently branched decane isomers:

2.9Ir/Na_{0.90},H_{0.10}-Y: $T_r = 300\text{ }^\circ\text{C}$; $X_{\text{B-CHX}} = 65\%$; $Y_{\text{OCDs}} = 29\%$; $S_{\text{OCDs}} = 45\%$.

3.0Pt/Na_{0.88},H_{0.12}-Y: $T_r = 340\text{ }^\circ\text{C}$; $X_{\text{B-CHX}} = 85\%$; $Y_{\text{OCDs}} = 41\%$; $S_{\text{OCDs}} = 49\%$.

At the lowest conversion of $X_{\text{B-CHX}} = 15\%$ when no multiple hydrogenolysis occurs ($\Sigma S_j^* = 201\%$), the selectivity of direct hydrogenolysis products assumes a value of 70% on 2.9Ir/Na_{0.90},H_{0.10}-Y. Due to its isomerization activity this value is lower compared to 91% on 2.73Ir/silica (see Table 9.1, page 102). A roughly similar molar distribution of the direct hydrogenolysis products with six to ten carbon atoms as on the silica catalyst was observed. The main differences were a higher mole fraction of 4-ethyloctane (65%) and a smaller fraction of methylcyclohexane (8%) on 2.9Ir/Na_{0.90},H_{0.10}-Y. On the zeolitic platinum catalyst the selectivity of direct hydrogenolysis products assumes a value of only 12% at the lowest conversion, due to the high amounts of skeletal isomers, whereas a value of 68% was obtained on 2.69Pt/silica (see Table 9.1, page 102).

An attempt was made to understand the ring-opening mechanism of butylcyclohexane on the bifunctional iridium and platinum catalysts and on 2.69Pt/silica. Due to the occurrence of bifunctional isomerization of type A, pentylcyclopentane is the main skeletal isomer on 3.0Pt/Na_{0.88},H_{0.12}-Y and accounts for 61% of all sk-Isos at the lowest conversion of 17%. Also on 2.9Ir/Na_{0.90},H_{0.10}-Y and 2.69Pt/silica $S_{\text{Pn-CPn}} / S_{\text{sk-Isos}}$ assumes values of 17 and 38%, respectively, at the lowest conversions.

Hence, if it is assumed that OCDs are formed by a hydrogenolytic ring opening either of butylcyclohexane or pentylcyclopentane, the following five OCDs would be formed (see Table 10.2). From butylcyclohexane: n-decane, 5-methylnonane and 4-ethyloctane. From pentylcyclopentane: n-decane, 4-methylnonane and 3-ethyloctane. The relative selectivities of these five OCDs are plotted versus conversion in Figure 10.9a together with the relative selectivities of 2-methylnonane and 3-methylnonane which

are also formed in high amounts. On 3.0Pt/Na_{0.88}H_{0.12}-Y the fraction of these seven plotted OCDs in the product group of OCDs is 100 % at the lowest conversion and 89 % at the maximum conversion.

Table 10.2: Main OCDs formed on 3.0Pt/Na_{0.88}H_{0.12}-Y and possible precursors for a hydrogenolytic ring opening.

OCD	Can be formed by hydrogenolytic ring opening of	
	butylcyclohexane	pentylcyclopentane
n-decane	+	+
2-methylnonane	-	-
3-methylnonane	-	-
4-methylnonane	-	+
5-methylnonane	+	-
3-ethyloctane	-	+
4-ethyloctane	+	-

On this catalyst, 5-methylnonane and 4-ethyloctane, which are assumed to stem only from the hydrogenolysis of butylcyclohexane, have a maximal relative selectivity at the lowest conversion, *i.e.* these are primary products. In contrast, 4-methylnonane and 3-ethyloctane, the products of a direct hydrogenolysis of pentylcyclopentane, show an increase of the relative selectivity from the lowest to the second lowest conversion. n-Decane is a hydrogenolysis product of butylcyclohexane and pentylcyclopentane, hence a detailed interpretation of the S_{n-De} / S_{OCDs} values is not possible.

The differences of the dependencies of relative selectivities *vs.* conversion can be interpreted in the following manner: At the lowest conversion mainly butylcyclohexane is opened hydrogenolytically on platinum, but with increasing conversion, higher amounts of pentylcyclopentane are formed by bifunctional isomerization. At the second lowest conversion pentylcyclopentane becomes the main OCDs precursor. From the conversion dependence of the selectivities it is obvious that 2-methylnonane and 3-methylnonane, which cannot be formed by a hydrogenolytic ring opening of butylcyclohexane or pentylcyclopentane are formed later in the reaction network. Presumably, they are formed by bifunctional type A isomerization of the other five OCDs.

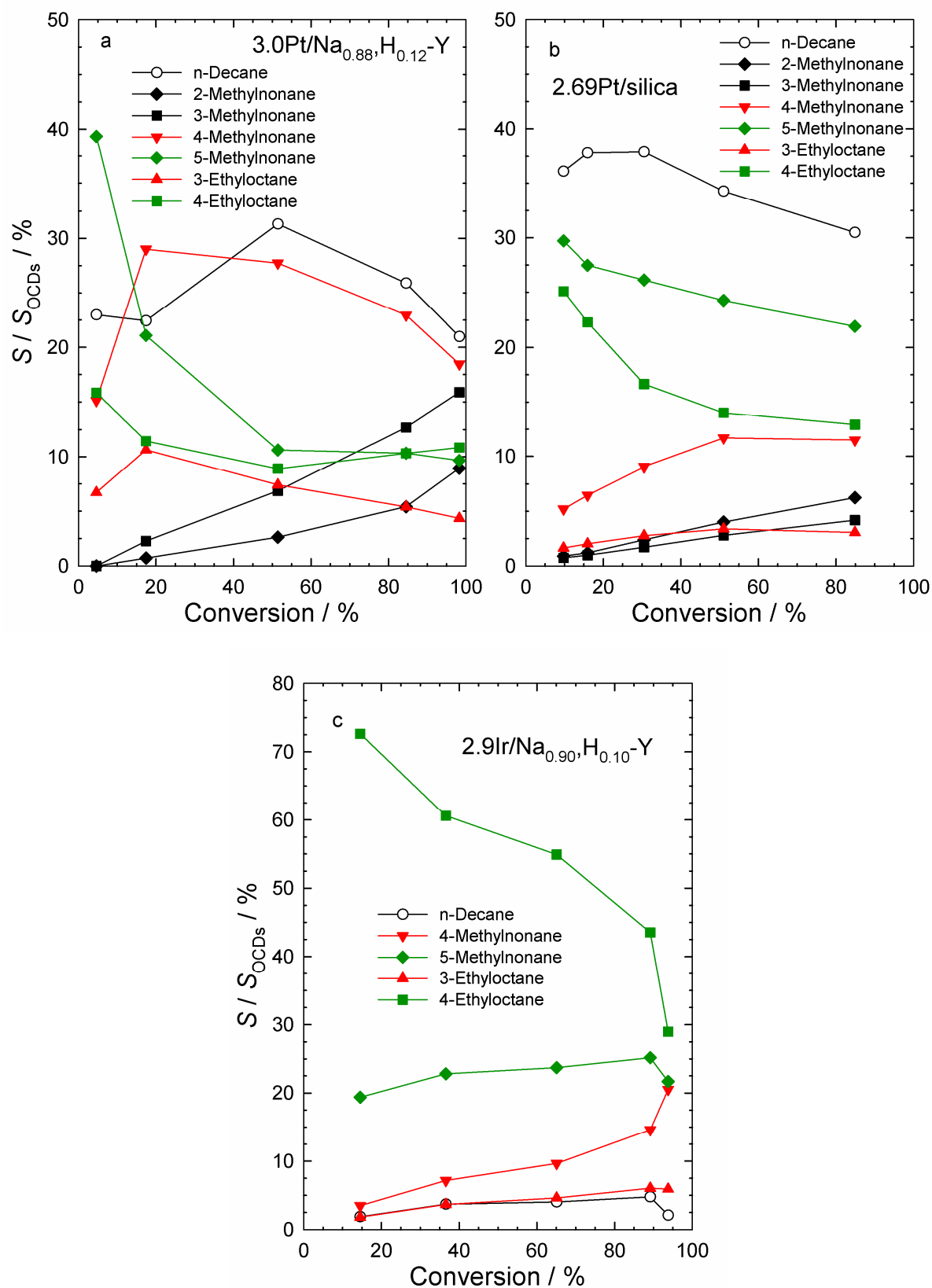


Figure 10.9: Hydroconversion of butylcyclohexane: relative selectivities of the major OCDs on three isomerization active catalysts at different conversions.

On non-acidic 2.69Pt/silica (see Figure 10.9b), most of the OCDs seem to stem from a hydrogenolytic ring opening of butylcyclohexane as indicated by the high relative selectivities of 5-methylnonane and 4-ethyloctane. But also the ring-opening products of pentylcyclopentane, *i.e.* 4-methylnonane and 3-ethyloctane, are formed to a certain extent with increasing conversion. As on the zeolite Y-supported platinum catalyst, also 2- and 3-methylnonane, which are presumably formed by an isomerization of the other OCDs are formed in intermediate amounts at higher conversions. From low to high conversion, 99 to 90 % of all OCDs consist of these seven OCDs mentioned.

Hence, for the two platinum catalysts a simplified reaction network for the formation of the OCDs n-decane (n-De), 4-methylnonane (4-M-No), 5-methylnonane (5-M-No), 3-ethyloctane (3-E-Oc) and 4-ethyloctane (4-E-Oc) is depicted in Figure 10.10. In addition the exocyclic hydrogenolysis to methylcyclohexane is shown, since, as shown in Table 9.1, page 102, the major products of hydrogenolysis in the butyl side-chain of butylcyclohexane are methylcyclohexane plus propane. Of course, this is a simplified reaction network which can explain the main products only at low conversion. With increasing conversion the isomerization activity of the platinum catalysts (either the metal alone or its combination with Brønsted acid sites) makes the product mixture and, hence, the reaction network more complex.

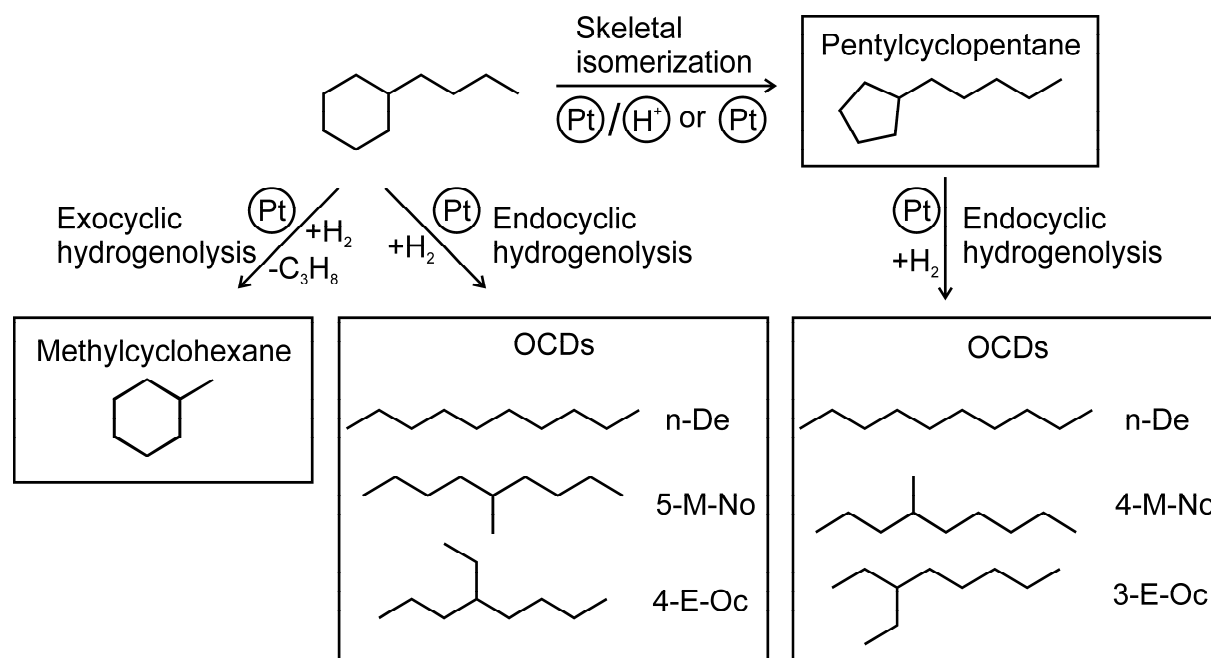


Figure 10.10: Proposed simplified reaction network for the hydroconversion of butylcyclohexane on the platinum catalysts 2.69Pt/silica and the HIPEROX 3.0Pt/Na_{0.88}H_{0.12}-Y.

On the mildly acidic iridium catalyst 2.9Ir/Na_{0.90},H_{0.10}-Y very small amounts of sk-Isos with maximal selectivities of 7 % were formed. However, at the lowest conversion, 99 % of all OCDs consist of n-decane, 5-methylnonane and 4-ethyloctane but also of the products from the ring opening of pentylcyclopentane: 4-methylnonane and 3-ethyloctane (see Figure 10.9c). At the second highest conversion of 89 %, 94 % of all OCDs consist of these five OCDs. Only at the maximal conversion of 94 %, at which hydrocracking to C₉- is too severe, a very low $S_{\text{OCDs}} = 3 \%$ is obtained. Since the different OCDs are not equally prone to consecutive hydrocracking, at this high reaction temperature of 330 °C a different OCD distribution is found, so that only 79 % of all OCDs are the five ones mentioned before. In contrast to the Pt/Na,H-Y catalyst, the strong preference for the formation of the OCDs 5-methylnonane and 4-ethyloctane on Ir/Na,H-Y can be understood in terms of a lower isomerization activity to pentylcyclopentane and a preference for cleaving the unsubstituted endocyclic C-C bonds in butylcyclohexane. However, as indicated by the formation of intermediate amounts of 4-methylnonane and 3-ethyloctane, more and more pentylcyclopentane is presumably formed and ring-opened by hydrogenolysis, as the conversion is increased.

McVicker *et al.* [4] found similar OCD distributions in the hydroconversion of pentylcyclopentane on Ir/ γ -alumina as in the hydroconversion of butylcyclohexane on a mixture of Ir/ γ -alumina and Pt/USY and on Ir/USY. They suspected that pentylcyclopentane could be an intermediate in the ring opening of butylcyclohexane on catalysts consisting of iridium and a component with an isomerization function.

These experiments with butylcyclohexane facilitate the understanding of OCD formation pathways on high-performance ring-opening catalysts (HIPEROCS). Strong hints were obtained for OCD formation occurring to a large extent on the noble metal, when acid sites catalyze the isomerization to five-membered rings in a preceding step. When platinum is the noble metal isomerization can also occur by metal catalysis to a smaller extent. In view of the low activity of platinum for hydrogenolytic opening of six-membered rings, this is a very valuable result which helps to explain the high amounts of OCDs formed in the hydroconversion of butylcyclohexane and presumably also in the hydroconversion of decalin [5].

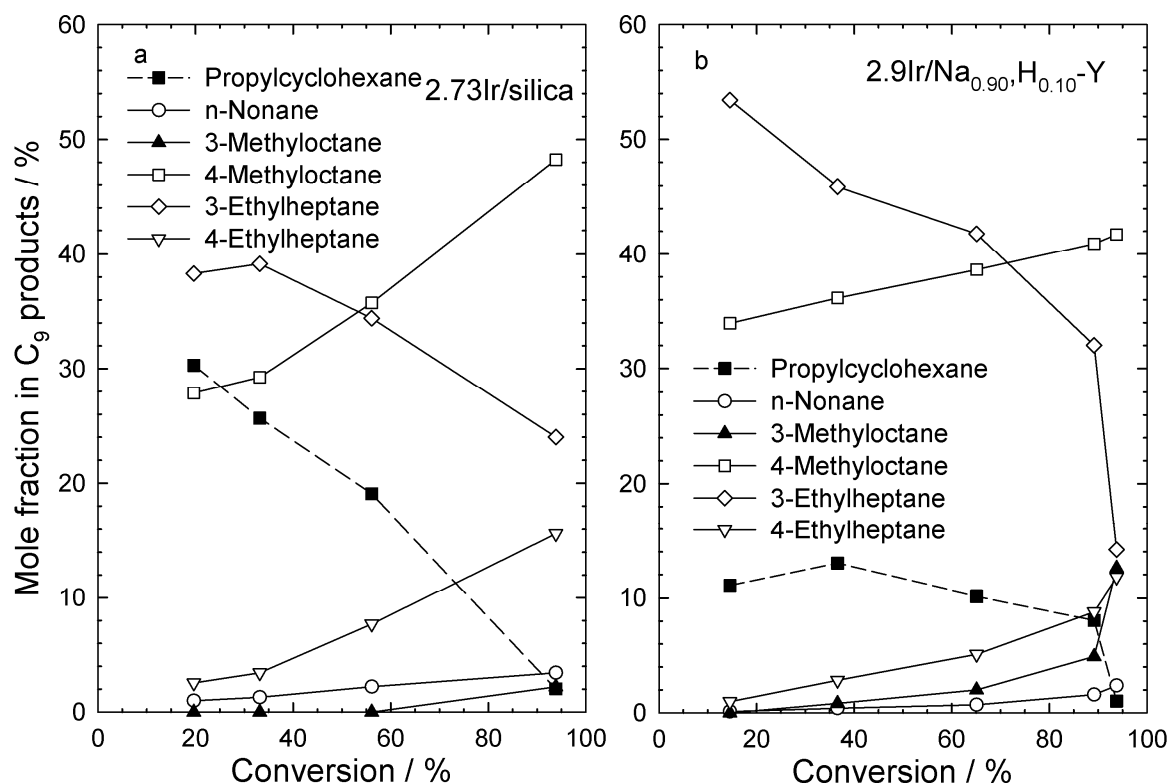


Figure 10.11: Hydroconversion of butylcyclohexane: relative selectivities of the major C_9 hydrocarbons on two iridium catalysts at different conversions.

A detailed analysis of the C_9 products which were formed from butylcyclohexane in high amounts on both iridium catalysts is shown in Figure 10.11. On both catalysts a mole fraction of 94 to 100 % of all C_9 products consisted of propylcyclohexane and the five OCNs n-nonane, 3- and 4-methyloctane and 3- and 4-ethylheptane which can be formed by the reaction scheme presented in Figure 10.12. A smaller mole fraction of these six compounds was only found on $2.9\text{Ir}/\text{Na}_{0.90},\text{H}_{0.10}\text{-Y}$ at the maximal conversion of 94 %.

The reaction network assumes, as the first steps on non-acidic iridium catalysts, the exo- and endocyclic hydrogenolysis to propylcyclohexane plus methane and the three OCDs n-decane, 5-methylnonane and 4-ethyloctane, respectively. Consecutive ring opening of propylcyclohexane furnishes n-nonane (n-No), 4-methyloctane (4-M-Oc) and 4-ethylheptane (4-E-Hp). In addition, the abstraction of methane from the three mentioned OCDs furnishes also 3-ethylheptane. When acid sites are present, butylcyclohexane can also be isomerized *via* bifunctional catalysis to pentylcyclopentane in the first step. Its consecutive ring opening would give n-decane, 4-methylnonane and 3-ethyloctane which can yield four different OCNs after methane abstraction: n-nonane, 3-methyloctane, 4-methyloctane and 3-ethylheptane. From Figure 10.12 it can easily be seen that the formation of 3-methyloctane requires an

isomerization step to pentylcyclopentane prior to the hydrogenolytic steps. This nicely explains the higher amounts of 3-methyloctane on the acidic catalyst 2.9Ir/Na_{0.90}H_{0.10}-Y (see Figure 10.11).

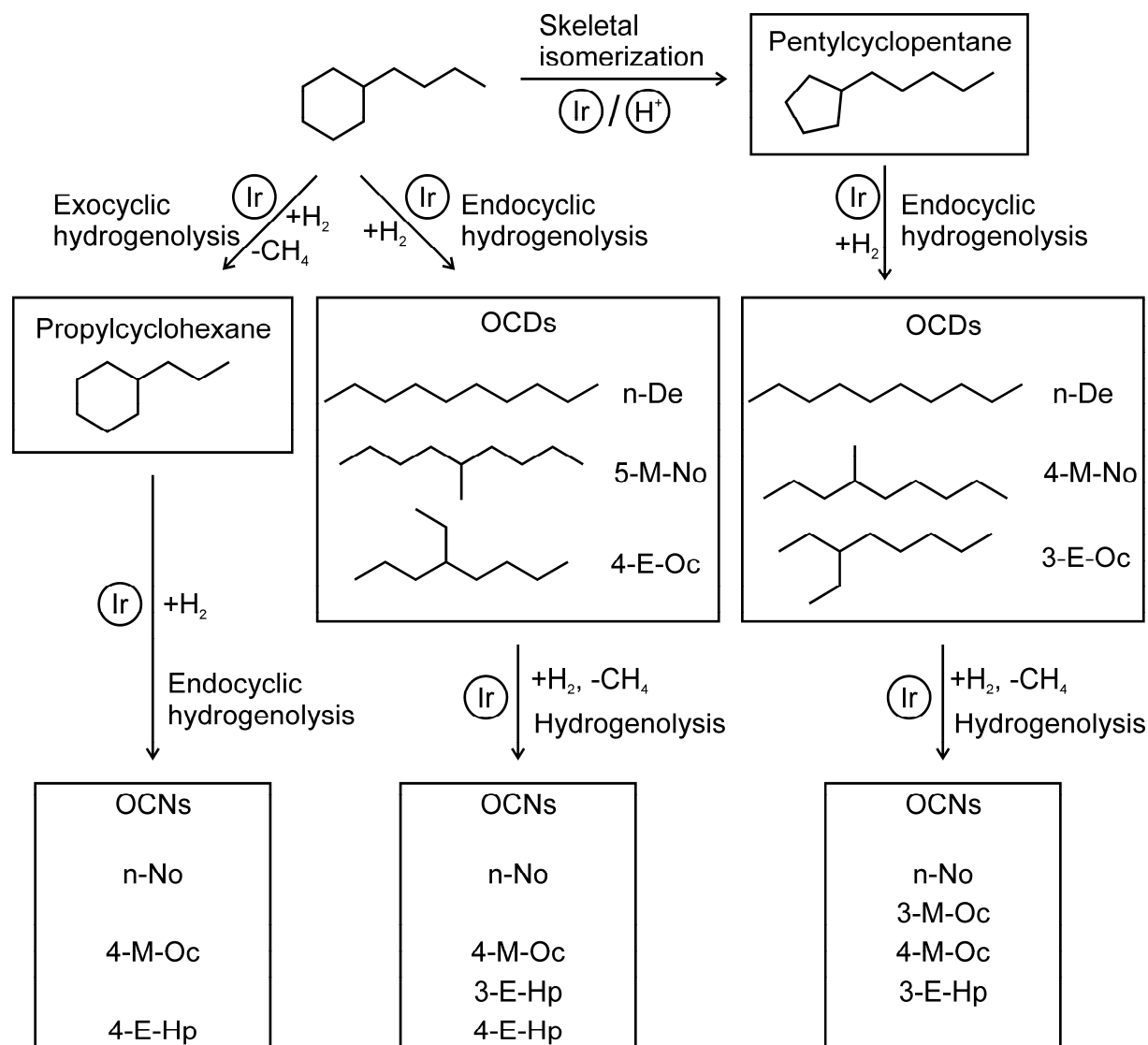


Figure 10.12: Proposed reaction network for the hydroconversion of butylcyclohexane on the iridium catalysts 2.73Ir/silica and the HIPEROc 2.9Ir/Na_{0.90}H_{0.10}-Y.

In Figure 10.13 the distribution of the hydrocracked products at reaction conditions of a maximal $Y_{\text{OGDs}} = 30\%$ is shown for 2.9Ir/Na_{0.90}H_{0.10}-Y. Compared to the curve shape obtained on 2.73Ir/silica (see Figure 9.13, page 104) the values of C₁ and C₉ are much higher and those of C₃ and C₇ are much lower. The increased amount of C₉ products when Brønsted acid sites are present is essentially due to the formation of 4-methyloctane and 3-ethylheptane. Each of them makes up *ca.* 40% of all C₉ products formed. Since the major difference between the reactions on 2.9Ir/Na_{0.90}H_{0.10}-Y and 2.73Ir/silica is the skeletal isomerization capability of the

zeolitic catalyst, the high amounts of C₉ products can only be rationalized by the reaction path *via* pentylcyclopentane (see right part of Figure 10.12).

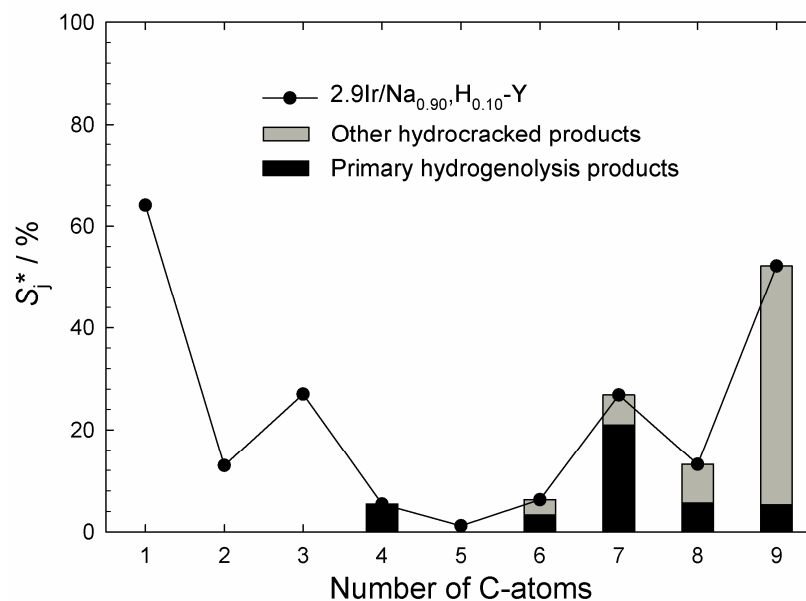


Figure 10.13: Modified hydrocracking selectivities S_j^* on 2.9Ir/Na_{0.90},H_{0.10}-Y in the hydroconversion of butylcyclohexane and fraction of primary hydrogenolysis products:

$T_r = 300\text{ }^\circ\text{C}$; $X_{\text{B-CH}_x} = 65\%$; $Y_{\text{C}_9^-} = 34\%$; $\Sigma S_j^* = 209\%$.

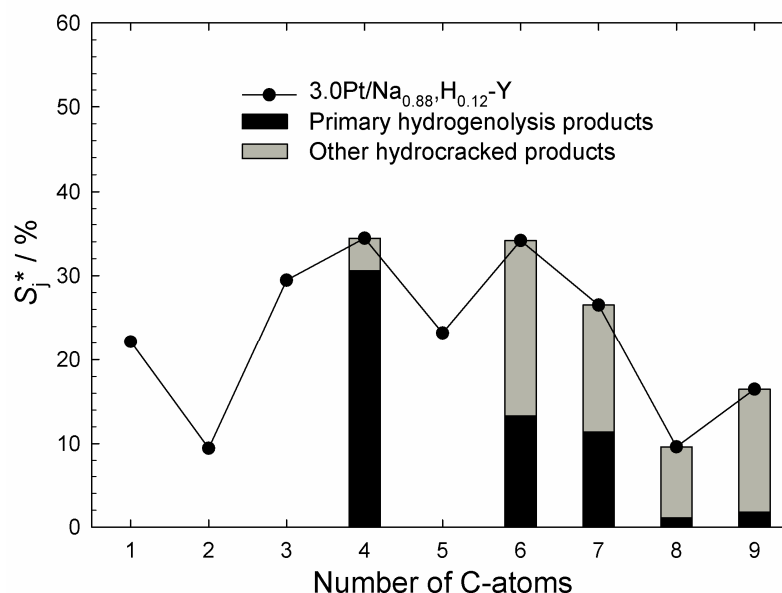


Figure 10.14: Modified hydrocracking selectivities S_j^* on 3.0Pt/Na_{0.88},H_{0.12}-Y in the hydroconversion of butylcyclohexane and fraction of primary hydrogenolysis products:

$T_r = 360\text{ }^\circ\text{C}$; $X_{\text{B-CH}_x} = 98\%$; $Y_{\text{C}_9^-} = 48\%$; $\Sigma S_j^* = 205\%$.

Due to the presence of Brønsted acid sites on 3.0Pt/Na_{0.88}H_{0.12}-Y (see Figure 10.14), significantly smaller amounts of C₃ and C₇ but higher amounts of C₄ and C₆ are formed compared to 2.69Pt/silica (see Figure 9.14, page 105). However, from the fact that the C₄ fraction consists mainly of n-butane, the paring reaction can be safely ruled out as the underlying mechanism. Since the C₆ to C₉ hydrocarbons consist mainly of other products than those of a direct hydrogenolysis and since skeletal isomerization is the prevailing type of reaction at low conversions, isomerization prior to hydrocracking seems to be the origin of the hydrocracked products distribution. A qualitatively similar distribution curve was observed with n-decane as reactant, see Figure 10.4, page 164. Although the compositions of the various C_n fractions differ, the rough similarity demonstrates that a certain fraction of C₉- products seems to stem from hydrocracking of n-decane which is indeed formed on 3.0Pt/Na_{0.88}H_{0.12}-Y with $S_{n-De} / S_{OCDs} = 26 \%$ (see Figure 10.8b, page 169).

On the same catalyst a very similar distribution curve was obtained with decalin as feed hydrocarbon [5]. The similarity indicates that butylcyclohexane is a representative hydrocarbon for the ring-opening intermediates in the decalin hydroconversion on this type of catalyst. Also in the decalin hydroconversion on this catalyst, more n-butane than iso-butane was formed. At $X_{Dec} = 96 \%$ and $Y_{C_9^-} = 33 \%$ a fraction of 59 % of the C₄ products were n-butane with an increasing amount of n-butane in the C₄ fraction with decreasing conversion. In spite of the qualitatively similar hydrocracked products distribution curves with the three C₁₀ reactants n-decane, butylcyclohexane and cis-decalin on 3.0Pt/Na_{0.88}H_{0.12}-Y it is not clear whether this finding is indicative of analogous reaction paths or just a coincidental similarity.

10.2.2 Hydroconversion on a Bifunctional Isomerization Catalyst and a Two-Bed Arrangement with 2.69Pt/Silica

In the hydroconversion of butylcyclohexane, 1.1Pd/Na_{0.93}H_{0.07}-Y (see Figure 10.15a) is a very pronounced isomerization catalyst, as already known from the conversion of n-decane (see Figure 10.2a, page 162). At the lowest conversion, 55 % of the skeletal isomers are pentylcyclopentane with a decreasing fraction of this specific isomer with increasing conversion. Its formation can be explained by a bifunctional isomerization of type A, see Section 4.2.2.1. Also the selectivity of sk-Isos decreases, and S_{OCDs} increases slowly with increasing conversion. Hydrocracking to C₉- becomes substantial at relatively high temperatures of $T_r = 400 \text{ }^\circ\text{C}$ with a selectivity of 17 %

and higher. A maximal OCD selectivity of 14 % is detected at $T_r = 390$ °C. At all temperatures, dehydrogenation to butylbenzene is negligible.

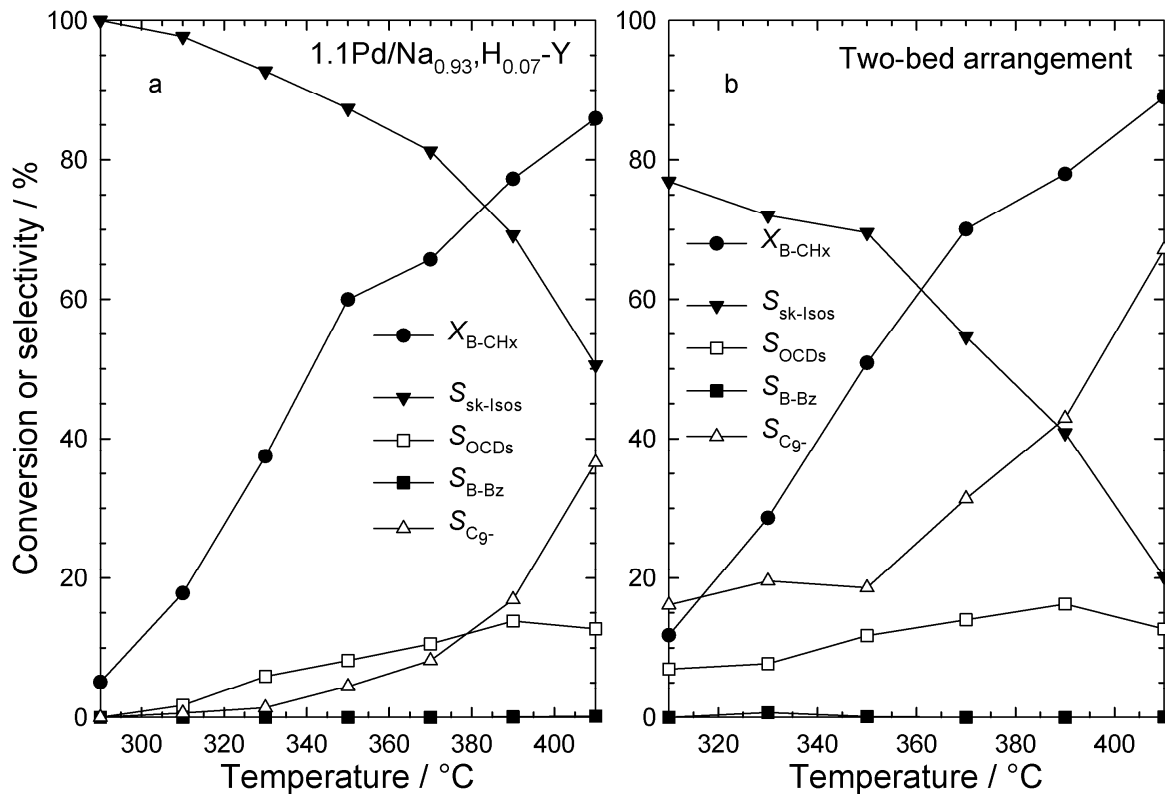


Figure 10.15: Conversion of butylcyclohexane and selectivities of different groups of products at different temperatures on a bifunctional isomerization catalyst and on a two-bed arrangement of catalysts 1.1Pd/Na_{0.93}H_{0.07}-Y and 2.69Pt/silica.

In Figure 10.15b the results of the butylcyclohexane hydroconversion on a two-bed arrangement of catalyst 1.1Pd/Na_{0.93}H_{0.07}-Y in the first bed and catalyst 2.69Pt/silica in the second bed are shown. Compared to the results obtained on the single catalysts (see Figure 10.15a and Figure 9.10b, page 101), intermediate conversions and selectivities are found. It was expected that skeletal isomers of butylcyclohexane, *e.g.* pentylcyclopentane, that are formed on Pd/Na,H-Y are opened readily on Pt/silica by hydrogenolysis. However, the combination of the two catalysts does not increase the maximal yield of OCDs, see Table 10.1, page 168. Presumably, the activities of the catalysts were too similar, resulting in a too small concentration of skeletal isomers that came into contact with the hydrogenolysis catalyst. Perhaps, by combining a more active isomerization catalyst and/or a less active hydrogenolysis catalyst a higher yield of sk-Isos would have been formed in the first bed and subsequently ring-opened by hydrogenolysis.

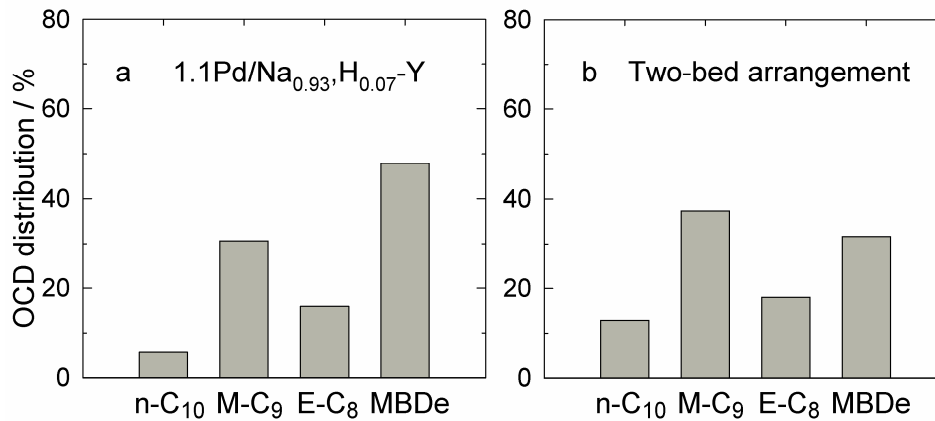


Figure 10.16: Breakdown of the selectivities of OCDs into differently branched decanes formed from butylcyclohexane (a) on the bifunctional isomerization catalyst and (b) on a two-bed arrangement of catalysts 1.1Pd/Na_{0.93},H_{0.07}-Y and 2.69Pt/silica:

1.1Pd/Na_{0.93},H_{0.07}-Y: $T_r = 410\text{ }^\circ\text{C}$; $X_{\text{B-CH}_x} = 86\%$; $Y_{\text{OCDs}} = 11\%$; $S_{\text{OCDs}} = 13\%$.
 Two-bed: $T_r = 390\text{ }^\circ\text{C}$; $X_{\text{B-CH}_x} = 78\%$; $Y_{\text{OCDs}} = 13\%$; $S_{\text{OCDs}} = 16\%$.

On 1.1Pd/Na_{0.93},H_{0.07}-Y rather multiply branched decanes are formed (see Figure 10.16a) Also on the two-bed arrangement (see Figure 10.16b) a relatively high degree of branching in the OCDs is found. This distribution seems to be a superposition of the results obtained in the experiments with the single catalysts (see Figure 10.16a and Figure 9.12b, page 103).

On 1.1Pd/Na_{0.93},H_{0.07}-Y the distribution curve of the hydrocracked products is “M-shaped” and nearly symmetrical (see Figure 10.17). It is unknown, why higher molar amounts of C₉ than of methane are formed. This peculiarity was also found in the hydroconversion of decalin, for example on several bifunctional palladium catalysts [96]. Since the C₉ fraction consists of several products of roughly similar amounts, a single erroneous peak assignment in the gas chromatogram cannot be the reason. Perhaps, cationic disproportionation-type side reactions occurred as observed also in the hydroconversion of different naphthenes on bifunctional catalysts [58, 97].

In Figure 10.17 also the amount of the paring reaction products iso-butane and methylcyclopentane in the C₄ and C₆ fraction, respectively, are shown. Due to the fact that 68 % of the C₄ fraction consists of iso-butane and 42 % of the C₆ fraction of methylcyclopentane, a major reaction path for the formation of C₄ and C₆ hydrocarbons appears to be the paring reaction (see Section 4.2.2.3). Nevertheless, since 18 % of the C₆ fraction consist of cyclohexane and the remaining 32 % of the C₄ products are n-butane, also the β -scission of a butylcyclohexyl cation could play a role. No hydrogenolysis seems to be responsible for the formation of n-butane and

cyclohexane since virtually no methane, an indicator for hydrogenolysis on palladium (see Figure 9.19, page 113), is formed.

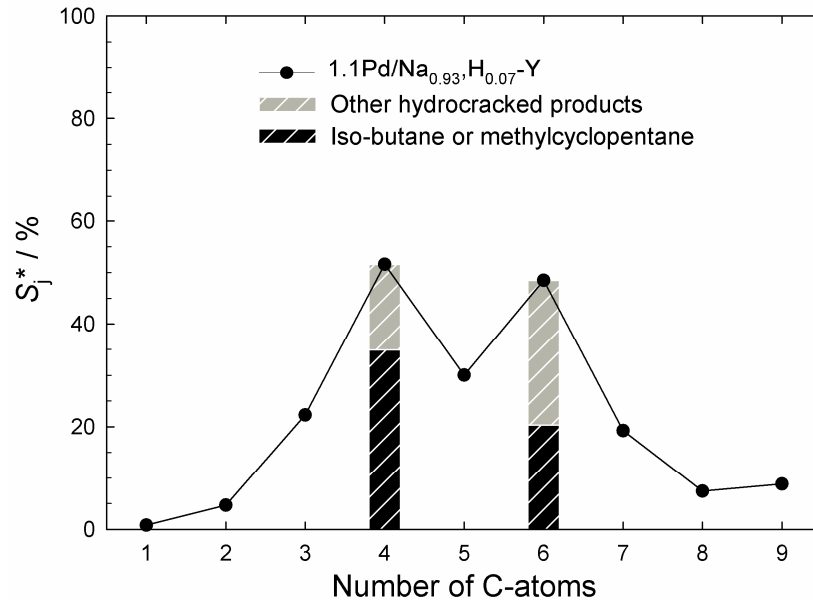


Figure 10.17: Modified hydrocracking selectivities S_j^* on 1.1Pd/Na_{0.93},H_{0.07}-Y in the hydroconversion of butylcyclohexane and fraction of iso-butane and methylcyclopentane:

$$T_r = 410 \text{ }^\circ\text{C}; X_{\text{B-CH}_x} = 86 \text{ } \%; Y_{\text{C}_0^-} = 31 \text{ } \%; \sum S_j^* = 193 \text{ } \%.$$

To understand the formation of n-butane and cyclohexane, a short mechanistic interpretation will be given. The formation of primary carbenium ions is strongly hindered due to their high energy content. Primary carbenium ions as products of the β -scission of butylcyclohexyl cations can be avoided, if the positive charge is assumed to be located at one of two positions shown in Figure 10.18. In both cases the β -scissions that occur are of the relatively slow type C [53], and they are expected to lead to cyclohexane and n-butane or n-decane as products. Presumably, due to the strong isomerization activity of this catalyst, n-decane is isomerized to branched decanes, in agreement with the finding that n-decane occurs in the product mixture only in small amounts (see Figure 10.16).

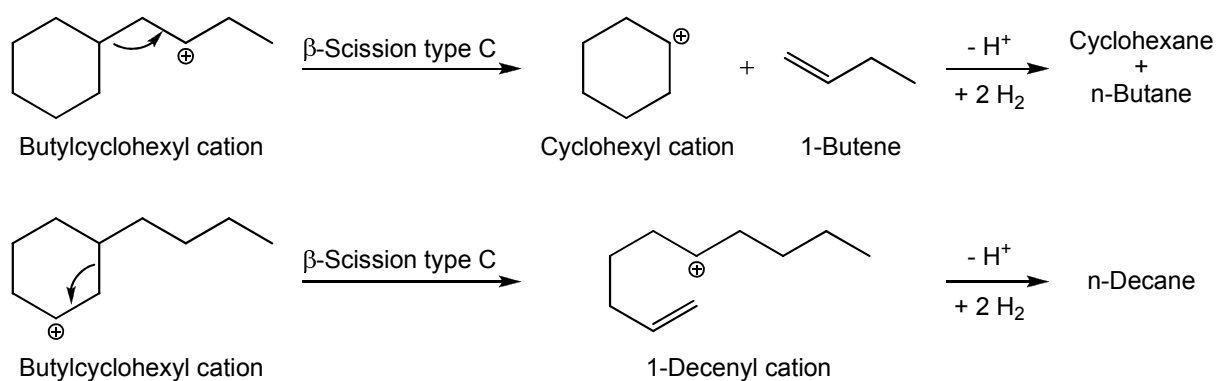


Figure 10.18: Secondary butylcyclohexyl cations and products of their β -scission without forming primary carbocations.

The carbon number distribution of the hydrocracked products on the two-bed arrangement with the Pd/Y and Pt/silica catalysts (not shown) is a mixture of the distribution curves obtained with the single catalysts. Hence, it seems that in both catalyst beds mainly butylcyclohexane was converted into C_9 - products. If mainly sk-Isos which were formed on the zeolite catalyst would have undergone hydrogenolysis on Pt/silica rather a different curve type was expected which is not a superimposition of those obtained on the single catalysts.

10.3 Perhydroindan

In the hydroconversion of perhydroindan on the non-acidic catalyst 0.60Pd/silica it turned out that palladium is almost inactive in the hydrogenolysis of C-C bonds, the main reaction was dehydrogenation (see Figure 9.16c, page 109). To investigate if bifunctional catalysis allows the opening of a five-membered ring when the paring reaction [3, 57, 58], which requires a hydrocarbon with at least 10 carbon atoms, is not possible, perhydroindan is hydroconverted on 1.0Pd/Na_{0.70}H_{0.30}-[Al]Beta-14.0. This bifunctional catalyst combines a noble metal which is virtually inactive in hydrogenolysis with an acidic zeolite support. Due to its higher n_{Si} / n_{Al} ratio of 14 compared to a ratio of 2.4 in zeolite Y it is expected to contain Brønsted acid sites of higher strength which are expected to result in a higher hydrocracking activity [96].

The presence of Brønsted acid sites on catalyst 1.0Pd/Na_{0.70}H_{0.30}-[Al]Beta-14.0 leads to a very strong increase of activity (see Figure 10.19) compared to 0.60Pd/silica (see Figure 9.16c, page 109). Similar conversions were attained at *ca.* 150 °C higher temperatures on Pd/silica. At conversions from 13 to 90 % the mole fraction of cis-perhydroindan assumed values of 50 to 51 % compared to values in the range of 47 to

61 % on different noble metal/silica catalysts. As discussed in Section 9.4, this stereoisomerization occurs most likely on the noble metal.

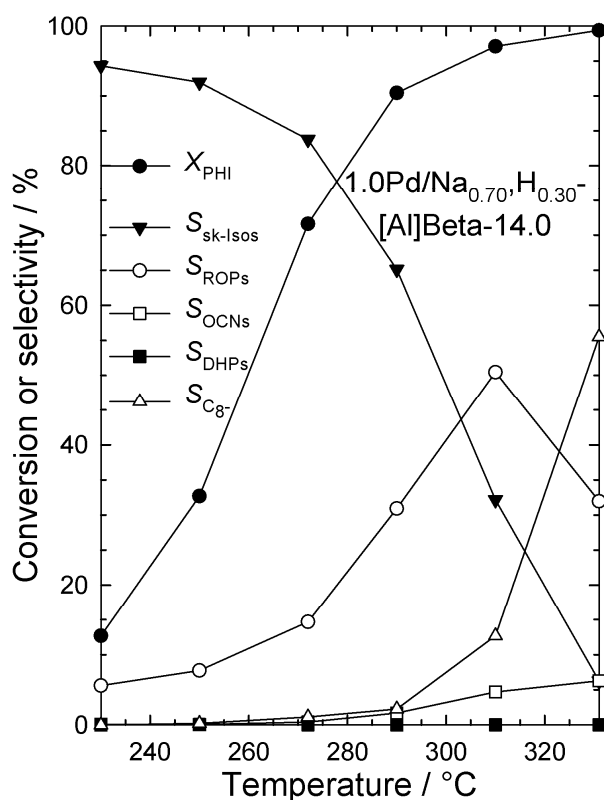


Figure 10.19: Conversion of perhydroindan and selectivities of different groups of products at different temperatures on the bifunctional catalyst 1.0Pd/Na_{0.70},H_{0.30}-[Al]Beta-14.0.

The selectivity pattern differs substantially from those of the two HIPEROcs [67] and from that of Pd/silica (see Figure 9.16c, page 109): Skeletal isomers of perhydroindan strongly dominate at low to moderate conversion, and the selectivity of open-chain nonanes is very low throughout. Since Pd/silica did not show any isomerization activity at these reaction temperatures, a bifunctional mechanism must be invoked for the extremely selective formation of skeletal isomers at low to moderate conversions. Indeed, even though the concentration of Brønsted acid sites on Pd/Na,H-Beta is not high, these sites are relatively strong as indicated by FT-IR measurements with pyridine as probe molecule [67].

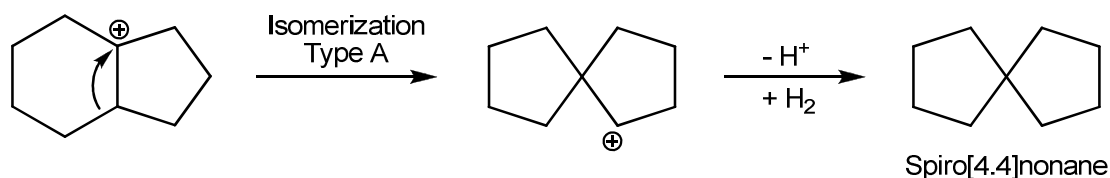


Figure 10.20: Cationic type A isomerization of perhydroindan.

If the reasonable assumption is made that, because of their high ring strain, no four-membered naphthenic rings are formed, then a single product of cationic type A isomerization of perhydroindan is expected, namely spiro[4.4]nonane (see Figure 10.20). In fact, if decalin is used as reactant and if the catalyst contains Brønsted acid sites, the analogous product spiro[4.5]decane does form at low conversions, as shown recently [52]. Hence, an attempt was made to find out whether spiro[4.4]nonane occurred as a primary product of perhydroindan conversion. On Pd/Na,H-Beta and Pt/Na,H-Y two skeletal isomers ($M = 124 \text{ g} \cdot \text{mol}^{-1}$) were indeed formed at low conversions with combined selectivities of up to 67 % which were eluted from the capillary column in the range of retention times which was considered to be consistent with the published boiling point of spiro[4.4]nonane (156 to 157 °C [98, 99]). A section of the gas chromatogram obtained at $T_r = 230 \text{ °C}$ is given in Figure 10.21.

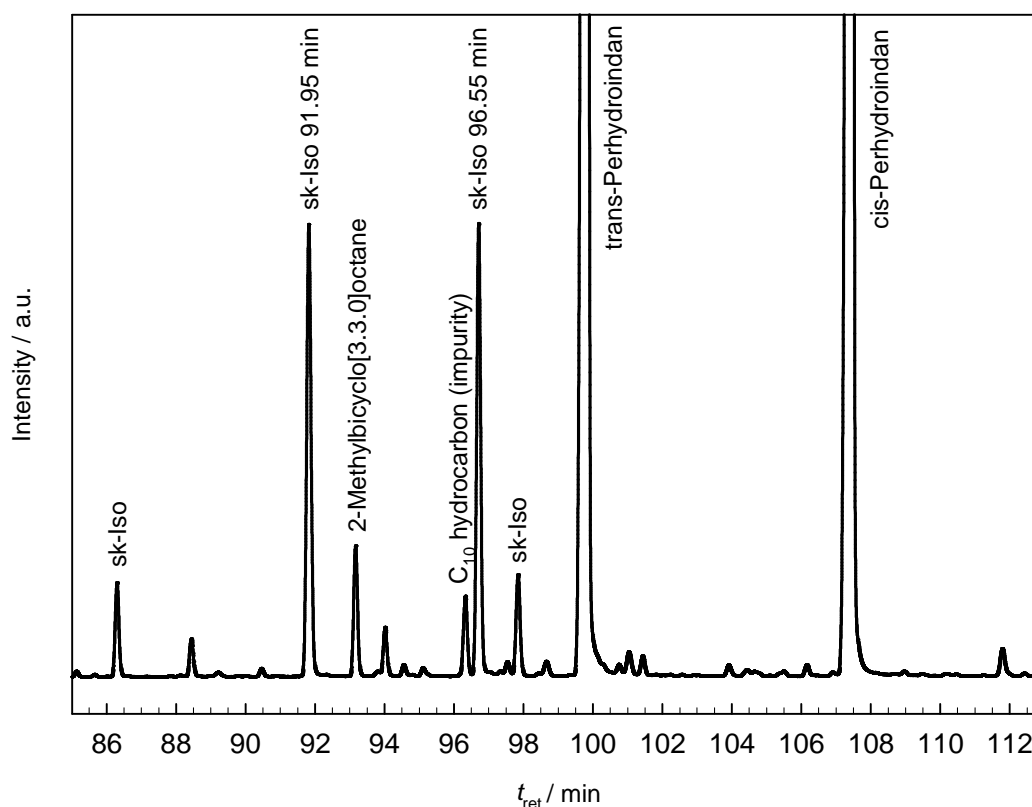


Figure 10.21: Gas chromatogram of the products obtained in the hydroconversion of perhydroindan on 1.0Pd/Na_{0.70}H_{0.30}-[Al]Beta-14.0 at $T_r = 230 \text{ °C}$.

As another piece of information, the two sk-Isos in question were not formed to a significant extent on the non-acidic silica-supported catalysts. Finally, the selectivities of the two sk-Isos *vs.* the perhydroindan conversion are plotted and compared to the results with the analogous plot of $S_{\text{spiro}[4.5]\text{decane}}$ against X_{Dec} for decalin conversion on the same catalysts [74, 100,] (see Figure 10.22). For one of the two unidentified sk-Isos, namely the one which appears in the chromatogram of perhydroindan conversion at $t_{\text{ret}} = 96.55$ min, the selectivity plot against X_{PHI} strongly resembles the one for $S_{\text{spiro}[4.5]\text{decane}}$ versus X_{Dec} . A conclusion is, even though the assignment of the peak in question is not safe, that evidence exists for spiro[4.4]nonane being formed from perhydroindan along a cationic reaction path, if the catalyst contains Brønsted acid sites.

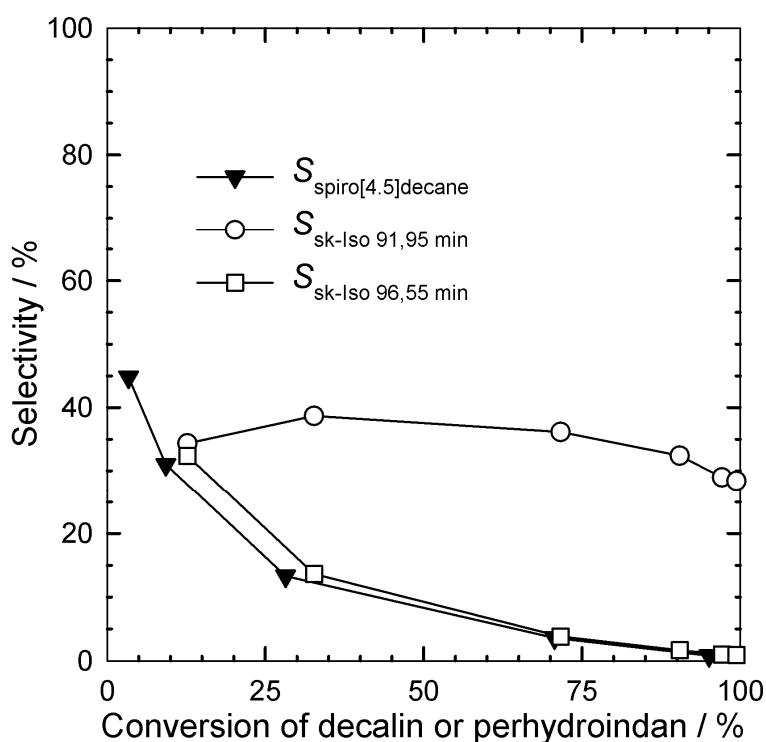


Figure 10.22: Selectivities of spiro[4.5]decane in the conversion of decalin and of two sk-Isos that were formed in the conversion of perhydroindan on 1.0Pd/Na_{0.70}H_{0.30}-[Al]Beta-14.0.

Most ring-opening products that are formed on 1.0Pd/Na_{0.70}H_{0.30}-[Al]Beta-14.0 are substituted cyclohexanes (CH_x-ROPs), see Figure 10.23. At low conversions (1-methylethyl)cyclohexane is the major ROP with $S / S_{\text{ROPs}} = 59\%$ at $T_r = 230\text{ }^\circ\text{C}$. Most likely, this product is formed by ring opening of a skeletal isomer and not by isomerization of the ROP propylcyclohexane, since on 0.60Pd/silica no ring opening occurs at such low temperatures (see Figure 9.16c, page 109). Unfortunately, the major

skeletal isomers were identified by GC/MS due to their molecular ion signal of $m/z = 124$ only. Hence, no reaction pathway for the formation of ROPs can be drawn.

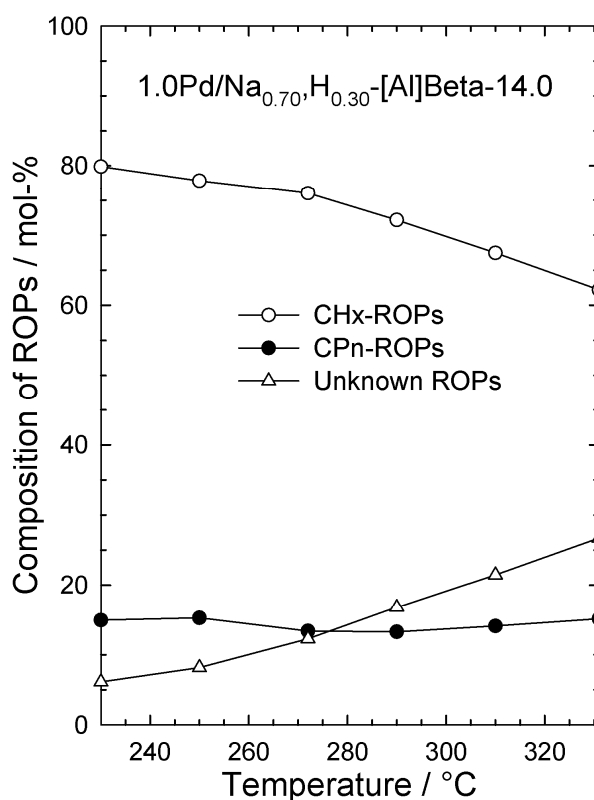


Figure 10.23: Breakdown of the ring-opening products into ROPs with a remaining six-membered ring (CHx-ROPs), with a remaining five-membered ring (CPn-ROPs) and into ROPs that have been identified by the molar mass of $M = 126 \text{ g}\cdot\text{mol}^{-1}$ only (unknown ROPs) in the hydroconversion of perhydroindan.

With increasing temperature the total amount of ROPs increases but the fraction of CHx-ROPs decreases. This is due to the formation of unknown ROPs which are probably substituted cyclopentanes since the larger number of carbon atoms in the alkyl side-chains allows a larger variety of skeletal isomers and renders peak assignment by GC/MS difficult. No aromatic ROPs were formed.

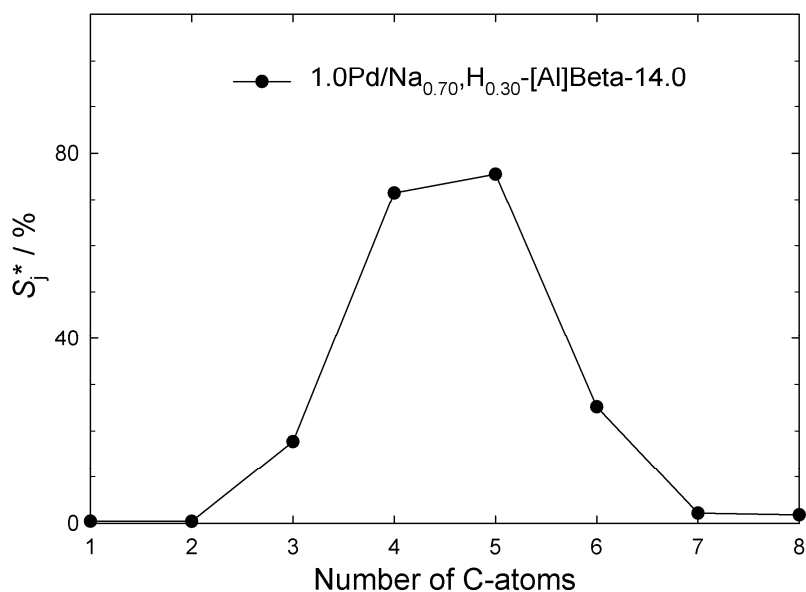


Figure 10.24: Modified hydrocracking selectivities S_j^* on 1.0Pd/Na_{0.70},H_{0.30}-[Al]Beta-14.0 in the hydroconversion of perhydroindan:
 $T_r = 331\text{ }^\circ\text{C}$; $X_{\text{PHI}} = 99\%$; $Y_{\text{C}_8^-} = 55\%$; $\Sigma S_j^* = 195\%$.

In comparison to results on the non-acidic catalysts (see Figure 9.19, page 113) or the HIPEROCS [67] a principally different distribution curve results for hydrocracking of perhydroindan on Pd/Na,H-Beta (see Figure 10.24): This curve is volcano-shaped with no C₁ and C₂ and very little C₇ and C₈. Mainly C₄ and C₅ moieties are formed, besides C₃ and C₆ hydrocarbons occur to a much lesser extent. The C₄ fraction consists of n-butane (22 mol-%) and iso-butane (78 mol-%), the C₅ fraction of n-pentane (27 mol-%), 2-methylbutane (55 mol-%), and cyclopentane (18 mol-%), and the C₆ fraction of n-hexane (11 mol-%), methylpentanes (28 mol-%), 2,2-dimethylbutane (2 mol-%), methylcyclopentane (49 mol-%), and cyclohexane (10 mol-%). Very similar product distributions have been reported for hydrocracking of one-ring naphthenes with nine carbon atoms, such as 1,2,4-trimethylcyclohexane [58] or propylcyclohexane [97] on bifunctional catalysts like NiS/silica-alumina or Pd/La-Y, respectively. Even the slight asymmetry of the distribution curve with $S_{\text{C}_5} > S_{\text{C}_4}$, $S_{\text{C}_6} > S_{\text{C}_3}$ and some small amounts of C₇ and C₈ were observed in these prior studies with bifunctional catalysts [58, 97] and attributed to the occurrence of cationic disproportionation-type side reactions. It is also noteworthy that the product distributions observed on Pd/Na,H-Y, especially the relatively large amounts of C₅ and C₆ naphthenes, are not consistent with a bifunctional hydrocracking mechanism starting from open-chain nonanes [48, 83]. Rather, hydrocracking of C₉ one-ring naphthenes seems to be the main reaction path.

10.4 Spiro[4.5]decane

The isomerization of spiro[4.5]decane was studied on 1.0Pd/Na_{0.93}H_{0.07}-Y. Conversion and selectivities are shown in Table 10.3. At both reaction temperatures, isomerization is essentially the only reaction with selectivities of 96 and 99 %.

Table 10.3: Conversion of spiro[4.5]decane and selectivities of different groups of products on catalyst 1.0Pd/Na_{0.93}H_{0.07}-Y at different temperatures.

$T_r / ^\circ\text{C}$	$X_{\text{spiro}} / \%$	$S_{\text{sk-Isos}} / \%$	$S_{\text{ROPs}} / \%$	$S_{\text{OCDs}} / \%$	$S_{\text{C}_9} / \%$
240	9.0	96	4.0	0.0	0.2
300	64	99	1.0	0.1	0.0

The skeletal isomers formed on 1.0Pd/Na_{0.93}H_{0.07}-Y (see Table 10.4) are, like on 2.69Pt/silica (see Table 9.11, page 139), composed mainly of decalin. Moreover, an analogous distribution of all sk-Isos at similar conversions is obtained, and the range of $n_{\text{tr-Dec}} / (n_{\text{tr-Dec}} + n_{\text{c-Dec}}) = 0.86$ to 0.88 is identical.

Table 10.4: Composition of skeletal isomers on catalyst 1.0Pd/Na_{0.93}H_{0.07}-Y at different temperatures.

$T_r / ^\circ\text{C}$	$X_{\text{spiro}} / \%$	$S_{\text{sk-Isos}} / \%$	$S_{\text{Dec}} / S_{\text{sk-Isos}} / \%$	$S_{\text{bicyclo[5.3.0]decane}} / S_{\text{sk-Isos}} / \%$	$S_{\text{bicyclopentyl}} / S_{\text{sk-Isos}} / \%$	$S_{\text{other sk-Isos}} / S_{\text{sk-Isos}} / \%$
240	9.0	96	88	11	0.6	0.3
300	64	99	92	1.0	0.8	6.4

To find an explanation for this similarity, the relevant knowledge so far acquired with both catalysts will be summarized: On Pt/silica pure metal catalysis takes place, as demonstrated for example in the test reaction with n-octane (see Section 8). On 1.0Pd/Na_{0.93}H_{0.07}-Y metal catalysis and bifunctional catalysis can occur, since in the hydroconversion of decalin on a similar Pd/Na,H-Y catalyst [96], a superimposition of hydrogenolysis (methane and C₉ formation) and the paring reaction (high amounts of C₄ and C₆) were observed. However, in the hydroconversion of perhydroindan on 0.60Pd/silica (Figure 9.16c, page 109) it was demonstrated that palladium on a non-acidic support is essentially only a dehydrogenation catalyst with a negligible isomerization activity. Hence, it seems unlikely that on a Pd/Na,H-Y catalyst skeletal isomerization occurs by pure metal catalysis.

Therefore, an alternative explanation could be given: The products obtained by applying a cyclic (see Figure 9.41, page 140) or a bond-shift mechanism (see Figure 9.40, page 140) can, theoretically, furnish similar products as bifunctional isomerization of type A *via* carbocations (see Figure 10.25).

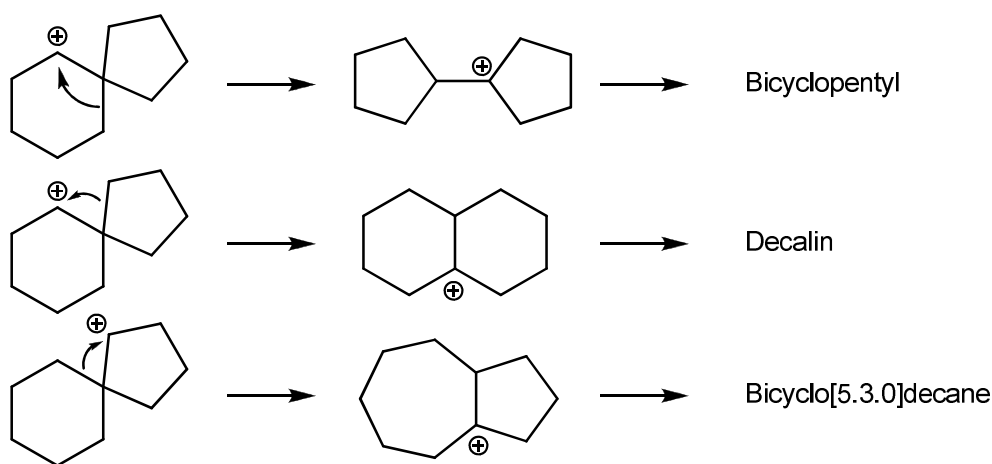


Figure 10.25: Carbocationic isomerization mechanisms of type A for the carbocations derived from spiro[4.5]decane.

The catalytic results obtained on the high-performance ring-opening catalyst 3.3Ir/H_{0.58},Cs_{0.42}-[Al]Beta-14.0 are presented in Table 10.5. A comparable conversion of *ca.* 80 % is obtained on a similar catalyst with decalin as reactant at a *ca.* 45 °C higher temperature [96], demonstrating the higher reactivity of spiro[4.5]decane. This zeolitic catalyst is also more active than 2.73Ir/silica in the spiro[4.5]decane conversion (see Table 9.8, page 135).

Table 10.5: Conversion of spiro[4.5]decane and selectivities of different groups of products on catalyst 3.3Ir/H_{0.58},Cs_{0.42}-[Al]Beta-14.0 at different temperatures.

$T_r / ^\circ\text{C}$	$X_{\text{spiro}} / \%$	$S_{\text{sk-Isos}} / \%$	$S_{\text{ROPs}} / \%$	$S_{\text{OCDs}} / \%$	$S_{\text{C}_9} / \%$
200	82	33	67	0.7	0.1
283	100	3.1	3.2	19	75

93 % of all ROPs are 1-methyl-1-propylcyclohexane and 1,1-diethylcyclohexane, at the lower conversion of $X_{\text{spiro}} = 82 \%$ on 3.3Ir/H_{0.58},Cs_{0.42}-[Al]Beta-14.0. At the same conversion also sk-Isos are formed with $S_{\text{sk-Isos}} = 33 \%$ which can only be generated *via* carbocationic mechanisms since iridium is not active in isomerization. However, as indicated by the high amounts of the two 1,1-disubstituted ROPs formed, the main reaction pathway is the hydrogenolysis of the five-membered ring in spiro[4.5]decane

rather than the hydrogenolysis of sk-Isos. At $T_r = 283\text{ °C}$ most hydrocarbons are hydrocracked to C_9 - products ($S_{C_9} = 75\%$) and OCDs are formed with $S_{OCDs} = 19\%$, hence the maximal OCD selectivity would probably lie between $T_r = 200$ and 283 °C . As expected by the selective ring-opening mechanism that is operative on iridium, most OCDs are highly branched, see Figure 10.26.

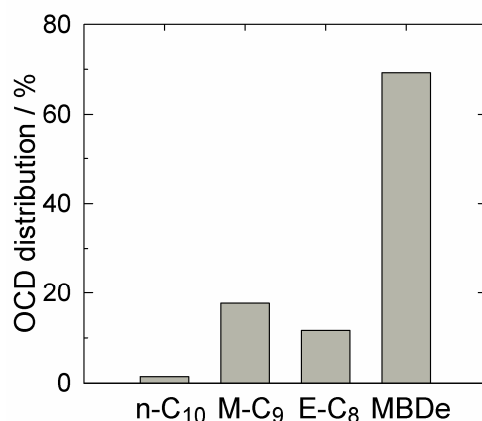


Figure 10.26: Breakdown of the selectivities of OCDs into differently branched decanes on 3.3Ir/H_{0.58},Cs_{0.42}-[Al]Beta-14.0:

$T_r = 283\text{ °C}$; $X_{\text{spiro}} = 100\%$; $Y_{\text{OCDs}} = 19\%$; $S_{\text{OCDs}} = 19\%$.

On the HIPEROc 3.3Pt/Na_{0.85},H_{0.15}-Y, spiro[4.5]decane is more reactive (see Table 10.6) than decalin on the similar HIPEROc 3.0Pt/Na_{0.88},H_{0.12}-Y [5]. With spiro[4.5]decane as reactant, skeletal isomerization is the main reaction at all temperatures and at the highest conversion of $X_{\text{spiro}} = 94\%$, skeletal isomers are formed with $S_{\text{sk-Isos}} = 84\%$. With decalin as reactant and at a similar conversion (achieved at a reaction temperature which is about 40 °C higher), skeletal isomers of decalin are almost completely consumed by hydrocracking [5].

Table 10.6: Conversion of spiro[4.5]decane and selectivities of different groups of products on catalyst 3.3Pt/Na_{0.85},H_{0.15}-Y at different temperatures.

$T_r / \text{°C}$	$X_{\text{spiro}} / \%$	$S_{\text{sk-Isos}} / \%$	$S_{\text{ROPs}} / \%$	$S_{\text{OCDs}} / \%$	$S_{C_9} / \%$
240	17	95	5.1	0.0	0.1
280	85	96	4.3	0.0	0.1
320	94	84	11	3.2	1.0

Again, the skeletal isomers consist largely of decalin, see Table 10.7, and the composition of the other isomers resembles that obtained with 2.69Pt/silica (see Table 9.11, page 139) and 1.0Pd/Na_{0.93},H_{0.07}-Y (see Table 10.4). The high reactivity of

spiro[4.5]decane in the isomerization to decalin and the similarity of the composition of the skeletal isomers on different catalysts lead to the following assumption: The ring-opening reactions could be preceded by an isomerization of the reactant decalin or spiro[4.5]decane on 3.3Pt/Na_{0.85}H_{0.15}-Y to a similar mixture of two-ring naphthenes which are subsequently ring-opened to a comparable extent. Indeed, the yields of ROPs and OCDs on the similar catalysts 3.3Pt/Na_{0.85}H_{0.15}-Y (see Table 10.6) and 3.0Pt/Na_{0.88}H_{0.12}-Y [5] with spiro[4.5]decane and cis-decalin, respectively, as reactants are similar: With spiro[4.5]decane $Y_{\text{ROPs}} = 11\%$ and $Y_{\text{OCDs}} = 3.0\%$ at $T_r = 320\text{ }^\circ\text{C}$. In the case of decalin and when the values obtained at $T_r = 309$ and $330\text{ }^\circ\text{C}$ are interpolated to $T_r = 320\text{ }^\circ\text{C}$, $Y_{\text{ROPs}} = 12\%$ and $Y_{\text{OCDs}} = 3.5\%$ are reached.

Table 10.7: Composition of skeletal isomers on catalyst 3.3Pt/Na_{0.85}H_{0.15}-Y at different temperatures.

T_r / $^\circ\text{C}$	X_{spiro} / $\%$	$S_{\text{sk-Isos}}$ / $\%$	S_{Dec} / $S_{\text{sk-Isos}}$ / $\%$	$S_{\text{bicyclo[5.3.0]decane}}$ / $S_{\text{sk-Isos}}$ / $\%$	$S_{\text{bicyclopentyl}}$ / $S_{\text{sk-Isos}}$ / $\%$	$S_{\text{other sk-Isos}}$ / $S_{\text{sk-Isos}}$ / $\%$
240	17	95	91	7.6	0.8	0.5
280	85	96	98	0.4	0.4	1.4
320	94	84	87	0.3	0.7	12

Only for 3.3Ir/H_{0.58}Cs_{0.42}-[Al]Beta-14.0 the yield of C₉- was high enough to plot a distribution curve of the hydrocracked products, see Figure 10.27. The curve is shaped very similar to that obtained with 3.4Ir/H_{0.58}Cs_{0.42}-[Al]Beta-14.0 and decalin as reactant [96]. Indeed, spiro[4.5]decane was formed in the ring opening of decalin on this type of catalyst. However, spiro[4.5]decane was also formed in the decalin conversion on the HIPEROX 2.9Ir/Na_{0.90}H_{0.10}-Y, but with this catalyst the distribution curve of the hydrocracked products resembles the hammock-type as in the decalin conversion [5]. Such a distribution observed in the hydroconversion of decalin can be explained with a strong contribution of hydrogenolysis on iridium (see Section 9.5.2). Also in the pure hydrogenolysis of spiro[4.5]decane on Ir/silica (see Figure 9.42, page 142) a similar curve type was observed.

Hence, on this Beta zeolite catalyst a different kind of reaction network seems to prevail. By carbocationic hydrocracking of C₁₀ ROPs *via* the paring reaction an M-shape with maxima at C₄ and C₆ is expected, see Figure 10.17, page 180. Bifunctional hydrocracking of OCDs would result in a volcano-shaped curve with much C₄ to C₆, see Figure 10.5, page 164. Consequently, hydrocracking of ROPs and OCDs could be the underlying mechanism for the formation of C₄ to C₆ products which is superimposed by hydrogenolysis as indicated by the formation of methane and ethane.

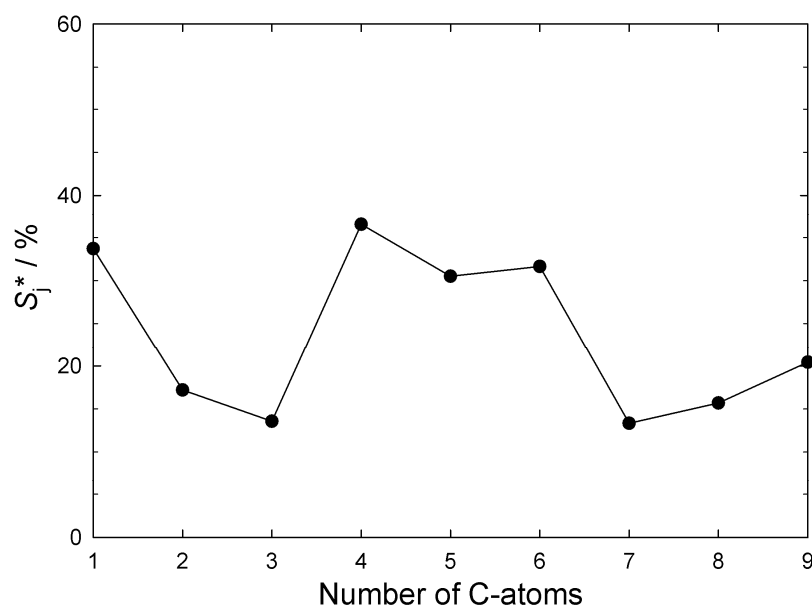


Figure 10.27: Modified hydrocracking selectivities S_j^* on 3.3Ir/H_{0.58},Cs_{0.42}-[Al]Beta-14.0 in the hydroconversion of spiro[4.5]decane:
 $T_r = 283 \text{ }^\circ\text{C}$; $X_{\text{spiro}} = 100 \%$; $Y_{\text{C}_9} = 75 \%$; $\Sigma S_j^* = 213 \%$.

10.5 Conclusions

On the zeolite-Y-based HIPEROCS Ir/Na,H-Y and Pt/Na,H-Y the cleavage of C-C bonds occurs almost exclusively by hydrogenolysis on the respective noble metal. In case of the platinum-containing HIPEROCS OCDs are formed in much higher yields from butylcyclohexane than on Pt/silica. A detailed examination of the products revealed that the main reason is the isomerization to pentylcyclopentane, the ring of which can be readily opened by hydrogenolysis on the noble metal. Also on Ir/Na,H-Y this reaction sequence occurs but, with butylcyclohexane as reactant, this does not lead to an increase of the OCD yield in comparison with Ir/silica. Most probably this is due to the relatively fast endocyclic hydrogenolysis of six-membered rings on iridium, whereas platinum-containing catalysts require an isomerization function to form five-membered ones as precursors for a fast ring opening on platinum

On the typical bifunctional catalysts 1.1Pd/Na_{0.93},H_{0.07}-Y and 1.0Pd/Na_{0.70},H_{0.30}-[Al]Beta-14.0 the main products were skeletal isomers and with increasing temperature hydrocracking occurred. With n-decane or butylcyclohexane a volcano-shaped or M-shaped distribution curve, respectively, was obtained. In the hydroconversion of perhydroindan large amounts of C₄ and C₅ hydrocarbons were formed as also found by others. This indicates that on these catalysts the main role of

the noble metal is to enable the interconversion of olefinic and aliphatic hydrocarbons and that hydrocracking occurs mainly *via* carbocations on the acid sites. Ring opening of butylcyclohexane and perhydroindan occurred to a certain extent on these palladium-containing acidic catalysts. Hence, it seems that also by bifunctional hydrocracking the cleavage of endocyclic C-C bonds is possible, since Pd/silica is virtually inactive in hydrogenolysis (see Section 9.4).

By converting spiro[4.5]decane it was demonstrated that bifunctional isomerization can furnish a similar mixture of skeletal isomers as pure metal catalysis on Pt/silica. Moreover, hints were obtained that on the zeolite-Y-based HIPEROC Pt/Na,H-Y ring opening starts from a similar mixture of skeletal isomers as in the hydroconversion of decalin on this catalyst. On the HIPEROC 3.3Ir/H_{0.58},Cs_{0.42}-[Al]Beta-14.0 a similar distribution of hydrocracked products is obtained with spiro[4.5]decane as in the hydroconversion of decalin [96]. This demonstrates that on both HIPEROCs this spiro compound is probably an important intermediate.

For experiments with a two-bed arrangement for studying the hydrogenolysis of a mixture of skeletal isomers a good adjustment of the catalyst activities has to be performed. In the hydroconversion of n-decane and butylcyclohexane on two-bed arrangements of 1.1Pd/Na_{0.93},H_{0.07}-Y in the first and 2.69Pt/silica in the second catalyst bed the $Y_{sk-Isos}$ on the zeolitic catalyst was too low. Hence, a large fraction of unconverted reactant was converted on the non-acidic metal catalyst in the second bed, resulting in an intermediate catalytic behavior related to the single catalysts.

11 References

- [1] International Energy Outlook 2010, U.S. Energy Information Administration.
- [2] DIN EN 590:2009+A1:2010, "Kraftstoffe für Kraftfahrzeuge – Dieselkraftstoff – Anforderung und Prüfverfahren".
- [3] J. Weitkamp, in: "Handbook of Heterogeneous Catalysis", 2nd Edn., G. Ertl, H. Knözinger, F. Schüth, J. Weitkamp (Eds.), Vol. 7, Wiley-VCH, Weinheim, 2008, p. 3133-3152.
- [4] G.B. McVicker, M. Daage, M.S. Touvelle, C.W. Hudson, D.P. Klein, W.C. Baird, Jr., B.R. Cook, J.G. Chen, S. Hantzer, D.E.W. Vaughan, E.S. Ellis, O.C. Feeley, *J. Catal.* 210 (2002) 137-148.
- [5] S. Rabl, D. Santi, A. Haas, M. Ferrari, V. Calemma, G. Bellussi, J. Weitkamp, *Microporous Mesoporous Mater.* 146 (2011) 190-200.

- [6] M.D. Moser, P.L. Bogdan, in "Handbook of Heterogeneous Catalysis", 2nd Edn., G. Ertl, H. Knözinger, F. Schüth, J. Weitkamp (Eds.), Vol. 6, Wiley-VCH, Weinheim, 2008, p. 2729-2741.
- [7] A.M. Ruppert, B.M. Weckhuysen, in: "Handbook of Heterogeneous Catalysis", 2nd Edn., G. Ertl, H. Knözinger, F. Schüth, J. Weitkamp (Eds.), Vol. 2, Wiley-VCH, Weinheim, 2008, p. 1178-1188.
- [8] R. Schlögl, in: "Handbook of Heterogeneous Catalysis", 2nd Edn., G. Ertl, H. Knözinger, F. Schüth, J. Weitkamp (Eds.), Vol. 1, Wiley-VCH, Weinheim, 2008, p. 357-427.
- [9] <http://www.aerosil.com/product/aerosil/en/products/hydrophilic-fumed-silica/Pages/default.aspx>, access on September 09, 2011.
- [10] D. Zhao, J. Feng, Q. Huo, N. Melosh, G.H. Fredrickson, B.F. Chmelka, G.D. Stucky, *Science* 279 (1998) 548-552.
- [11] C.T. Kresge, M.E. Leonowicz, W.J. Roth, J.C. Vartuli, J.S. Beck, *Nature* 359 (1992) 710-712.
- [12] E. Marceau, X. Carrier, M. Che, O. Clause, C. Marcilly, in: "Handbook of Heterogeneous Catalysis", 2nd Edn., G. Ertl, H. Knözinger, F. Schüth, J. Weitkamp (Eds.), Vol. 1, Wiley-VCH, Weinheim, 2008, p. 467-484.
- [13] J.T. Miller, M. Schreier, A.J. Kropf, J.R. Regalbuto, *J. Catal.* 225 (2004) 203-212.
- [14] L. Jiao, J.R. Regalbuto, *J. Catal.* 260 (2008) 342-350.
- [15] L. Jiao, J.R. Regalbuto, *J. Catal.* 260 (2008) 329-341.
- [16] P. Gallezot, in: "Molecular Sieves: Science and Technologies", H.G. Karge, J. Weitkamp (Eds.), Vol. 3, Springer, Berlin, 2002, p. 257-305.
- [17] D.S. Santilli, B.C. Gates, in: "Handbook of Heterogeneous Catalysis", 2nd Edn., G. Ertl, H. Knözinger, F. Schüth, J. Weitkamp (Eds.), Vol. 3, Wiley-VCH, Weinheim, 2008, p. 1624-1637.
- [18] G.C. Bond, in: "Metal-Catalysed Reactions of Hydrocarbons", M.V. Twigg, M.S. Spencer (Eds.), *Fundamental and Applied Catalysis*, Springer, New York, 2005, p. 604.
- [19] J.H. Sinfelt, in: "Bifunctional Catalysis", T.B. Drew, J.W. Hoopes Jr., T. Vermeulen, G.R. Cokelet (Eds.), *Advances in Chemical Engineering*, Vol. 5, Academic Press, New York, 1964, p. 37-74.
- [20] M.M. Bhasin, J.H. McCain, B.V. Vora, T. Imai, P.R. Pujad, *Appl. Catal. A: Gen.* 221 (2001) 397-419.
- [21] F.M. Dautzenberg, J.C. Platteuw, *J. Catal.* 19 (1970) 41-48.
- [22] F.G. Gault, in: "Advances in Catalysis", D.D. Eley, H. Pines, P.B. Weisz (Eds.), Vol. 30, Academic Press, New York, 1981, p. 1-95.
- [23] J. Weitkamp, in: "Proceedings of the 9th Iberoamerican Symposium on Catalysis", Sociedad Iberoamericana de Catálise (Eds.), Vol. 2, Lissabon, 1984, p. 1332-1341.
- [24] J.R. Anderson, N.R. Avery, *J. Catal.* 2 (1963) 542-544.
- [25] G.C. Bond, in: "Fundamental and Applied Catalysis", M.V. Twigg, M.S. Spencer (Eds.), Springer, New York, 2005, p. 625-628.
- [26] Y. Barron, G. Maire, J.M. Muller, F.G. Gault, *J. Catal.* 5 (1966) 428-445.

- [27] F. Garin, F.G. Gault, *J. Am. Chem. Soc.* 97 (1975) 4466-4476.
- [28] G.C. Bond, in: "Metal-Catalysed Reactions of Hydrocarbons", M.V. Twigg, M.S. Spencer (Eds.), *Fundamental and Applied Catalysis*, Springer, New York, 2005, p. 626.
- [29] P. Légaré, F. Garin, *J. Catal.* 241 (2003) 336-340.
- [30] J.R. Anderson, N.R. Avery, *J. Catal.* 5 (1966) 446-463.
- [31] J.L. Carter, J.A. Cusumano, J.H. Sinfelt, *J. Catal.* 20 (1971) 223-229.
- [32] G.C. Bond, R.H. Cunningham, *J. Catal.* 166 (1997) 172-185.
- [33] G. Maire, G. Plouidy, J.C. Prudhomme, F.G. Gault, *J. Catal.* 4 (1965) 556-569.
- [34] D. Teschner, K. Mátusek, Z. Paál, *J. Catal.* 192 (2000) 335-343.
- [35] D. Teschner, Z. Paál, D. Duprez, *Catal. Today* 65 (2001) 185-190.
- [36] B. Coq, R. Dutartre, F. Figueras, T. Tazi, *J. Catal.* 122 (1990) 438-447.
- [37] Z. Paál, N. Györfly, A. Wootsch, L. Tóth, I. Bakos, S. Szabó, U. Wild, R. Schlögl, *J. Catal.* 250 (2007) 254-263.
- [38] E.M. Engler, J.D. Andose, P. von R. Schleyer, *J. Am. Chem. Soc.* 95 (1973) 8005-8025.
- [39] R.J. Chimentão, G.P. Valença, F. Medina, J. Pérez-Ramírez, *Appl. Surf. Sci.* 253 (2007) 5888-5893.
- [40] U. Nylén, L. Sassu, S. Melis, S. Järås, M. Boutonnet, *Appl. Catal. A: Gen.* 299 (2006) 1-13.
- [41] S.L. González-Cortés, S. Dokjampa, P.T. Do, Z. Li, J.M. Ramallo-López, F.G. Requejo, *Chem. Eng. J.* 139 (2008) 147-156.
- [42] S. Dokjampa, T. Rirksomboon, D.T.M. Phuong, D.E. Resasco, *J. Mol. Catal. A: Chem.* 274 (2007) 231-240.
- [43] P.T. Do, W.E. Alvarez, D.E. Resasco, *J. Catal.* 238 (2006) 477-488.
- [44] B. Coq, E. Crabb, F. Figuéras, *J. Mol. Catal. A: Chem.* 96 (1995) 35-48.
- [45] H. Shi, O.Y. Gutiérrez, J.A. Lercher, in: "Preprints of the Conference – Catalysis – Innovative Applications in Petrochemistry and Refining", S. Ernst, U. Balfanz, A. Jess, J.A. Lercher, J. Lichtscheidl, M. Marchionna, F. Nees, E. Santacesaria (Eds.), *DGMK Tagungsbericht 2011-2*, DGMK, Hamburg, 2011, p. 153-157.
- [46] J. Weitkamp, M. Hunger, in: "Introduction to Zeolite Science and Practice", J. Čejka, H. van Bekkum, A. Corma, F. Schüth (Eds.), *Studies in Surface Science and Catalysis*, Vol. 168, Elsevier, Amsterdam, 2007, p. 787-835.
- [47] J. Weitkamp, *Ind. Eng. Chem. Prod. Res. Dev.* 21 (1982) 550-558.
- [48] J.A. Martens, P.A. Jacobs, J. Weitkamp, *Appl. Catal.* 20 (1986) 239-281.
- [49] M. Santikunaporn, W.E. Alvarez, D.E. Resasco, *Appl. Catal. A: Gen.* 325 (2007) 175-187.
- [50] D. Kubička, N. Kumar, P. Mäki-Arvela, M. Tiitta, V. Niemi, H. Karhu, T. Salmi, D.Y. Murzin, *J. Catal.* 227 (2004) 313-327.
- [51] D. Kubička, M. Ronnholm, S.-P. Reinikainen, T. Salmi, D.Y. Murzin, *Anal. Chim. Acta* 537 (2005) 339-348.
- [52] S. Rabl, A. Haas, D. Santi, C. Flego, M. Ferrari, V. Calemma, J. Weitkamp, *Appl. Catal. A: Gen.* 400 (2011) 131-141.
- [53] J. Weitkamp, P.A. Jacobs, J.A. Martens, *Appl. Catal.* 8 (1983) 123-141

- [54] J. Weitkamp, H. Schulz, Erdöl Kohle, Erdgas, Petrochem. Brennst.-Chem. 28 (1975) 37.
- [55] K. Hedden, J. Weitkamp, Chem. Ing. Tech. 55 (1983) 907-914.
- [56] D.M. Brouwer, H. Hogeveen, Recl. Trav. Chim. Pays-Bas 89 (1970) 211-224.
- [57] R.F. Sullivan, C.J. Egan, G.E. Langlois, R.P. Sieg, J. Am. Chem. Soc. 83 (1961) 1156-1160.
- [58] C.J. Egan, G.E. Langlois, R.J. White, J. Am. Chem. Soc. 84 (1962) 1204-1012.
- [59] M. Santikunaporn, J.E. Herrera, S. Jongpatiwut, D.E. Resasco, W.E. Alvarez, E.L. Sughrue, J. Catal. 228 (2004) 100-113.
- [60] M.A. Arribas, A. Corma, M.J. Díaz-Cabañas, A. Martínez, Appl. Catal. A: Gen. 273 (2004) 277-286.
- [61] K.C. Mouli, V. Sundaramurthy, A.K. Dalai, Z. Ring, Appl. Catal. A: Gen. 321 (2007) 17-26.
- [62] R. Contreras, J. Ramírez, R. Cuevas-García, A. Gutiérrez-Alejandre, P. Castillo-Villalón, G. Macías, I. Puente-Lee, Catal. Today 148 (2009) 49-54.
- [63] K.C. Mouli, V. Sundaramurthy, A.K. Dalai, J. Mol. Catal. A: Chem. 304 (2009) 77-84.
- [64] A. Arribas, P. Concepción, A. Martínez, Appl. Catal. A: Gen. 267 (2004) 111-119.
- [65] D. Kubička, M. Kangas, N. Kumar, M. Tiitta, M. Lindblad, D.Y. Murzin, Top. Catal. 53 (2010) 1438-1445.
- [66] J. Weitkamp, S. Rabl, A. Haas, D. Santi, M. Ferrari, V. Calemma, (a) in: "Preprints of the Conference - The Future Role of Hydrogen in Petrochemistry and Energy Supply", S. Ernst, A. Lercher, J. Lichtscheidl, M. Marchionna, F. Nees, E. Santacesaria (Eds.), DGMK Tagungsbericht 2010-3, DGMK, Hamburg, 2010, p. 77-86. (b) Oil Gas European J. 37 (2) (2011) 94-98.
- [67] G. Bellussi, A. Haas, S. Rabl, D. Santi, M. Ferrari, V. Calemma, J. Weitkamp, Chin. J. Catal. (2012), accepted.
- [68] V.R.R. Marthala, S. Rabl, J. Huang, S.A.S. Rezai, B. Thomas, M. Hunger, J. Catal. 257 (2008) 134-141.
- [69] G. Bergeret, P. Gallezot, B. Imelik, J. Phys. Chem. 85 (1981) 411-416.
- [70] K. Kunimori, T. Wakasugi, F. Yamakawa, H. Oyanagi, J. Nakamura, T. Uchijima, Catal. Lett. 9 (1991) 331-338.
- [71] G.B. McVicker, R.T. Baker, R.L. Garten, E.L. Kugler, J. Catal. 65 (1980) 207-220.
- [72] S. Koutsopoulos, T. Johannessen, K.M. Eriksen, R. Fehrmann, J. Catal. 238 (2006) 206-213.
- [73] L.B. Okhlopkova, A.S. Lisitsyn, V.A. Likholobov, M. Gurrath, H.P. Boehm, Appl. Catal. A: Gen. 204 (2000) 229-240.
- [74] S. Rabl, Ph.D. Thesis, University of Stuttgart, 2011.
- [75] S. Brunauer, P.H. Emmett, E. Teller, J. Am. Chem. Soc. 60 (1938) 309-319.
- [76] J.A. Anderson. M. Fernández-García, A. Martínez-Arias, in: "Supported Metals in Catalysis", J.A. Anderson. M. Fernández-García (Eds.), Catalytic Science Series, Vol. 5, Imperial College Press, London, 2005, p. 139.

- [77] J. Weitkamp, R. Gläser, in: "Handbook of Heterogeneous Catalysis", 2nd Edn., G. Ertl, H. Knözinger, F. Schüth, J. Weitkamp (Eds.), Vol. 4, Wiley-VCH, Weinheim, 2008, p. 2045-2053.
- [78] J.M. Prausnitz, R.N. Lichtenthaler, E.G. de Azevedo, "Molecular Thermodynamics of Fluid-Phase Equilibria", 3rd Edn., Prentice-Hall PTR, Upper Saddle River, 1999, p. 40-43.
- [79] <http://www.iza-structure.org/databases/> (Access on 04.11.2011).
- [80] G.B. McVicker, R.T. Baker, R.L. Garten, E.L. Kugler, *J. Catal.* 65 (1980) 207-220.
- [81] A. de Oliveira, I. Costilla, C. Gigola, I.M. Baibich, V.T. da Silva, S.B.C. Pergher, *Catal. Lett.* 136 (2010) 185-191.
- [82] P. Reyes, G. Pecchi, J.L.G Fierro, *Langmuir*, 17 (2001) 522-527.
- [83] J. Weitkamp, in: "Hydrocracking and Hydrotreating", J.W. Ward, S.A. Qader (Eds.), Amer. Chem. Soc. Symp. Ser., Vol. 20, American Chemical Society, Washington, D.C., 1975, p. 1-27.
- [84] A. Haas, Diploma Thesis, University of Stuttgart, 2008.
- [85] C.F. Frye, A.W. Weitkamp, *J. Chem. Eng. Data* 14 (1969) 372-376.
- [86] N.L. Allinger, J.L. Coke, *J. Am. Chem. Soc.* 82 (1960) 2553-2556.
- [87] A.W. Weitkamp, in: "Advances in Catalysis", D.D. Eley, H. Pines, P.B. Weisz (Eds.), Vol. 18, Academic Press, New York, 1968, p. 1-110.
- [88] U. Nylén, J.F. Delgado, S. Järås, M. Boutonnet, *Appl. Catal. A: Gen.* 262 (2004) 189-200.
- [89] C.L. Yaws "Yaws' Handbook of Thermodynamic and Physical Properties of Chemical Compounds" Knovel, 2003, <http://www.knovel.com/knovel2/Toc.jsp?BookID=667&VerticalID=0>, Accessed on May 29, 2008.
- [90] W.-C. Lai, C. Song, *Catal. Today* 31 (1996) 171-181.
- [91] J.A. Moulijn, A.E. van Diepen, F. Kapteijn, in: "Handbook of Heterogeneous Catalysis", 2nd Edn., G. Ertl, H. Knözinger, F. Schüth, J. Weitkamp (Eds.), Vol. 4, Wiley-VCH, Weinheim, 2008, p. 1829-1846.
- [92] R.C. Santana, P.T. Do, M. Santikunaporn, W.E. Alvarez, J.D. Taylor, E.L. Sughrie, D.E. Resasco, *Fuel* 85 (2006) 643-656.
- [93] R.K. Herz, W.D. Gillespie, E.E. Petersen, G.A. Somorjai, *J. Catal.* 67 (1981) 371-386.
- [94] D. Teschner, D. Duprez, Z. Paál, *J. Mol. Catal. A: Chem.* 179 (2002) 201-212.
- [95] C.L. Yaws, "Thermophysical Properties of Chemicals and Hydrocarbons", William Andrew Inc., Norwich, 2008, p. 501.
- [96] D. Santi, Ph.D. Thesis, University of Stuttgart, in preparation.
- [97] S. Ernst, J. Weitkamp, in: "Proceedings of the International Symposium of Zeolite Catalysis", Siófok, Hungary, May 13 to 16, 1985, p. 457-466.
- [98] M.B. Turova-Polyak, I.S. Sosnina, N.A. Belikova, A.F. Plate, *Zh. Org. Khim.* 2 (1966) 2162-2164.
- [99] M.P. Kozina, A.K. Mirzaeva, I.E. Sosnina, N.V. Elagina, S.M. Skuratov, *Dokl. Akad. Nauk SSSR* 155 (1964) 1123-1125.
- [100] D. Santi, personal communication, 2011.

12 Appendices

12.1 Retention Times

Tables containing the retention times of products in the GC can be found on the attached CD.

12.2 Calculation of Conversion, Yields and Selectivities in the Catalytic Conversion of Hydrocarbons with Hydrogen

With cis-decalin as hydrocarbon, an evaluation method for the calculation of conversion, yields and selectivities was developed by Rabl [1]. For the present work a generalized version is required since several different feed hydrocarbons are used.

12.2.1 Nomenclature

12.2.1.1 Symbols

Symbol	Unit	Designation
A	-	Dimensionless peak area in the chromatogram
f	-	Compound-specific correction factor of the flame-ionization detector
m	kg	Mass
\dot{m}	$\text{g}\cdot\text{h}^{-1}$	Mass flux
M	$\text{g}\cdot\text{mol}^{-1}$	Molar mass
n	mol	Molar amount
\dot{n}	$\text{mol}\cdot\text{h}^{-1}$	Molar flux
s	kg	Reciprocal sensitivity of the flame ionization detector
S	-	Selectivity
S^*	-	Modified selectivity

x	-	Stoichiometric coefficient of hydrogen consumed in Eq. (12.1)
X	-	Conversion
y	-	Stoichiometric coefficient of hydrogen formed in Eq. (12.1)
Y	-	Yield
ν	-	Stoichiometric factor

12.2.1.2 Indices

conv	Converted
in	Entering the reactor
out	Leaving the reactor

12.2.1.3 Abbreviations

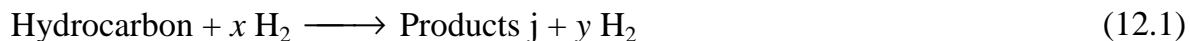
B	Butyl-
Bz	Benzene
C ₇ -	Hydrocarbons with less than 8 carbon atoms (hydrocracked products)
C ₈ aromatics	Aromatic hydrocarbons with 8 carbon atoms
C ₈ -	Hydrocarbons with less than 9 carbon atoms (hydrocracked products)
C ₉ -	Hydrocarbons with less than 10 carbon atoms (hydrocracked products)
C ₁₀ -	Hydrocarbons with less than 11 carbon atoms (hydrocracked products)
DHP(s)	Dehydrogenated products
E-	Ethyl-
Eq(s).	Equation(s)
FID	Flame ionization detector
GSL	Gas sampling loop

j	Product or group of products in Eq. (12.1)
OCD(s)	Open-chain decane(s)
OCN(s)	Open-chain nonane(s)
OCO(s)	Open-chain octane(s)
OCU(s)	Open-chain undecane(s)
RCP(s)	Ring-closure product(s)
ROP(s)	Ring-opening product(s)
sk-Iso(s)	Skeletal isomer(s)

12.2.2 Conversion X_{feed}

12.2.2.1 Fundamentals

In the present work different hydrocarbons, *viz.* n-alkanes and hydrocarbons with one or two naphthenic rings, were converted with a large excess of hydrogen in a fixed-bed reactor. As basis for the subsequent considerations, the simplified stoichiometry is given in Eq. (12.1).



Depending on the feed hydrocarbon, different classes of products were formed, see Section 5.5.1. In Table 12.8 the stoichiometric coefficients x and y for the hydrogen consumed and formed, respectively, are tabulated for the different feed hydrocarbons and reactions.

Table 12.8: Stoichiometric coefficients x and y for the hydrogen consumed and formed, respectively, for the different feed hydrocarbons and reactions.

Feed Hydrocarbon	Reaction	Product Group	x	y
n-Octane	Isomerization	sk-Isos	0	0
	Dehydrocyclization	RCPs	0	1
	Aromatization	C ₈ aromatics	0	4
	Hydrocracking	C ₇ -	≥ 1	0
n-Decane	Isomerization	sk-Isos	0	0
	Dehydrocyclization	RCPs	0	1
	Hydrocracking	C ₉ -	≥ 1	0
Ethylcyclohexane	Isomerization	sk-Isos	0	0
	Ring opening	OCOs	1	0
	Dehydrogenation	E-Bz	0	3
	Hydrocracking	C ₇ -	≥ 1	0
Butylcyclohexane	Isomerization	sk-Isos	0	0
	Ring opening	OCDs	1	0
	Dehydrogenation	B-Bz	0	3
	Hydrocracking	C ₉ -	≥ 1	0
Perhydroindan	Isomerization	sk-Isos	0	0
	Ring opening	ROPs	1	0
	Double ring opening	OCNs	2	0
	Dehydrogenation	DHPs	0	3 or 4
	Hydrocracking	C ₈ -	≥ 1	0
Decalin	Isomerization	sk-Isos	0	0
	Ring opening	ROPs	1	0
	Double ring opening	OCDs	2	0
	Dehydrogenation	DHPs	0	3 or 5
	Hydrocracking	C ₉ -	≥ 1	0
Spiro[4.5]decane	Isomerization	sk-Isos	0	0
	Ring opening	ROPs	1	0
	Double ring opening	OCDs	2	0
	Hydrocracking	C ₉ -	≥ 1	0

Table 12.8 (continued).

Methyldecalin	Isomerization	sk-Isos	0	0
	Ring opening	ROPs	1	0
	Double ring opening	OCUs	2	0
	Dehydrogenation	DHPs	0	3 or 5
	Hydrocracking	C ₁₀ -	≥ 1	0

The conversion defined in Eq. (5.1), page 69 with molar fluxes \dot{n} can also be expressed with mass fluxes \dot{m} :

$$X_{\text{feed}} = \frac{(\dot{m}_{\text{feed}})_{\text{in}} - (\dot{m}_{\text{feed}})_{\text{out}}}{(\dot{m}_{\text{feed}})_{\text{in}}} \quad (12.2)$$

Since the products were analyzed in an on-line gas chromatograph equipped with a gas sampling loop (GSL), Eq. (12.2) can be transformed into Eq. (12.3) under incorporation of absolute masses inside the GSL.

$$X_{\text{feed}} = \frac{(m_{\text{feed}})_{\text{GSL at } X=0} - (m_{\text{feed}})_{\text{GSL}}}{(m_{\text{feed}})_{\text{GSL at } X=0}} \quad (12.3)$$

While $(m_{\text{feed}})_{\text{GSL at } X=0}$ is the hypothetical mass of feed hydrocarbon that would have been captured in the gas sampling loop if no reaction would have occurred, $(m_{\text{feed}})_{\text{GSL}}$ is the mass of feed hydrocarbon that is actually stored in the GSL. In the gas chromatogram, the area of the feed hydrocarbon allows a direct calculation of $(m_{\text{feed}})_{\text{GSL}}$ (see Section 12.2.2.2), whereas $(m_{\text{feed}})_{\text{GSL at } X=0}$ has to be evaluated *via* another method (see Section 12.2.2.3).

12.2.2.2 Calculation of $(m_{\text{feed}})_{\text{GSL}}$ from the Area in the Gas Chromatogram

In the flame ionization detector, the mass of a given hydrocarbon is proportional to an instrument-specific proportionality factor s times the compound-specific FID correction factor f_{feed} times the dimensionless peak area A_{feed} :

$$(m_{\text{feed}})_{\text{GSL}} = s \cdot f_{\text{feed}} \cdot A_{\text{feed}} \quad (12.4)$$

A determination of s by calibration experiments is not required since, as will be shown in Section 12.2.2.3, in the calculation of X_{feed} this factor s can be cancelled. The

compound-specific FID correction factor is usually related to benzene, for which $f_{\text{Bz}} = 1.000$ is set:

$$f_{\text{feed}} = \frac{m_{\text{feed}} \cdot A_{\text{feed}}}{m_{\text{Bz}} \cdot A_{\text{Bz}}} \quad (12.5)$$

Principally, f_{feed} and also the compound-specific FID correction factor f_j of all products could be obtained with Eq. (12.5) by injection of known masses of the respective compounds and measuring the areas in the gas chromatogram. However, an alternative determination of the FID factor is required due to (i) the large number of products, (ii) the fact that not every signal in the chromatogram can be assigned to a specific compound and (iii) the commercial unavailability of some hydrocarbons in its pure form.

It is well-known [2] that the signal intensity in the FID stems almost completely from the carbon atoms in the respective molecule, whereas the hydrogen atoms appear virtually “FID-silent”. Hence, for hydrocarbons with a higher fraction of hydrogen in the molecule compared to benzene, f is larger than unity and *vice versa*. For calculating f_{feed} Eq. (12.6) will be applied:

$$f_{\text{feed}} = \frac{\frac{M_{\text{feed}}}{M_{\text{C, feed}}}}{\frac{M_{\text{Bz}}}{M_{\text{C, Bz}}}} \quad (12.6)$$

Here, M_{feed} and M_{Bz} are the molar masses of the feed hydrocarbon and benzene, respectively. $M_{\text{C, feed}}$ and $M_{\text{C, Bz}}$ are the molar masses of carbon in the feed hydrocarbon and benzene, respectively. A slight modification of Eq. (12.6) allows the calculation of the FID factor of the products f_j with M_j and $M_{\text{C, j}}$ as the molar masses of the product j and of carbon in the product j , respectively:

$$f_{\text{feed}} = \frac{\frac{M_j}{M_{\text{C, j}}}}{\frac{M_{\text{Bz}}}{M_{\text{C, Bz}}}} \quad (12.7)$$

12.2.2.3 Calculation of $(m_{\text{feed}})_{\text{GSL}}$ at $X = 0$

In Eq. (12.3) the hypothetical mass of the feed hydrocarbon that would be entrapped in the GSL at zero conversion $(m_{\text{feed}})_{\text{GSL}}$ at $X = 0$ was introduced. According to Eq. (12.8) it

is the sum of masses of the unconverted feed hydrocarbon $(m_{\text{feed}})_{\text{GSL}}$ (calculation in Section 12.2.2.2) and of the converted feed hydrocarbon $(m_{\text{feed}})_{\text{conv}}$.

$$(m_{\text{feed}})_{\text{GSL at } X=0} = (m_{\text{feed}})_{\text{GSL}} + (m_{\text{feed}})_{\text{conv}} \quad (12.8)$$

For each product, the mass of decalin that was converted into this product has to be calculated. In analogy to Eq. (12.4), the mass of each product $(m_j)_{\text{GSL}}$ can be determined:

$$(m_j)_{\text{GSL}} = s \cdot f_j \cdot A_j \quad (12.9)$$

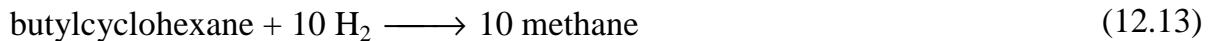
With Eq. (12.9) a calculation of $(m_{\text{feed}})_{\text{converted to product } j}$ is possible for each product j :

$$(m_{\text{feed}})_{\text{converted to product } j} = \frac{|v_{\text{feed}}|}{v_j} \cdot \frac{M_{\text{feed}}}{M_j} \cdot s \cdot f_j \cdot A_j \quad (12.10)$$

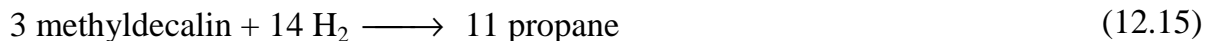
Here, v_{feed} and v_j are the stoichiometric factors of the reactant and the product j , respectively. In reactions furnishing products with the same number of carbon atoms like the feed hydrocarbon, v_{feed} and v_j equal unity. Only in hydrocracking reactions the feed hydrocarbon can furnish products with a lower number of carbon atoms than the feed hydrocarbon, *i.e.* v_{feed} and v_j can assume values larger than one. Exemplarily, some hydrocracking reactions and the corresponding stoichiometric factors are given:



$$v_{\text{feed}} = -1; v_j = 2; \frac{|v_{\text{feed}}|}{v_j} = \frac{1}{2} \quad (12.12)$$



$$v_{\text{feed}} = -1; v_j = 10; \frac{|v_{\text{feed}}|}{v_j} = \frac{1}{10} \quad (12.14)$$



$$v_{\text{feed}} = -3; v_j = 11; \frac{|v_{\text{feed}}|}{v_j} = \frac{3}{11} \quad (12.16)$$

By summing up $(m_{\text{feed}})_{\text{converted to product } j}$ (Eq. (12.10)) for all products the total mass of feed hydrocarbon that was converted can be determined:

$$(m_{\text{feed}})_{\text{conv}} = s \cdot \sum_j \frac{|v_{\text{feed}}|}{v_j} \cdot \frac{M_{\text{feed}}}{M_j} \cdot f_j \cdot A_j \quad (12.17)$$

Finally, the conversion X_{feed} results by substituting Eqs. (12.4) and (12.17) into Eq. (12.8), and Eqs. (12.4) and (12.8) in Eq. (12.3), followed by cancellation of s :

$$X_{\text{feed}} = \frac{\sum_j \frac{|v_{\text{feed}}|}{v_j} \cdot \frac{M_{\text{feed}}}{M_j} \cdot f_j \cdot A_j}{f_{\text{feed}} \cdot A_{\text{feed}} + \sum_j \frac{|v_{\text{feed}}|}{v_j} \cdot \frac{M_{\text{feed}}}{M_j} \cdot f_j \cdot A_j} \quad (12.18)$$

12.2.3 Yield Y_j

In this work, the yield of products is defined as:

$$Y_j = \frac{(\dot{n}_j)_{\text{out}} - (\dot{n}_j)_{\text{in}}}{(\dot{n}_{\text{feed}})_{\text{in}}} \cdot \frac{|v_{\text{feed}}|}{v_j} \quad (12.19)$$

Since $(\dot{n}_j)_{\text{in}}$ will be zero throughout this work and in analogy to the evaluation discussed in Section 12.2.2.1, Eq. (12.19) can be transformed into Eqs. (12.20) and (12.21).

$$Y_j = \frac{(n_j)_{\text{GSL}}}{(n_{\text{feed}})_{\text{GSL at X=0}}} \cdot \frac{|v_{\text{feed}}|}{v_j} \quad (12.20)$$

$$Y_j = \frac{(m_j)_{\text{GSL}}}{(m_{\text{feed}})_{\text{GSL at X=0}}} \cdot \frac{|v_{\text{feed}}|}{v_j} \cdot \frac{M_{\text{feed}}}{M_j} \quad (12.21)$$

As developed for the conversion in Section 12.2.2.3, substituting Eqs. (12.4) and (12.17) into Eq. (12.8), and Eqs. (12.4) and (12.8) into Eq. (12.21) gives the yield of products Y_j after cancellation of s :

$$Y_j = \frac{f_j \cdot A_j}{f_{\text{feed}} \cdot A_{\text{feed}} + \sum_j \frac{|v_{\text{feed}}|}{v_j} \cdot \frac{M_{\text{feed}}}{M_j} \cdot f_j \cdot A_j} \cdot \frac{|v_{\text{feed}}|}{v_j} \cdot \frac{M_{\text{feed}}}{M_j} \quad (12.22)$$

12.2.4 Selectivity S_j

In this work, the selectivity of products is defined as shown in Eq. (12.23). A summation of S_j over all products equals 100 %.

$$S_j = \frac{(\dot{n}_j)_{\text{out}} - (\dot{n}_j)_{\text{in}}}{(\dot{n}_{\text{feed}})_{\text{in}} - (\dot{n}_{\text{feed}})_{\text{out}}} \cdot \frac{|v_{\text{feed}}|}{v_j} \quad (12.23)$$

Since $(\dot{n}_j)_{\text{in}}$ will be zero throughout this work and in analogy to the evaluation discussed in Section 12.2.2.1, Eq. (12.23) can be transformed into Eqs. (12.24) and (12.25):

$$S_j = \frac{(n_j)_{\text{GSL}}}{(n_{\text{feed}})_{\text{conv}}} \cdot \frac{|v_{\text{feed}}|}{v_j} \quad (12.24)$$

$$S_j = \frac{(m_j)_{\text{GSL}}}{(m_{\text{feed}})_{\text{conv}}} \cdot \frac{|v_{\text{feed}}|}{v_j} \cdot \frac{M_{\text{feed}}}{M_j} \quad (12.25)$$

As developed for the conversion in Section 12.2.2.3, substituting Eqs. (12.4) and (12.17) into Eq. (12.8) and Eqs. (12.4) and (12.8) into Eq. (12.25) gives the selectivity of products S_j after cancellation of s :

$$S_j = \frac{f_j \cdot A_j}{\sum_j \frac{|v_{\text{feed}}|}{v_j} \cdot \frac{M_{\text{feed}}}{M_j} \cdot f_j \cdot A_j} \cdot \frac{|v_{\text{feed}}|}{v_j} \cdot \frac{M_{\text{feed}}}{M_j} \quad (12.26)$$

12.2.5 Modified Selectivity S_j^*

For the quantitative discussion of the hydrocracking reactions to hydrocarbons with a smaller number of carbon atoms than the feed hydrocarbon, the modified hydrocracking selectivity S_j^* will be used. It is defined as the molar amount of a hydrocracked product j formed divided by the molar amount of reactant converted into hydrocracked products:

$$S_j^* = \frac{(\dot{n}_j)_{\text{out}}}{(\dot{n}_{\text{feed}})_{\text{converted into hydrocracked products}}} \quad (12.27)$$

Substituting the molar fluxes in Eq. (12.27) with total molar amounts in the GSL and converting them into total masses furnishes Eq. (12.28).

$$S_j^* = \frac{\frac{1}{M_j} \cdot (m_j)_{\text{GSL}}}{\frac{1}{M_{\text{feed}}} \cdot (m_{\text{feed}})_{\text{converted into hydrocracked products}}} \quad (12.28)$$

By substituting the nominator and denominator with Eqs. (12.9) and (12.17), respectively, and cancellation of s it results for the hydrocracked products j :

$$S_j^* = \frac{\frac{1}{M_j} \cdot f_j \cdot A}{\frac{1}{M_{\text{feed}}} \cdot \sum_j \frac{|v_{\text{feed}}|}{v_j} \cdot \frac{M_{\text{feed}}}{M_j} \cdot f_j \cdot A_j} \quad (12.29)$$

12.2.6 References

- [1] S. Rabl, Ph.D. Thesis, University of Stuttgart, 2011.
- [2] E. Leibnitz, H.G. Struppe, "Handbuch der Gaschromatographie", 3rd Edn., Akademische Verlagsgesellschaft Geest & Portig, Leipzig, 1984, p. 422.

12.3 Simulation of the Distribution of Hydrocracked Products in the Hydroconversion of Decalin on Ir/silica

12.3.1 Underlying Reaction Network

The distribution of the hydrocracked products is simulated by assuming the reaction sequence that is depicted in Figure 12.1. It is derived from the catalytic results obtained on 2.59Ir/silica in the decalin conversion (see Section 9.5.2). Accordingly, hydrocracked products (C_9^-) are formed from decalin on iridium/silica via two principal pathways: Both start with the hydrogenolytic opening of one six-membered ring to the five direct ROPs. The latter are key intermediates on the way to hydrocarbons with nine or less carbon atoms: in path 1, C_9^- products are readily made from direct ROPs by hydrogenolysis in an alkyl side-chain. Alternatively, in path 2 direct OCDs are first formed by endocyclic hydrogenolysis of direct ROPs, and the direct OCDs undergo a consecutive hydrogenolysis to C_9^- hydrocarbons.

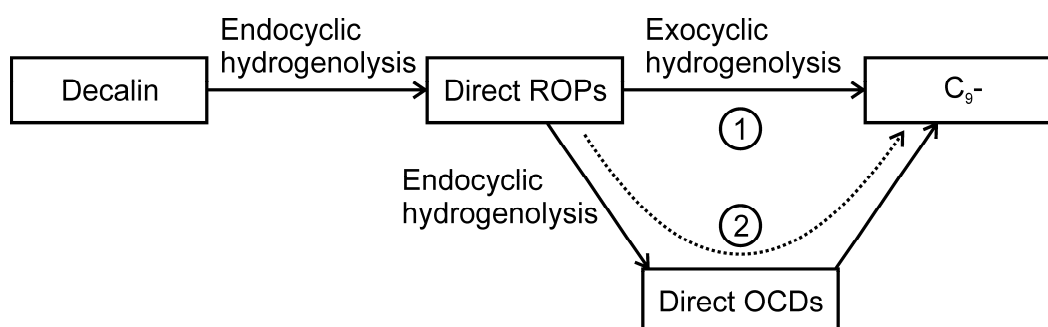


Figure 12.1: Assumed reaction sequence of the hydrogenolysis of decalin on Ir/silica.

12.3.1.1 Hydrogenolytic Ring Opening of One Six-Membered Ring in Decalin

As described in Section 9.5.2 a direct hydrogenolytic ring opening of decalin results in the formation of five different direct ROPs. Hydrogenolysis of the tertiary-secondary C-C bond yields butylcyclohexane whereas a ring opening at the two bissecondary C-C bonds results in the formation of the cis- and trans-isomers of 1-methyl-2-propylcyclohexane and of 1,2-diethylcyclohexane, see Figure 12.2.

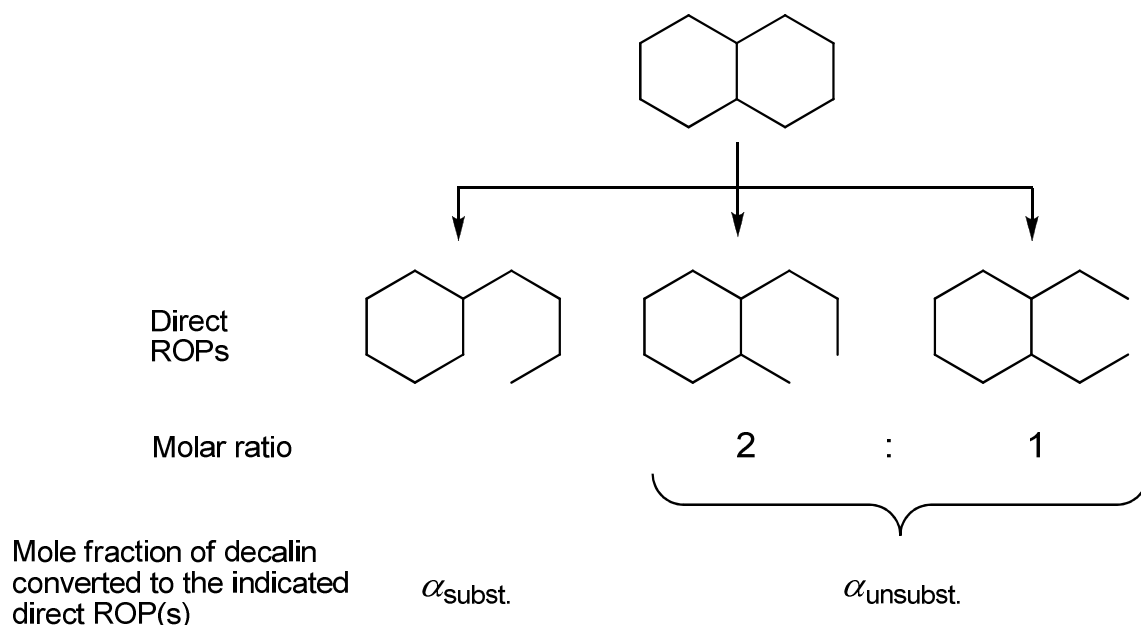


Figure 12.2: Hydrogenolysis of decalin on iridium under the formation of direct ROPs.

Different metals exhibit different regioselectivities in hydrogenolysis: Substituted C-C bonds, that comprise at least one tertiary or quaternary carbon atom, and unsubstituted C-C bonds between secondary and/or primary carbon atoms, are broken with different rates as demonstrated, for example in the ring opening of ethylcyclohexane (see Figure 9.8, page 97). In decalin, of the five C-C bonds to be broken, three are unsubstituted, while two are substituted. To account for this regioselectivity in a quantitative manner, the factors $\alpha_{\text{unsubst.}}$ or $\alpha_{\text{subst.}}$ are, respectively, defined:

$$\alpha_{\text{unsubst.}} \equiv \frac{\text{number of hydrogenolyzed C-C bonds between unsubstituted C-atoms}}{\text{total number of C-C bonds hydrogenolyzed}} \quad (12.30)$$

$$\alpha_{\text{subst.}} \equiv \frac{\text{number of hydrogenolyzed C-C bonds involving substituted C-atoms}}{\text{total number of C-C bonds hydrogenolyzed}} \quad (12.31)$$

$$\text{and } \alpha_{\text{unsubst.}} = 1 - \alpha_{\text{subst.}} \quad (12.32)$$

For the first ring opening step from decalin to direct ROPs $\alpha_{\text{unsubst.}}$ equals the mole fraction of decalin that undergoes hydrogenolysis at the unsubstituted C-C bonds, while $\alpha_{\text{subst.}}$ equals the mole fraction of decalin that is hydrogenolyzed at substituted C-C bonds. 1-Methyl-2-propylcyclohexane and 1,2-diethylcyclohexane will usually be formed in a ratio 2 : 1, since, statistically, the rupture of two equivalent bonds leads to

the former ROP, as opposed to the rupture of just one bond leading to 1,2-diethylcyclohexane.

12.3.1.2 Consecutive Hydrogenolysis of the Direct ROPs and Direct OCDs

For the consecutive hydrogenolysis of direct ROPs again the factors $\alpha_{\text{unsubst.}}$ or $\alpha_{\text{subst.}}$ are taken into account. By exocyclic hydrogenolysis (route 1 in Figure 12.1), *i.e.* when C-C bonds in the alkyl side-chain are cleaved, C₉- products are obtained. When C-C bonds are cleaved which form part of the six-membered ring (route 2 in Figure 12.1) direct OCDs are formed. These are again assumed to undergo hydrogenolysis into C₉- products in dependence of the degree of C-C bond substitution using the respective α factors.

However, in the direct OCD n-decane no substituted C-C bonds are available. When in addition, $\alpha_{\text{subst.}} > 0$ defines that a fraction of n-decane should undergo hydrogenolysis at substituted positions the formalism would lead to a loss of C₉- due to the absence of substituted C-C bonds. To avoid this loss of carbon atoms it is assumed that n-decane undergoes complete hydrogenolysis at unsubstituted C-C bonds, *i.e.* $\alpha_{\text{unsubst.}} = 1$ is set for n-decane leading to a statistical rupture of all nine C-C bonds in n-decane.

12.3.2 Calculation Method for the Distribution of the Hydrocracked Products

For each single reaction path which is possible by combining the assumed mechanistic steps described in Section 12.3.1, the amount of the two C₉- hydrocarbons formed can be calculated. At first the mole fractions of each single C₉- precursor for each single reaction path are multiplied. Subsequently, the amounts per group of C_n are summed up to obtain a simulated S_j^* curve. As an exemplary reaction path the ring opening to 1-methyl-2-propylcyclohexane and further the endocyclic hydrogenolysis to 5-methylnonane followed by hydrogenolysis to n-butane and n-hexane is shown in Figure 12.3.

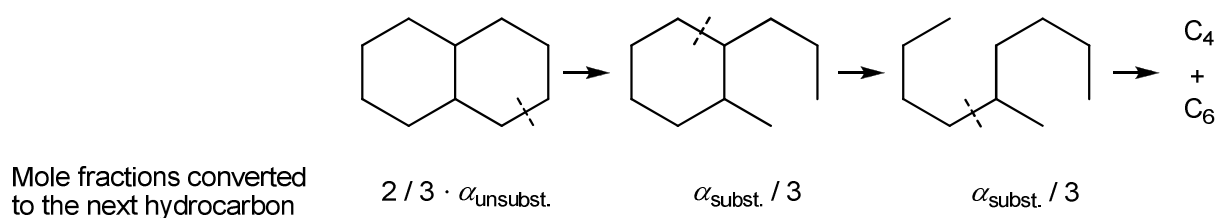


Figure 12.3: Exemplary reaction path together with the mole fractions of each hydrocarbon which is converted in the manner shown.

The mole fraction of decalin converted into 1-methyl-2-propylcyclohexane contains the factor $\alpha_{\text{unsubst.}}$ since an unsubstituted position is cleaved. Due to the molar ratio of 2 : 1 of the two possible direct ROPs by cleaving unsubstituted bonds 1-methyl-2-propylcyclohexane and 1,2-diethylcyclohexane, the factor $2/3$ is required. For the endocyclic hydrogenolysis of 1-methyl-2-propylcyclohexane at the substituted position the factor $\alpha_{\text{subst.}}$ is needed, together with $1/3$, since one out of three different substituted endocyclic bonds is cleaved. A rupture in 5-methylnonane at the marked substituted position furnishes equal amounts of C_4 and C_6 . The factor $\alpha_{\text{subst.}}$ stems from the rupture of a substituted bond, and the factor $1/3$ is due to the availability of three substituted bonds. By multiplication, for both C_4 and C_6 a mole fraction of $2/3 \cdot \alpha_{\text{unsubst.}} \cdot \alpha_{\text{subst.}} / 3 \cdot \alpha_{\text{subst.}} / 3$ is obtained by this pathway. As the broken bond in the symmetric 5-methylnonane occurs twice, this pathway occurs two times and will be added twice to the total ΣS_j^* for all pathways is calculated, a value of 200 % is obtained.

12.3.3 Results

At first some simulation results will be shown that are obtained when an equal probability of opening each C-C bond in decalin, direct ROPs and direct OCDs is assumed, *i.e.* without using factors α . With these assumptions a V-shaped curve is obtained, see Figure 12.4. Although the highest values are calculated for carbon numbers of 1 and 9 like on the iridium catalyst, the curve shapes match only moderately. A better approach starts from the real mixture of direct ROPs as obtained on 2.59Ir/silica at the lowest conversion with a molar ratio of butylcyclohexane : 1-methyl-2-propylcyclohexane : 1,2-diethylcyclohexane = 13 : 51 : 36. This results in the curve with the black triangles depicted in Figure 12.4 which coincides slightly better with the experimental result.

Now, both factors α are taken into account to include the specific regioselectivity of iridium in the simulation. By calculating $S_{\text{B-CH}_X} / S_{\text{direct ROPs}}$ at low decalin conversions,

the value of $\alpha_{\text{subst.}} = 0.13$ for catalyst 2.59Ir/silica was found. This value stands for a preferred rupture of unsubstituted C-C bonds. As result, the curve with open triangles in Figure 12.4 is obtained. Especially the high amounts of C_1 and C_9 correspond rather nicely to the measured curve.

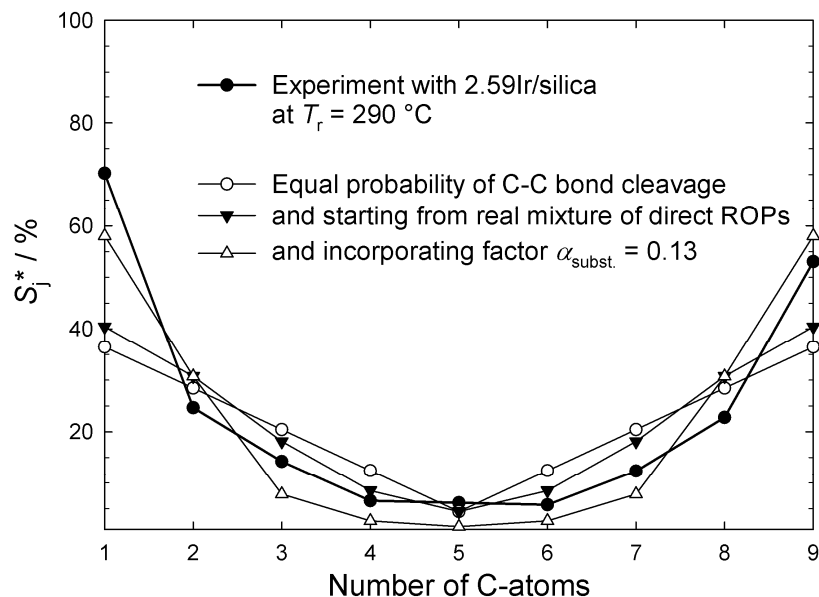


Figure 12.4: Modified hydrocracking selectivities in the experiment with 2.59Ir/silica and simulated values.